Synthesis and Application of Gold and Glycogold Nanoparticles

A thesis submitted in partial fulfillment of the requirements for the degree of **Doctor of Philosophy** in **Chemistry** at the **University of Canterbury**

Vivek Poonthiyil

Supervisors: **Prof. Antony J. Fairbanks**
&
Dr. Vladimir B. Golovko

University of Canterbury
Christchurch
New Zealand 8041.

2016

Table of Contents

Table of Contents

Table of Contents

Abstract

Gold nanoparticles have drawn significant interest in recent years due to their unique optical, electronic, and molecular recognition properties. It is widely known that the key properties of gold nanoparticles are dependent on their size, morphology, and nature of the ligands that stabilize them against aggregation. A recent development in the field of gold nanoparticle chemistry is the synthesis and application of glycogold nanoparticles, which are water-soluble three-dimensional multivalent systems based on carbohydrate-decorated gold nanoparticles. Glycogold nanoparticles are typically synthesized by attaching carbohydrates to the surface of gold nanoparticles *via* thiol-terminated linkers. They have been used to detect many toxic proteins such as concanavalin A, *Ricinus communis* agglutinin 120, cholera toxin, and viral hemagglutinin. Facile methods for the synthesis of gold and glycogold nanoparticles and the demonstration of the efficient use of glycogold nanoparticles as colorimetric sensors for toxic proteins are highly sought after.

The work in this thesis focuses on the synthesis of gold nanoparticles of various shapes and sizes using the Turkevich reaction and the synthesis of glycogold nanoparticles using Brust-Schiffrin method, ligand exchange method, and the copper(I)-catalysed azide-alkyne Huisgen cycloaddition. Also, the application of galactose-capped gold nanoparticles and full-length sialic acid terminated complex bi-antennary *N*-glycan-capped gold nanoparticles as colorimetric sensors for the detection of the lectin heat-labile enterotoxin and influenza viral particles respectively has been presented.

Acknowledgements

I would like to thank my supervisors, Prof. Antony Fairbanks and Dr. Vladimir Golovko, for their constant guidance throughout my PhD. Prof. Fairbanks` method of conducting group meetings in every week and making us to write experimental sections once in every six months and painstakingly correcting them has been really helpful in building my knowledge in organic chemistry and also helped me to finish my thesis writing in a short time frame. Also, I would like to thank him for correcting all the chapters in my thesis the very day I sent them to him. Certainly, he has shown me how to be efficient in one`s professional life and I would like to emulate that in my own life. The long discussions that I had with Dr. Golovko in his office have also certainly helped me to improve my knowledge in nanochemistry. Also, I would like to thank him for treating me like a friend throughout the duration of my PhD.

I would like to thank Dr. Yusuke Tomabechi for teaching me all the basic techniques in the lab at the beginning of my PhD and also training me in natural product extraction methods. Special thanks also go to Drs. Andrew Watson and Akshita Wason for the support during their tenure.

The best part of my Ph.D. at UC have been meeting and getting to know the other Ph.D. students and the interns in Fairbanks`s group. Evan (captain Nimmo), Pragya, Govind (GP sir), Davey (thanks buddy for helping all of us whenever we needed it and also for reading my thesis), Kajitha (Kajithakka!), Stewart (for helping me with a lot of doubts

and reading my thesis), Jesse (thanks my Swedish buddy for drawing that amazing cover image), Preeti, Sivasinthujah Paramasivam (thankachi), Hélène, Patrycja, and Aoife (free Irish Tavern) - thank you all for the wonderful time we shared together.

I really appreciate the service provided by the technical staffs at UC. Thank you Drs. Marie, Amelia, and Alexander for your assistance with NMR and Mass spec. Thanks also to Wayne, Rob, Nick, Gill, and Laurie - you all make a fantastic team and the department is currently thriving because of it! My special thanks to Dr.Matthew Polson, who has helped me with his extensive knowledge in various fields at various stages of my Ph.D.

I also would like to thank UC Doctoral scholarship for funding me for the entire three years of my Ph.D. Finally I would like to thank my family, friends, and Vrinda (my fiancée) back in India who have been supporting and encouraging me throughout.

Vivek Poonthiyil

Abbreviations

The following abbreviations have been used in this thesis:

General

1D	one-dimensional
2D	two-dimensional
3D	three-dimensional
δ	chemical shift
ν_{max}	wavenumber
ºC	degrees Celsius
µm	micrometre
µM	micromolar
Å	Angstrom
AAC	azide-alkyne Huisgen cycloaddition
Ac	acetyl
ADMP	2-azido-1,3-dimethylimidazolium hexafluorophosphate
aq	aqueous
Ar	aromatic
at	apparent triplet (in NMR)
ATT	alkyne-terminated thiol
ATT-AuNP	alkyne-terminated thiol-functionalized gold nanoparticle
AU	absorbance units
AuNP	gold nanoparticle
$BF_3{\cdot}Et_2O$	boron trifluoride diethyl etherate

Bn	benzyl
br.	broad (in NMR)
BSA	bovine serum albumin
BSM	Brust-Schiffrin method
Bz	benzoyl
c	concentration
Calcd.	calculated
Cer	ceramide
Cit-AuNP	citrate-functionalized gold nanoparticle
cm	centimetre
ConA	concanavalin A
CT	cholera toxin
CTAB	cetyltrimethylammonium bromide
CuAAC	copper-catalysed azide-alkyne cycloaddition
d	doublet (in NMR)
D_2O	deuterated water
Da	Dalton(s)
DBU	1,8-diazabicyclo[5.4.0]undec-7-ene
DC	dendritic cells
DCC	*N*,*N*′-dicyclohexylcarbodiimide
DCM	dichloromethane
dd	doublet of doublets (in NMR)

DEPT	distortionless enhancement by polarization transfer
DIPEA	di-isopropylethylamine
DLS	dynamic light scattering
DMAP	4-dimethylaminopyridine
DMC	2-chloro-1,3-dimethylimidazolinium chloride
DMF	dimethylformamide
DMSO	dimethylsulfoxide
DNA	deoxyribonucleic acid
DTT	dithiothreitol
EA	elemental analysis
E. coli	Escherichia coli
EG	ethylene glycol
e.g.	*exempli gratia* (for example)
ELISA	enzyme-linked immunosorbent assay
EM	electron microscopy
Enz	enzyme
ESI	electrospray ionization
et al.	*et alia* (and others)
EtOAc	ethyl acetate
EtOH	ethanol
ev	electron volt
FTIR	fourier transform infrared spectroscopy
Fuc	fucose

g	gram(s)
Gal	D-galactose
Gal-gAuNP	galactose-functionalized gold nanoparticle
GalNAc	*N*-acetyl-D-galactosamine
gAuNP	glycogold nanoparticle
GlcNAc	*N*-acetyl-D-glucosamine
GSL	glycosphingolipid
Glu	D-glucose
h	hour(s)
HA	hemagglutinin
HRMS	high resolution mass spectrometry
HPLC	high performance liquid chromatography
HSQC	heteronuclear single quantum coherence spectroscopy
Hz	Hertz
IgG	immunoglobulin
IR	infrared
I-SPAAC	interfacial strain promoted azide-alkyne cycloaddition
J	coupling constant
L	litre
Le^X	Lewis X trisaccharide
Le^Y	Lewis Y tetrasaccharide
LT	heat-labile enterotoxin
LTB	B subunit of heat-labile enterotoxin

lit.	literature
M	molar
m	multiplet (in NMR)
m	meta
m.p.	melting point
m/z	mass/charge ratio
M^+	molecular mass ion
Man	mannose
mbar	millibar
Me	methyl
MeCN	acetonitrile
MeOH	methanol
mg	milligram(s)
MHz	megahertz
min	minute(s)
mL	millilitre(s)
mM	millimolar
mmol	millimole
mol	mole
mol. sieves	molecular sieves
MS	mass spectrometry
MsCl	mesyl cholride
NeuAc	*N*-acetylneuraminic acid

NIR	near-infrared
nm	nanometre
nM	nanomolar
nmol	nanomole
NMR	nuclear magnetic resonance
NP	nanoparticle
NSET	nanoparticle surface energy transfer
O/N	overnight
p	para
PBS	phosphate buffer saline
PCR	polymerase chain reaction
PEG	polyethylene glycol
PFU	plaque forming unit
Ph	phenyl
ppm	parts per million
p-TSA	*para*-toluenesulfonic acid
py	pyridine
q	quartet (in NMR)
quant.	quantitative
R	The molar ratio of trisodium citrate to $HAuCl_4$
RCA_{120}	*Ricinus communis* agglutinin
R_f	retention factor
rpm	revolutions per minute

rt	room temperature
s	singlet (in NMR)
SAM	self-assembled monolayer
SDS-PAGE	sodium dodecyl sulfate polyacrylamide gel electrophoresis
sec	second(s)
SEC	size exclusion chromatography
SGP	sialylglycopeptide
SG-gAuNP	sialylglycan-functionalized gold nanoparticle
SPR	surface plasmon resonance
t	tertiary
t	triplet (in NMR)
TEA	triethylamine
TEM	transmission electron microscopy
TFA	trifluoroacetic acid
TGA	thermogravimetric analysis
THF	tetrahydrofuran
t.l.c.	thin layer chromatography
TMSOTf	trimethylsilyl trifluoromethanesulfonate
TOAB	tetraoctylammonium bromide
Tris	tris(hydroxymethyl)aminomethane
UV-Vis	ultraviolet-visible
v/v	volume by volume
w/v	weight by volume

XPS	x-ray photoelectron spectroscopy

Amino acids:

A	Ala	Alanine
C	Cys	Cysteine
D	Asp	Aspartic acid
E	Glu	Glutamic acid
F	Phe	Phenylalanine
G	Gly	Glycine
H	His	Histidine
I	Ile	Isoleucine
K	Lys	Lysine
M	Met	Methionine
N	Asn	Asparagine
P	Pro	Proline
Q	Gln	Glutamine
R	Arg	Arginine
S	Ser	Serine
T	Thr	Threonine
V	Val	Valine
W	Trp	Tryptophan
Y	Tyr	Tyrosine

Publications

Parts of this thesis have been published in the following publications:

- Poonthiyil, V.; Golovko, V.B.; Fairbanks, A.J. Control of gold nanostructure morphology by variation of temperature and reagent ratios in the Turkevich Reaction, *Aust. J. Chem.* **2015**, 68 (6), 858-862.

- Poonthiyil, V.; Golovko, V.B.; Fairbanks, A.J. Size-optimized galactose-capped gold nanoparticles for the colorimetric detection of heat-labile enterotoxin at nanomolar concentrations, *Org. Biomol. Chem*. **2015**, 13, 5215-5223.

- Poonthiyil, V.; Golovko, Nagesh, P.T.; Husain, M.; Fairbanks, A.J. Gold nanoparticles decorated with sialic acid terminated bi-antennary N-Glycans for the detection of influenza virus at nanomolar concentrations, *ChemistryOpen*, **2015**, 4, 708-716.

A note concerning terminologies related to nanoparticles

Dispersity is a measure of the heterogeneity of the sizes of the nanoparticles in a sample. A monodisperse sample is composed of particles of same size, whereas a polydisperse sample contains particles of different sizes.

Nanoclusters are particles smaller than 1 nm, and have a precisely defined size without any polydispersity, whereas nanoparticles have size larger than 1 nm and are polydisperse.[1]

Multivalency refers to the property of nanoparticles to be able to bind to a multiple number of ligands.

Multifunctionality refers to the property of nanoparticles to be able to bind to different kind of ligands.

Reference

1. Parker, J. F.; Fields-Zinna, C. A.; Murray, R. W. *Acc. Chem. Res.* **2010,** *43* (9), 1289-1296.

Chapter 1: Introduction

1.1. Background

1.1.1. Nanoparticles

One of the most significant developments in science in the last five decades has been the emergence of materials with morphology defined down to the nanometre scale. Nanoparticles (NPs) comprise an important sub-class of nanomaterials with all 3 dimensions smaller than a specific threshold value (1 micron). NPs are assemblies of atoms that have different shapes, and typically have size in the range from 1 to 100 nm (Figure 1.1).[1] Metal NPs, with their unique physicochemical properties, have drawn significant interest in recent years. They are expected to form the basis of many of the biological and technological innovations of the 21st century.[2] Since the size of the most metal atoms falls in the range of 0.1 to 0.2 nm, metal NPs generally contain hundreds to several thousands of metal atoms depending on the size of the NP.[3] There have been a large number of reports detailing the synthesis of metal NPs in the literature, especially those made from noble metals.[2]

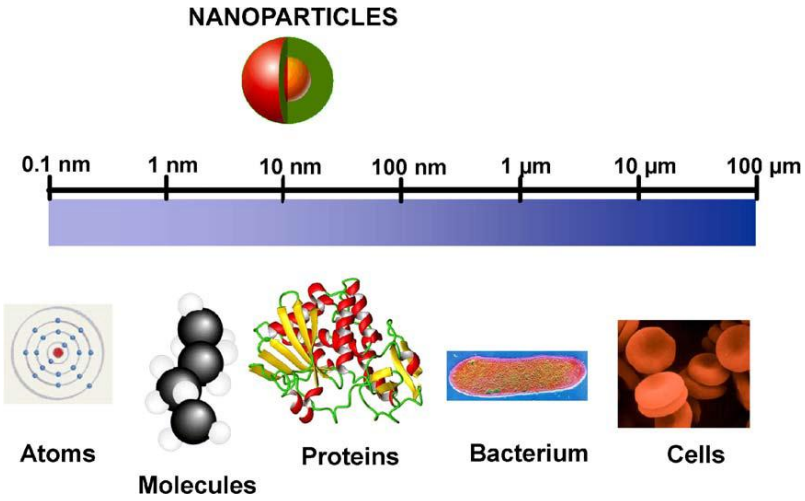

Figure 1.1. A schematic representation depicting the relative size of NPs in comparison with other biological entities. Image reproduced from Ref. 4 with permission from Elsevier.

1.1.2. Gold nanoparticles

Gold nanoparticles (AuNPs) are one of the most significant classes of metal NPs.[5] AuNPs are one of the most stable metal NPs, and are known to have potential applications in optics,[6] biology,[7] and catalysis.[8] To date, more than 70,000 reports focused on AuNPs have appeared in the literature showing the growing importance of this class of nanomaterial.[5] In 1857, Michael Faraday reported the first synthesis of AuNPs (deep red in colour) by the reduction of an aqueous solution of tetrachloroaurate ($AuCl_4^-$) using phosphorus in CS_2 (a two-phase system).[9] Faraday`s synthesis inspired many scientists to invent new synthetic methods for AuNPs in the 20th century.[10-13] Over the past decade, different groups have been conducting extensive studies on AuNPs mainly due to their increasing applications in various fields.[5]

1.1.3. The Chemistry of Gold.

Gold, a noble metal with the atomic number 79 and chemical symbol Au, is located below copper and silver in group 11 (IB) in the periodic table. The ground state electronic configuration of Au is $[Xe]4f^{14}5d^{10}6s^{1}$. Au is known to exist in several different oxidation states, namely (-I), (0), (I), (II), (III), (IV), and (V); however, only species containing Au (0), (I), and (III) are typically stable in aqueous solution.[2] Therefore, *in vivo*, Au exists in equilibrium between its metallic ground state of (0) and its oxidized states (I) or (III).[14] Au is distributed in nature either in its metallic form or as a component of ores of other transition metals. In its metallic form, Au is soft and is one of the most ductile of the elements. Metallic Au is also one of the least reactive metals and it does not oxidize or burn in air, even when heated. It is also inert to strong acids and alkali.[15] Even nitric acid is not a strong enough oxidizing agent to oxidize Au. However, aqua regia, a mixture of nitric and hydrochloric acid in a 1:3 molar ratio, can dissolve Au as the Au ion is complexed by the chloride ion to give tetrachloroauric acid ($HAuCl_4$):[16]

$$2Au + 11HCl + 3HNO_3 \longrightarrow 2H^+ + 2AuCl_4^- + 3NOCl + 6H_2O$$

The $AuCl_4^-$ complex is a strong oxidizing agent, and is easily reduced by various reducing agents to give coloured colloidal solutions of Au metal.[17]

1.2. Methods of AuNP synthesis

AuNPs are prepared by both “top down” and “bottom up” procedures.[18] In the “top down” approach, a bulk state metallic Au is systematically broken down to produce

AuNPs of different sizes.[19] However, the "top down" approach is limited in its use as the control over the shape and further functionalization of particles is difficult.[19] Alternatively, in the "bottom up" method AuNPs are formed from individual Au atoms which are themselves formed by chemical reduction.[20] This process involves two steps: nucleation and successive growth; when these occur in the same reaction process, AuNP synthetic strategy is called an *in situ* synthesis and otherwise it is called a seed-mediated growth method.[5]

The LaMer theory proposed by LaMer and Dinegar in the early 1950's explains the correlation between the nucleation and the growth of the produced nuclei, and how monodisperse NPs are formed in a homogenous solution.[21] This mechanism is based upon an extensive study of the solution-phase synthesis of sulfur colloids. In the context of metal NP synthesis, the concentration of metal atoms (C) increases steadily with time as the precursor compound is reduced (or decomposed) to give metal atoms (region (I) in Figure 1.2).[22] Once C reaches a point of critical level for nucleation (C_{min} or C_{crit}), the atoms begin to aggregate to form nuclei (region (II) in Figure 1.2). In this stage, C still continues to increase for a while until critical limiting supersaturation is reached (C_{max}).[23] C then decreases because of the increased consumption of metal atoms for the growth of nuclei, and then reaches the critical level for nucleation again. This stage corresponds to the end of the nucleation. Finally, the system enters and goes through the growth stage (region (III) in Figure 1.2) until the metal concentration is lowered so that it is close to the solubility level C_s. A clear separation between the nucleation and the growth stages is the major requirement for the formation of monodisperse particles.[24] Hence, if the

nucleation rate is not high enough, *i.e*, the metal concentration C lingers between C_{min} and C_{max}, growth of the particles occurs along with the nucleation resulting in the formation of polydisperse NPs.

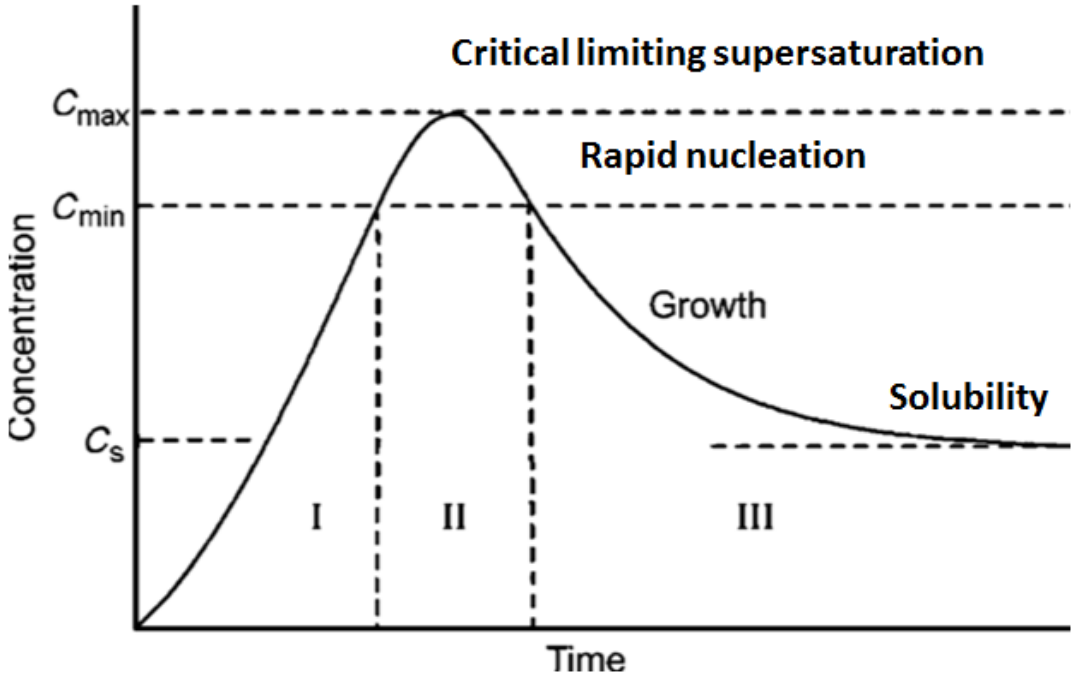

Figure 1.2. A schematic representation of the LaMer model of nucleation and growth of NPs. The regions I, II, and III indicate the prenucleation, nucleation, and growth stages respectively. Image reproduced from Ref. 25 with permission from the Royal Society of Chemistry.

1.2.1. *In situ* synthesis of AuNPs

The *in situ* synthesis of AuNPs consists two major parts: **(i)** formation of NPs from individual Au atoms which are themselves formed by reduction of the Au precursor. Reagents generally used for the reduction are $NaBH_4$,[26] trisodium citrate,[12] polyols[27] etc. **(ii)** Stabilization of particles by ligands against aggregation, and the ligands generally used for stabilization are trisodium citrate,[12] sulphur-,[26] phosphorus-,[28] and nitrogen-based ligands[29], polymers,[30] and dendrimers.[31] AuNPs synthesized through the *in situ*

process can also be used as seeds for the seed-mediated growth for the synthesis of larger NPs, and also for further functionalization.[5]

1.2.1.1. The Turkevich reaction (citrate reduction method)

The citrate reduction method, developed by Turkevich in 1951, is the most popular *in situ* synthesis of AuNPs.[10] Typically, an aqueous solution of trisodium citrate dihydrate (hereafter referred as citrate) is added to a boiling aqueous solution of $HAuCl_4 \cdot 3H_2O$ with vigorous stirring (Scheme1.1). The yellow coloured solution turns colourless and then deep wine-red, indicating the formation of citrate-stabilized AuNPs (Cit-AuNPs). In 1973, Frens reported an improved method, in which Cit-AuNPs of various sizes (from 15 to 150 nm) were synthesized by controlling the ratio of trisodium citrate to $HAuCl_4$.[12] However, any NPs formed in this way which were larger than 20 nm size were always found to be polydisperse.

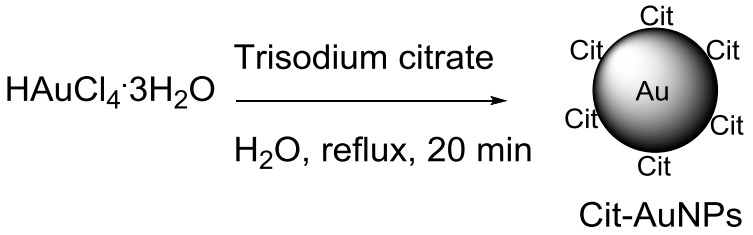

Scheme 1.1. Synthesis of Cit-AuNPs in the Turkevich reaction.

Over the last decade, several groups have improved the Turkevich method, and have proposed different possible mechanisms for Cit-AuNP formation. These improved methods and the proposed mechanisms are discussed in detail in Chapter 2.

In reactions at relatively low temperatures and with strong reducing agents such as $NaBH_4$, citrate only acts as a stabilizing agent due to its weak reducing nature. In 1985, Slot *et al.* reported AuNP synthesis at 60 ^oC using a mixture of tannic acid and citrate in which the tannic acid acted as a reducing agent and the citrate as the stabilizing agent.[32] Subsequently, in 1996, Brown *et al.* reported AuNP synthesis in which $NaBH_4$ was used as the reducing agent and citrate as a stabilizing agent (Scheme 1.2).[33] In this case AuNPs were obtained at room temperature simply upon the addition of a $NaBH_4$/citrate mixture to the $HAuCl_4$ solution.

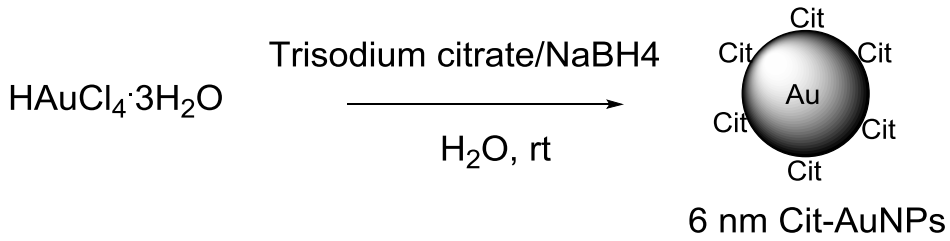

Scheme 1.2. Synthesis of 6 nm sized Cit-AuNPs using $NaBH_4$ as the reducing agent and citrate as the stabilizing agent.

1.2.1.2. The Brust-Schiffrin method

In 1993, Giersig and Mulvaney demonstrated the use of alkylthiols of various chain lengths to stabilize AuNPs.[34] Later, in 1994, an *in situ* synthesis of thiol-stabilized AuNPs, the two-phase Brust-Schiffrin method (BSM), was published.[26] In the BSM, $HAuCl_4$ was first transferred from an aqueous phase to toluene using tetraoctylammonium bromide (TOAB) as a phase transfer agent (Scheme 1.3).[26] The two phases were then separated, and dodecanethiol was added to the organic phase, which caused the solution to change colour from orange to colourless, indicating the reduction of Au^{3+} to Au^{+}.[35] An aqueous solution of $NaBH_4$ was then added to the organic phase

with vigorous stirring. The colour of the toluene solution then immediately changed from colourless to deep-brown indicating the formation of AuNPs (Scheme 1.3).

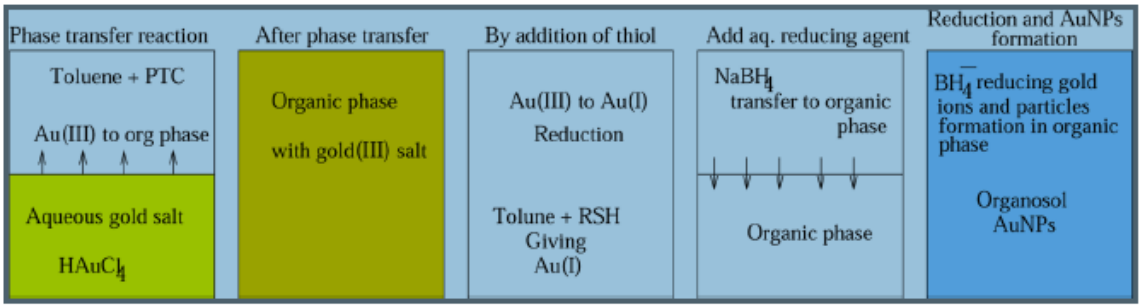

Scheme 1.3. A schematic representation of AuNP formation in BSM. Reprinted with permission from Ref. 35. Copyright (2016) American Chemical Society.

$HAuCl_4$ was phase-transferred from water to toluene using TOAB according to the following reaction:[26]

$$H^+AuCl^-_{4(aq)} + (R_{oct})_4N^+Br^-_{(org)} \longrightarrow (R_{oct})_4N^+AuX^-_{4(org)} + HX_{(aq)} \qquad (1.1)$$

In equation 1.1, X represents either Br or Cl as the extent of exchange between Cl^- and Br^- is not known. The reduction of Au^{3+} to Au^+ with dodecanethiol (RSH) yielded a thiolated polymer $-(AuSR)_n-$ and disulfide RSSR as shown in equation 1.2:[26, 36-37]

$$(R_{oct})_4N^+AuX^-_4 + 3RSH \longrightarrow -(AuSR)_n- + RSSR + (R_{oct})_4N^+ + 4X^- + 3H^+ \qquad (1.2)$$

$NaBH_4$ then reduced any remaining Au^{3+} and Au^{1+} to Au^0 by the following reactions:[36-37]

$$-(AuSR)_n- + BH_4^- + RSH + RSSR \longrightarrow Au_x(SR)_y \qquad (1.3)$$

$$(R_{oct})_4N^+AuX_4^- + BH_4^- + RSH + RSSR \longrightarrow Au_x(SR)_y \qquad (1.4)$$

However, recent reports from Goulet and Lennox[38] and Li *et al.*[39] showed that a thiolate polymer $-(AuSR)_n-$ was not formed in the BSM. Instead the reduction of AuX_4^- by alkanethiol actually produced a new intermediate, AuX_2^-, by the following reaction:

$$(R_{oct})_4N^+AuX_4^- + 2RSH \longrightarrow (R_{oct})_4N^+AuX_2^- + RSSR + 2HX \qquad (1.5)$$

As shown in equation 1.5, two moles of RSH reduced one mole of Au^{3+} to Au^+. Thus, when thiol to Au ratios are less than 2, the Au precursor exists as both Au^{3+} and Au^+ in the solution before the addition of $NaBH_4$ (Scheme 1.4).

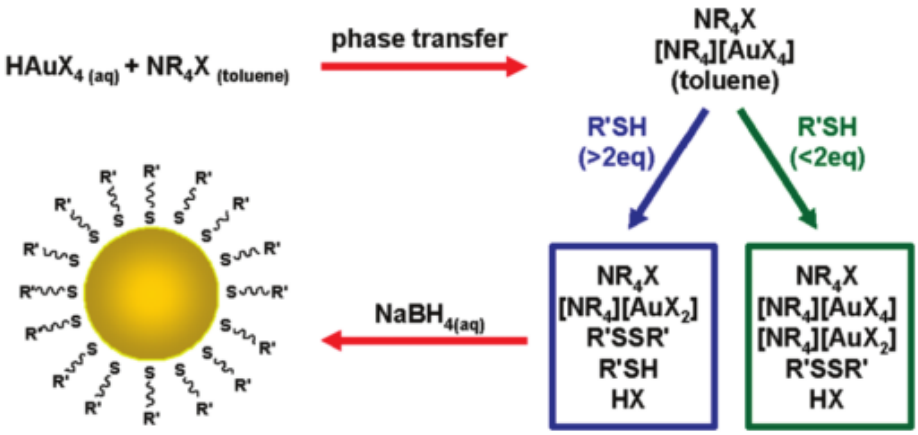

Scheme 1.4. Revised BSM by Goulet and Lennox.[38] Image reprinted with permission from Ref. 38. Copyright (2016) American Chemical Society.

The BSM was a major breakthrough in AuNP synthesis for multiple reasons: (1) the easy synthesis of AuNPs under mild reaction conditions, (2) the AuNPs synthesized are highly stable, (3) the particles can be dried and re-dissolved without any decomposition or aggregation, (4) smaller particles (2 - 5 nm range) with a narrow size distribution can be obtained, and (5) the functionalization of the particles produced is relatively easy.[5]

In the BSM, higher S to Au molar ratios and a faster addition of $NaBH_4$ are known to produce smaller AuNPs with very narrow particle size distributions.[40] The particles obtained are highly stable due to the strong Au-S covalent bonds formed on the particle surface.[41] The Au-S covalent bond is believed to be formed by the oxidative addition of the S-H bond onto two adjacent Au^0 atoms on the surface of the AuNPs.[5] The Au-H bonds formed are known to have fluxional properties (the dynamic property that allows the atoms to interchange between symmetry-equivalent positions), allowing the swift movement of H atoms on the NP surface. This movement eventually results in two Au-H bonds reaching close proximity with each other, and the consequent reductive elimination of H_2.[5]

Due to the advantages of the BSM that were explained above, it is now widely used for the synthesis of thiol-functionalized AuNPs.[38] The synthesis of precise Au clusters has also been reported using this method.[42,43]

In 1995, Brust *et al.* published a modified BSM in which *p*-mercaptophenol-functionalized AuNPs were synthesized in MeOH (Scheme 1.5) without the use of a

phase transfer reagent, which avoided the TAOB impurities that were observed in previous cases.[44] This finding led to a large number of follow-up publications that focused on the synthesis of thiol-functionalized AuNPs through the BSM in a single-phase system.[41] It is now understood that any thiol that is soluble in the same solvent as $HAuCl_4$, such as H_2O, MeOH, or EtOH, can be used for the synthesis of thiol-stabilised AuNPs using the single-phase BSM.[40]

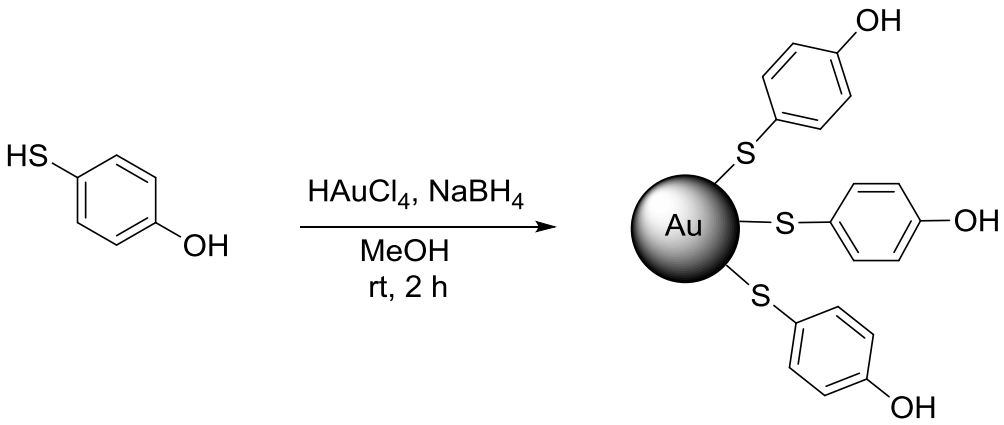

Scheme 1.5. AuNP synthesis by the one-phase BSM.[44]

$NaBH_4$, the reducing agent used in the BSM, is much stronger than the citrate used in the Turkevich reaction. Thus, the rate of reduction in the BSM is much faster than that observed in the Turkevich reaction, which results in the formation of smaller AuNPs in the BSM as compared to the Turkevich reaction.[5]

1.2.1.3. Place exchange reactions to form mixed monolayer AuNPs

In 1996, Hostetler *et al.* reported the first 'place exchange reactions' a term which refers to a reaction involving the substitution of the thiol ligands on the surface of an AuNP by another thiol (Scheme 1.6).[40] This reaction allowed the introduction of different

functionality onto the surface of AuNPs. The place exchange reaction involves the transfer of the hydrogen atom from the S-H bond of the incoming thiol to the S atom bonded to the AuNP surface (equation 1.6).[5]

$$\text{Au-SR} + \text{R`SH} \longrightarrow \text{Au-S(R)}\cdots\text{H}\cdots\text{SR`} \longrightarrow \text{HSR} + \text{Au-SR`} \qquad (1.6)$$

The extent of exchange on the AuNP surface is dependent on the reaction time and the amount of the added thiol.[45] The major advantage of using place exchange reactions is that AuNPs decorated with different functional thiols can be synthesized without subjecting the labile functional thiols to the strong reducing conditions of the BSM.[7]

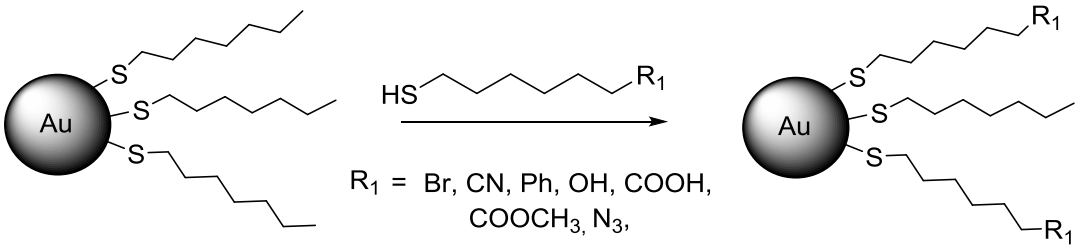

Scheme 1.6. A general scheme for place exchange reaction for alkanethiol-functionalized AuNPs with functionalized thiols.[7]

However, place exchange reactions are known to have some disadvantages, such as: (1) difficulty in controlling the extent of ligand substitution, (2) the possibility of irreversible particle aggregation, (3) the difficulty in determining the amount of ligands that have exchanged, and (4) incompatibilities between the incoming thiols and the solvent in which the AuNPs are dissolved.[5]

1.2.1.4. AuNPs stabilized with phosphorus-based ligands

AuNPs stabilized by phosphorus-based ligands are good precursors for ligand-substitution reactions to give functionalized AuNPs.[28] These AuNPs also have potential applications in sensing, imaging, catalysis, and for therapeutic uses.[5] The most popular phosphorus ligand-stabilized Au nanosystem is the Schmid's cluster. In 1981, Schmid *et al.* reported the synthesis of the phosphine-stabilized Au_{55} cluster ($[Au_{55}(PPh_3)_{12}Cl_6]$), which is now known as Schmid's cluster.[46] Triphenylphosphine acts as a good stabilizing ligand for 1.4 nm sized Au_{55} clusters in $Au_{55}(PPh_3)_{12}Cl_6$. The cluster was synthesized by the reduction of Ph_3PAuCl with gaseous diborane in either toluene or benzene at elevated temperatures. Later, in 2000, Weare *et al.* modified Schmid's method by adding $NaBH_4$ (instead of the diborane used in Schmid's method) and triphenylphosphine to $HAuCl_4$ and TOAB in a toluene-water mixture.[47] The cluster $[Au_{101}(PPh_3)_{21}C_{l5}]$ was produced, along with $[Au(PPh_3)Cl]$ as an impurity. In 2009, Shem *et al*. used the mild reducing agent, 9-borabicyclo-[3.3.1] nonane (9-BBN) for the synthesis of triphenylphosphine-stabilized AuNPs.[48] These particles had sizes in the range of 1.2 - 2.8 nm with a narrow size distribution. Recently, many groups have reported different methods for synthesizing AuNPs stabilized with phosphines or phosphine derivatives.[49-51]

1.2.1.5. Other capping ligands

Although thiol compounds are the most commonly used ligands to functionalize AuNPs, a variety of other ligands have also been used. Apart from sulfur containing ligands, nitrogen- and oxygen-based ligands having functional groups such as amines, carbonyls, carboxylates, and phenols also have been used to stabilize AuNPs. In particular amines

have widely been used as ligands for AuNPs because of their abundant presence in biosystems.[52]

Amongst the amine ligands used, 4-(*N*,*N*-dimethylamino) pyridine (DMAP) is particularly common, and DMAP-stabilized AuNPs have been extensively used for ligand-substitution reactions.[53] These DMAP-stabilized AuNPs can be synthesized by mixing an aqueous solution of DMAP with the TOAB-stabilized AuNPs *via* a phase transfer reaction.[54]

1.2.2. The seed-mediated growth method

The seed-mediated growth method is another common procedure used for AuNP synthesis. In this growth method, particles are increased in size step-by-step, and it is much easier to control the shapes and sizes of the AuNPs.[55] This method has two steps: in the first step, small AuNP seeds are synthesized; in the second step, the seeds are added to a "growth" solution containing both reducing and stabilizing agents, and also a source of Au precursor (typically $HAuCl_4$).[55] The newly formed Au^0 atoms adsorb onto the surface of the seeds resulting in the formation of larger AuNPs. Mild reducing agents are always used in the second step so that the Au^{3+} to Au^0 reduction only occurs in the presence of Au seeds as catalysts.[56] Hence, no new nucleation events occur under such conditions, and the deposition of the newly formed Au^0 atoms onto the seed surface is the only prevalent process.[56]

In 1998, Brown and Natan reported the first seed-mediated synthesis of AuNPs.[57] The 12 nm sized seeds they used in that reaction were synthesized following the Turkevich procedure. The growth step was based on the colloidal Au surface-catalysed reduction of Au^{3+} by NH_2OH and spherical AuNPs with sizes between 30 and 100 nm were synthesized. Subsequently Murphy's group used 3.5 nm sized citrate-capped Au seeds for the seed-mediated growth reaction.[56] The seeds were synthesized by adding an ice-cold aqueous solution of $NaBH_4$ to an aqueous solution containing $HAuCl_4$ and citrate. The seeds were also used for the synthesis of Au nanorods. In 2003, El-Sayed's group modified the seed synthesis by using hexadecyltrimethylammonium bromide as the stabilizing agent instead of citrate.[58] Au seeds with a size smaller than 4 nm were used to reduce the dispersity of Au nanorods produced in the growth step. Now seed-mediated growth has been widely used for the synthesis of monodisperse, large, spherical or quasi-spherical AuNPs, Au nanorods, and AuNPs of other shapes (rectangle, hexagon, cube, triangle, and star like shapes).[20, 59]

1.3. The physical properties of AuNPs

The physical properties of NPs are significantly different to those of bulk materials and molecular or ionic compounds which contain the same element. Typically NPs have a range of interesting properties, such as size-related magnetic, electronic, and optical effects (a quantum size effect), and also properties related to their higher surface area to volume ratio.[60] The quantum size effect of AuNPs arises due to the fact that the wavelength of the metallic electrons ($6s^1$) is the same order of magnitude as the size of the NPs themselves ($\lambda \sim 1$ nm).[61] This property results in the particles behaving

electronically as zero-dimensional quantum dots or quantum boxes, where they are subjected to quantum-mechanical rules.[61] Apart from their size, the physical properties of NPs also depend strongly on the distance between the particles, their structure, and also on the type of the stabilising organic ligands.[62]

In regard to the structure of thiol-functionalized AuNPs, recent X-ray crystallographic studies of Au_{25} and Au_{102} clusters have revealed that the thiol ligands form linear RS-Au-SR units on the AuNP surface, in contrast to the generally accepted model for flat surfaces, in which thiol ligands form head-on single covalent bonds with the close-packed Au core.[63-65] Thus, many of the Au atoms make bonds with thiol ligands and form semiring structures, and these Au atoms are not part of the main particle core.[18] However, since the synthesis of larger sized AuNPs always produce polydisperse particles, their structural studies have been limited and to what extent the structural aspects of the clusters match with the large particles remain to be explored.

1.3.1. Surface Plasmon Resonance

When a metal NP is exposed to light, the oscillating electromagnetic field of the light induces a collective coherent oscillation of the conduction band electrons of the metal. This electron oscillation around the NP surface results in a charge separation, which in turn causes a dipole oscillation along the direction of the electric field of the light (Figure 1.3). The amplitude of the oscillation is a maximum at a specific frequency, which is known as surface plasmon resonance (SPR).[66] The SPR induces a strong absorption of incident light, and thus can be measured using a UV-Vis absorption spectrophotometer.

The wavelength and intensity of the SPR band depend on the factors affecting the electron charge density on the NP surface, such as the particle size, structure, shape, the metal type, and the nature of the surrounding medium.[67]

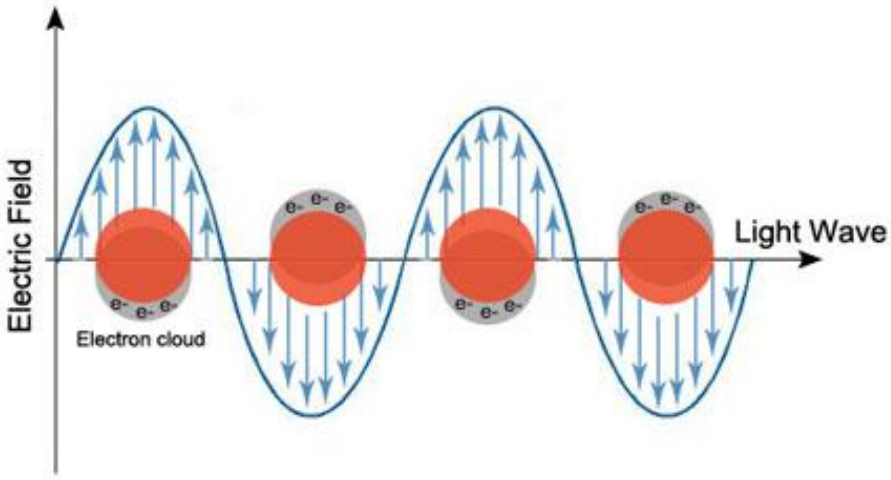

Figure 1.3. SPR of AuNPs; the collective oscillation of surface electrons with incident light at a specific wavelength.[68]

AuNPs in the size range of 5-20 nm exhibit their SPR band near 520 nm in the visible region. The SPR peak position is affected by the NP size (Figure 1.4) and the peak red shifts with an increase in NP size, *i.e*, the wavelength of the SPR peak increases.[69]

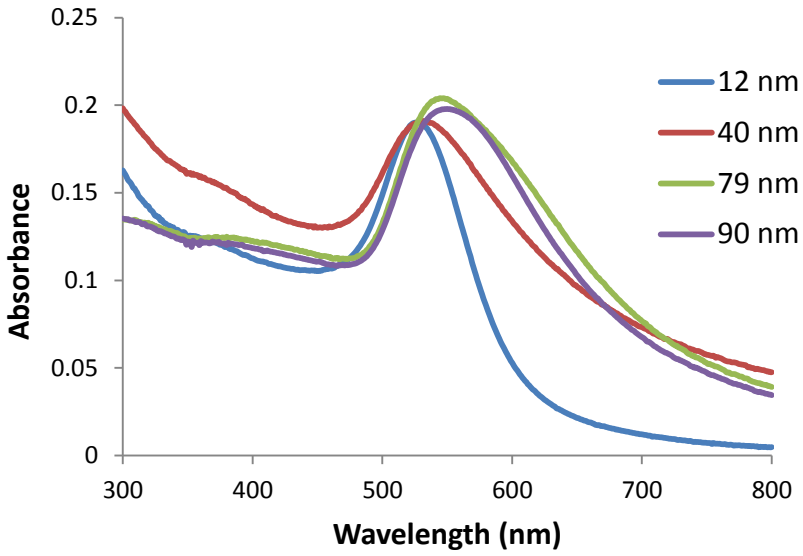

Figure 1.4. UV-Vis absorption spectra of AuNPs with different sizes.

In addition, the SPR frequency is very sensitive to the interparticle distance. Specifically, if particles aggregate the SPR band shifts to lower energies i.e. to higher wavelengths (typically a red-shift from ~520 to ~650 nm).[70] This shift results in a change in the colour of the AuNP solution from red to blue, and this property of AuNPs has been exploited for the development of colorimetric sensors.

1.3.2. Fluorescence

Various studies have demonstrated that AuNPs contribute to the fluorescent activity of the fluorophores attached on their surface or freely present in solution.[7, 71] AuNPs are known to be good fluorescent quenchers of a wide range of fluorophores.[71] Fluorescence quenching is mainly observed when fluorescent ligands are attached to the surface of AuNPs. The fluorescent quenching occurs when the emission spectrum of the fluorophores matches the SPR band of the AuNPs.[72] Apart from the frequency matching,

the size and shape of the NPs, the distance between the particle core and the fluorophores, and the dipole orientation with respect to NP-dye axis also affect the fluorescent quenching of the fluorophores by NPs.[72]

1.3.3. Ligand presentation

Any desired ligand can be attached to the spherical or quasi-spherical scaffold of AuNPs. The multivalent presentation of such functionalized ligands in these AuNPs makes them good candidates for a variety of applications such as sensing, receptor specific multivalent binding, and biosystem mimicking.[73] In addition, AuNPs carrying several different ligands, known as 'hybrid AuNPs,' have also attracted considerable attention.[74] The extent of multifunctionalization in these particles can be controlled by regulating the relative molar ratios of the different ligands added during their synthesis, the way in which the ligands bind to the NP core, and the core size of the particles itself.[74]

1.4. Synthesis and application of glycogold nanoparticles

1.4.1. Biofunctionalized NPs

Biofunctionalized NPs represent hybrid systems that combine inorganic nanostructures with biomolecules.[75] A large variety of novel biofunctionalized NPs has been synthesized and used to study biologically relevant interactions.[76] The wide range of metals that can be used as the metal core of these systems permits tuning of the electronic, optical, and magnetic properties of such NPs.[77] The size of the biofunctionalized NPs can be varied, and their surface can be modified with multivalent and multifunctional ligands.[78] Biofunctionalized NPs can have sizes similar to those of the naturally occurring scaffolds

made from nucleic acids and proteins which enables these particles to be used as biomimetic systems and also for the study of biorecognition processes at the molecular level.[78]

Au has been the most popular choice of metal for the core of biofunctionalized NPs.[20] The first studies of AuNPs decorated with peptides, antibodies, DNA, and proteins appeared in 1990's.[4] In 2001, the Penadés group reported the synthesis of AuNPs attached to carbohydrates for the first time.[79] These systems were comprised of AuNPs with the Au atoms covalently attached to thiols of the thiol-terminated carbohydrate derivatives, and these particles were termed 'glycogold nanoparticles (gAuNPs).'[79] After the first report on gAuNPs by the Penadés group,[79] the number of studies focusing on the synthesis, characterization, and applications of gAuNPs has grown exponentially (Section 1.4.5).[4]

1.4.2. Carbohydrates

Carbohydrates, also known as saccharides, are one of the most abundant biomolecules. Along with lipids and peptides, they constitute the essential molecules for life.[80-81] Carbohydrates are poly-hydroxylated aldehydes or ketones, and can exist as monosaccharides, disaccharides, oligosaccharides, and polysaccharides. The monosaccharides and disaccharides, which are smaller carbohydrates, are generally referred to as sugars. Carbohydrates are synthesized by plants through photosynthesis; in the presence of light, CO_2 reacts with water to give oxygen and carbohydrates, with the general formula $C_m (H_2O)_n$:[81]

$$CO_2 + H_2O \xrightarrow{\text{Light}} C_m(H_2O)_n + O_2 \quad (1.7)$$

Carbohydrates contain a large variety of monosaccharide units with backbones of varying length. The monosaccharides have carbonyl groups, either as aldehydes or ketones, also primary and secondary alcohols. The sequence of stereogenic centres presents in the monosaccharide influences how it occupies in a 3-dimensional space. Each monosaccharide has its own enantiomer with respect to the most distant stereogenic centre from the carbonyl group. The prefixes D and L are assigned to distinguish between the two enantiomers (Figure 1.5). In the D form, the hydroxyl group (higher priority group) on the last chiral carbon of the open chain Fischer projection is on the right side, whereas in the L form the hydroxyl group is on the left.[82]

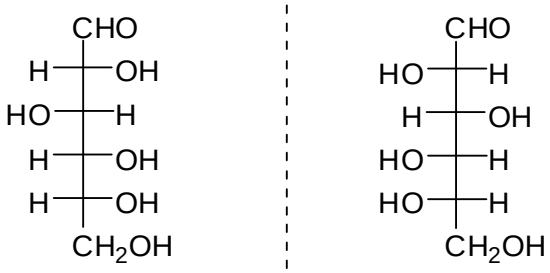

Figure 1.5. Fischer projections of D-glucose (left) and L-glucose (right).

The open chain form of monosaccharides can undergo intramolecular reaction; a nucleophilic attack of one of the hydroxyl groups at the intrachain aldehyde or ketone results in the formation of a cyclic hemiacetal or hemiketal respectively.[83] The most commonly formed ring structures are furanoses (five membered rings) and pyranoses (six

membered rings) as shown in Scheme 1.7. The newly formed stereocenter is called the anomeric centre. The two possible stereochemistries formed at the anomeric centre are called anomers,[82] which are diastereoisomers of one another. The configuration at the anomeric carbon is termed as alpha- (α-) or beta- (β-) with respect to the stereocenter that decides the absolute configuration (D or L form).[84] As shown in Figure 1.6, cyclic sugars can be represented in different ways such as Mills, Fischer, Haworth, and chair representations. In a Fischer projection, if the hydroxyl group at the anomeric centre is on the same side as the hydroxyl group of the configurational (D- or L-) carbon, it is the α-anomer of the sugar.[82] If it is in the opposite side, then it is the β-anomer. In general, the functionalization of the anomeric hydroxyl group blocks ring opening/closing mechanisms, locking the ring in its cyclic conformation.[82]

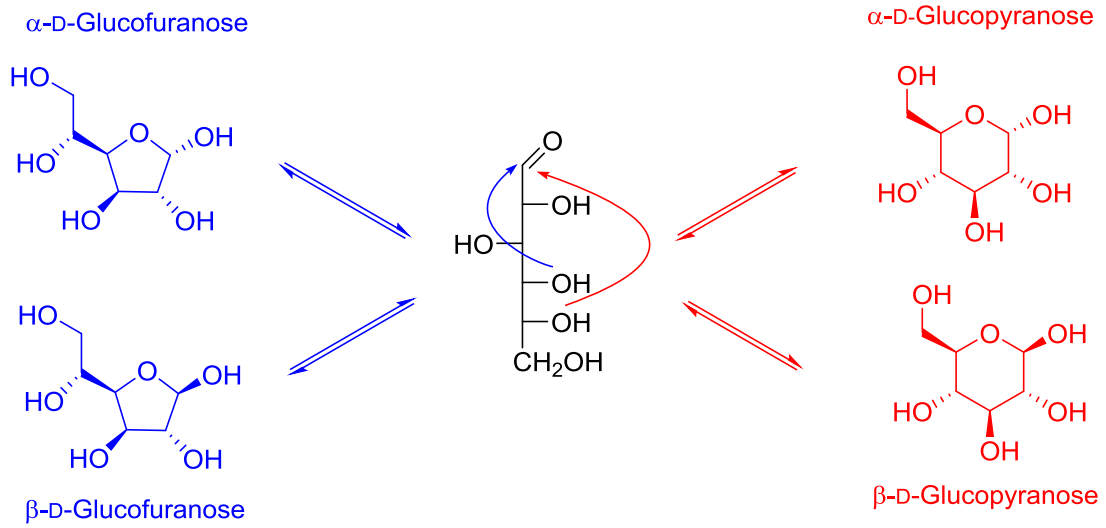

Scheme 1.7. Formation of furanose and pyranose from D-glucose open chain form.

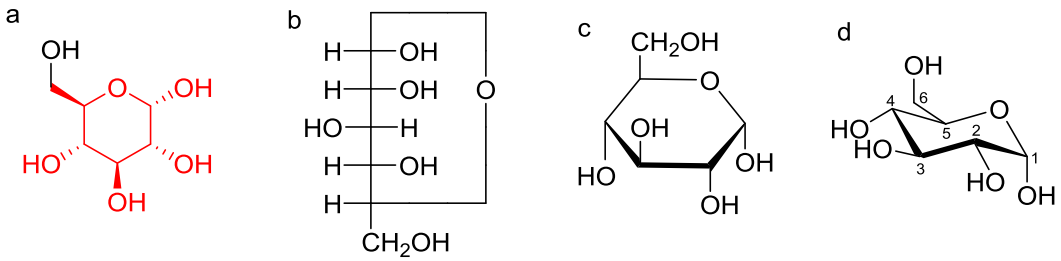

Figure 1.6. (a) Mills, (b) Fischer, (c) Haworth, and (d) chair representations of α-D-glucopyranose.

With pyranoses, various ring conformations are possible. Generally, a chair conformation with C2, C3, C5, and the ring oxygen occupying the same plane is preferred as shown in Figure 1.6d.[82] The chair form can have two conformations depending on where the C1 and C4 are located. A conformation in which the C4 is above and the C1 is below the plane is known as the $^4C_1$ conformation, whereas when the C1 is above and the C4 is below the plane, it is called a $^1C_4$ conformation. One conformation is preferred over the other based on the stereochemical placement of substituents on the ring (Scheme 1.8). Typically, substituents prefer to occupy the equatorial positions, however a trade-off between maximizing orbital overlaps between the orbital with electron lone pair in the ring oxygen and the $\sigma^*_{C1\text{-}O1}$ orbital of the axial (exocyclic)

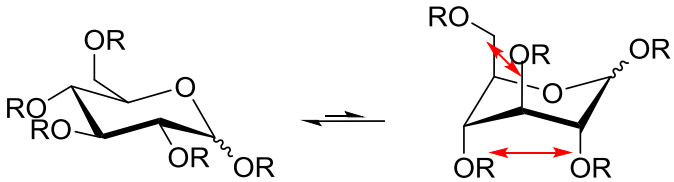

Scheme 1.8. $^4C_1$ (left) and $^1C_4$ (right) ring conformations of D-glucose derivative. Here $^4C_1$ is preferred over $^1C_4$ due to the 1-3 diaxial steric hindrance (shown in red double headed arrows) present in $^1C_4$ conformation. This preference is observed to increase with increasing size of substituent R.

C-O bond (the anomeric effect) and minimizing the 1,3-diaxial steric interactions is most often made. The anomeric effect is a stereoelectronic effect that explains why electronegative heteroatomic substituents attached to the anomeric carbon prefer the axial position over the less hindered equatorial position.[82] Amongst the many explanations provided, a most widely accepted one is based on hyperconjugation. A stabilizing interaction, hyperconjugation, is seen between the lone pair of electrons in the ring oxygen and the $\sigma^*_{C1\text{-}Y1}$ orbital of the axial (exocyclic) C-Y bond (Y is an electronegative heteroatom). Hyperconjugation occurs only when the orbital with the lone pair in the ring oxygen is aligned antiperiplanar (180^o) to the σ* orbital of the C-Y bond (Scheme 1.9, Y is Oxygen in this case).[85] Thus, when C-Y bond is placed in the axial position, the overall energy is lowered and the molecule achieves more stability.

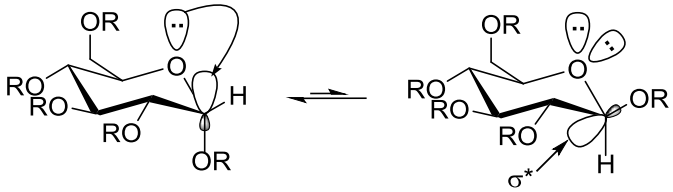

Scheme 1.9. The anomeric effect is seen when the electronegative heteroatomic substituent at the anomeric position is in axial position.

1.4.2.1. Glycosylation

Glycosylation refers to the reactions in which a glycosyl donor, typically bearing a labile leaving group at the anomeric centre, is joined to a hydroxyl or other functional groups of another compound (glycosyl acceptor).[86] The new bond formed through glycosylation between the hemiacetal or hemiketal groups of a sugar with the glycosyl acceptor is called a glycosidic bond, and the compound containing such a bond is called a

glycoside.[86] By choosing both the glycosyl donor and acceptor as monosaccharides, disaccharides can be made. Through further glycosylation of the disaccharide, tri-, tetra-, oligo-, and polysaccharides can also be synthesized. In biological systems, enzyme-catalysed glycosylation reactions produce the necessary carbohydrate molecules, and conjugate them to lipids, peptides, and proteins to give glycolipids, glycopeptides, and glycoproteins respectively.[87]

In a glycosylation reaction, the monosaccharide is attached to the acceptor *via* the anomeric carbon. Typically, the donor molecule is modified to have a suitable leaving group at the anomeric position. The leaving group, in general, is activated using an activator, such as a Lewis acid, and eliminated *via* the formation of an oxocarbenium ion intermediate (Scheme 1.10). A nucleophilic attack of a glycosyl acceptor at the reactive anomeric carbon of the oxocarbenium ion of the donor results in the formation of a glycosidic bond. The bond can be axial or equatorial (α linkage or β linkage respectively for glucose), or a mixture of both depending on the nature of the donor, acceptor, and the reaction conditions (Scheme 1.10).[86]

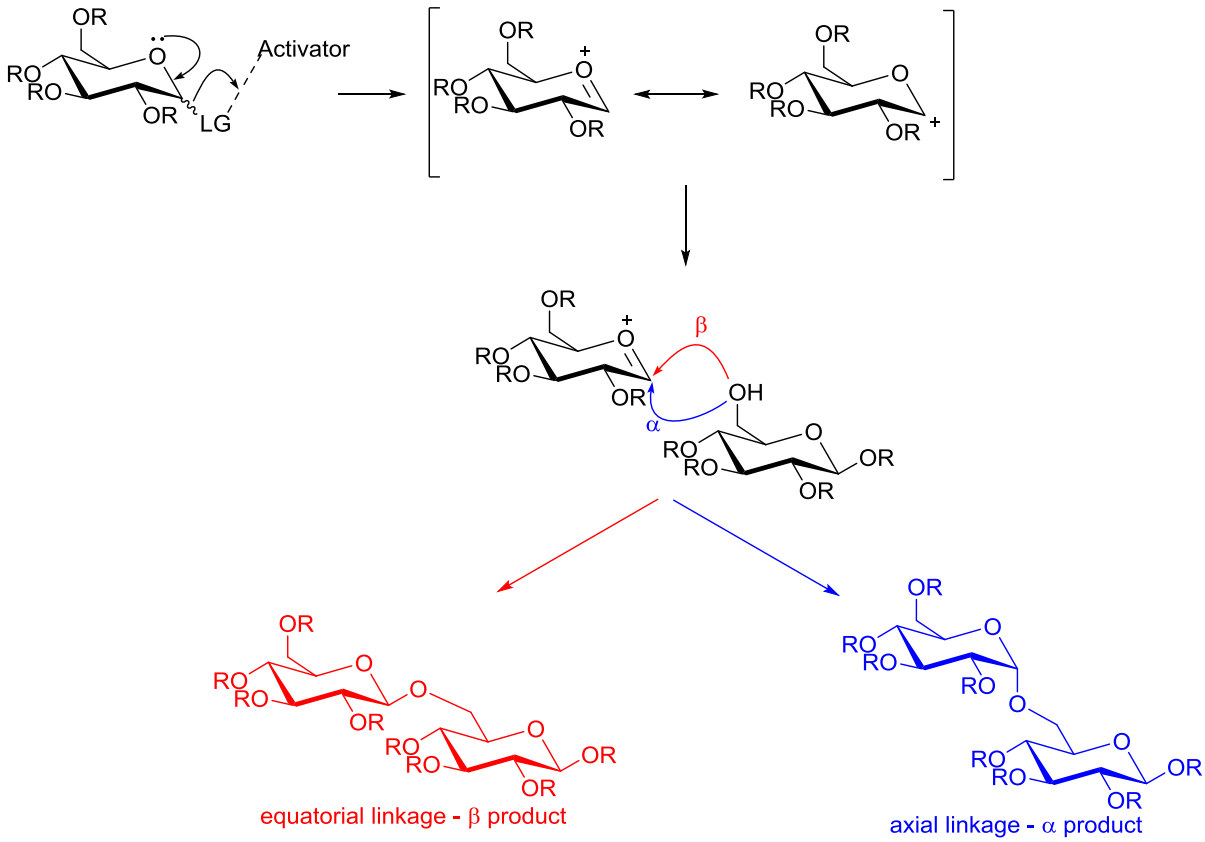

Scheme 1.10. A glycosylation reaction between two monosaccharides through oxocarbenium intermediate formation giving α- and β- glycosides.

Oligo- and polysaccharides are known to be highly flexible due to the significant freedom of rotation about the glycosidic bond joining the monosaccharide subunits.[88] Due to this flexibility, oligosaccharides are known to possess conformational heterogeneity and often various conformations are attainable at ambient conditions.[88] The alcohol groups in a monosaccharide can be modified by reduction, oxidation, or substitution to give deoxy-, carboxylic acid, or amines, sulfates, phosphates etc. respectively.[89]

A wide variety of polysaccharides can be made by choosing different monosaccharide units, by functionalizing the anomeric positions with different acceptors, and also functionalizing the hydroxyl groups with various molecules.[89] Such a variety of

combinations of functionalities in a carbohydrate results in them having different physical, chemical, and structural properties for each variation.[89]

1.4.3. The biological importance of carbohydrates

The multitude of structural variations possible within a macromolecular carbohydrate unit enables them to function as an essential component in biological systems. They serve as the energy storage and transport units, in the form of glycogen and starch in animals and plants respectively, and they also act as the structural units in plants and crustaceans, for example as cellulose and chitin.[90]

Apart from serving as the energy sources and structural materials, carbohydrates also mediate biorecognition events through their interactions with proteins and other biological units. For example, carbohydrates are known to be involved in immune response, cell communication and trafficking, fertilization, tumour genesis and progression, infection, and apoptosis.[91] However, there have been many challenges which hamper the study and understand these processes in detail. The major hindrances in the development of glycoscience have been the complexity of the glycan structures involved, their low natural abundance, and also the weak affinities of carbohydrate-protein interactions.[91] However, recent progress in the synthesis of complex carbohydrate structures, methods for glycan analysis, and glyconanotechnology have assisted researchers to overcome some of the barriers to studying processes involving carbohydrates.[92]

Lectins are carbohydrate-binding proteins which are known for their specificity for sugar molecules.[93] One of the most significant developments in the field of glycoscience was the realisation that carbohydrates bind lectins in a highly cooperative way in order to enhance the weak affinity of individual carbohydrate-lectin interactions.[94] The tremendous increase in the binding constant when multiple copies of carbohydrates interact with a lectin as compared to the simple sum of the total number of carbohydrate interactions is known as the 'cluster glycoside' effect.[94]

The understanding of the 'cluster glycoside effect' has inspired researchers to explore the carbohydrate interaction processes with renewed interest.[95] Various groups have attached multiple copies of carbohydrates to the scaffolds such as peptides, proteins, lipids, and synthetic polymers in order to study the multivalent effect.[96] New synthetic strategies have been developed to control the spatial orientation and the number of ligands on the scaffold, and also the structure of the scaffold itself, all of which affect the binding affinity between the glycoconjugate and the receptor.[96] It is expected that carbohydrate-based therapeutics may be developed with these synthetic multivalent glycoconjugates as they could bind to receptors competitively serving as the inhibitors for the natural ligands.[97]

1.4.4. Glycogold nanoparticles

The quest for a better scaffold for the synthesis of multivalent carbohydrates structures has led to the development of self-assembled monolayers (SAMs) of carbohydrates on the spherical surface of the AuNPs; a method that was termed the 'glyconanotechnology

strategy.'[98] In 2001, the Penadés group defined glycogold nanoparticles (gAuNPs) as "a new, water-soluble, three-dimensional polyvalent model system based on sugar-modified gold nanoclusters. These so-called glyconanoparticles provided a glycocalyx-like surface with a globular carbohydrate display, and chemically well-defined compositions for the study of carbohydrate interactions and to interfere with cell-cell adhesion processes."[79]

A suitably arranged saccharide layer on the surface of gAuNPs makes them soluble, stable, and compatible with biological media.[75] The entity that binds the desired sugar moiety to the surface of AuNPs is termed a linker, and the length and nature (hydrophobic or hydrophilic) of the linker influence the flexibility and the accessibility of the sugars during any interaction with receptors.[99] Multifunctional gAuNPs which contain a combination of carbohydrates, lipids, peptides, RNA, DNA, or fluorescent molecules on the surface of the same AuNP allow for the creation of an "artificial glycocalyx."[99] Moreover, the magnetic, electronic, and optical properties of gAuNPs can be altered by varying the size of the AuNP core.[99]

1.4.5. The synthesis of gAuNPs

In general, there are three methods that can be used to synthesize gAuNPs: (A) a direct method involving the reduction of $HAuCl_4$ in the presence of carbohydrate derivatives with linkers bearing a thiol end-group (Figure 1.7A); (B) a ligand exchange reaction involving the replacement of the ligands on preformed AuNPs with carbohydrate derivatives with linkers bearing a thiol end group (Figure 1.7B); (C) a method involving a

chemical reaction between functional groups of the ligands attached to the surface of preformed AuNPs and suitably functionalized carbohydrates (Figure 1.7C).[75]

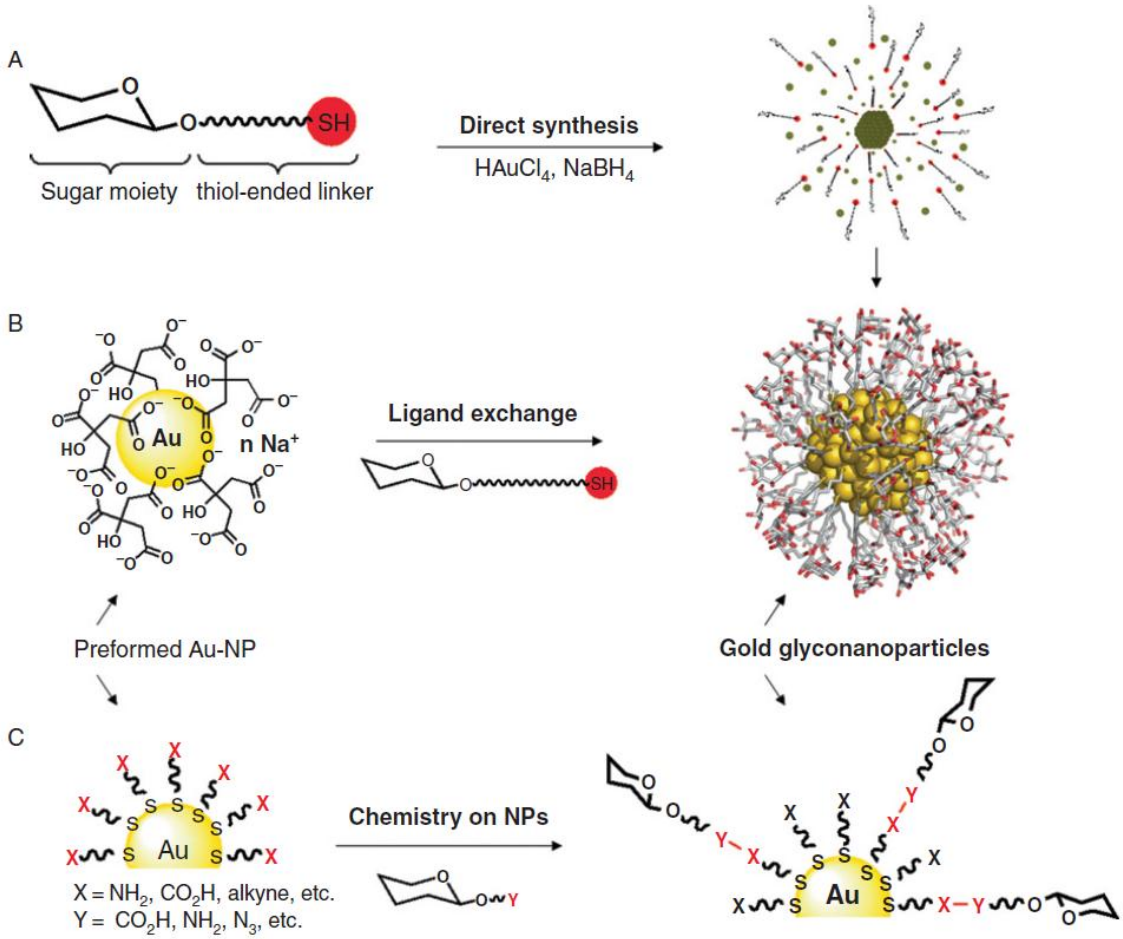

Figure 1.7. Common methods for the preparation of gAuNPs. (A) Direct synthesis, (B) ligand exchange, and (C) ligand modification methods. Image reprinted from Ref. 75 with permission from Elsevier.

1.4.5.1. Direct *in situ* formation of gAuNPs

In 2001, Fuente *et al.* reported the first ever synthesis of gAuNPs, and the single-phase BSM was used for the synthesis.[79] Stable gAuNPs of 2 nm average size were synthesized by the addition of either an aqueous or methanolic solution of thiol-derivatives of the

disaccharide lactose [β-Gal-(1→4)-Glc] and the Lewis X trisaccharide [β-Gal-(1→4)-[α-Fuc-(1→3)]-β-GlcNAc, Le^X] to an aqueous solution of $HAuCl_4$ and the subsequent reduction of the Au salts with $NaBH_4$. (Scheme 1.11) The gAuNPs formed were used to study the selective self-recognition of Le^X antigens by carbohydrate-carbohydrate interactions.

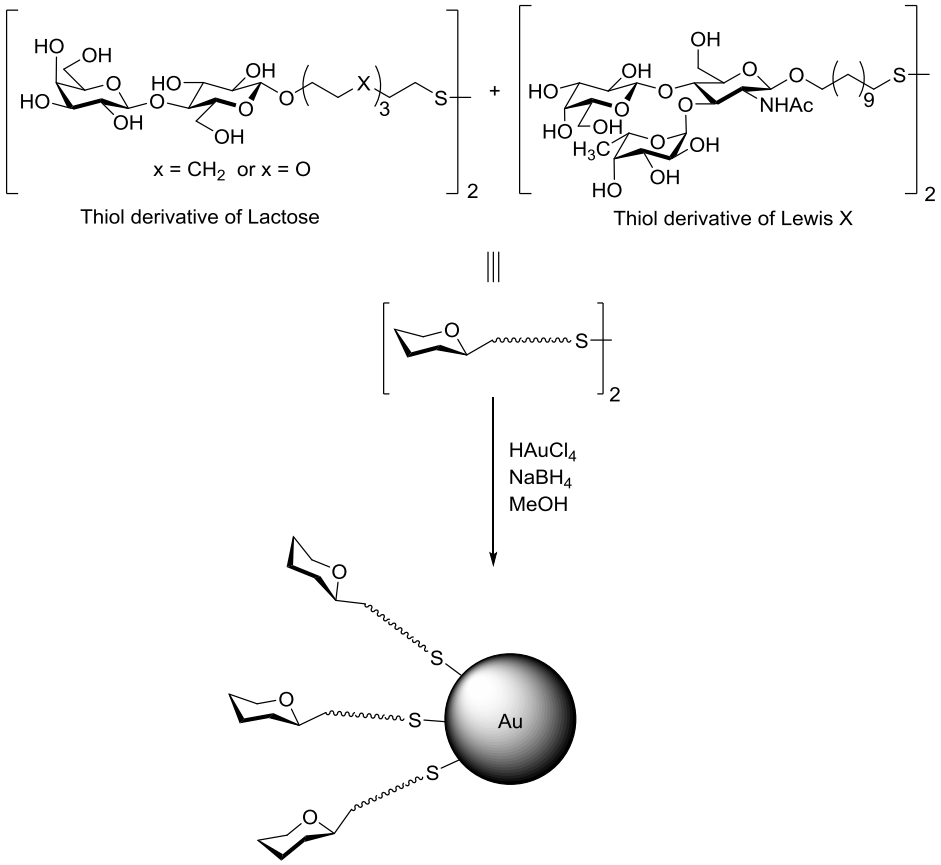

Scheme 1.11. Structures of the thiol derivatives of the disaccharide lactose and the trisaccharide Lewis X synthesized by Fuente *et al.*[79] Adapted from Fuente *et al.*[79]

Subsequently many other groups have used the direct reduction method to synthesize gAuNPs decorated with various sugars. [100-108] Different thiolated linkers, such as hydrophilic polyethylene glycol derivatives and hydrophobic alkanes, have been used to

attach saccharides to the surface of AuNPs.[75] The size of AuNP core can be varied approximately from 1 to 10 nm by changing the ratio of the thiol ligands to the amount of $HAuCl_4$ in a direct in situ synthesis of gAuNPs.[75] Herein larger particles are formed when the ratio is small, and smaller particles are formed when the ratio is high. Also, by manipulating the ratio of the carbohydrate ligands to non-carbohydrate ligands during the synthesis, gAuNPs with varied carbohydrate ligand surface densities can be synthesized. These gAuNPs can be used as model systems to study the influence of carbohydrate density on molecular-recognition processes.

The most complex hybrid gAuNPs reported in the literature to date have four different ligands on the same AuNP (Scheme 1.12).[109] These gAuNPs contain a peptide from tetanus toxoid (T-cell helper peptide), glucose, a Le^Y antigen, and a sialyl Tn epitope [α-Neu*p*5Ac-(2→6)-α-GalNAc] were synthesized in one step by single-phase BSM and characterized by Transmission Electron Microscopy (TEM) and ^{1}H NMR.[109]

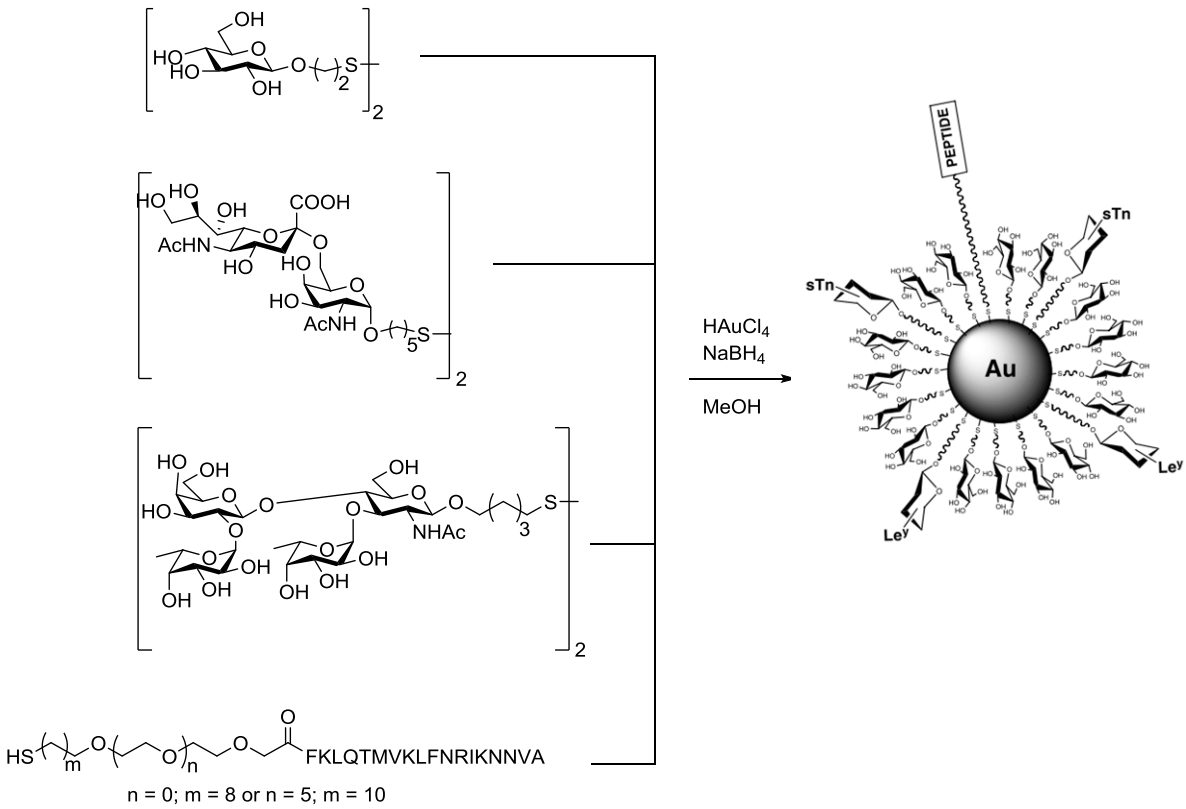

Scheme 1.12. Hybrid gAuNPs containing four different ligands. Image adapted from Ref. 109 with permission from Elsevier.

1.4.5.2. Two-step synthesis of gAuNPs by ligand exchange

Cit-AuNPs synthesized by the Turkevich reaction have been used to synthesize gAuNPs by replacing the citrate ligands with thiolated-carbohydrate derivatives. Citrate to thiol ligand exchange is one of the most commonly used methods to synthesize thiol-functionalized AuNPs in the 7 to 100 nm size range.[110] Ligand exchange on the AuNP surface is driven by the higher binding affinity of Au for the thiol than for the citrate due to the significant energy difference between Au-S (~ 40 kcal·mol^{-1}) and Au-O_{COOH} (~ 2 kcal·mol^{-1}) bonds.[111]

In 2003, the Russell group synthesized gAuNPs decorated with mannose ligands by a ligand exchange reaction achieved by incubating Cit-AuNPs with 2-mercaptoethyl α-D-mannopyranoside for 48 h (Scheme 1.13).[112] Centrifugal filtering was used to remove the salts and the excess mannose ligands. gAuNPs bearing thiolated lactose derivatives have also been synthesized by the ligand exchange method.[110]

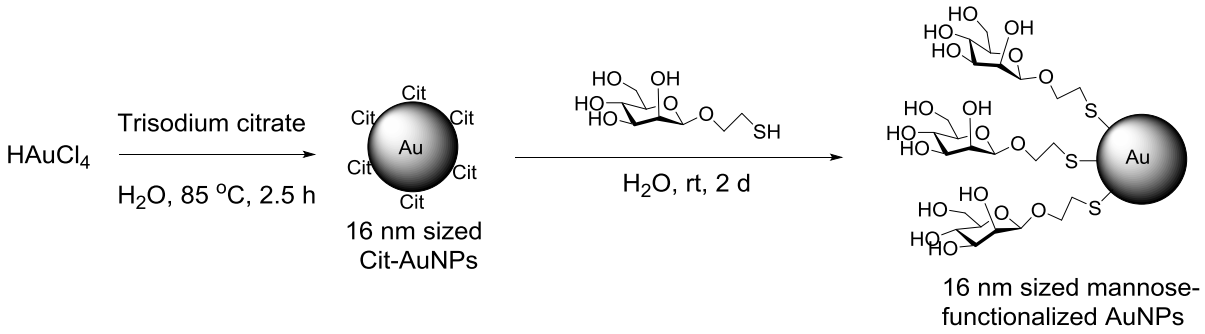

Scheme 1.13. Synthesis of 16 nm sized mannose-functionalized gAuNPs by ligand exchange method.[112]

Later, in 2006, Lee *et al*. performed a peptide coupling between hyaluronic acid and cystamine to obtain a thiolated-hyaluronic acid (Figure 1.8).[113] This thiolated ligand was then used to displace the citrate ligands of Cit-AuNPs to obtain gAuNPs decorated with hyaluronic acid.[113]

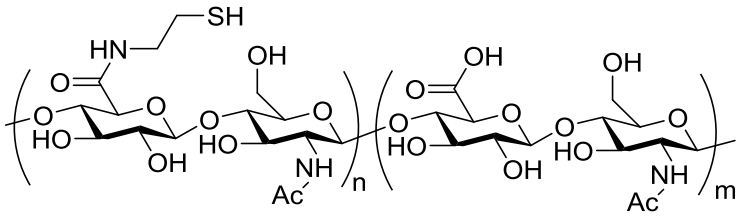

Figure 1.8. Structure of thiolated hyaluronic acid.

AuNPs stabilized with ligands other than citrate have also been used to synthesize gAuNPs through ligand exchange. For example, gAuNPs functionalized with thiolated oligosaccharide moieties which were the synthetic analogues of type A *Neisseria meningitides* antigens were synthesized by exchanging the dioctylamine ligands on the dioctylamine-stabilized AuNPs with the corresponding thiolated saccharide derivatives.[114]

1.4.5.3. Two-step synthesis involving chemical modifications of the AuNP surface.

Multistep reactions involving different chemical modifications of the surface of AuNPs have been used for the synthesis of gAuNPs. In 2001, Otsuka *et al.* attached lactose and mannose to AuNPs functionalized with acetal-terminated mercaptopoly(ethylene glycol). The acetal group was first converted to an aldehyde under acidic conditions, followed by reductive amination with the corresponding *p*-aminophenyl glycosides in the presence of $(CH_3)_2NHBH_3$ to produce gAuNPs (Scheme 1.14).[115] This was the first example of monolayer-protected gAuNPs that had been synthesized by a three-step reaction. Subsequently, in 2009, Nagahori *et al*. reacted aminooxy-functionalized AuNPs with aldehydes derived from glycosphingolipids (GSL) to produce gAuNPs as mimics of the

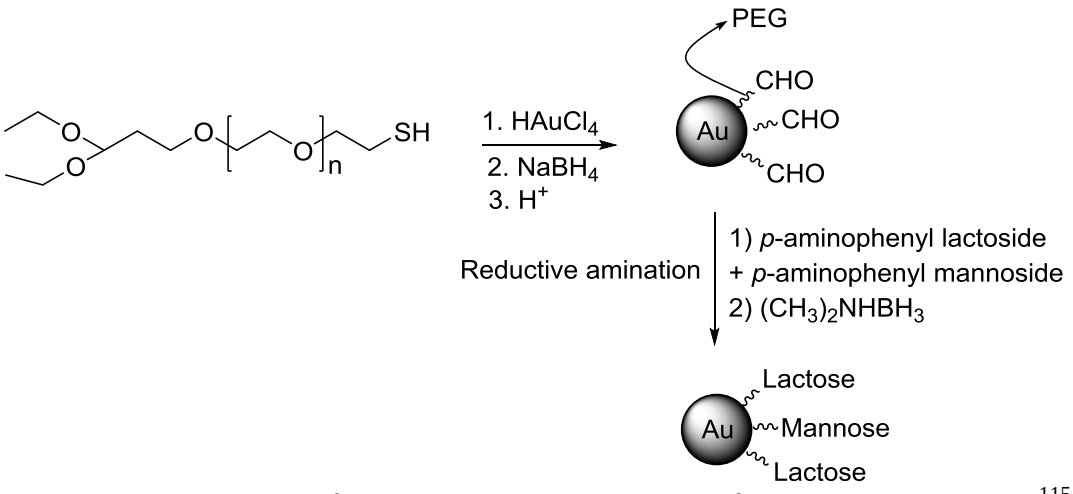

Scheme 1.14. Synthesis of gAuNPs using chemical modification by Otsuka *et al*.[115]

self-assembled microdomain model of multivalent GSLs that is seen on the cell surface (Scheme 1.15).[116] The double bond in the ceramide units of different GSLs was selectively converted to an aldehyde by ozonolysis. These aldehydes were then reacted with the aminooxy groups of the previously synthesized AuNPs to attach the GSL units to the particle surface by oxime formation. The aminooxy functionalized AuNPs were synthesized in two steps; firstly AuNPs functionalized with the *N*-tert-butoxycarbonyl-protected aminooxy group were made by direct synthesis, and then the *N*-tert-butoxycarbonyl group was removed by treatment with an aqueous HCl at 40 ^{o}C. The GSL aldehydes were then coupled directly with the aminooxy functionalized AuNPs under mild conditions. Another potential method that can be used to convert AuNPs to gAuNPs is "Click Chemistry." A detailed discussion of the synthesis of gAuNPs *via* "Click Chemistry" is presented in Chapter 5.

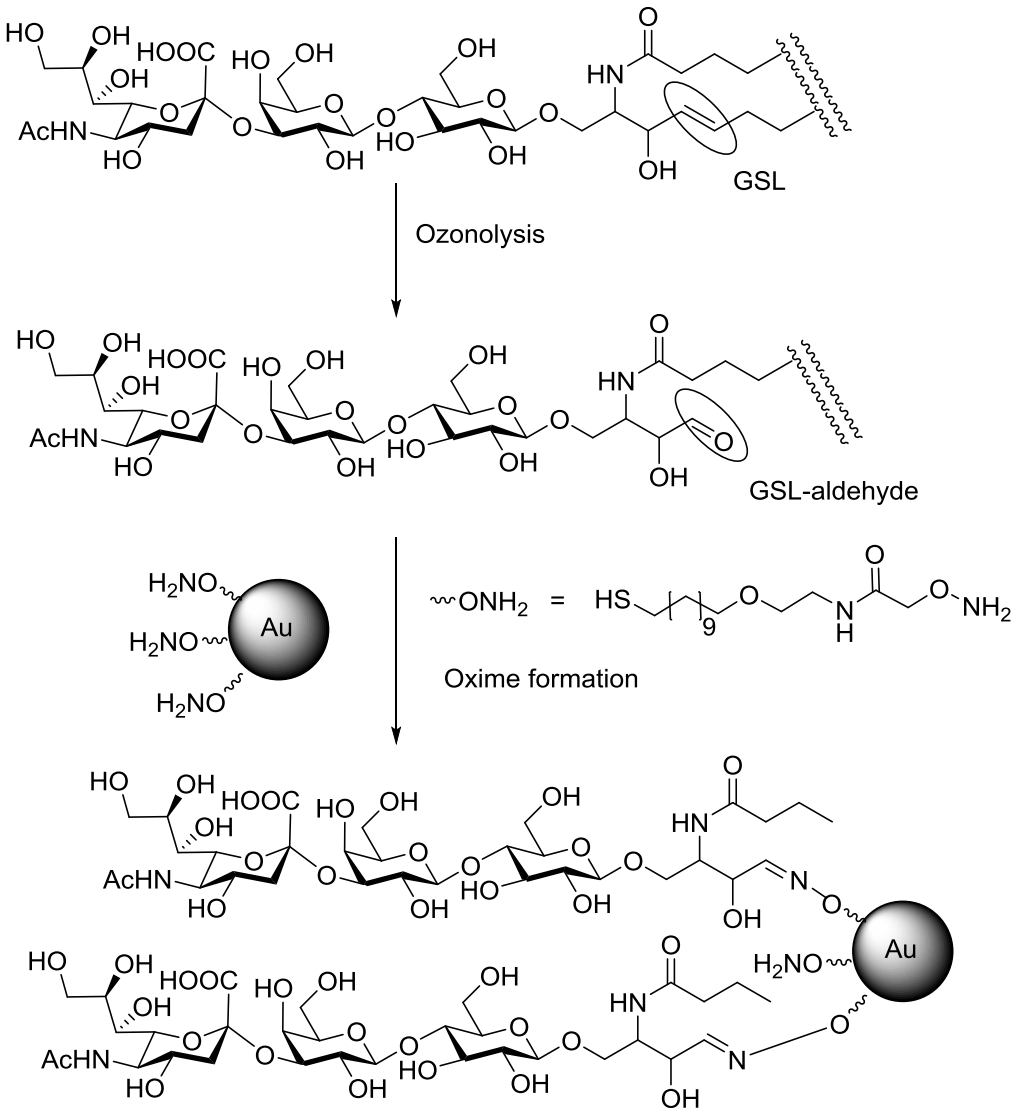

Scheme 1.15. Synthesis of gAuNPs using chemical modification by Nagahori et al.[116]

1.4.6. Applications of gAuNPs

Various aspects of gAuNPs, such as the controllable shape and size of the metallic core, the facile methods established to decorate the surface of the particles with various sugars and other functionalised ligands, and their relatively high chemical stability mean that they are promising systems for the study of various processes involving sugars.[99]

1.4.6.1. Carbohydrate-protein interactions

Carbohydrate-protein interactions are very specific and in general multivalent interactions are required in order to effect strong binding between the two types of units.[94] Several model systems have been prepared comprising multivalent presentations of carbohydrates using suitable scaffolds, to study multivalent carbohydrate-protein interactions.[75] gAuNPs have also been used for this purpose, and in particular, colorimetric bio-assays based on the aggregation and dispersion of gAuNP solutions, controlled by the interactions between proteins and carbohydrate derivatives on the gAuNP surface, have gained significant interest in the last decade.[75]

Most studies have used the aggregation of gAuNPs in the presence of a target protein as the strategy to study carbohydrate-protein interactions for the detection of lectins.[70, 117] The gAuNPs, which are well-dispersed in solution, undergo aggregation in the presence of a suitable protein due to the specific binding of the sugars on the surface of gAuNPs with multiple binding sites present on the protein. This mechanism of gAuNP aggregation is explained in detail in Chapter 3.

While the optical properties of AuNPs are determined by its SPR, there is significant change in these properties when NPs come close and form aggregates due to the coupling of the plasmon oscillations of the interacting particles.[118] The plasmon oscillation produces an electric field localized on the AuNP surface which decays with distance away from the NP. The near-field of particles present in close proximity can interact with each other strongly. Thus the electric field felt by each particle is the sum of the incident

light field and the perturbation due to the presence of the electric dipole present on the neighbouring particle.[118] The coupling of the plasmon oscillations causes a change in the position of the SPR peak and that can be observed using UV-Vis spectrophotometry. The aggregation process can also be observed with the naked eye as the colour of the AuNP solution typically turns from red to purple.

In 2001, the Kataoka group used gAuNPs to study carbohydrate-protein interactions for the first time.[115] gAuNPs functionalized with lactosyl-poly(ethylene glycol) were synthesized and used to detect the bivalent lectin, *Ricinus communis agglutinin* (RCA_{120}).[115] The lactose units on the surface of the gAuNPs selectively interacted with the lectin, causing reversible aggregation (upon the addition of galactose the aggregates were redispersed) of the gAuNPs. UV-Vis studies showed that the extent of the aggregation was proportional to the concentration of RCA_{120}. In addition, investigation with gAuNPs of varying lactoside ligand density (0-65%) demonstrated that particle aggregation also depended on that parameter; a critical lactoside density (>20%) was essential for aggregation to occur.

Later, in 2003, Russell and co-workers synthesized mannose-functionalized gAuNPs for the selective detection of the lectin concanavalin A (ConA).[112] Rapid detection of sub-micromolar concentrations of ConA was achieved with the gAuNPs as monitored by UV-Vis spectrophotometry. The Russell group also synthesized gAuNPs functionalized with thiolated galactose, mannose, and lactose derivatives for the colorimetric detection of RCA_{120}, ConA, and cholera toxin respectively.[70] In general these studies showed that the

gAuNP size, the length of the linker, and the sugar density on the particle surface all affected the performance of the gAuNPs in their analytical detection of the various proteins.[70]

Subsequently, in 2003, Lin *et al.* reported the first quantitative study into the multivalent interactions between gAuNPs and lectins.[101] SPR binding assay studies with mannose-functionalized gAuNPs showed that ConA had an affinity that was one to two orders of magnitude higher for multivalent presentation as compared to monovalent presentation of the mannose ligands. These results confirmed that the multivalent presentation of sugars on a NP surface significantly increases their binding affinity without altering their specificity for lectins.

1.4.6.2. Carbohydrate-carbohydrate interactions

Carbohydrate-carbohydrate interactions are known for their specificity, their weak affinities, and their dependency on bivalent cations.[75] Weak individual binding affinities are overcome by multivalent interactions.[75] In the late 1980s, Eggens *et al.*[119] and Misevic *et al.*[120] independently introduced the concept of carbohydrate-carbohydrate interaction in cell adhesion processes. This finding inspired the development of various model systems to undertake studies into the quantification of carbohydrate-carbohydrate interactions.[98, 121-122] However the precise details of these interactions are still not clear and so further research is on-going. One difficulty lies in the design and preparation of well-defined carbohydrate conjugates which can be used to analyse carbohydrate-carbohydrate interactions. Several groups have studied these interactions with the help of model systems, such as micelles, giant vesicles, and artificial glycoviruses.[75]

In 2004, the Penadés group demonstrated that gAuNPs can be used as multivalent model systems to quantify carbohydrate-carbohydrate interactions at the molecular level.[98] gAuNPs decorated with the trisaccharide Le^X were used to study the Ca^{2+} dependency of the Le^X self-aggregation process. Two different 2 nm sized gAuNP systems, one decorated with thiolated-lactose derivatives and the other with thiolated-Le^X derivatives were synthesized. TEM was used to follow the aggregation of these gAuNPs in the presence and absence of Ca^{2+} ions. The lactose-functionalized gAuNPs showed no aggregation in the presence of Ca^{2+} ions. In contrast, the Le^X-functionalized gAuNPs aggregated reversibly in the presence of Ca^{2+} ions (the aggregates could be redispersed by the addition of ethylenediaminetetraacetic acid (EDTA)) at all the Ca^{2+} concentrations tested (0.1-0.9 mg/mL).

Subsequently, in 2006, the Russell group synthesized a series of gAuNPs (16 nm) decorated with lactosyl derivatives bearing thiolated oligoethylene glycol linkers of varying lengths.[110] TEM and UV-Vis studies showed that the length and the nature of the oligoethylene glycol linkers used had a significant effect on the Ca^{2+}-induced aggregation of these particles. UV-Vis studies also revealed that the aggregation of particles was rapid; the absorbance intensity changed 30 only seconds after the addition of the Ca^{2+} ions. In contrast, previous studies using smaller gAuNPs (~2 nm) functionalized with lactose and other carbohydrates, showed either no aggregation or that it only occurred after several hours. [79, 98, 123] These results indicate that the size of the NPs used in gAuNP model systems has a significant effect on the self-aggregation of the carbohydrates.

1.4.6.3. gAuNPs as anti-adhesion agents

Carbohydrate interactions are directly involved in a variety of cell-cell adhesion processes which, unfortunately, also include undesired pathogenic ones.[75] In general, adhesion of pathogens to host tissues is a necessary condition for the initiation of the infection. The adhesion of pathogens to host receptor cells can be mediated by carbohydrate-carbohydrate and/or carbohydrate-protein interactions.[75] The crucial role of carbohydrates in these types of recognition events has led to the development of new antimicrobial agents that are carbohydrate-based mimics of host glycoconjugates. These new anti-adhesion agents have been considered as potential alternatives to the existing antibiotic-based cures.[124]

For instance, in 2004, Rojo *et al.* demonstrated that gAuNPs can be used as anti-adhesion agents against the advancement of lung metastasis in mice.[125] A murine melanoma cell line (B16) that causes metastasis in lungs was used as a model system to study the inhibitory effect of gAuNPs in metastasis and tumour progression. Previously Hakomori *et al*. have shown that a carbohydrate-carbohydrate interaction between lactosylceramide of endothelium cells and the ganglioside GM3 (α-Neu5Ac(2→3)-β-Gal(1→4)-β-Glc(1→1)-Cer) of B16 cells is the first and the crucial step of the adhesion of tumour cells to the endothelium.[126] This step can therefore be considered as a possible target for the inhibition of the progression of metastasis. Thus, Rojo *et al.* synthesized gAuNPs (1.8 nm size) each bearing 70 lactose units as potential inhibitors of the binding of melanoma cells to endothelial cells.[125] Glucose-functionalized gAuNPs, which are not involved in

the adhesion process, were also synthesized and used as a control. The structures of the thiolated lactose and glucose derivatives used as ligands are shown in Figure 1.9.

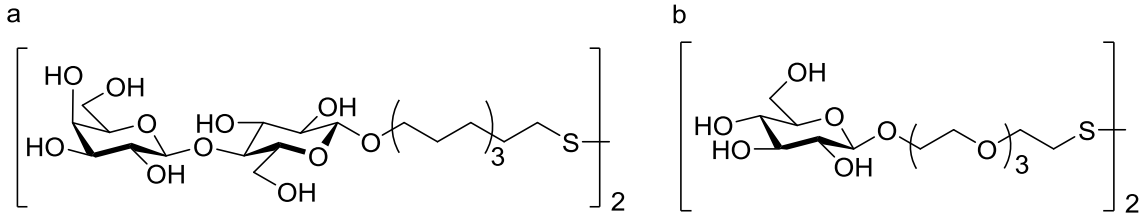

Figure 1.9. Structures of the thiolated (a) lactose and (b) glucose derivatives used by Rojo *et al.*[125] for the synthesis of gAuNPs.

Mice were inoculated with melanoma cells (B16F10), which were pre-incubated with the lactose- and glucose-functionalized gAuNPs (Figure 1.10a). They were sacrificed after three weeks and the tumour foci in the lungs were observed under a microscope. *Ex vivo* pre-incubation of the tumour cells with the lactose-functionalized gAuNPs at 90 μM concentration was seen to inhibit cancer metastasis by up to 70%. Comparison studies in which mice were injected either only with the melanoma cells, or with the melanoma cells incubated with glucose-functionalized gAuNPs were also conducted. Analysis of the images (Figure 1.10b) at two different magnifications (x 8 and x 80) revealed that at the same particle concentration (90 μM), many large (>1 mm; blue arrows) and small tumoural foci (<1 mm; black arrows in Figure 1.10b) were seen when glucose-functionalized gAuNPs were used, whereas tumoural foci were only very scarcely seen when the lactose-functionalized gAuNPs were used.

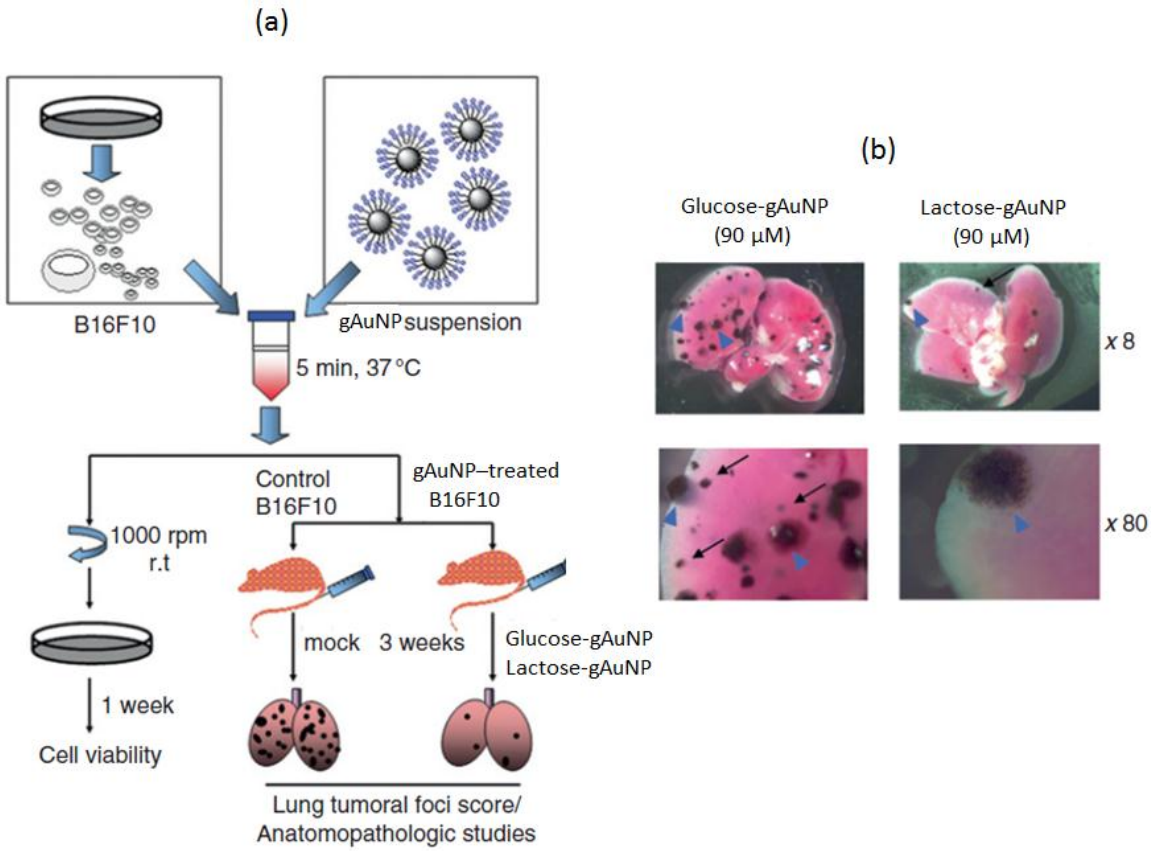

Figure 1.10. (a) Schematic representation of *ex vivo* studies evaluating cell viability and the anti-metastatic effect of gAuNPs functionalized with glucose derivatives (Glucose-gAuNPs) and lactose derivatives (Lactose-gAuNPs). (b) Images of the lungs taken at two different magnifications (x 8, x 80) corresponding to mice subjected to B16F10 cells and Glucose-gAuNP (left) and Lactose-gAuNP (right). Blue triangles indicate the presence of large foci (>1 mm) and black arrows shows the small foci (<1 mm). Image reprinted from Ref. [125]. Copyright (2016) WILEY-VCH Verlag GmbH & Co. KGaA.

1.4.6.4. gAuNPs in cellular and molecular imaging

Cellular and molecular imaging probes that are highly stable under biological conditions, which are very specific to the desired target, and also non-toxic to the biological system, are highly sought after. The use of gAuNPs as non-invasive bio-imaging tools has been explored. In 2008, Lee *et al.* synthesized gAuNPs functionalized with hyaluronic acid derivatives which were labelled with the near-infrared fluorescence (NIRF) dye Hilyte-647 (Figure 1.11).[127] The gAuNPs were denoted as HHAuNPs. The fluorescence of the

dye was quenched (Figure 1.11, left) due to the NP surface energy transfer (NSET) between the dye-labelled hyaluronic acid and the AuNP core. Highly metastatic tumour and rheumatoid arthritis are known to express excess amount of hyaluronidase (HAdase) and reactive oxygen species (ROS), respectively, and cause the degradation of local hyaluronic acid in the extracellular matrix.[128-129] In the study by Lee *et al*., i*n vivo* imaging of mice with tumour and arthritic inflammation after injection of HHAuNPs showed the sensitive detection capability of these particles.[127] When the HHAuNPs reached the target zone (tumours and arthritic joints) the excess amount HAdase and ROS present there cleaved and released the dye-labelled oligo-hyaluronic acid conjugates. The release of the dye from the gAuNP surface deactivated the NSET and resulted in the recovery of fluorescence (Figure 1.11, right) and thus allowed the ultra-sensitive detection of the target zone by *in vivo* fluorescence imaging.

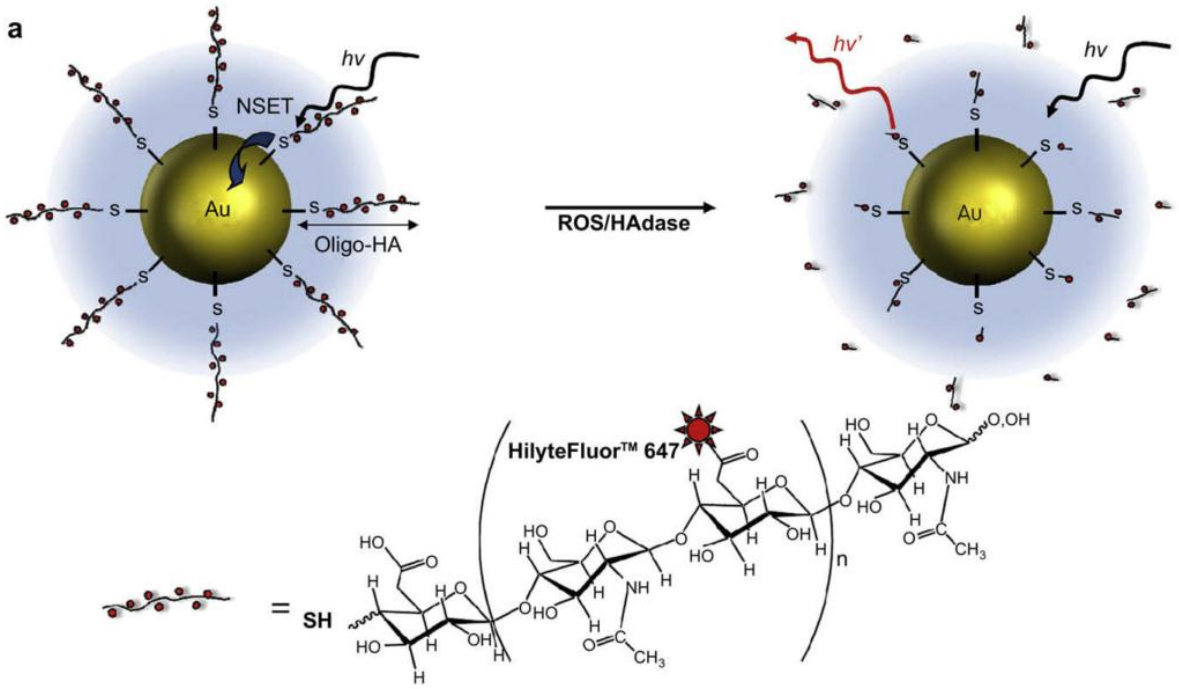

Figure 1.11. A schematic representation of NSET interaction between a AuNP and a Hilyte-647 dye labelled oligo-hyaluronic acid. Left: fluorescence quenching by NSET between the AuNP core and the dye-labelled oligo-hyaluronic acid and; Right: fluorescence recovery in the presence of HAdase/ROS, which cleaved and released the surface immobilized dye-labelled oligo-hyaluronic acid conjugates. Image reprinted from Ref.[127] with permission from Elsevier

1.5. Characterization of AuNPs and gAuNPs.

Several analytical techniques are commonly employed for the characterization of AuNPs and gAuNPs. Some techniques are used for the analysis of the organic ligands on the surface of the particles, whilst other methods focus on the metallic core.[41] In the following section, only the techniques that were used in this project will be discussed.

1.5.1. UV-Vis spectrophotometry

UV-Vis spectrophotometry has been used to analyse the optical properties of AuNP solutions. AuNPs with sizes larger than *ca*. 2 nm exhibit an SPR band in the visible region in the UV-Vis absorption spectrum. [61] The SPR of an AuNP solution is not only

dependent on the size of the NPs, but also on the solvent, the temperature, and the ligand shell.[130] When the temperature, solvent, and the ligand shell are the same for two samples, the absorption maximum depends solely on the particle size and shape. The width of the SPR band is a measure of the polydispersity of the particles in solution.[130] Moreover, using UV-Vis spectrophotometry, the aggregation of AuNPs can be studied. When AuNPs are in close proximity, the surface electrons of the neighbouring particles are delocalized causing a shift in the SPR band to longer wavelengths which can be followed using UV-Vis spectrophotometry.[70]

1.5.2. Electron microscopy

Electron Microscopy (EM) is used to determine the mean metallic core size of NPs. An electron microscope uses a beam of electrons as an illumination source. Since electron wavelengths can be up to 10^5 times smaller than that of visible light photons, an electron microscope has a much larger resolution (smallest distance between two points in the sample that can be seen as two separate entities) than a light microscope.[131] Thus, an electron microscope can be effectively used to analyse the size of NPs.

Transmission electron microscope (TEM), one of several electron microscopes, uses a high voltage electron beam to image the sample. The electron beam is generated by an electron gun, which is generally fitted with a tungsten filament or lanthanum hexaboride as the source of electron. The electron beam is then accelerated by an electric potential and focused on the sample by a number of electromagnetic and electrostatic lenses.

For the imaging, samples are prepared by drying NPs on a Cu grid that is coated with a thin layer of carbon. Successful imaging of NPs using TEM depends on the contrast of the sample compared to the background in the grid. Materials that have significantly large number of electrons as compared to carbon are easily imaged because of the enhanced scattering from these high atomic number materials.[132]

The electron beam is transmitted through the NP sample prepared on the grid, which is placed in the sample holder of the microscope. The beam that emerges from sample is magnified by the objective lens (Figure 1.12). The image is viewed by projecting the magnified beam onto a fluorescent screen. Alternatively, the image can be recorded photographically by projecting the beam onto a charge-coupled device (CCD) camera or a complementary metal-oxide semiconductor (CMOS) camera.

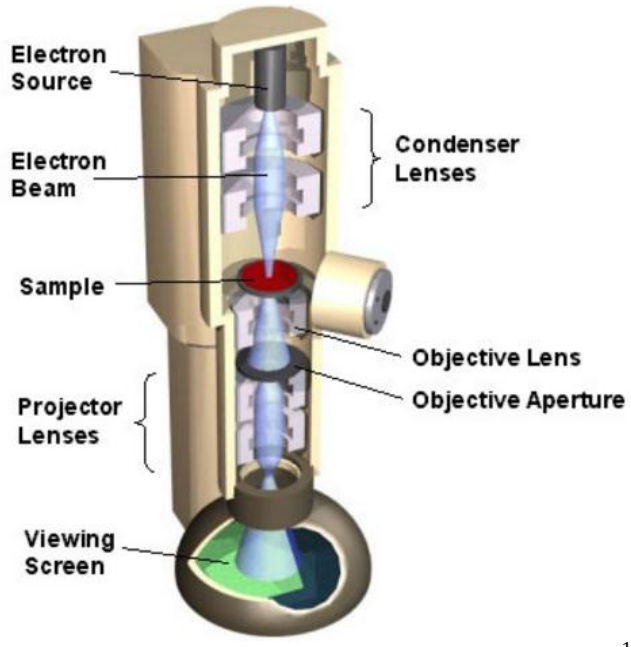

Figure 1.12. Layout of the components in a TEM.[133]

Although TEM is effective for imaging and measuring the size of NPs due to its high resolution, it has several drawbacks. Firstly in TEM, the field of view is relatively small, thus there is a chance that the region viewed may not be a true representation of the whole sample. Secondly the sample structure may be altered during the sample preparation, and in some cases there is a chance that the sample can be damaged by the electron beam.

1.5.3. Dynamic light scattering

Dynamic light scattering (DLS, also known as photon correlation spectroscopy) is a non-invasive technique used to measure the size distribution of proteins, polymers, and nanoparticles.[134-135] DLS gives the size of the particles by measuring the speed at which the particles diffuse in the solvent due to the Brownian motion. Brownian motion is defined as the random movement of particles due to their bombardment by solvent molecules that surround them, and is inversely proportional to the size of the particles. The DLS measurement is performed by passing a monochromatic light beam through a solution containing particles and measuring fluctuation of the scattered light intensity. The solution temperature must be stable in order to obtain accurate DLS measurements; otherwise any convection current in the solution may cause non-random movements that would give an incorrect interpretation of the particle size. The diameter of the particles obtained by DLS is referred to as the hydrodynamic diameter since its measurement relies on particle diffusion in the solvent. The hydrodynamic diameter does not just depend on the core size of the particles, but also on the surface structures, and the type, and concentration of ions in the system.[136]

The light absorption and scattering properties of AuNPs are strongly enhanced due to the SPR oscillation of the surface electrons. For example, a AuNP with a diameter of 60 nm has a light-scattering cross-section 200-300 times larger than that of a polystyrene bead of the same size, and is 4-5 orders of magnitude larger than that of a fluorescent dye, such as fluorescein.[137] Therefore, AuNP-based DLS assays have been extensively used for the detection of various analytes.[73, 138] Moreover, the scattered light intensity from AuNPs is much stronger than that from biological samples, and thus there is no background interference from the sample matrix. AuNP size measurements with DLS have been performed in biological samples, such as tissues, cells, and serum.[73]

Unlike TEM, DLS is very easy to use and it provides a quick method of analysis. Also, a large number of particles are measured in one measurement, giving a dataset that is statistically significant. However, there is a major drawback to DLS; since the intensity of scattered light changes with the sixth power of the particle diameter, relatively small amounts of impurities can severely interfere with the measurements.

1.5.4. Thermogravimetric and Elemental Analysis

Thermogravimetric analysis (TGA) is a technique in which the sample mass is measured as a function of time or temperature as the sample is heated in a controlled atmosphere.[139] It is generally used to determine the properties of materials that show either mass gain or loss because of oxidation, decomposition, or the loss of volatile components upon heating.[139] In the case of AuNPs, TGA is used to determine the relative mass of the organic ligands on the particle surface.[139] As the temperature is increased, the organic

ligands that comprise the AuNPs decompose forming solid carbon and the weight change that accompanies this process can be measured. As the metallic core of the particle simply produces elemental bulk Au which does not react at temperatures below 1000 ^{o}C, any changes in the mass that are measured below 1000 ^{o}C correspond to the decomposition or reaction of the organic shell of the AuNPs.[36] Thus, in effect, the use of TGA can be used to measure the metal-to-ligand ratio of a NP sample. Also, if the decomposition temperature of different ligands attached to the particle is known, the relative ratios of these ligands to each other can also be determined.[140]

Elemental analysis (EA) is used for the determination of the elemental composition of a compound. Generally, the relative mass percentage of carbon, hydrogen, and nitrogen (CHN) are determined by the combustion of a sample and detection of the resulting combustion products. In the case of AuNPs, EA is used to quantify the ligand shell composition and to confirm the metal-to-ligand ratio.[100] In addition, if the theoretical elemental composition of AuNPs is known, EA can be used to confirm the purity of the sample.

1.5.5. Nuclear Magnetic Resonance Spectroscopy

Nuclear Magnetic Resonance (NMR) has been extensively used to characterize thiolate-functionalized AuNPs. The ^{1}H and ^{13}C NMR signals of the solutions of thiolate-functionalized AuNPs are quite broad as compared to those of the corresponding free alkanethiols.[36] The ^{13}C NMR spectra of alkanethiolate-functionalized AuNPs show that that linewidths change systematically with the position of carbon relative to the particle

surface.[141] Hostetler *et al.* showed that ^{1}H and ^{13}C NMR peaks of the methyl group of the octanethiolate ligand in octanethiolate-functionalized AuNPs were broader than those of the methyl group of the dodecanethiolate ligand in the dodecanethiolate-functionalized AuNPs.[142] Also, the ^{13}C methylene linewidths were seen to increase as the position of the methylene groups get closer to the particle surface.

Spectral broadening of particular signals of AuNPs can arise from a number of factors:
(1) Spin-lattice relaxation (T_1, also known as longitudinal relaxation, or relaxation in the z-direction) is the process by which energy absorbed by the excited spins is released back into the surrounding lattice to regain thermal equilibrium. T_1 relaxation corresponds to the process of re-establishing the normal Gaussian population distribution of the spin states in the magnetic field. In AuNPs, the methylene groups closest to the particle surface are the most densely packed, and they behave like a solid, i.e. they undergo fast T_1 relaxation from dipolar interactions; short relaxation time implies faster signal decay and low signal information and thus broad signals.[143] In contrast, the methylene groups furthest away from the particle surface experience freedom of motion, and their spin-lattice relaxations are similar to those of dissolved species.[144]

(2) It has been proposed that difference in the nature of the binding site (vertices, edges, and terraces) of the ligands at the particle surface may cause α- and β-methylene groups to have a distribution of chemical shifts, and thus resulting in the broadening of the ^{13}C resonance peak for α- and β-methylene groups.[144]

(3) Spin-spin relaxation (T_2, also known as transverse relaxation, or relaxation in the x-y plane) is the random and temporary interaction between two excited spins that results in a cumulative loss in phase causing an overall loss of signal. T_2 broadening is dependent on the rate of tumbling of the particles in solution, and for the methyl resonance T_2 changes as r^{-3}, where r is the mean distance between the methyl group and the centre of the Au core.[142]

1.5.6. Infrared Spectroscopy

In infrared (IR) spectroscopy, the vibrational modes of atoms in molecules are excited and the corresponding absorption is detected. The absorption spectrum covers the range from 400-4000 cm^{-1} of the electromagnetic spectrum, and is generally given in units of wavenumbers. In the case of AuNPs, IR spectroscopy can also be used to analyse the ligand shell.[141] The specific IR bands of functional groups can be identified to confirm the nature of species present in the ligand shell. Sometimes, additional insights about the particles can be obtained; for instance, Brust *et al.* have reported that the S-H vibrational mode disappeared when the thiol ligand was attached to the NPs, and they used that result as confirmation of the binding of the ligand with the particles.[44]

1.6. Project Objectives

The goal of this research project was to explore new methods for the production and application of AuNPs and gAuNPs. This thesis describes the use of the Turkevich method to synthesize Cit-AuNPs of various shapes and sizes, and the use these NPs in ligand exchange reactions with different saccharide derivatives to make gAuNPs. Studies of

applications of gAuNPs that were synthesised were focused on the colorimetric sensing of heat-labile enterotoxin and influenza virus particles and hemagglutinin.

Chapter 2 describes the synthesis of AuNPs with different sizes and shapes by tuning the conditions of the Turkevich reaction.

Chapter 3 describes the synthesis of galactose-functionalized gAuNPs, and their application for the colorimetric sensing of the lectin, heat-labile enterotoxin.

Chapter 4 describes the extraction of sialylglycopeptide from egg yolks, the synthesis of gAuNPs decorated with sialylglycans, and application of these gAuNPs for the colorimetric detection of influenza hemagglutinin and influenza virus particles.

Chapter 5 describes attempts to synthesize gAuNPs in a one-pot reaction by use of the copper(I)-catalysed azide-alkyne Huisgen cycloaddition.

Chapter 6 provides full experimental details for the work reported in Chapters 2-5.

1.7. References

1. Eustis, S.; El-Sayed, M. A. *Chem. Soc. Rev.* **2006,** *35* (3), 209-217.

2. Thakor, A.; Jokerst, J.; Zavaleta, C.; Massoud, T.; Gambhir, S. *Nano Lett.* **2011,** *11* (10), 4029-4036.

3. Slater, J. C. *J. Chem. Phys.* **1964,** *41* (10), 3199-3204.

4. Fuente, J. M. d. l.; Penadés, S. *Biochim. Biophys. Acta Gen. Subj.* **2006,** *1760* (4), 636-651.

5. Zhao, P.; Li, N.; Astruc, D. *Coord. Chem. Rev.* **2013,** *257* (3), 638-665.

6. Elghanian, R.; Storhoff, J. J.; Mucic, R. C.; Letsinger, R. L.; Mirkin, C. A. *Science* **1997,** *277* (5329), 1078-1081.

7. Saha, K.; Agasti, S. S.; Kim, C.; Li, X.; Rotello, V. M. *Chem. Rev.* **2012,** *112* (5), 2739-2779.

8. Turner, M.; Golovko, V. B.; Vaughan, O. P.; Abdulkin, P.; Berenguer-Murcia, A.; Tikhov, M. S.; Johnson, B. F.; Lambert, R. M. *Nature* **2008,** *454* (7207), 981-983.

9. Faraday, M. *Philos. Trans. R. Soc. London* **1857,** *147*, 145-181.

10. Turkevich, J.; Stevenson, P. C.; Hillier, J. *Discuss. Faraday Soc.* **1951,** *11* (0), 55-75.

11. Hayat, M. A. *Colloidal gold: principles, methods, and applications*. Academic Press: New York, 1989.

12. Frens, G. *Nat. Phys. Sci.* **1973,** *241*, 20.

13. Schmid, G. *Chem. Rev.* **1992,** *92* (8), 1709-1727.

14. Merchant, B. *Biologicals* **1998,** *26* (1), 49-59.

15. Beliles, R. P. *Patty's industrial hygiene and toxicology*. 4 ed.; John Wiley & Sons: New York, 1994; p 2021-2032.

16. Wulfsberg, G. Inorganic Chemistry. University Science Books: California, 2000; p 270.

17. Pricker, S. *Gold Bull.* **1996,** *29* (2), 53-60.

18. Sardar, R.; Funston, A. M.; Mulvaney, P.; Murray, R. W. *Langmuir* **2009,** *25* (24), 13840-13851.

19. Nguyen, D. T.; Kim, D.-J.; Kim, K.-S. *Micron* **2011,** *42* (3), 207-227.

20. Daniel, M.-C.; Astruc, D. *Chem. Rev.* **2004,** *104* (1), 293-346.

21. LaMer, V. K.; Dinegar, R. H. *J. Am. Chem. Soc.* **1950,** *72* (11), 4847-4854.

22. Xia, Y.; Halas, N. J. *MRS Bull.* **2005,** *30* (05), 338-348.

23. Viswanatha, R.; Sarma, D. Growth of nanocrystals in solution. In *Nanomaterials Chemistry: Recent Developments and New Directions*, Rao, C.; Muller, A.; Cheetham, A. k., Eds. Wiley-VCH: Weinheim, 2007; pp 139-170.

24. Sugimoto, T. *J. Colloid Interface Sci.* **2007,** *309* (1), 106-118.

25. Bahrig, L.; Hickey, S. G.; Eychmüller, A. *CrystEngComm* **2014,** *16* (40), 9408-9424.

26. Brust, M.; Walker, M.; Bethell, D.; Schiffrin, D. J.; Whyman, R. *J. Chem. Soc., Chem. Commun.* **1994,** (7), 801-802.

27. Silvert, P.-Y.; Tekaia-Elhsissen, K. *Solid State Ionics* **1995,** *82* (1), 53-60.

28. Zheng, N.; Fan, J.; Stucky, G. D. *J. Am. Chem. Soc.* **2006,** *128* (20), 6550-6551.

29. Aslam, M.; Fu, L.; Su, M.; Vijayamohanan, K.; Dravid, V. P. *J. Mater. Chem.* **2004,** *14* (12), 1795-1797.

30. Corbierre, M. K.; Cameron, N. S.; Sutton, M.; Mochrie, S. G.; Lurio, L. B.; Rühm, A.; Lennox, R. B. *J. Am. Chem. Soc.* **2001,** *123* (42), 10411-10412.

31. Shi, X.; Sun, K.; Baker Jr, J. R. *J. Phys. Chem. C* **2008,** *112* (22), 8251-8258.

32. J.W. Slot; Geuze, H. J. *Eur. J. Cell Biol.* **1985,** *38*, 87.

33. Brown, K. R.; Fox, A. P.; Natan, M. J. *J. Am. Chem. Soc.* **1996,** *118* (5), 1154-1157.

34. Giersig, M.; Mulvaney, P. *Langmuir* **1993,** *9* (12), 3408-3413.

35. Perala, S. R. K.; Kumar, S. *Langmuir* **2013,** *29* (31), 9863-9873.

36. Shon, Y.-S.; Mazzitelli, C.; Murray, R. W. *Langmuir* **2001,** *17* (25), 7735-7741.

37. Chen, S.; Templeton, A. C.; Murray, R. W. *Langmuir* **2000,** *16* (7), 3543-3548.

38. Goulet, P. J.; Lennox, R. B. *J. Am. Chem. Soc.* **2010,** *132* (28), 9582-9584.

39. Li, Y.; Zaluzhna, O.; Xu, B.; Gao, Y.; Modest, J. M.; Tong, Y. J. *J. Am. Chem. Soc.* **2011,** *133* (7), 2092-2095.

40. Hostetler, M. J.; Green, S. J.; Stokes, J. J.; Murray, R. W. *J. Am. Chem. Soc.* **1996,** *118* (17), 4212-4213.

41. Templeton, A. C.; Wuelfing, W. P.; Murray, R. W. *Acc. Chem. Res.* **2000,** *33* (1), 27-36.

42. Miles, D. T.; Murray, R. W. *Anal. Chem.* **2003,** *75* (6), 1251-1257.

43. Parker, J. F.; Fields-Zinna, C. A.; Murray, R. W. *Acc. Chem. Res.* **2010,** *43* (9), 1289-1296.

44. Brust, M.; Fink, J.; Bethell, D.; Schiffrin, D.; Kiely, C. *J. Chem. Soc., Chem. Commun.* **1995,** (16), 1655-1656.

45. Templeton, A. C.; Hostetler, M. J.; Kraft, C. T.; Murray, R. W. *J. Am. Chem. Soc.* **1998,** *120* (8), 1906-1911.

46. Schmid, G.; Pfeil, R.; Boese, R.; Bandermann, F.; Meyer, S.; Calis, G. H. M.; van der Velden, J. W. A. *Chem. Ber.* **1981,** *114* (11), 3634-3642.

47. Weare, W. W.; Reed, S. M.; Warner, M. G.; Hutchison, J. E. *J. Am. Chem. Soc.* **2000,** *122* (51), 12890-12891.

48. Shem, P. M.; Sardar, R.; Shumaker-Parry, J. S. *Langmuir* **2009,** *25* (23), 13279-13283.

49. Pettibone, J. M.; Hudgens, J. W. *ACS Nano* **2011,** *5* (4), 2989-3002.

50. de Silva, N.; Ha, J.-M.; Solovyov, A.; Nigra, M. M.; Ogino, I.; Yeh, S. W.; Durkin, K. A.; Katz, A. *Nat. Chem.* **2010,** *2* (12), 1062-1068.

51. Ha, J.-M.; Solovyov, A.; Katz, A. *Langmuir* **2009,** *25* (18), 10548-10553.

52. Porta, F.; Krpetić, Ž.; Prati, L.; Gaiassi, A.; Scarì, G. *Langmuir* **2008,** *24* (14), 7061-7064.

53. Griffin, F.; Fitzmaurice, D. *Langmuir* **2007,** *23* (20), 10262-10271.

54. Yu, A.; Liang, Z.; Cho, J.; Caruso, F. *Nano Lett.* **2003,** *3* (9), 1203-1207.

55. Jana, N. R.; Gearheart, L.; Murphy, C. J. *Adv. Mater.* **2001,** *13* (18), 1389.

56. Jana, N. R.; Gearheart, L.; Murphy, C. J. *J. Phys. Chem. B.* **2001,** *105* (19), 4065-4067.

57. Brown, K. R.; Natan, M. J. *Langmuir* **1998,** *14* (4), 726-728.

58. Nikoobakht, B.; El-Sayed, M. A. *Chem. Mater.* **2003,** *15* (10), 1957-1962.

59. Sau, T. K.; Murphy, C. J. *J. Am. Chem. Soc.* **2004,** *126* (28), 8648-8649.

60. Boisselier, E.; Astruc, D. *Chem. Soc. Rev.* **2009,** *38* (6), 1759-1782.

61. Motl, N.; Smith, A.; DeSantis, C.; Skrabalak, S. *Chem. Soc. Rev.* **2014,** *43* (11), 3823-3834.

62. Brust, M.; Kiely, C. J. *Colloids Surf A: Physicochem Eng Asp.* **2002,** *202* (2–3), 175-186.

63. Jadzinsky, P. D.; Calero, G.; Ackerson, C. J.; Bushnell, D. A.; Kornberg, R. D. *Science* **2007,** *318* (5849), 430-433.

64. Zhu, M.; Aikens, C. M.; Hollander, F. J.; Schatz, G. C.; Jin, R. *J. Am. Chem. Soc.* **2008,** *130* (18), 5883-5885.

65. Heaven, M. W.; Dass, A.; White, P. S.; Holt, K. M.; Murray, R. W. *J. Am. Chem. Soc.* **2008,** *130* (12), 3754-3755.

66. Huang, X.; El-Sayed, M. A. *J. Adv. Res.* **2010,** *1* (1), 13-28.

67. Mie, G. *Ann. Phys.* **1908,** *25*, 377-445.

68. Gold Nanoparticle Properties. http://www.cytodiagnostics.com/store/pc/Gold-Nanoparticle-Properties-d2.htm (accessed Jan 16).

69. Link, S.; El-Sayed, M. A. *J. Phys. Chem. B.* **1999,** *103* (21), 4212-4217.

70. Marin, M. J.; Schofield, C. L.; Field, R. A.; Russell, D. A. *Analyst* **2015,** *140* (1), 59-70.

71. Cheng, P. P. H.; Silvester, D.; Wang, G.; Kalyuzhny, G.; Douglas, A.; Murray, R. W. *J. Phys. Chem. B.* **2006,** *110* (10), 4637-4644.

72. Sapsford, K. E.; Berti, L.; Medintz, I. L. *Angew. Chem. Int. Ed.* **2006,** *45* (28), 4562-4589.

73. Jans, H.; Huo, Q. *Chem. Soc. Rev.* **2012,** *41* (7), 2849-2866.

74. Hill, H. D.; Millstone, J. E.; Banholzer, M. J.; Mirkin, C. A. *ACS Nano* **2009,** *3* (2), 418-424.

75. Marradi, M.; Martín-Lomas, M.; Penadés, S. *Adv. Carbohydr. Chem. Biochem.* **2010,** *64*, 211-290.

76. Wang, J. *small* **2005,** *1* (11), 1036-1043.

77. Edelstein, A. S.; Cammaratra, R. *Nanomaterials: synthesis, properties and applications*. CRC Press: Bristol, 1996.

78. You, C.-C.; Chompoosor, A.; Rotello, V. M. *Nano today* **2007,** *2* (3), 34-43.

79. de la Fuente, J. M.; Barrientos, A. G.; Rojas, T. C.; Rojo, J.; Cañada, J.; Fernández, A.; Penadés, S. *Angew. Chem. Int. Ed.* **2001,** *113* (12), 2317-2321.

80. Davis, B. G.; Fairbanks, A. J. *Carbohydrate Chemistry*. Oxford University Press: Oxford, 2002.

81. Pigman, W.; Horton, D. *The carbohydrates: chemistry and biochemistry*. Academic Press: San Diego, 1972.

82. Gold, V.; Loening, K.; McNaught, A.; Shemi, P. *IUPAC Compendium of Chemical Terminology*. Blackwell Science: Oxford, 1997.

83. Ionescu, A. R.; Bérces, A.; Zgierski, M. Z.; Whitfield, D. M.; Nukada, T. *J. Phys. Chem. A* **2005,** *109* (36), 8096-8105.

84. Biarnés, X.; Ardèvol, A.; Planas, A.; Rovira, C.; Laio, A.; Parrinello, M. *J. Am. Chem. Soc.* **2007,** *129* (35), 10686-10693.

85. Juaristi, E.; Cuevas, G. *The anomeric effect*. CRC press: Florida, 1994.

86. Boons, G.-J.; Hale, K. J. *Organic synthesis with carbohydrates*. Blackwell Science: Sheffield, 2008.

87. Varki, A.; Cummings, R. D.; Esko, J. D.; Freeze, H. H.; Stanley, P.; Marth, J. D.; Bertozzi, C. R.; Hart, G. W.; Etzler, M. E. *Proteomics* **2009,** *9* (24), 5398-5399.

88. Kirschner, K. N.; Woods, R. J. *Proc. Natl. Acad. Sci. USA* **2001,** *98* (19), 10541-10545.

89. Horton, D. *Advances in carbohydrate chemistry and biochemistry*. Academic Press: London, 2012.

90. Candy, D. J. *Biological functions of carbohydrates*. Springer: Netherlands, 1980.

91. Wang, X.; Ramström, O.; Yan, M. *Adv. Mater.* **2010,** *22* (17), 1946-1953.

92. Blow, N. *Nature* **2009,** *457* (7229), 617-620.

93. Berg, J. M.; Tymoczko, J. L.; Stryer, L. *Biochemistry*. 5 ed.; W H Freeman: New york, 2002.

94. Lee, Y. C.; Lee, R. T. *Acc. Chem. Res.* **1995,** *28* (8), 321-327.

95. Lundquist, J. J.; Toone, E. J. *Chem. Rev.* **2002,** *102* (2), 555-578.

96. Jayaraman, N. *Chem. Soc. Rev.* **2009,** *38* (12), 3463-3483.

97. Ernst, B.; Magnani, J. L. *Nat. Rev. Drug Discov.* **2009,** *8* (8), 661-677.

98. Jesus, M.; Penadés, S. *Glycoconj. J.* **2004,** *21* (3-4), 149-163.

99. Marradi, M.; Chiodo, F.; Garcia, I.; Penadés, S. *Chem. Soc. Rev.* **2013,** *42* (11), 4728-4745.

100. Barrientos, Á. G.; de la Fuente, J. M.; Rojas, T. C.; Fernández, A.; Penadés, S. *Chem. Eur. J.* **2003,** *9* (9), 1909-1921.

101. Lin, C.-C.; Yeh, Y.-C.; Yang, C.-Y.; Chen, G.-F.; Chen, Y.-C.; Wu, Y.-C.; Chen, C.-C. *Chem. Commun.* **2003,** (23), 2920-2921.

102. Lin, C.-C.; Yeh, Y.-C.; Yang, C.-Y.; Chen, C.-L.; Chen, G.-F.; Chen, C.-C.; Wu, Y.-C. *J. Am. Chem. Soc.* **2002,** *124* (14), 3508-3509.

103. Svarovsky, S. A.; Szekely, Z.; Barchi, J. J. *Tetrahedron: Asymmetry* **2005,** *16* (2), 587-598.

104. Sundgren, A.; Barchi, J. J. *Carbohydr. Res.* **2008,** *343* (10), 1594-1604.

105. de Paz, J.-L.; Ojeda, R.; Barrientos, Á. G.; Penadés, S.; Martín-Lomas, M. *Tetrahedron: Asymmetry* **2005,** *16* (1), 149-158.

106. Carvalho De Souza, A.; Halkes, K. M.; Meeldijk, J. D.; Verkleij, A. J.; Vliegenthart, J. F. G.; Kamerling, J. P. *Eur. J. Org. Chem.* **2004,** (21), 4323-4339.

107. de Souza, A. C.; Vliegenthart, J. F.; Kamerling, J. P. *Org. Biomol. Chem.* **2008,** *6* (12), 2095-2102.

108. Chien, Y. Y.; Jan, M. D.; Adak, A. K.; Tzeng, H. C.; Lin, Y. P.; Chen, Y. J.; Wang, K. T.; Chen, C. T.; Chen, C. C.; Lin, C. C. *ChemBioChem* **2008,** *9* (7), 1100-1109.

109. Ojeda, R.; de Paz, J. L.; Barrientos, A. G.; Martín-Lomas, M.; Penadés, S. *Carbohydr. Res.* **2007,** *342* (3-4), 448-459.

110. Reynolds, A. J.; Haines, A. H.; Russell, D. A. *Langmuir* **2006,** *22* (3), 1156-1163.

111. Park, J.-W.; Shumaker-Parry, J. S. *ACS nano* **2015,** *9* (2), 1665-1682.

112. Hone, D. C.; Haines, A. H.; Russell, D. A. *Langmuir* **2003,** *19* (17), 7141-7144.

113. Lee, H.; Choi, S. H.; Park, T. G. *Macromolecules* **2006,** *39* (1), 23-25.

114. Manea, F.; Bindoli, C.; Fallarini, S.; Lombardi, G.; Polito, L.; Lay, L.; Bonomi, R.; Mancin, F.; Scrimin, P. *Adv. Mater.* **2008,** *20* (22), 4348-4352.

115. Otsuka, H.; Akiyama, Y.; Nagasaki, Y.; Kataoka, K. *J. Am. Chem. Soc.* **2001,** *123* (34), 8226-8230.

116. Nagahori, N.; Abe, M.; Nishimura, S.-I. *Biochemistry* **2008,** *48* (3), 583-594.

117. Zhao, W.; Brook, M. A.; Li, Y. *ChemBioChem* **2008,** *9* (15), 2363-2371.

118. Jain, P. K. Plasmons in assembled metal nanostructures: radiative and nonradiative properties, near-field coupling and its universal scaling behaviour. Georgia Institute of Technology, 2008.

119. Eggens, I.; Fenderson, B.; Toyokuni, T.; Dean, B.; Stroud, M.; Hakomori, S.-I. *J. Biol. Chem.* **1989,** *264* (16), 9476-9484.

120. Misevic, G. N.; Finne, J.; Burger, M. *J. Biol. Chem.* **1987,** *262* (12), 5870-5877.

121. Hakomori, S. *Arch. Biochem. Biophys.* **2004,** *426* (2), 173-181.

122. Rojo, J.; Morales, J. C.; Penadés, S. Carbohydrate-carbohydrate interactions in biological and model systems. In *Host-Guest Chemistry*, Springer: 2002; pp 45-92.

123. Carvalho de Souza, A.; Halkes, K. M.; Meeldijk, J. D.; Verkleij, A. J.; Vliegenthart, J. F.; Kamerling, J. P. *ChemBioChem* **2005,** *6* (5), 828-831.

124. Sharon, N. *Biochim. Biophys. Acta Gen. Subj.* **2006,** *1760* (4), 527-537.

125. Rojo, J.; Díaz, V.; De La Fuente, J. M.; Segura, I.; Barrientos, A. G.; Riese, H. H.; Bernad, A.; Penadés, S. *ChemBioChem* **2004,** *5* (3), 291-297.

126. Otsuji, E.; Park, Y.; Tashiro, K.; Kojima, N.; Toyokuni, T.; Hakomori, S. *Int. J. Oncol.* **1995,** *6* (2), 319-327.

127. Lee, H.; Lee, K.; Kim, I. K.; Park, T. G. *Biomaterials* **2008,** *29* (35), 4709-4718.

128. Bresnihan, B. *J. Rheumatol.* **1999,** *26* (3), 717-719.

129. Liu, D.; Pearlman, E.; Diaconu, E.; Guo, K.; Mori, H.; Haqqi, T.; Markowitz, S.; Willson, J.; Sy, M.-S. *Proc. Natl. Acad. Sci. USA* **1996,** *93* (15), 7832-7837.

130. Jain, P. K.; Huang, X.; El-Sayed, I. H.; El-Sayed, M. A. *Acc. Chem. Res.* **2008,** *41* (12), 1578-1586.

131. Hawkes, P. W. *Advances in Imaging and Electron Physics*. Elsevier: California, 2010.

132. Transmission electron microscopy analysis of nanoparticles. http://50.87.149.212/sites/default/files/nanoComposix%20Guidelines%20for%20TEM%20Analysis.pdf (accessed Jan 22).

133. Transmission Electron Microscope. http://binoculas.net/scanning-and-transmission-electron-microscope/ (accessed March 06).

134. Dai, Q.; Liu, X.; Coutts, J.; Austin, L.; Huo, Q. *J. Am. Chem. Soc.* **2008,** *130* (26), 8138-8139.

135. Ipe, B. I.; Shukla, A.; Lu, H.; Zou, B.; Rehage, H.; Niemeyer, C. M. *ChemPhysChem* **2006,** *7* (5), 1112-1118.

136. Goldburg, W. *Am. J. Phys.* **1999,** *67* (12), 1152-1160.

137. Jain, P. K.; Lee, K. S.; El-Sayed, I. H.; El-Sayed, M. A. *J. Phys. Chem. B.* **2006,** *110* (14), 7238-7248.

138. Du, B.-A.; Li, Z.-P.; Liu, C.-H. *Angew. Chem. Int. Ed.* **2006,** *45* (47), 8022-8025.

139. Coats, A.; Redfern, J. *Analyst* **1963,** *88* (1053), 906-924.

140. Shi, W.; Sahoo, Y.; Swihart, M. T. *Colloids Surf A: Physicochem Eng Asp.* **2004,** *246* (1), 109-113.

141. Badia, A.; Cuccia, L.; Demers, L.; Morin, F.; Lennox, R. B. *J. Am. Chem. Soc.* **1997,** *119* (11), 2682-2692.

142. Hostetler, M. J.; Wingate, J. E.; Zhong, C.-J.; Harris, J. E.; Vachet, R. W.; Clark, M. R.; Londono, J. D.; Green, S. J.; Stokes, J. J.; Wignall, G. D.; Glish, G. L.; Porter, M. D.; Evans, N. D.; Murray, R. W. *Langmuir* **1998,** *14* (1), 17-30.

143. Terrill, R. H.; Postlethwaite, T. A.; Chen, C.-h.; Poon, C.-D.; Terzis, A.; Chen, A.; Hutchison, J. E.; Clark, M. R.; Wignall, G. *J. Am. Chem. Soc.* **1995,** *117* (50), 12537-12548.

144. Badia, A.; Gao, W.; Singh, S.; Demers, L.; Cuccia, L.; Reven, L. *Langmuir* **1996,** *12* (5), 1262-1269.

Chapter 2: Control of gold nanostructure morphology in the Turkevich reaction

2.1. Objective

The aim of this chapter was to perform a detailed and systematic study to elucidate the effect of the reagent molar ratios and the reaction temperature on the shape and size of the AuNPs produced in the Turkevich reaction. The Turkevich reaction has been widely used throughout my work to obtain citrate-stabilized AuNPs used as a precursor compound to synthesize glycogold nanoparticles.

2.2. Introduction

2.2.1. AuNPs with various shapes

AuNPs have drawn significant interest in recent years due to their unique physicochemical properties which have led to their applications in sensors,[1-3] imaging,[4] catalysis,[5-6] and biomedicine.[7] It is widely known that the magnetic, electronic, and optical properties of AuNPs are often dependent upon their size and morphology. Recent developments in the synthesis of shape-specific AuNPs have opened further exciting opportunities for applications in the fields of plasmonics (the study of the interaction between electromagnetic field and electrons in a metal)[8] and cancer hyperthermia (a medical treatment in which tissue is exposed to higher temperatures either to kill cancer cells or to increase the effect of radiation and anti-cancer drugs on cancer cells).[9]

Therefore, there is now a considerable impetus to develop methods that allow the synthesis of size- and shape-specific AuNPs.

Various methods have been used to synthesize Au nanosystems in the forms of rods,[10-14] cubes,[15-18] disks,[19] prisms,[20] plates,[21-22] and polyhedrons.[23-25] In addition to the synthesis of AuNPs with a desired morphology, it is also important to be able to control their assembly into various secondary structures, such as nanochains, nanowires, and networks, as these structures could be advantageous for applications in biosensors,[26-27] catalysis,[28-29] and electronics.[30] Nanochains can be defined as elongated one-dimensional assemblies of NPs arranged one after another, like the beads in a chain, in which it is possible to easily distinguish the individual particles. Nanowires can be defined as elongated one-dimensional assemblies of fused NPs in which the adjacent particles strongly overlap, making it impossible to distinguish them individually. Methods used for the fabrication of such complex Au nanostructures include template-assisted assembly formation,[31-33] functional crosslinking[34-35] or agglomeration,[36-37] and manipulation using an atomic force microscope (AFM).[38]

2.2.2. The Turkevich reaction

Although a number of different methods have been employed for the synthesis of AuNPs, the citrate reduction method, also known as the Turkevich reaction originally developed by Turkevich[39] and further modified by Frens,[40] is still very popular due to its simplicity and efficiency. In the Turkevich reaction, trisodium citrate reduces Au^{3+} ions to Au atoms and also stabilizes the AuNPs that are formed from clustered Au atoms. Citrate-stabilized

AuNPs (Cit-AuNPs) are commonly used as the starting material for a range of AuNP-based studies and applications such as ligand exchange reactions,[41] controlled NP self-assembly formation,[42] surface charge studies,[43] linker conjugation reactions,[44] catalysis by AuNPs,[45] NP growth mechanism studies,[46] and studies of the effect of NPs on biological systems.[47] Investigations into the Turkevich reaction by various groups over the last 50 years have shown that when the citrate to Au ratio was increased by a factor of 5, i.e. from 0.4 to 2, the AuNP size was decreased by a factor of 7 (Figure 2.1).[39-40, 48-49] However when the ratio was further increased from 2 to 7 very little changes were observed in the size of the NPs formed.

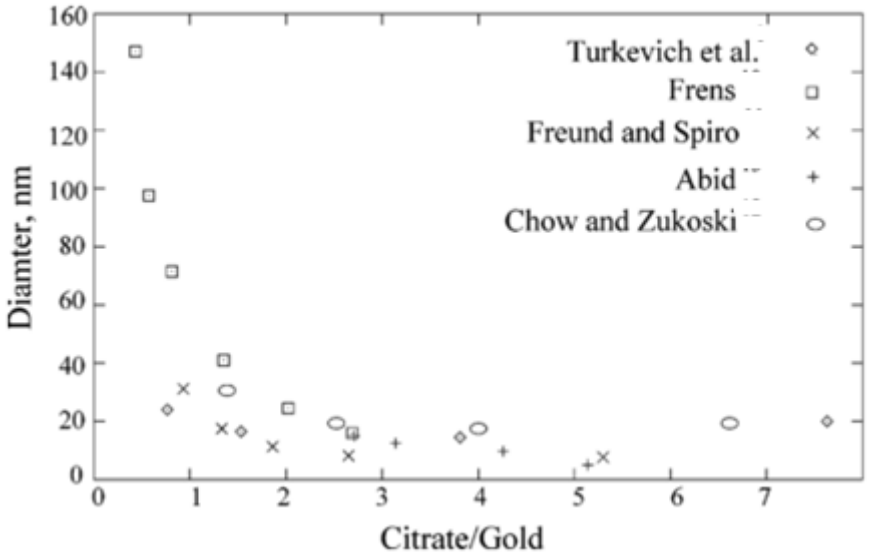

Figure 2.1. Change in AuNP size with ratio of concentrations of citrate to gold. Adapted from Kumar *et al*.[50] Reprinted with permission from Ref. 50. Copyright (2016) American Chemical Society.

2.2.3. Mechanism of AuNP formation in the Turkevich reaction

In 2007, Kumar *et al.* developed a model that explains the various steps in the Turkevich reaction in detail.[50] The oxidation of trisodium citrate to dicarboxyacetone is the first step of this multistep reaction:

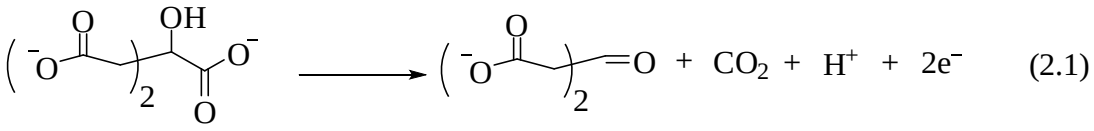

(2.1)

The second step is the reduction of Au^{3+} to Au^{+} :

$$AuCl_3 + 2e^- \longrightarrow AuCl + 2Cl^- \qquad (2.2)$$

The third step is the disproportionation of Au^{+} ions to Au^{0} atoms and Au^{3+} ions:

$$3AuCl \longrightarrow 2Au^0 + AuCl_3 \qquad (2.3)$$

According to Abid[48] and Turkevich[39] the disproportionation step is driven by dicarboxy acetone, which forms a complex with AuCl molecules as shown in Figure 2.2. In the complex, three AuCl molecules interact with a minimum of two dicarboxy acetone molecules. According to Gammons *et al.*[51] once AuNPs are formed the disproportionation reaction can then occur on the surface of the particles too.

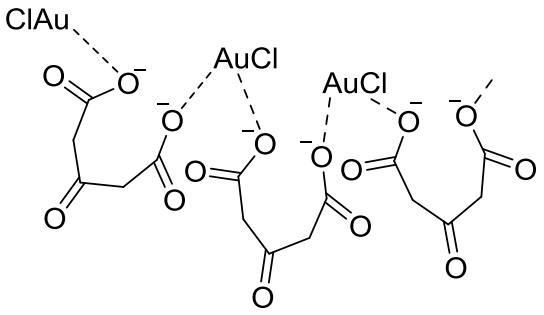

Figure 2.2. Dicarboxy acetone-AuCl complex.

Thus the overall stoichiometry of the reaction can be written as:

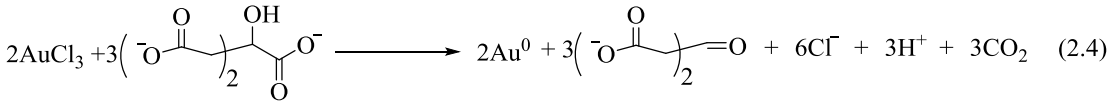

(2.4)

According to the equation 2.4, three citrate ions are required to reduce two $AuCl_3$ molecules. But Frens has reported the complete reduction of $AuCl_3$ with a citrate to Au ratio as low as 0.43.[40] Kumar *et al.* hypothesised that the products formed from the degradation of dicarboxy acetone can also reduce the $AuCl_3$ molecules.[50] Dicarboxy acetone is known to form acetone at high temperatures as shown in equation 2.5:

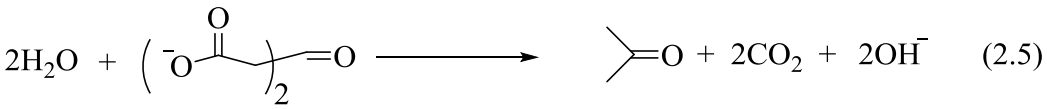

(2.5)

Davies *et al.*[52] and Turkevich *et al.*[39] have demonstrated that $AuCl_3$ can be reduced to AuNPs by reaction with acetone. Therefore Kumar *et al.* assumed that in the Turkevich reaction the acetone formed from dicarboxy acetone reduces $AuCl_3$ to AuCl as shown in

equation (2.6), and that accounts for the complete reduction of $AuCl_3$.[50] According to this assumption three moles of $AuCl_3$ can be reduced by one mole of citrate.

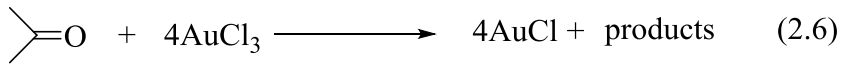

Thus the overall mechanism of AuNP formation proposed by Kumar *et al.* can be summarized as follows. Firstly citrate reduces the Au^{3+} in solution to Au^{+}, and then the dicarboxy acetone formed from the oxidation of citrate forms a multimolecular complex with the Au^{+}. The disproportionation of the complex results in the formation of Au^{0} atoms, and these atoms then adsorb Au^{+} species. Further complexation of the Au^{+} with dicarboxy acetone and disproportionation of the complex results in the formation of larger Au aggregates. The disproportionation and aggregation of Au atoms continues until a critical size is reached at which point a nucleus of Au atoms is formed. The Au atoms produced by ongoing disproportionation become adsorbed onto this nucleus, resulting in its growth and the formation of the NP. [39, 50]

2.2.4. Nucleation and particle growth in the Turkevich Reaction

Different groups have proposed various theories to account for the nucleation and growth of Cit-AuNPs in the Turkevich reaction. Turkevich and co-workers, through their extensive work on the Turkevich reaction came to the conclusion that Cit-AuNPs are formed following the classical LaMer growth model (discussed in Chapter 1, Section 1.5),[53] *i.e.* the particles are formed through a burst of nucleation.[39, 54-57] Takiyama[58] and Frens[40] also studied the formation of Cit-AuNPs and came to the same conclusion that

uniform Cit-AuNPs are formed as a result of a burst of nucleation followed by particle growth. However, later studies showed that the classical LaMer growth model failed to explain the stability of small AuNPs which are in general very difficult to stabilize against aggregation.[59]

In 1994, Chow and Zukoski reported that the size of the Cit-AuNPs decreased as a function of time during the Turkevich reaction.[60] It was observed that large NPs were formed in the beginning of the reaction, which then shrank to produce smaller particles as the reaction proceeded. The large NPs appeared to be made of smaller NPs. Chow and Zukoski proposed a model for Cit-AuNP formation that explained these observations as follows: citrate reduces $AuCl_4^-$ ions to produce Au^0 atoms which adsorb to other $AuCl_4^-$ and citrate ions. The reduction continues along with the growth of the particles. The preferential binding of the particles to $AuCl_4^-$ as opposed to citrate results in the growing particles to have a low surface potential and causes the particles to aggregate.[61] The steric barrier created by the adsorbed ions prevents irreversible particle aggregation. The on-going reduction process completely consumes the $AuCl_4^-$ ions resulting in an increase in the surface potential of the particles. The electrostatic repulsive forces generated by the increase in surface potential causes the particles to break away from the aggregate and to form a stable colloidal system.

In 2006, Kimling *et al*. proposed a different multistep mechanism. Herein the entire amount of Au^{3+} is reduced to Au^0 atoms.[62] These Au^0 atoms form clusters, and in turn they assemble into larger polycrystalline NPs, which is followed by further aggregation.

In contrast, the mechanism proposed by Pong *et al*. involves the formation of nanochains and networks followed by their fragmentation to produce NPs.[63] Here it is proposed that Au^{3+} undergoes fast reduction to give Au^{0} atoms, which is followed by the formation of clusters with an average radius of 2.5 nm (Figure 2.3a). These clusters then assemble themselves into chains and networks (Figure 2.3b and c). A TEM study revealed that the chains and networks were comprised of crystalline particles with an approximate size of 4 nm, and that these particles were interconnected by amorphous Au. As the reaction proceeded, the chains and networks were observed to grow in diameter and then to fragment into smaller particles (Figure 2.3d). The fragmentation proceeded along the segments until these segments were cleaved into small spherical-like particles (Figure 2.3e and f). These particles undergo Ostwald ripening to give the final large spherical particles. Ostwald ripening, a process first described by Wilhelm Ostwald in 1896, is a phenomenon observed in colloidal suspensions or in solid solutions, and is the process through which smaller colloidal particles or crystals dissolve and then are redeposited onto bigger colloidal particles or crystals over time.[64] Ostwald ripening is a thermodynamically-driven process, and it occurs because larger particles are more energetically stable than smaller particles. The higher stability of the larger particles arises from the fact that molecules on the surface of a particle are energetically less stable than the interior ones which are packed and well ordered. As a system tends to reduce its overall energy, the energetically unstable molecules on the surface of a small particle detach and defuse in the solution and then attach to the surface of bigger particles. Thus, the number of smaller particles continues to decrease, whilst the larger particles continue to grow in size.[65]

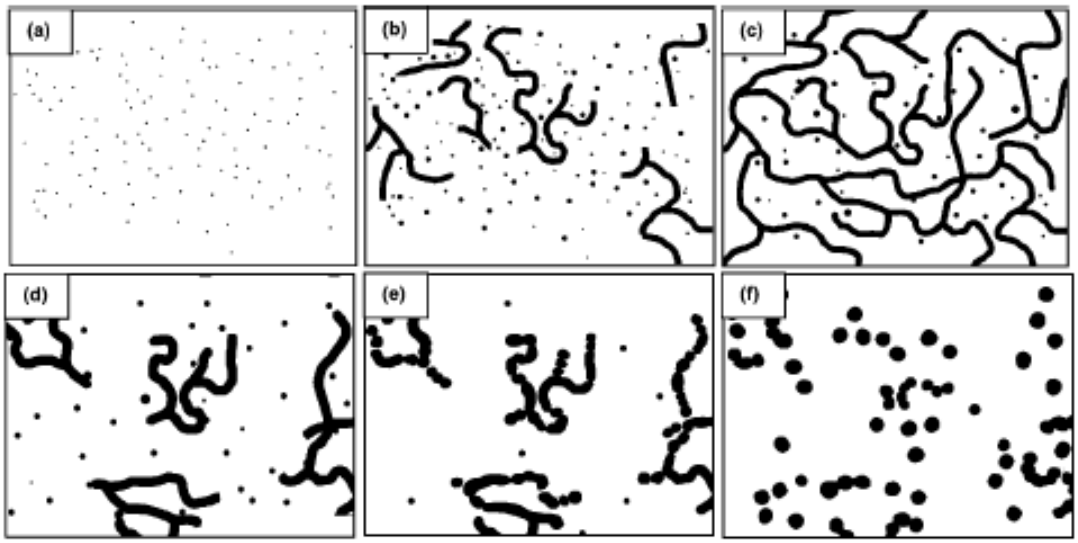

Figure 2.3. A schematic representation of the growth mechanism for the spherical Cit-AuNP formation according to Pong *et al*.[63] Reprinted with permission from Ref. 63. Copyright (2016) American Chemical Society.

In 2010, Polte *et al*. proposed a sequential process for AuNP formation consisting of a four-step nucleation and growth model.[46] The first step is fast formation of nuclei, which is then followed by aggregation of these nuclei into bigger particles. The third step consists of slow diffusion controlled growth of the bigger particles that is maintained by the continued reduction of Au^{3+} ions and also further aggregation. In the fourth and final step, the particles grow quickly to their final size (Figure 2.4).

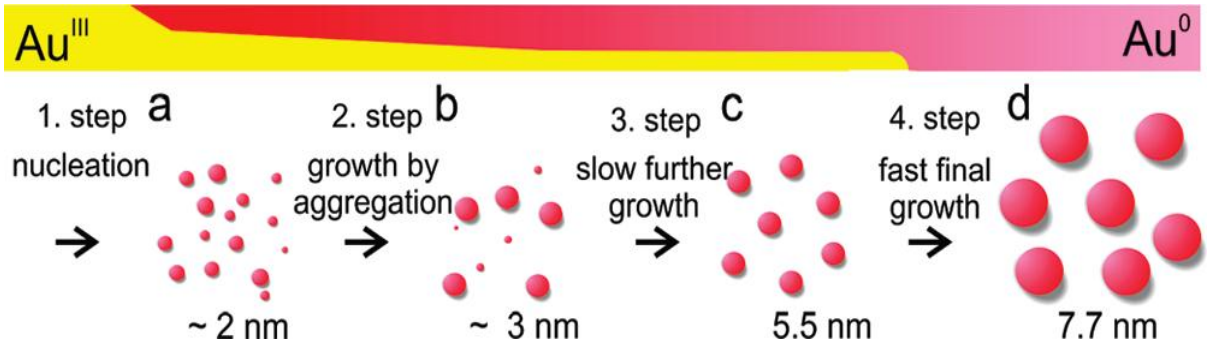

Figure 2.4. A schematic representation of the mechanism of AuNP formation according to Polte *et al*.[46] Reprinted with permission from Ref. 46. Copyright (2016) American Chemical Society.

2.2.5. The Structure of citrate layers of Cit-AuNPs

Biggs *et al*.[66] and Chow *et al*.[60] have reported that in Cit-AuNPs, the citrate anions are coordinated to the Au surface through inner sphere complexation of the carboxylate groups. Trace amounts of OH^-, Cl^-, and $AuCl_4^-$ are also present on the Au surface. In 2014, Park *et al*. demonstrated by infrared (IR) and X-ray photoelectron spectroscopy (XPS) analysis that a specific coordination of adsorbed citrate is prevalent on Cit-AuNPs;[67] dihydrogen citrate anions are attached to the metal surface through η^2-COO^- coordination of the central carboxylate group (Figure 2.5). These IR studies also showed that dangling citrate ions not in direct contact with the Au surface are also present along with the coordinated citrate ions.[67] The citrate ions that are directly coordinated to the Au surface interact with adjacent adsorbed citrate ions and dangling citrate ions by hydrogen bonding between the terminal carboxylic acid moieties. The hydrogen bonded dihydrogen citrate ions form one-dimensional chains, in which the ions interact with each other through van der Waals interactions between nearby CH_2 groups, resulting in the formation of a self-assembled layer of citrate ions on the AuNP surface (Figure 2.5).[67] It is well-known that electrostatic repulsion between particles due to the negatively charged

surface bound citrate anions confers stability to the Cit-AuNPs.[68] Various studies also indicate that steric repulsion between citrate layers of various particles also has a role in stabilizing Cit-AuNPs.[66, 69] Prior to the study of Park *et al*., only the free carboxylate groups of the adsorbed citrate ions were thought to be the source of the negatively charged surfaces of Cit-AuNPs.[68] However, the investigation by Park *et al*. suggested that the negative charge of the outer layer comprised of the dangling citrate anions may be the origin of the electrostatic repulsion between the Cit-AuNPs.[67]

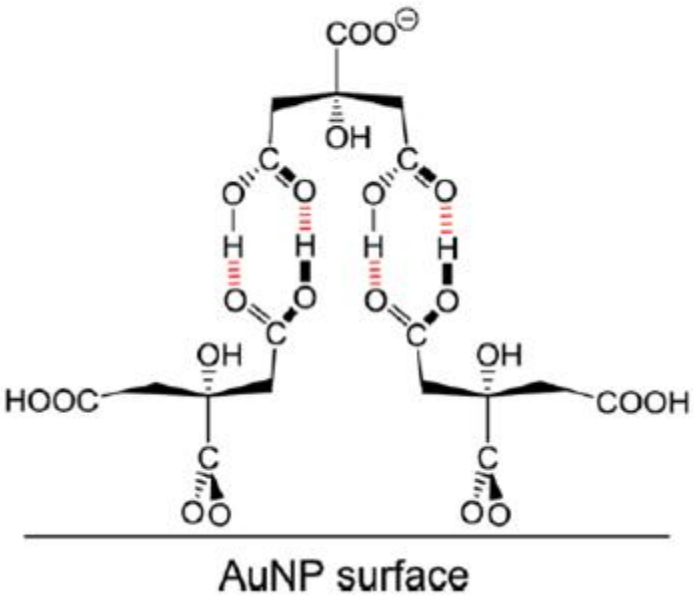

Figure 2.5. A diagrammatic representation of the surface structure of Cit-AuNPs. Reprinted with permission from Ref. 67. Copyright (2016) American Chemical Society.

2.2.6. Turkevich reaction and non-spherical nanostructures

In general, the Turkevich method typically yields spherical AuNPs. However, several groups have recently attempted to fine-tune this method in order to synthesise anisotropic AuNPs, nanochains, wires, and networks. For example, Shankar *et al.* reported the

synthesis of mixtures containing spherical and triangular AuNPs at low temperature.[70] Reaction temperature is an important parameter that influences the shape of the AuNPs formed. By reducing the temperature, the rate of the reduction of the Au ions can be slowed down, resulting in the growth of Au nanotriangles. The TEM and UV-Vis-NIR studies reported by Shankar *et al*. indicated that the formation of Au nanotriangles was a kinetically controlled process.[70] They also observed that halide ions influenced the shape of the particles formed in the Turkevich reaction. Cl^- ions favoured Au nanotriangle formation whereas Br^- and I^- ions promoted the formation of spherical NPs.

Pei *et al*.[71] and Liu *et al*.[72] reported the synthesis of Au nanowires and chains at low molar ratios of citrate to $HAuCl_4$. According to Pei *et al*. the crucial factor in the formation of Au nanowires is the adsorption of $AuCl_4^-$ instead of citrate ions onto the surface of the AuNPs.[71] In 2009, Qiu *et al*. selectively fabricated nanochains and nanowires by seed-mediated shape evolution of Cit-AuNPs[73] using 13 nm Cit-AuNPs as the seeds. It was observed that both the presence of the seeds and the use of a low citrate to $HAuCl_4$ molar ratio (< 0.3) yielded nanochains and nanowires. Patungwasa *et al.* reported the synthesis of AuNPs with predominantly polyhedral shapes by performing the reaction at lower pH.[74] The pH of the solution was regulated by the citrate and citric acid equilibrium that acted as a buffer in the 3.5-7.5 pH range. When the reaction was performed below pH 5 AuNPs of predominantly polyhedral shapes were obtained. The shape-selective AuNP synthesis was achieved at a lower pH by altering the charge on the citrate ions, which in turn affected their stabilizing effects during AuNP growth. At a lower pH the selective detachment of citrate ions from certain faces of the AuNPs might

have been promoted due to the protonation of the carboxyl groups resulting in different growth rates at the different faces of the crystals.

Although the Turkevich reaction has been examined in detail by various groups, a systematic study focused on the effect of the reagent molar ratios at low temperature has not been reported. To the best of our knowledge, the selective synthesis of nanostructured Au systems comprising only polygonal particles and only chains without the presence of any spherical NPs simply by tuning the temperature and reagent ratios of the Turkevich reaction has not been previously reported. The remaining sections of this chapter will detail the synthesis of Cit-AuNPs of various shapes (spheres, polyhedrons, chains, wires, and networks) and sizes as well as providing possible explanations for the formation of these anisotropic structures.

2.3. Results and discussion

2.3.1. The Turkevich reaction under various reaction conditions and TEM analysis

The reactions carried out in this study, namely the reduction of $HAuCl_4$ by trisodium citrate in water at various temperatures and reactant ratios, are summarized in Table 2.1. The molar ratio of trisodium citrate to $HAuCl_4$ is referred to as R. In a typical reaction, 150 mL of 0.25 mM aqueous solution of $HAuCl_4 \cdot 3H_2O$ was refluxed (**2.1a**) or heated to the desired temperature (70 ^{o}C for **2.1b**, **2.2a**, **2.3a**, and **2.4b**, and 95 ^{o}C for **2.4a**) in a temperature-controlled oil bath with continuous magnetic stirring (500 rpm). The required amount of trisodium citrate was rapidly added as an aqueous solution (38.8 mM) and the reaction was continued for 15 min, after which the reaction mixture was cooled to

room temperature. In the case of **2.4a**, the reaction was additionally carried out for 60 minutes.

In the entire range of the R values employed in this study, *i.e*. from 8.7 to 0.7, refluxing the reaction mixture **(2.1a)** resulted in the formation of only spherical and quasi spherical AuNPs (Figure 2.6), with the AuNP size ranging from 12 to 86 nm (Table 2.1). These results are in accordance with previous reports in the literature.[39-40, 75-76] For example, Frens *et al*. synthesized AuNPs with sizes ranging from 16 to 97 nm by varying the R values from 3.1 to 0.6 respectively.[40] Histograms of the particle size distributions of the spherical and quasi-spherical particles synthesized in this study are provided in Figure 2.7. Analysis of the TEM images of the Cit-AuNPs (in each case at least 200 particles were measured) were performed using ImageJ software.

Exp set	R	Temperature (^{o}C)	Shape	Mean particle size (nm)
2.1a	8.7	reflux	spherical NPs	12 ± 1
2.1a	0.7	reflux	spherical & quasi spherical NPs	92 ± 5
2.1b	8.7	70	spherical NPs	12 ±1
2.1b	1.7	70	spherical& quasi spherical NPs	40 ± 4
2.2a	1.6-1.1	70	spherical & polygonal NPs	57 ± 11
2.3a	1.0-0.8	70	polygonal NPs	53 ± 13
2.4a	0.7	95	Wires & networks	11 ± 2 (diameter)
2.4b	0.7	70	Chains made of spherical & polygonal NPs	86 ± 15 (size of NPs within chains)

Table 2.1. Summary of the reagent molar ratios (R) and reaction temperatures used, which resulted in formation of AuNPs with the listed shapes and sizes (averaged along all axes for non-spherical particles).

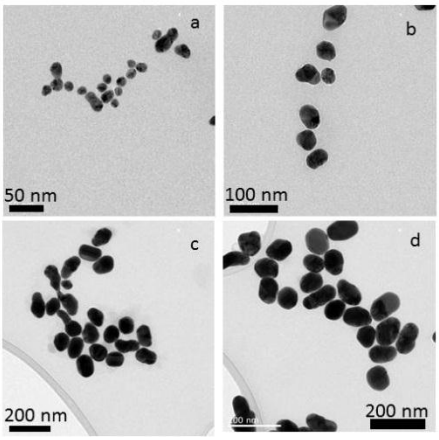

Figure 2.6. TEM images of spherical and quasi spherical Au NPs obtained in experiments **(2.1a)** and **(2.1b)**:(a) R value of 8.7 (reflux or 70 ^{o}C), (b) R value of 1.7 (reflux or 70 ^{o}C), (c) R value of 0.8 (reflux), and (d) R value of 0.7 (reflux).

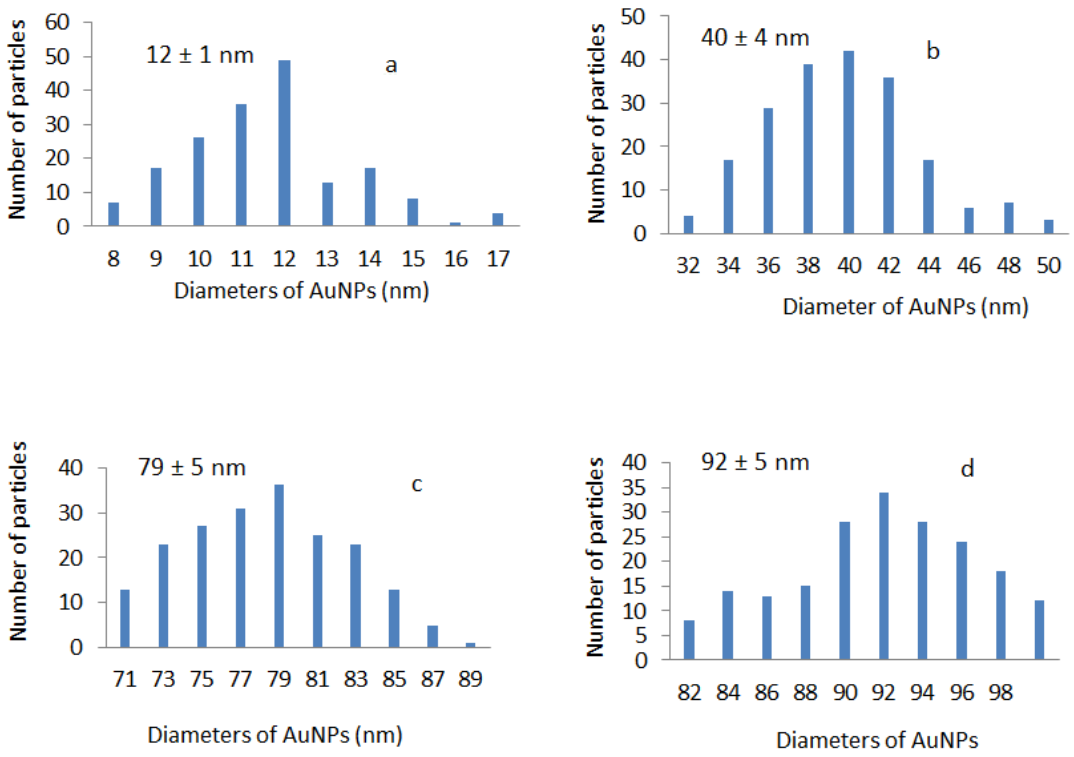

Figure 2.7. Size distribution histograms of spherical and quasi spherical Au NPs obtained in experiments **(2.1a)** and **(2.1b):** a) R value of 8.7 (reflux or 70 ^{o}C), (b) R value of 1.7 (reflux or 70 ^{o}C), (c) R value of 0.8 (reflux), and (d) R value of 0.7 (reflux).

Reduction of the reaction temperature to 70 ^{o}C did not result in any change in the shapes of the AuNPs formed, within the range of R values from 8.7 to 1.7 **(2.1b)**. However, reduction of the R value below 1.7 while carrying out reaction at 70 ^{o}C resulted in the formation of nanostructures with different morphologies. When the R value was maintained within the range of 1.6 to 1.1 **(2.2a)**, a mixture of spherical and polygonal AuNPs was obtained (Figure 2.8a). The AuNPs formed in **(2.2a)** were quite polydisperse with a mean particle size of 57 ± 11 nm (Figure 2.9a). However, when the R value was maintained in the range of 1.0 to 0.8 **(2.3a)** at the same temperature, only polygonal AuNPs were obtained (Figure 2.8b). Though the particles obtained in this case were quite

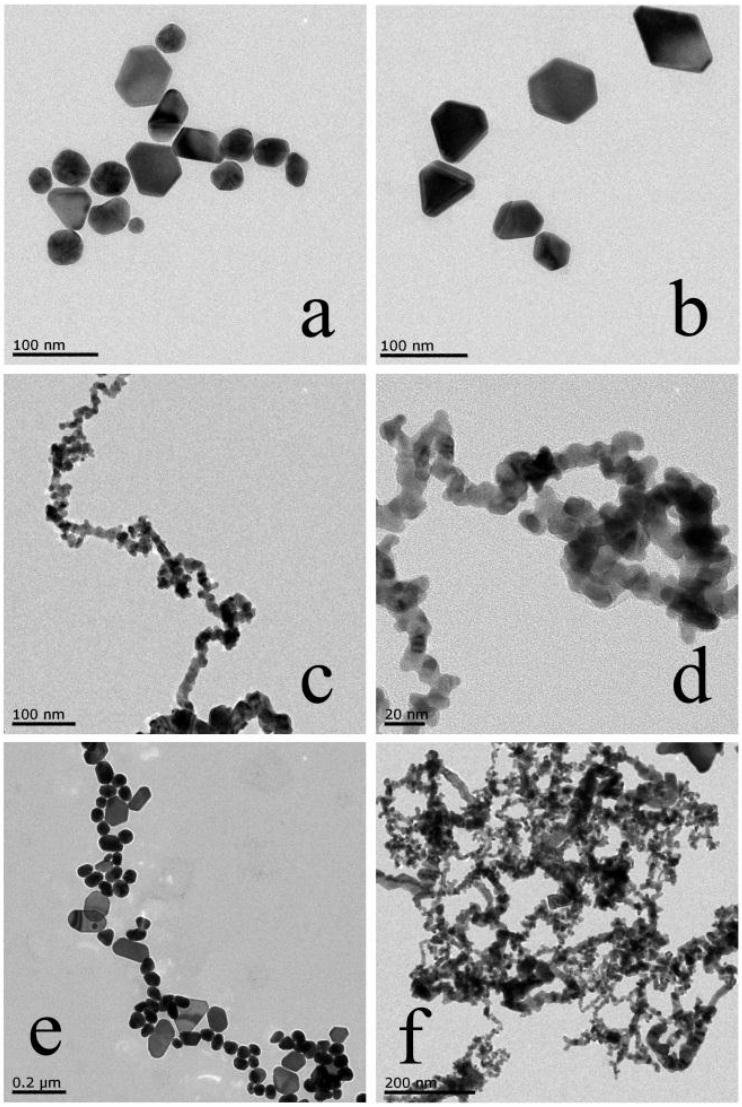

Figure 2.8. TEM images of the nanosystems obtained under different reaction conditions: (a) **2.2a**, (b) **2.3a**, (c) **2.4a** (time:15 min), (d) **2.4a** (time: 15 min) at higher magnification, (e) **2.4b**, and (f) **2.4a** (time: 60 min). Table 1 summarizes the reaction conditions employed for the preparation of the different Au nanosystems.

polydisperse with mean particle size of 53 ± 13nm (Figure 2.9b), the selective formation of only the polygonal AuNPs by simple control of both the temperature and reagent ratio in the Turkevich reaction is a very interesting result. From Figure 2.8a and Figure 2.8b it is clear that in **(2.2a)** and (**2.3a**) the polygonal particles were comprised of triangular, tetragonal, pentagonal, and hexagonal AuNPs. In **(2.2a)** approximately 60% of the

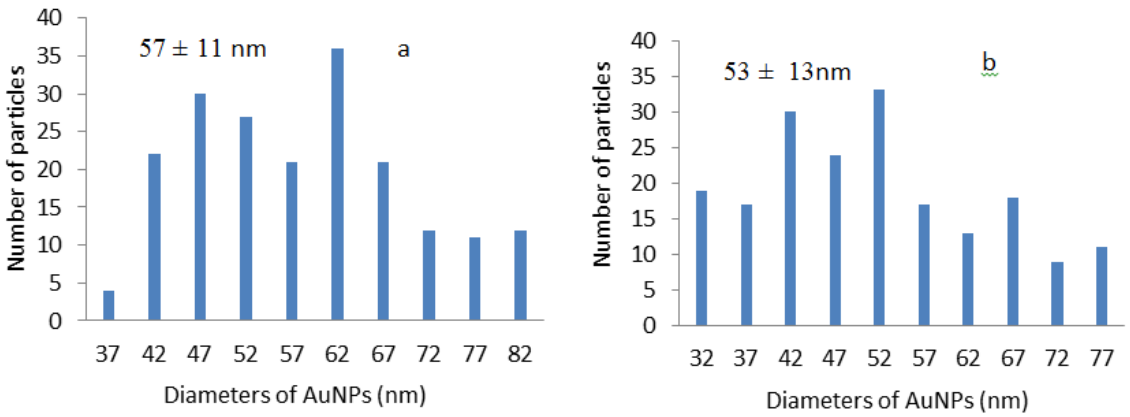

Figure 2.9. Size distribution histograms of Au NPs obtained in **(2.2a)** and **(2.3a)**.

particles were spheres, whilst the remaining particles were triangular (*ca*. 9%), tetragonal (*ca*. 11%), pentagonal (*ca*. 8%), and hexagonal (*ca*. 12%)**.** In **(2.3a)** no spherical particles were formed and the ratio of the populations of the triangular (*ca*. 23%), tetragonal (*ca*. 26%), pentagonal (*ca*. 23%), and hexagonal (*ca*. 28%) particles were approximately the same as in **(2.2a)**. The edge lengths of the polygonal AuNPs formed in (**2.2a**) and (**2.3a**) were not equal in size, and so the sizes of the AuNPs quoted here are the averages of their lengths along all axes. Since mixtures of particles with several different shapes were formed under these conditions the particle size distributions were somewhat wider than at the higher temperatures due to different growth rates of specific shapes.

A further, but relatively small reduction in the value of R from 0.8 to 0.7 led to a significant change in the growth regime. When the reaction temperature was maintained at 95 ^{o}C, and the R value was reduced to 0.7 **(2.4a)**, Au nanowires were obtained as shown in Figure 2.8c. Figure 2.8d shows a TEM image of the nanowire (**2.4a**) under high magnification from which the average diameter of the nanowire was found to be 11 ± 2 nm (Figure 2.10a). A further reduction of the reaction temperature to 70 ^{o}C with the same

R value of 0.7 (**2.4b**) resulted in the formation of nanochains comprised of spherical as well as polygonal AuNPs (Figure 2.8e). The AuNPs in the chain showed the greatest polydispersity, with a mean particle size of 86 ± 15 nm (Figure 2.10b). From Figure 2.8e it is clear that in (**2.4b**) there were no spherical or polygonal AuNPs that were not part of the chain. This demonstrates an added advantage of this method over to that reported by Liu *et al*.[72] in which spherical AuNPs were present along with the chain. Both the Au nanowires and chains prepared in (**2.4a**) and (**2.4b**) ranged from several hundred nanometres to more than 4 microns in length.

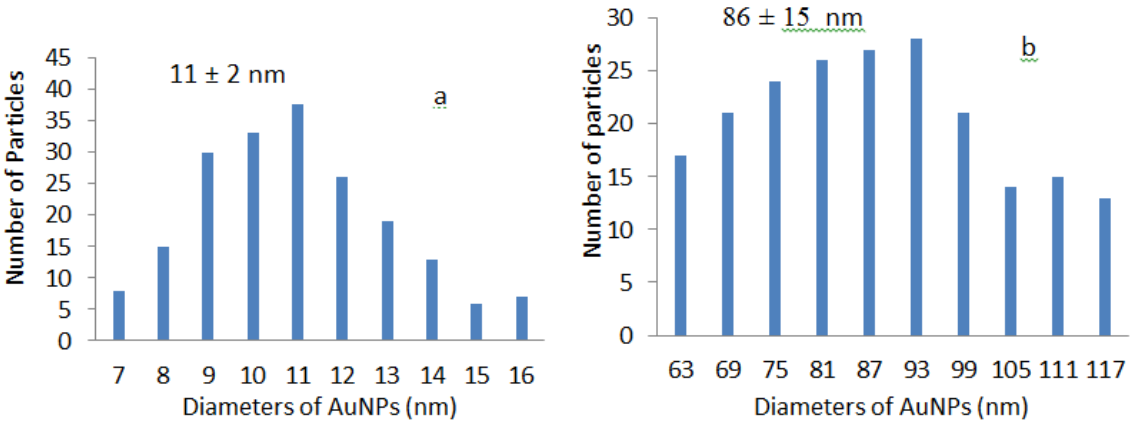

Figure 2.10. Size distribution histograms: (a) the diameter of the nanowires obtained in experiment (**4a**) and (b) individual particles discernable in the chains obtained in experiment **(4b)**.

All of the reactions discussed so far were carried out for 15 minutes. As the duration of Turkevich reaction can affect its outcome, an investigation into the effect of reaction time was also performed.[71,61] Pei *et al* have reported that the Au nanowires formed in the Turkevich reaction after 30 minutes were transformed into a network structure when the reaction duration was extended to 60 minutes.[71]

In our study it was found that reactions carried out for a longer duration (60 minutes) gave the same outcome, except for the case of (**2.4a**). Here (**2.4a**) when the reaction time was increased to 60 minutes or longer, Au nanonetworks uniformly covering the 2D space were obtained (Figure 2.8f) in accordance with the observations of Pei *et al*.[71] The AuNPs in (**2.1a**)-(**2.3b**) were found to be stable for more than a month and the wires, networks and chains in (**2.4a**) and (**2.4b**) were stable for at least two weeks in solution at room temperature.

2.3.2. UV-Vis analysis

Au nanosystems exhibit strong surface plasmon resonance (SPR) absorption that is dependent on their size and shape.[77-78] Spherical AuNPs in general show a single size-dependent narrow absorption band between 520 and 560 nm.[79] The UV-Vis spectra of the spherical particles made in experiments (**2.1a**) and (**2.1b**) are shown in Figure 2.11 and, as expected, the position of the SPR peak maximum shifted from 527 to 558 nm as the AuNPs increased in size from 12 nm to 90 nm.

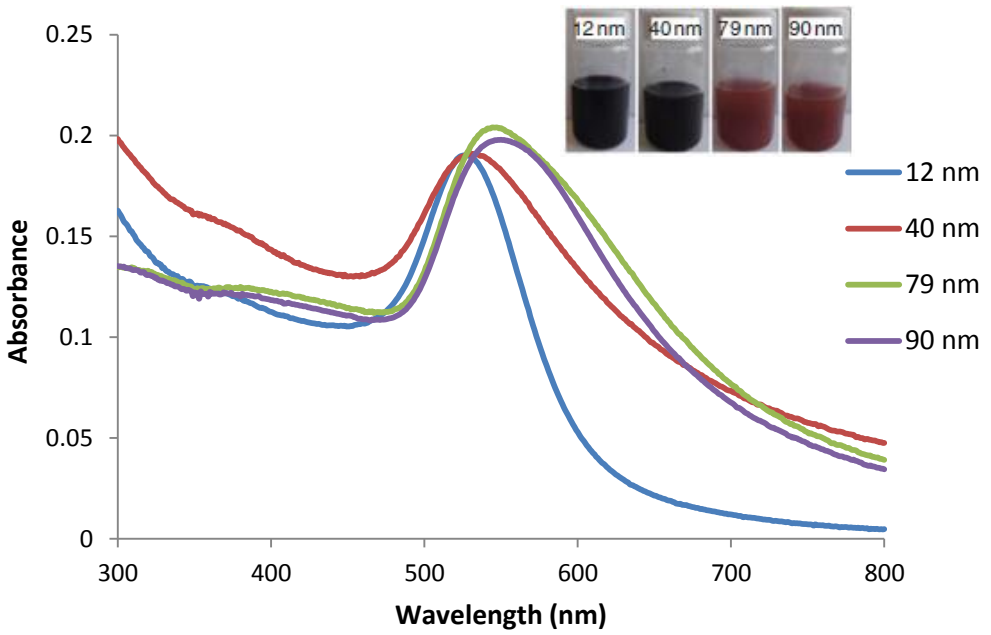

Figure 2.11. UV-Vis spectra of all different sized spherical AuNPs. The inset shows the corresponding photographs of the AuNP solutions.

From Figure 2.12, it is clear that two distinct SPR bands were observed for **(2.2a)** confirming that this sample was a mixture of polygonal and spherical AuNPs. The band centred at 535 nm in **(2.2a)** corresponds to spherical nanoparticles, whilst the band centred at 700 nm was attributed to polygonal AuNPs. In the case of (**2.3a**), Figure 2.12 clearly shows a broad SPR absorption band centred at 580 nm along with a smaller peak at around 700 nm. These observations match well with previous reports in the literature that showed that the polygonal AuNPs possess an additional broad band in the near-IR region, which is attributed to quadrupole plasmon resonance of the NPs.[80-82] The morphology of nanomaterials decides how they are polarized and the number of plasmonic peaks they possess.[83] For instance, absorption spectra of small NPs with the most symmetrical shape *i.e.* a sphere have just one plasmonic peak because a small sphere can be polarized only in dipole mode, whereas polygonal NPs can be polarized

both in dipole and quadrupole modes.[84] Thus, they exhibit two plasmonic peaks as shown in Figure 2.12.[85]

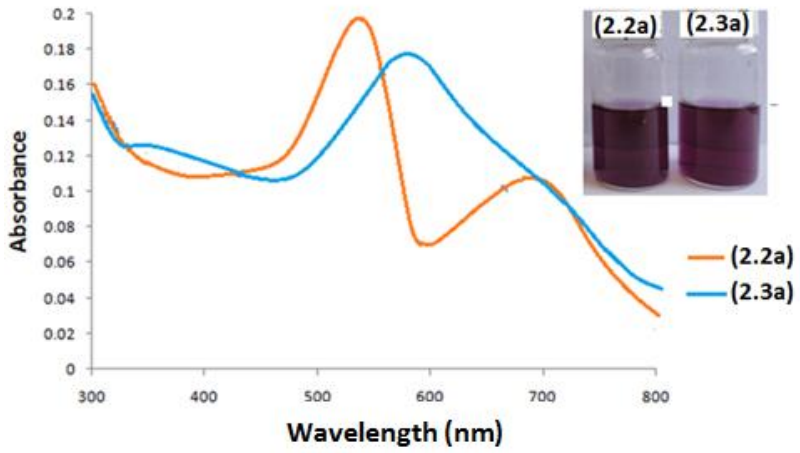

Figure 2.12. UV-Vis spectra of the solutions containing mixture of spherical and polygonal AuNPs, and polygonal AuNPs alone. The inset shows the corresponding photographs of the AuNPs solutions.

In general, non-spherical nanosystems exhibit two SPR peaks corresponding to their long and short axes.[10, 86] In samples (**2.4a**) and (**2.4b**), which contain the nanochains, wires, and network structures, both transverse and longitudinal bands were expected due to their anisotropy. However, it can be seen in Figure 2.13 that nearly flat absorption peaks were observed from 500 to 800 nm. This result can be explained by an earlier observation that when one axis of the one dimensional nanomaterial exceeds 60 nm in length the corresponding longitudinal absorption peak appears above 1000 nm.[86] Since the nanochains, wires, and network present in samples (**2.4a**) and (**2.4b**) have lengths greater than 60 nm, it is possible that the longitudinal peak appears beyond 1000 nm; this was not visible as the technical limitations of our UV-Vis instrument allow measurements only up to 800 nm. Nevertheless, the UV-Vis spectra for chains and wires observed here

match well with the ones reported by Pei *et al.*[71] and Qiu *et al.*[73] The transverse absorption peak corresponding to the short axis of the nanochains and wires appears between 400 to 900 nm as expected. Because of particle aggregation, both in the chains and the wires, the transverse absorption peaks were shifted to the higher wavelengths; 560 nm for the wires and 600 nm for the chains respectively.[87-88] It can also be seen that the SPR peak in the UV-Vis spectrum of the chains (**2.4b**) is not as flat as that of the wires made using the same reagent ratio but at a different temperature (**2.4a**). According to Liu *et al.* this is indicative of the relatively ordered one-dimensional NP formation present in chains, in contrast to the disordered aggregation in wires.[72]

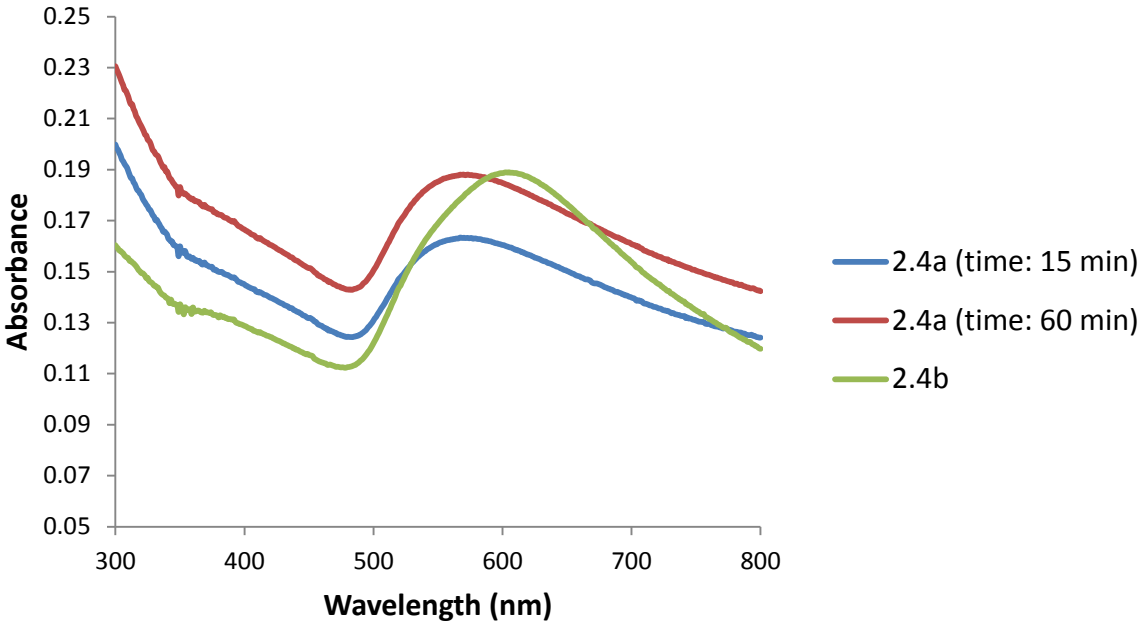

Figure 2.13. UV-Vis spectra of Au nanochains, wires, and networks.

2.3.3. Explanation for the chain and wire formation

When the R value is low the rate of reduction of Au^{3+} is relatively slow and only a small number of Au nuclei are formed.[71] Whereas when R is high, the reduction is very fast,

and a large number of nuclei are formed. After the initial nucleation, the continuous reduction of the remaining $AuCl_4^-$ in the solution creates more Au^0 atoms and the attachment of these newly formed atoms onto the nuclei results in the formation of AuNPs.[54] As the number of nuclei formed initially determines the size of the particles, under high R conditions very small particles are formed and under low R conditions, relatively large-sized particles are formed. As the reaction continues, AuNPs collide because of the attraction force due to the adsorption of $AuCl_4^-$ and they become stuck together.[63] Atomic Force Microscopy (AFM) measurements have demonstrated that repulsive interactions were dominant between Au surfaces in citrate solution due to the adsorption of citrate anions at the Au/water interface.[66, 89] However, only attractive forces were observed in $AuCl_4^-$ solution, that is, both in $AuCl_4^-$ without any citrate ions and also in the case of competitive adsorption of citrate ions and $AuCl_4^-$ ions.[89] Also, the addition of $AuCl_4^-$ ions to the AFM cell pre-adsorbed with citrate ions caused the intermolecular forces to change from repulsion to attraction.[61] As the citrate anions were displaced by $AuCl_4^-$, the diffuse layer potential of the Au surface was seen to decrease.[66] It was therefore concluded that $AuCl_4^-$ is adsorbed as $AuCl_3$ with one of the Cl^- ligand displaced and not as a charged ion.[66] Also, $AuCl_4^-$ adsorption onto the Au surface can reduce the surface charge, which results in an increase of the van der Waals attractions between the Au surfaces.[66]

According to Pei *et al*. the Au atoms get preferentially adsorbed on the concave surface formed at the joint of two NPs as shown in Figure 2.14.[71] This preferential adsorption eventually results in the formation Au nanowires, and they grow in diameter and length

and with time form a 2D network structure. Under high R value conditions eventually all the Au^{3+} ions are completely reduced, resulting in the breakdown of Au nanowires to form AuNPs.[63] However when the R value is low, $AuCl_4^-$ remains on the Au surface and the Au nanowires survive.[63] Pei *et al* have confirmed through TEM and UV-Vis studies that irrespective of the difference between the experimental conditions Au nanowires were formed when a large amount of $AuCl_4^-$ was present in solution and these wires collapsed to spherical particles when the $AuCl_4^-$ ions had been completely consumed.[71] Thus it is clear that the low R value and the consequent presence of excess $AuCl_4^-$ in solution result in the formation of the wires.

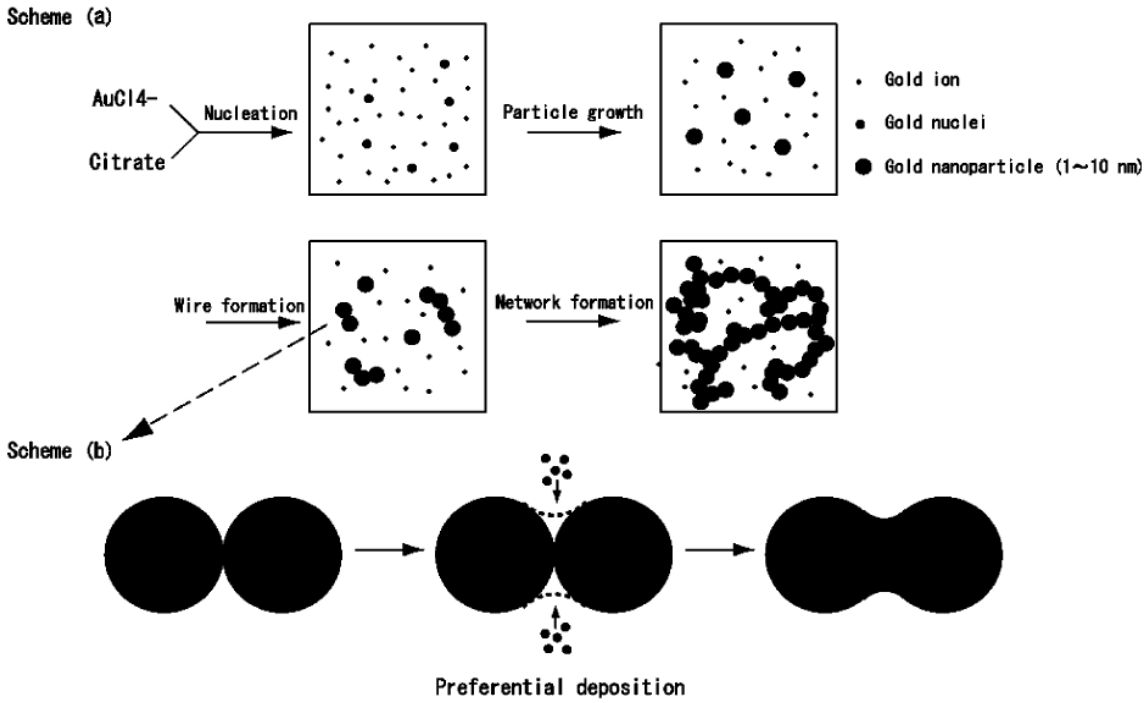

Figure 2.14. A Schematic representation of (a) the formation process of Au nanowires in the Turkevich reaction and (b) preferential deposition of Au^0 atoms on the concave surface when two particles are adhered together. Reprinted with permission from Ref. 71. Copyright (2016) American Chemical Society.

2.3.4. Explanation for the polygonal particle formation

The most widely used model for morphology control of crystals is given by the Gibbs-Curie-Wulff theorem.[90] This theorem suggests that the morphology of a crystal is determined by the surface energy of individual crystallographic faces of the crystal. The crystal attains its final morphology in such a way that the total surface energy of the crystal is minimized.[91] This theorem has been successful in explaining most of the shape control of crystals. However, since it is based on a thermodynamic model, it does not explain any morphology evolution in a single system.[90]

Thus the formation of polygonal AuNPs at lower temperatures in this study, as in the cases of **(2.2a)** and (**2.3a**), could be a result of the difference in change of the rates of nucleation and particle growth with temperature. It has been proposed that the final shape of NPs formed can be controlled by the kinetics of the crystal growth.[92] Under a thermodynamically controlled growth regime, isotropic growth of the nuclei into a thermodynamically favoured equilibrium shapes such as spherical or near-spherical polyhedral structures is preferred.[93] Previously, it has been shown that at high temperature the rate of nucleation is high, resulting in efficient consumption of Au atoms to form nuclei, and the subsequent Ostwald ripening process allows the isotropic growth of the nuclei to form thermodynamically favoured spherical AuNPs.[54, 94] Also, the higher reaction temperature favours higher rates of surface diffusion, and that also results in the formation of thermodynamically favoured spherical NPs.[54] In a kinetically controlled regime, the anisotropic growth of the nuclei into particles with different morphology is often observed due to different growth rates for specific crystal facets.[93-94] Kinetic control

of the reaction can be achieved by decreasing the rate of reduction of $AuCl_4^-$ ions.[92-94] Here, in the cases of **(2.2a)** and **(2.3a)** the low reaction temperature and the low molar ratios of citrate to $HAuCl_4$ result in a slowing down of the rate of the reduction of $AuCl_4^-$ ions, allowing kinetic control of the particle shape. Also, at a lower temperature, the rate of nucleation is expected to be reduced, which could favour the deposition of reduced atoms on existing nuclei along specific crystallographic directions, resulting in the formation of anisotropic structures rather than spherical NPs.[90, 95-98]

A previous study of the Turkevich reaction by Shankar *et al*.,[70] demonstrated that the formation of a mixture of triangular and spherical AuNPs could be ensured by choice of appropriate reaction temperature. In this study we have unravelled the effects of both the temperature and the reagent ratios with the aim of achieving better control over product morphology. The selective formation of polygonal-only AuNPs at the intermediate R ratio of 1.0 to 0.8, and the selective formation of only chains (without any individual spherical NPs) at the R ratio of 0.7 proves that the reagent ratio plays a significant role in the control of the morphology of the Au nanosystems along with the reaction temperature.

2.4. Conclusions

This chapter has described the significant role of the molar reagent ratios of citrate and $HAuCl_4$ in controlling the morphology of the Au nanosystems obtained by the Turkevich reaction when performed at various temperatures. High temperatures and molar ratios resulted in the formation of spherical and quasi-spherical particles, whilst reactions

involving intermediate molar ratios yielded polygonal-only AuNPs at low temperatures, and the use of the lowest molar ratios resulted in the formation of complex structures (chains, wires, and networks) at low temperatures. It would appear that combined control of the molar ratio of reagents and temperature in the Turkevich reaction opens new opportunities for the selective synthesis of polygonal AuNPs, nanochains, wires, and networks.

2.5. References

1. Ahmad, M. Z.; Golovko, V. B.; Adnan, R. H.; Abu Bakar, F.; Ruzicka, J. Y.; Anderson, D. P.; Andersson, G. G.; Wlodarski, W. *Int. J. Hydrogen Energy* **2013,** *38* (29), 12865-12877.

2. Ahmad, M. Z.; Sadek, A. Z.; Yaacob, M. H.; Anderson, D. P.; Matthews, G.; Golovko, V. B.; Wlodarski, W. *Sensor Actuat B-Chem.* **2013,** *179,* 125-130.

3. Saha, K.; Agasti, S. S.; Kim, C.; Li, X.; Rotello, V. M. *Chem. Rev.* **2012,** *112* (5), 2739-2779.

4. Boisselier, E.; Astruc, D. *Chem. Soc. Rev.* **2009,** *38* (6), 1759-1782.

5. Turner, M.; Golovko, V. B.; Vaughan, O. P.; Abdulkin, P.; Berenguer-Murcia, A.; Tikhov, M. S.; Johnson, B. F.; Lambert, R. M. *Nature* **2008,** *454* (7207), 981-983.

6. Donoeva, B. G.; Ovoshchnikov, D. S.; Golovko, V. B. *Acs Catal.* **2013,** *3* (12), 2986-2991.

7. Giljohann, D. A.; Seferos, D. S.; Daniel, W. L.; Massich, M. D.; Patel, P. C.; Mirkin, C. A. *Angew. Chem. Int. Ed.* **2010,** *49* (19), 3280-3294.

8. Maier, S. A.; Brongersma, M. L.; Kik, P. G.; Meltzer, S.; Requicha, A. A. G.; Atwater, H. A. *Adv. Mater.* **2001,** *13* (19), 1501-1505.

9. Hirsch, L. R.; Stafford, R. J.; Bankson, J. A.; Sershen, S. R.; Rivera, B.; Price, R. E.; Hazle, J. D.; Halas, N. J.; West, J. L. *Proc. Natl. Acad. Sci. USA* **2003,** *100* (23), 13549-13554.

10. Yu; Chang, S.-S.; Lee, C.-L.; Wang, C. R. C. *J. Phys. Chem. B.* **1997,** *101* (34), 6661-6664.

11. Nikoobakht, B.; El-Sayed, M. A. *Chem. Mater.* **2003,** *15* (10), 1957-1962.

12. Nann, T.; Riegler, J. *Chem. Eur. J.* **2002,** *8* (20), 4791-4795.

13. Zhang, J. B.; Balla, N. K.; Gao, C.; Sheppard, C. J. R.; Yung, L. Y. L.; Rehman, S.; Teo, J. Y.; Kulkarni, S. R.; Fu, Y. H.; Yin, S. J. *Aust. J. Chem.* **2012,** *65* (3), 290-298.

14. Kumar, S.; Nann, T. *Chem. Commun.* **2003,** (19), 2478-2479.

15. Sun, Y. Y. *Science* **2002,** *298* (5601), 2176-2179.

16. Ren, J.; Tilley, R. D. *J. Am. Chem. Soc.* **2007,** *129* (11), 3287-3291.

17. LaGrow, A. P.; Ingham, B.; Cheong, S.; Williams, G. V. M.; Dotzler, C.; Toney, M. F.; Jefferson, D. A.; Corbos, E. C.; Bishop, P. T.; Cookson, J.; Tilley, R. D. *J. Am. Chem. Soc.* **2011,** *134* (2), 855-858.

18. Warner, J. H.; Tilley, R. D. *Adv. Mater.* **2005,** *17* (24), 2997-3001.

19. Simakin, A. V.; Voronov, V. V.; Shafeev, G. A.; Brayner, R.; Bozon-Verduraz, F. *Chem. Phys. Lett.* **2001,** *348* (3–4), 182-186.

20. Millstone, J. E.; Park, S.; Shuford, K. L.; Qin, L.; Schatz, G. C.; Mirkin, C. A. *J. Am. Chem. Soc.* **2005,** *127* (15), 5312-5313.

21. Chu, H.-C.; Kuo, C.-H.; Huang, M. H. *Inorg. Chem.* **2005,** *45* (2), 808-813.

22. Grzelczak, M.; Perez-Juste, J.; Mulvaney, P.; Liz-Marzan, L. M. *Chem. Soc. Rev.* **2008,** *37* (9), 1783-1791.

23. Huang, W.-C.; Chen, Y.-C. *J. Nanopart. Res.* **2008,** *10* (4), 697-702.

24. Rashid, M. H.; Mandal, T. K. *Adv. Funct. Mater.* **2008,** *18* (15), 2261-2271.

25. Seo, D.; Park, J. C.; Song, H. *J. Am. Chem. Soc.* **2006,** *128* (46), 14863-14870.

26. Duan, J.; He, D.; Wang, W.; Liu, Y.; Wu, H.; Wang, Y.; Fu, M.; Li, S. *Talanta* **2013,** *115* (0), 992-998.

27. Yang, M.; Qu, F.; Li, Y.; He, Y.; Shen, G.; Yu, R. *Biosens. Bioelectron.* **2007,** *23* (3), 414-420.

28. Balachandran, S.; Selvam, K.; Babu, B.; Swaminathan, M. *Dalton Trans.* **2013,** *42* (46), 16365-16374.

29. Sinha, A. K.; Basu, M.; Sarkar, S.; Pradhan, M.; Pal, T. *J. Colloid Interface Sci.* **2013,** *398*, 13-21.

30. Gudiksen, M. S.; Lauhon, L. J.; Wang, J.; Smith, D. C.; Lieber, C. M. *Nature* **2002,** *415* (6872), 617-620.

31. Tang, Z.; Kotov, N. A. *Adv. Mater.* **2005,** *17* (8), 951-962.

32. Mucic, R. C.; Storhoff, J. J.; Mirkin, C. A.; Letsinger, R. L. *J. Am. Chem. Soc.* **1998,** *120* (48), 12674-12675.

33. Zhao, F.; Xun, J. K.; Liu, S. F. *Aust. J. Chem.* **2008,** *61* (1), 1-4.

34. Shenton, W.; Davis, S. A.; Mann, S. *Adv. Mater.* **1999,** *11* (6), 449-452.

35. Kanjanawarut, R.; Su, X. *Anal. Chem.* **2009,** *81* (15), 6122-6129.

36. Zhao, W.; Brook, M. A.; Li, Y. *ChemBioChem* **2008,** *9* (15), 2363-2371.

37. Gangula, A.; Chelli, J.; Bukka, S.; Poonthiyil, V.; Podila, R.; Kannan, R.; Rao, A. M. *J. Mater. Chem.* **2012,** *22* (43), 22866-22872.

38. Meltzer, S.; Resch, R.; Koel, B. E.; Thompson, M. E.; Madhukar, A.; Requicha, A. A. G.; Will, P. *Langmuir* **2001,** *17* (5), 1713-1718.

39. Turkevich, J.; Stevenson, P. C.; Hillier, J. *Discuss. Faraday Soc.* **1951,** *11* (0), 55-75.

40. Frens, G. *Nat. Phys. Sci.* **1973,** *241*, 20.

41. Lin, S.-Y.; Tsai, Y.-T.; Chen, C.-C.; Lin, C.-M.; Chen, C.-h. *J. Phys. Chem. B.* **2004,** *108* (7), 2134-2139.

42. Sardar, R.; Heap, T. B.; Shumaker-Parry, J. S. *J. Am. Chem. Soc.* **2007,** *129* (17), 5356-5357.

43. Brewer, S. H.; Glomm, W. R.; Johnson, M. C.; Knag, M. K.; Franzen, S. *Langmuir* **2005,** *21* (20), 9303-9307.

44. Gearheart, L. A.; Ploehn, H. J.; Murphy, C. J. *J. Phys. Chem. B.* **2001,** *105* (50), 12609-12615.

45. Zhou, X.; Xu, W.; Liu, G.; Panda, D.; Chen, P. *J. Am. Chem. Soc.* **2009,** *132* (1), 138-146.

46. Polte, J. r.; Ahner, T. T.; Delissen, F.; Sokolov, S.; Emmerling, F.; Thünemann, A. F.; Kraehnert, R. *J. Am. Chem. Soc.* **2010,** *132* (4), 1296-1301.

47. Chithrani, B. D.; Chan, W. C. W. *Nano Lett.* **2007,** *7* (6), 1542-1550.

48. Abid, J.-P. Laser induced synthesis and nonlinear optical properties of metal nanoparticles. Ph.D. Thesis, Ecole Polytechnique Federale de Lausanne, Switzerland, 2003.

49. Freund, P. L.; Spiro, M. *J. Phys. Chem.* **1985,** *89* (7), 1074-1077.

50. Kumar, S.; Gandhi, K.; Kumar, R. *Ind. Eng. Chem. Res.* **2007,** *46* (10), 3128-3136.

51. Gammons, C. H.; Yu, Y.; Williams-Jones, A. *Geochim. Cosmochim. Acta* **1997,** *61* (10), 1971-1983.

52. Davies, A. E. *J. Phys. Chem.* **1929,** *33* (2), 274-284.

53. LaMer, V. K.; Dinegar, R. H. *J. Am. Chem. Soc.* **1950,** *72* (11), 4847-4854.

54. Turkevich, J.; Stevenson, P. C.; Hillier, J. *J. Phys. Chem.* **1953,** *57* (7), 670-673.

55. Enustun, B. V.; Turkevich, J. *J. Am. Chem. Soc.* **1963,** *85* (21), 3317-3328.

56. Turkevich, J. *Gold Bull. 18* (3), 86-91.

57. Turkevich, J. *Gold Bull. 18* (4), 125-131.

58. Takiyama, K. *Bull. Chem. Soc. Jpn.* **1958,** *31*, 944.

59. Zukoski, C. Chapter 15. In *Particulate two-phase flow*, Butterworth-Heinemann Boston, 1993.

60. Chow, M. K.; Zukoski, C. F. *J. Colloid Interface Sci.* **1994,** *165* (1), 97-109.

61. Biggs, S.; Chow, M. K.; Zukoski, C. F.; Grieser, F. *J. Colloid Interface Sci.* **1993,** *160* (2), 511-513.

62. Kimling, J.; Maier, M.; Okenve, B.; Kotaidis, V.; Ballot, H.; Plech, A. *J. Phys. Chem. B.* **2006,** *110* (32), 15700-15707.

63. Pong, B.-K.; Elim, H. I.; Chong, J.-X.; Ji, W.; Trout, B. L.; Lee, J.-Y. *J. Phys. Chem. C* **2007,** *111* (17), 6281-6287.

64. Ostwald, W. *Z. phys. Chem* **1897,** *22* (3), 289-330.

65. Voorhees, P. W. *J. Stat. Phys.* **1985,** *38* (1-2), 231-252.

66. Biggs, S.; Mulvaney, P.; Zukoski, C. F.; Grieser, F. *J. Am. Chem. Soc.* **1994,** *116* (20), 9150-9157.

67. Park, J.-W.; Shumaker-Parry, J. S. *J. Am. Chem. Soc.* **2014,** *136* (5), 1907-1921.

68. Mpourmpakis, G.; Vlachos, D. G. *Phys. Rev. Lett.* **2009,** *102* (15), 155505.

69. Wagener, P.; Schwenke, A.; Barcikowski, S. *Langmuir* **2012,** *28* (14), 6132-6140.

70. Shiv Shankar, S.; Bhargava, S.; Sastry, M. *J. Nanosci. Nanotechnol.* **2005,** *5* (10), 1721-1727.

71. Pei, L.; Mori, K.; Adachi, M. *Langmuir* **2004,** *20* (18), 7837-7843.

72. Liu, Z.; Zu, Y.; Guo, S. *Appl. Surf. Sci.* **2009,** *255* (11), 5827-5830.

73. Qiu, P.; Mao, C. *J. Nanopart. Res.* **2009,** *11* (4), 885-894.

74. Patungwasa, W.; Hodak, J. H. *Mater. Chem. Phys.* **2008,** *108* (1), 45-54.

75. Vujačić, A.; Vasić, V.; Dramićanin, M.; Sovilj, S. P.; Bibić, N. a.; Milonjić, S.; Vodnik, V. *J. Phys. Chem. C* **2013,** *117* (13), 6567-6577.

76. Techane, S. D.; Gamble, L. J.; Castner, D. G. *J. Phys. Chem. C* **2011,** *115* (19), 9432-9441.

77. Nehl, C. L.; Hafner, J. H. *J. Mater. Chem.* **2008,** *18* (21), 2415-2419.

78. Dahmen, C.; von Plessen, G. *Aust. J. Chem.* **2007,** *60* (7), 447-456.

79. Haiss, W.; Thanh, N. T. K.; Aveyard, J.; Fernig, D. G. *Anal. Chem.* **2007,** *79* (11), 4215-4221.

80. Zhou, M.; Chen, S.; Zhao, S. *J. Phys. Chem. B.* **2006,** *110* (10), 4510-4513.

81. Malikova, N.; Pastoriza-Santos, I.; Schierhorn, M.; Kotov, N. A.; Liz-Marzán, L. M. *Langmuir* **2002,** *18* (9), 3694-3697.

82. Huang, H.; Yang, X. *Biomacromolecules* **2004,** *5* (6), 2340-2346.

83. Xia, Y.; Xiong, Y.; Lim, B.; Skrabalak, S. E. *Angew. Chem. Int. Ed.* **2009,** *48* (1), 60-103.

84. Ashkarran, A. A.; Bayat, A. *Int. Nano Lett.* **2013,** *3* (1), 50.

85. Zhang, S.; Bao, K.; Halas, N. J.; Xu, H.; Nordlander, P. *Nano Lett.* **2011,** *11* (4), 1657-1663.

86. Chang, S.-S.; Shih, C.-W.; Chen, C.-D.; Lai, W.-C.; Wang, C. R. C. *Langmuir* **1998,** *15* (3), 701-709.

87. Link, S.; El-Sayed, M. A. *J. Phys. Chem. B.* **1999,** *103* (40), 8410-8426.

88. Ung, T.; Liz-Marzán, L. M.; Mulvaney, P. *J. Phys. Chem. B.* **2001,** *105* (17), 3441-3452.

89. Wall, J. F.; Grieser, F.; Zukoski, h. F. *J. Chem. Soc., Faraday Trans.* **1997,** *93* (22), 4017-4020.

90. Kumar, S.; Nann, T. *Small* **2006,** *2* (3), 316-329.

91. Ringe, E.; Van Duyne, R. P.; Marks, L. D. *J. Phys. Chem. C* **2013,** *117* (31), 15859-15870.

92. Xiao, J.; Qi, L. *Nanoscale* **2011,** *3* (4), 1383-1396.

93. Cheong, S.; Watt, J. D.; Tilley, R. D. *Nanoscale* **2010,** *2* (10), 2045-2053.

94. Viswanath, B.; Kundu, P.; Halder, A.; Ravishankar, N. *J. Phys. Chem. C* **2009,** *113* (39), 16866-16883.

95. Ren, J.; Tilley, R. D. *Small* **2007,** *3* (9), 1508-1512.

96. Pérez-Juste, J.; Liz-Marzán, L. M.; Carnie, S.; Chan, D. Y. C.; Mulvaney, P. *Adv. Funct. Mater.* **2004,** *14* (6), 571-579.

97. Xie, J.; Lee, J. Y.; Wang, D. I. C. *J. Phys. Chem. C.* **2007,** *111* (28), 10226-10232.

98. Rai, A.; Singh, A.; Ahmad, A.; Sastry, M. *Langmuir* **2006,** *22* (2), 736-741.

Chapter 3: Galactose-capped gold nanoparticles for the colorimetric detection of heat-labile enterotoxin

3.1. Objective

The aim of this chapter was to develop a simple and rapid colorimetric sensing system for the B-subunits of heat-labile enterotoxin (LTB) using thiol-modified galactose capped glycogold nanoparticles (Gal-gAuNPs). The Gal-gAuNP-based colorimetric sensor described in this chapter is a step towards the development of a size-optimised, easy to use, cheap, selective, highly sensitive, and fast sensing platform for the detection of LTB.

3.2. Introduction

3.2.1. AuNP-based colorimetric assays

AuNP-based colorimetric assays have attracted significant interest over the past decade. The major advantages of AuNP-based colorimetric assays are:

1. Facile methods established for binding AuNPs to a wide variety of ligands.[1]

   It has been shown that a wide variety of molecules: sugars, ranging from monosaccharides to oligosaccharides, peptides and proteins, antibodies, dendrimers, drug molecules, DNA, and lipids can be bound to the surface of AuNPs.[1]

2. High extinction coefficients of AuNPs.[2]

   The molar extinction coefficient of AuNPs of 13 nm diameter is 2.7×10^8 $M^{-1}cm^{-1}$, which is around 1000 times higher than that of traditional organic dyes.[2] Thus,

AuNP solutions exhibit colour at nanomolar concentrations, allowing the detection of even small amounts of analytes with the naked eye.

3. The distinctive colour change of AuNP solutions.

   If the presence of the target analyte results in the aggregation of the NPs, the solution colour changes from red to purple/blue, and vice versa in the case of the redispersion of the aggregates (purple/blue to red).[3]

4. Simplicity and wide applicability.[3]

   The detection of target analytes using AuNP-based colorimetric assays is possible with the naked eye or with a UV-Vis spectrophotometer, which is commonly found in every Chemistry laboratory.

All these benefits make AuNPs an ideal choice to form the basis of a colorimetric sensor for a plethora of analytes.[4] To date, AuNP-based colorimetric sensors have been used to detect alkali and alkaline earth metal ions,[5-6] heavy metal ions,[7] lanthanides,[8] anions,[9] organic molecules,[10] oligonucleotides,[11] and proteins.[4, 12]

3.2.2. gAuNP-based colorimetric detection of toxic lectins

Lectins are carbohydrate-binding proteins that are highly specific for sugar moieties.[13] Generally a lectin contains two or more carbohydrate binding sites, whilst some lectins also form oligomeric structures, which therefore possess with multiple binding sites. A series of carbohydrates units present on the surface of one cell interact with the binding sites of lectins on the surface of another cell. In this way a number of relatively weak but specific interactions join the lectins and carbohydrates.

These interactions between the lectins and the carbohydrates resemble the action of Velcro; the interaction between each unit is relatively weak but the overall binding is strong.[13] Though lectins are essential for various biological functions in animals, there are certain plant lectins that are amongst the most poisonous compounds known. For example, extracts from the seeds of *Ricinus communis* (castor beans) and *Abrus precatorious* contain the lectins ricin and abrin respectively; consumption of these toxins even in small quantities can be lethal and can cause irreversible inhibition of host cellular protein synthesis and death of affected tissues and organs.[14-15]

Colorimetric sensors based on gAuNPs have been used to detect various toxic lectins. Otsuka *et al.* have shown that the AuNPs modified with α-lactosyl-ω-mercapto-poly(ethylene glycol) can be used to detect the lectin *Ricinus communis* agglutinin (RCA_{120}) - a ricin surrogate.[16] Hone *et al.* have developed a thiolated mannose-stabilized AuNP sensor, which was used to detect the lectin concanavalin A (Con A).[17] Con A, a toxic lectin isolated from the jack bean *Canavalia ensiformis*, causes agglutination of red blood cells, followed by hemolysis, and eventual cell death.[18] Schofield *et al*. have developed thiolated galactose-stabilized and thiolated lactose-stabilized AuNP sensors for the detection of RCA_{120} and cholera toxin respectively.[19,20] Cholera toxin, a lectin secreted by the bacterium *Vibrio cholerae*, is the pathogenic agent responsible for cholera, an acute infection affecting the intestine.[21] Recently, Wei *et al*. have shown that the AuNPs modified with structural analogues of sialylglycan can be used for the detection of influenza viral hemagglutinin.[22]

3.2.3. Effect of ligand density snd length, and size of AuNPs on their colorimetric detection

gAuNPs are typically synthesised by attaching saccharides or glycoconjugates to the surface of AuNPs *via* thiol-terminated linkers. Previous studies have shown that both the length of the linker and the density of the ligands on the gAuNP surface can affect the efficacy of subsequent colorimetric sensing assays.[16, 19,23-28] The chain length of the thiolated linker that binds the sugar to the AuNP surface has an influence on both the stability and the sensitivity of the gAuNPs.[4] The general trend observed is that ligands with a longer chain give a more stable monolayer, whilst a shorter chain length results in better detection limits for colorimetric aggregation assays.[4] The sugar density on the gAuNP surface is an important parameter that has a direct effect on the multivalent interaction between gAuNPs and lectins, and hence in the colorimetric aggregation assays. Previous studies have shown that the ligand density on the gAuNPs required for the optimal aggregation of the NPs depends on the specific lectin under investigation.[4]

It has been shown that size of AuNPs also has an influence on their performance in colorimetric sensing.[29-32] Krpetić *et al.* have shown the effect of AuNP size in the efficiency of colorimetric assays employing a model system for Ni^{2+} ion detection.[30] AuNPs with 45 nm diameter were found to be the optimal sensor for the detection of Ni^{2+} ions. Niikura *et al*. have studied the effect of the particle size in the efficiency of colorimetric bioassays.[31] AuNPs of 5, 10, and 15 nm diameter were capped with a

thiolated sialic acid derivative and used for the colorimetric detection of John Cunningham (JC) virus.[31] Optical detection of virus was only achieved with the 15 nm sized gAuNPs. Although the majority of the reported gAuNP-based colorimetric assays have used 8-20 nm diameter gAuNPs, there has been no specific study into the effect of gAuNP size on the colorimetric sensing of toxic lectins.

3.2.4. Heat-labile enterotoxin

Heat-labile enterotoxin (LT), a lectin secreted by enterotoxigenic *Escherichia coli*, is one of the pathogenic agents responsible for a form of intestinal disease, commonly called 'traveller's diarrhoea.'[33] Although in the case of a healthy adult this disease is either self-limiting or curable with antibiotics, it leads to the deaths of thousands of children per year in underdeveloped countries.[34] LT is a member of the AB_5 bacterial toxin family, which also includes cholera toxin, shiga toxin, shiga-like toxin, and pertussis toxin.[35] LT is very similar to cholera toxin (CT) in terms of structure, sequence, and function.[34] All the AB_5 toxins contain a disease causing A subunit, which is symmetrically surrounded by five carbohydrate binding B-subunits (Figure 3.1).[33] The B-subunits of heat-labile enterotoxin (LTB) bind to the ganglioside GM1, which is present on the surface of mammalian intestinal cells. In the GM1 ganglioside, ceramide is linked to the branched pentasaccharide β-Gal-(1→3)-β-GalNAc-(1→4)-[α-Neu5Ac-(2→3)]-β-Gal-(1→4)-β-Glc-ceramide.[33]

Binding of this pentasaccharide to the carbohydrate recognition domains of LTB is the first step in the entry of the LT into gut cells.[33]

Crystallographic studies have shown that interaction between GM1 and LTB occurs mainly through the terminal galactose residues of GM1; only minimal interactions have been observed between the N-acetylneuraminic acid of GM1 and LTB.[36] The significant contact between LTB and galactose, 79% of which is buried in the binding pocket, explains the high selectivity of LTB for GM1, compared to other gangliosides.[37] X-Ray crystallographic studies of the interaction of LTB with lactose revealed that that the high

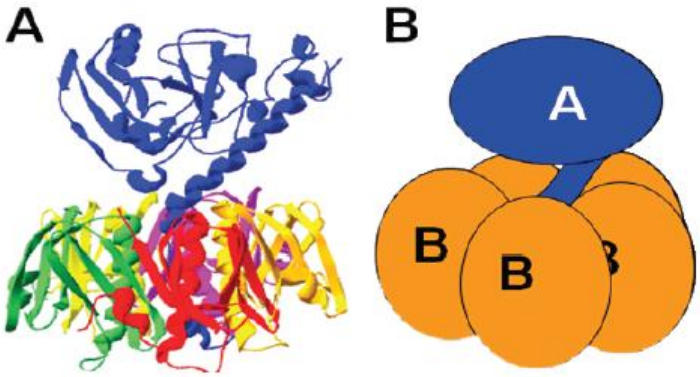

Figure 3.1. (A) LT holotoxin crystal structure and (B) a schematic representation of the subunit arrangement of LT. Adapted from Mudrak *et al*.[33]

specificity for galactose arises from the fact that every hydrogen-bond acceptor and donor of the galactose unit, other than the ring and anomeric oxygens, is involved in hydrogen bonding.[34, 38] Like others in their work on other AB_5 toxins,[20,39-40] we therefore chose galactose as the LTB binding motif for the development of a colorimetric sensing system.

Several methods have already been developed for the detection of LT. These include phenotypic assays based on recognition of monoclonal antibodies (MAbs),[41-47] genotypic methods based on DNA/DNA hybridization,[48] and the use of the polymerase chain

reaction (PCR), or real-time PCR techniques.[49-51] Ito *et al*. have reported that the automatic latex agglutination test is capable of measuring LT at a concentration of 1 ng/mL.[52] Ristaino *et al*. have shown that the least amount of toxin detected by GM1-ELISA was 7 ng/mL.[53] Menezes *et al* have reported that 25 µg/mL of anti-rabbit heat-labile toxin IgG enriched fraction and 10 µg/mL of IgG2B monoclonal antibody allowed the capture of less than 10 ng of the toxin.[54] Spangler *et al*. have used the Spreeta® surface plasmon resonance sensor and a quartz crystal microbalance and have shown that the least amount of toxin detected was 3 to 6 µg/mL,[55] which is similar to the detection level in our study. Although these methods have a high level of sensitivity and specificity, the majority of them require complex instrumentation and involve protracted operating procedures. More recently, colorimetric sensing of the heat-labile enterotoxin gene was reported by Jyoti *et al*.[56] using thiol-modified oligonucleotide capped AuNPs, indicating the desirability of an operationally straightforward colorimetric assay. Interestingly, so far there have been no reports that discuss the use of AuNPs stabilized with simple sugar moieties for the colorimetric detection of heat-labile enterotoxin.

The remaining sections of this chapter will detail the synthesis of Gal-gAuNPs of various sizes, containing AuNP metal cores of 2, 7, 12, and 20 nm, and investigations into their performance for the colorimetric sensing of LTB.

3.3. Results and discussion

3.3.1. Synthesis of the thiol-terminated galactose ligand

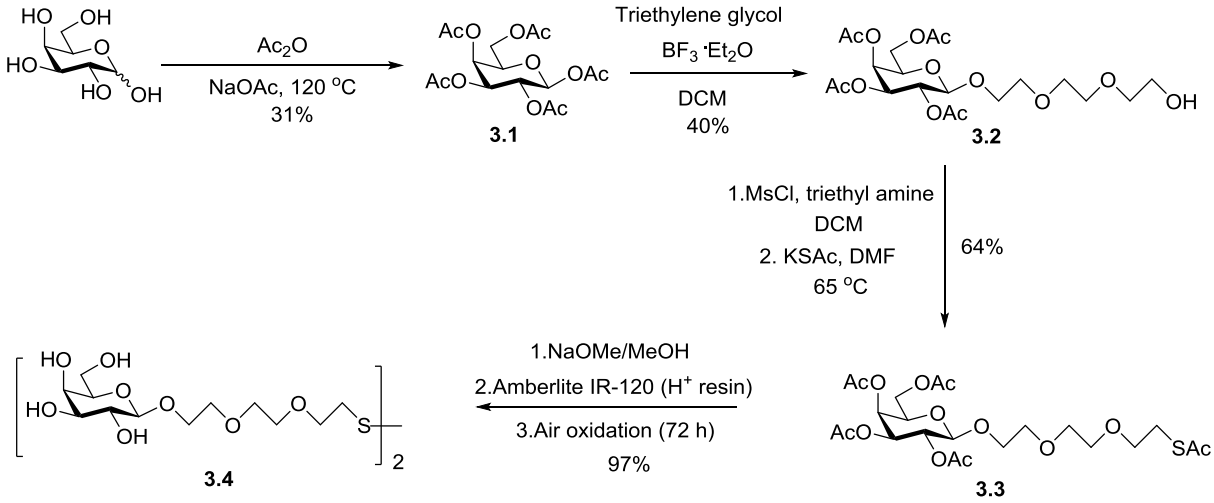

Scheme 3.1. Synthesis of the thiol-terminated galactose ligand.

The known disulfide 3.4 (Scheme 3.1) was accessed by following the procedure of Schofield *et al.* with slight modifications.[19] D-Galactose was acetylated by reaction with acetic anhydride and sodium acetate to give penta-*O*-acetyl-β-D-galactopyranose 3.1 (Scheme 3.1).[57-58] Reaction of 3.1 with triethyleneglycol in the presence of the Lewis acid, $BF_3{\cdot}Et_2O$, afforded the β-triethylene glycol glycoside 3.2.[19] Initially, for the introduction of a thioacetate at the terminus of the linker, alcohol 3.2 was reacted with tosylchloride (TsCl) in pyridine, to form an intermediate tosylate, which could be used to obtain the thioacetate 3.3. However, this reaction proved to be problematic, presumably due to the presence of water in the pyridine used. As an alternative approach, alcohol 3.2 was reacted with mesylchloride (MsCl) and triethylamine in DCM, to form an intermediate mesylate, which was then reacted with potassium thioacetate in DMF to

afford the thioacetate 3.3. Global deactylation of 3.3 by reaction with sodium methoxide, followed by air oxidation afforded the disulfide 3.4.[19]

3.3.2. Synthesis and characterization of different sized Gal-gAuNPs

Density of the thiol-terminated sugar ligands on the surface of gAuNPs can be manipulated by introducing additional 'spectator' or 'filler' ligands. By varying the ratio of the sugar ligands and the 'filler' ligands in the synthesis of gAuNPs, the desired sugar density on the surface of gAuNPs can be obtained. In this study, only the thiol-terminated galactose was used as a ligand to synthesize Gal-gAuNPs, so that the effect of the gAuNP size alone on the performance of these systems in colorimetric sensing could be specifically and systematically studied. The 2 nm sized Gal-gAuNPs (**Gal-gAuNP-2**) were synthesized following the procedure of Barrientos *et al.*, a modified version of Brust-Schiffrin method (BSM).[59-60] Disulfide 3.4, dissolved in MeOH, was added to an aqueous solution of $HAuCl_4$. Sodium borohydride, dissolved in water, was then added to reduce the $HAuCl_4$ to obtain **Gal-gAuNP-2** (Scheme 3.2).[59, 61]

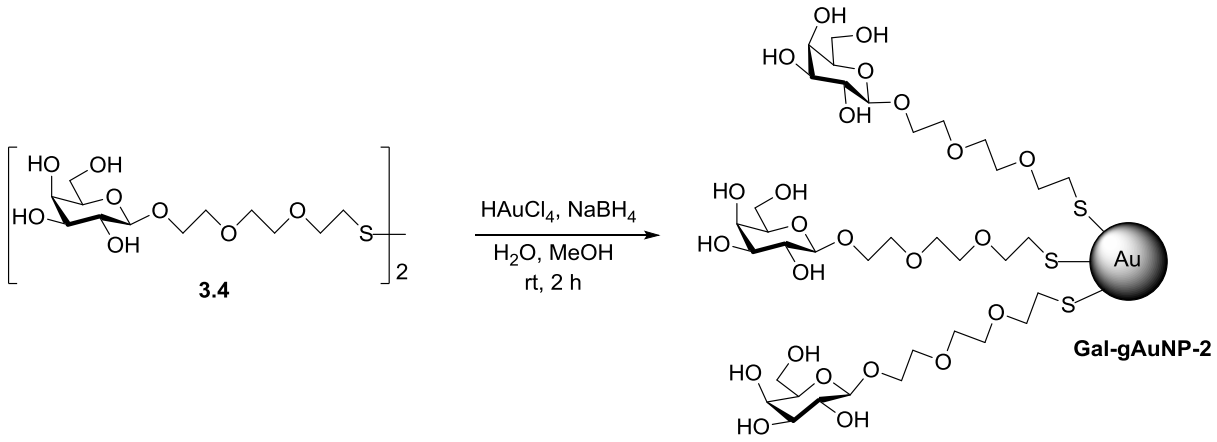

Scheme 3.2. Synthesis of **Gal-gAuNP-2** following a modified version of BSM.

The 7 nm (**Gal-gAuNP-7**), 12 nm (**Gal-gAuNP-12**), and 20 nm (**Gal-gAuNP-20**) sized Gal-gAuNPs were obtained by ligand exchange reactions of Cit-AuNPs of 7, 12, and 20 nm respectively with the disulfide 3.4 (Scheme 3.3).[17] The disappearance of the characteristic IR bands for citrate (at 1400 and 1600 cm^{-1} for the carboxylate and carbonyl groups, see Appendix, Figure A3.1-A3.5)[62] after the reaction of the Cit-AuNPs with the thiol confirmed that the citrate ligands had been were successfully replaced.

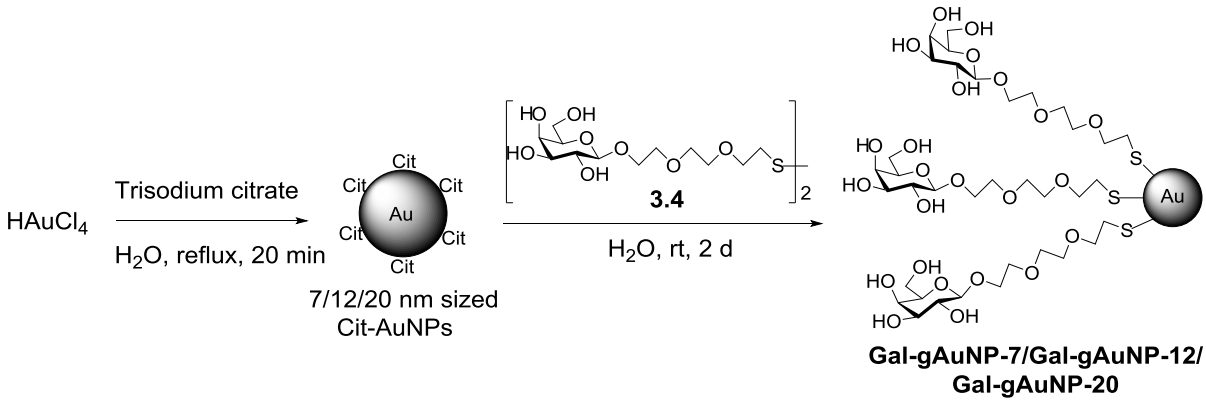

Scheme 3.3. Synthesis of **Gal-gAuNP-7**/**Gal-gAuNP-12**/**Gal-gAuNP-20** by ligand exchange method.

The 12 and 20 nm sized Cit-AuNPs used in these reactions were themselves synthesized using the standard Turkevich reaction.[63] The 7 nm sized Cit-AuNPs were synthesized by following a recently developed procedure by Sivaraman *et al.*[64] In this modified Turkevich process, the addition of a solution of $HAuCl_4$ to a solution of citrate, which is the reverse order compared to the standard Turkevich reaction, produced AuNPs of 7 nm size. Through their kinetic studies, Sivaraman *et al.* have shown that the pH of the reaction mixture and the initial molar ratio of citrate to $HAuCl_4$ both play a crucial role in producing the monodispersed AuNPs of 7 nm size.[64]

Particle size and size distributions (as demonstrated by TEM) and the UV-Vis absorption spectra of all of the AuNPs were essentially the same both before and after ligand exchange, indicating that the AuNP cores had not been affected. Analysis of the TEM images of the Gal-gAuNPs (in each case at least 200 particles were measured) using ImageJ software revealed the particle sizes to be 2.3 ± 0.5, 7.3 ± 0.9, 12.0 ± 1.7, and 20.3 ± 1.8 nm (histograms for the size distribution of the AuNPs are shown in the Appendix Figure A3.6) for **Gal-gAuNP-2**, **Gal-gAuNP-7**, **Gal-gAuNP-12**, and **Gal-gAuNP-20** respectively (Figure 3.2).

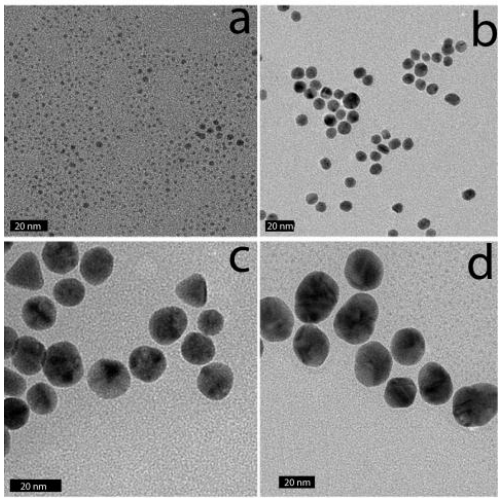

Figure 3.2. Representative TEM images of Gal-gAuNPs: a) **Gal-gAuNP-2**, b) **Gal-gAuNP-7,** c) **Gal-gAuNP-12,** and d) **Gal-gAuNP-20**. The scale bar is 20 nm.

It is known that as AuNPs increase in size, the corresponding SPR peaks in the UV-Vis absorption spectra shift toward longer wavelengths.[65] Here, the absorption maxima for **Gal-gAuNP-7, Gal-gAuNP-12,** and **Gal-gAuNP-20** were found to be 518, 523, and 527 nm respectively (Figure 3.3) whilst **Gal-gAuNP-2** had an absorption shoulder at 506 nm. ESI-MS and FT-IR analysis (see Appendix) also confirmed that the galactose ligands had been successfully incorporated. The average molecular formula of the Gal-gAuNPs was determined through TGA (see Appendix Figure A3.7-A3.10), and was also confirmed by elemental analysis. The average molecular formulae were found to be $Au_{377}(C_{12}H_{24}O_8S)_{162,}$ $Au_{12060}(C_{12}H_{24}O_8S)_{2181,}$ $Au_{53568}(C_{12}H_{24}O_8S)_{3074,}$ and $Au_{259328}(C_{12}H_{24}O_8S)_{9761}$ for **Gal-gAuNP-2, Gal-gAuNP-7, Gal-gAuNP-12** and **Gal-gAuNP-20** respectively.

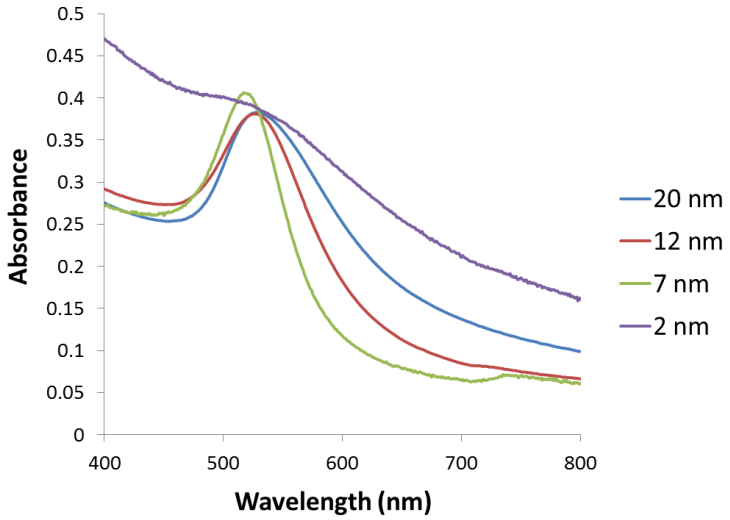

Figure 3.3. UV-Vis absorbance spectra of the Gal-gAuNPs.

The number of Au atoms (N_{Au}) and the number of thiolate ligands (N_L) per NP was calculated according to the following equation:[66-67]

$$N_{Au} = \frac{V_{NP} \text{ x APF}}{V_{Au}} = \frac{4\pi \frac{r_{NP}^3}{3} \text{x } 0.7405}{4\pi r_{Au}^3/3} = \frac{\left(\frac{d_{NP}}{2}\right)^3 \text{x } 0.7405}{0.144^3} = d_{NP}^3 \text{ x } 31$$

$m_{Au} = N_{Au}$ x 196.97

$m_L = m_{Au}$ x (wt% of L/ wt% of Au)

$N_L = m_L / M_L$

where V_{NP} is the volume of a spherical AuNP, V_{Au} is the volume of a Au atom, APF is atomic packing factor, r_{NP} and d_{NP} are the radius and the diameter of a AuNP, and r_{Au} is the radius of a Au atom. m_{Au}, m_L, and M_L are the mass of the Au atoms in the NP, mass of the ligands in the NP, and the molecular mass of the ligand respectively. The wt% of the ligand (L) and wt% of Au are obtained from TGA.

3.3.3. The effect of Gal-gAuNP size on the efficacy of colorimetric detection of LTB

To investigate the effect of the size of the Gal-gAuNPs on the colorimetric detection of LTB, purified Gal-gAuNPs with particle sizes 2, 7, 12, and 20 nm were freeze-dried, and then re-suspended in phosphate buffer (10 mM, pH 7.2) to give a NP concentration of 10 nM. A series of solutions with a range of LTB concentrations (300, 600, 900 and 1200 nM) were prepared separately in Milli-Q water. Then, an aliquot of each of the LTB solutions (150 μl) was added (with mixing) to an aliquot of the Gal-gAuNP solution (150 μl), and the progress of the reaction was monitored by UV-Vis spectroscopy, recording the absorption at 620 nm prior to recording of the whole UV-Vis absorbance spectrum.

Interestingly, it was found from both TEM and UV-Vis studies that **Gal-gAuNP-2** did not undergo any aggregation upon the addition of LTB; hence **Gal-gAuNP-2** was not suitable for the colorimetric sensing of LTB. However in the cases of the 7, 12, and 20 nm diameter Gal-gAuNPs a correlation was observed between the concentration of the LTB that was added, and the degree of Gal-gAuNP aggregation. In these cases both the red-shift and the intensity of the SPR peak increased with increasing amounts of LTB due to the formation of larger Gal-gAuNP aggregates.[17]

TEM analysis (Figure 3.4b-d) clearly showed that, following the addition of LTB, the Gal-gAuNPs were no longer present as individual particles, but had assembled into networks of aggregated NPs, except in the case of **Gal-gAuNP-2** (Figure 3.4a). LTB detection was possible with the naked eye as the colour of the colloidal solution changed from ruby red to purple upon Gal-gAuNP aggregation (Figure 3.5).

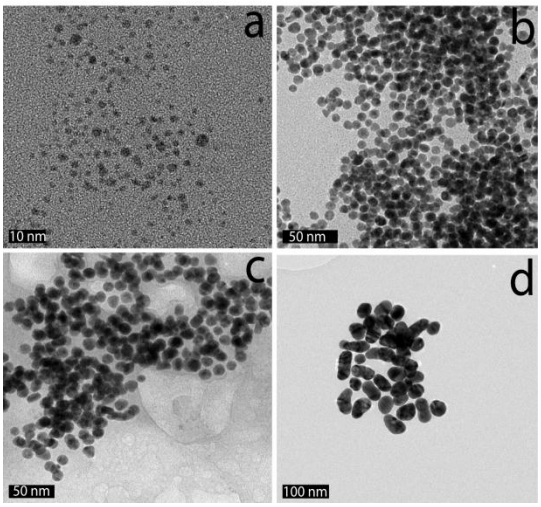

Figure 3.4. Representative TEM images of Gal-gAuNPs after the addition of LTB: non-aggregated a) **Gal-gAuNP-2** (with 10 μM LTB) and aggregated b**) Gal-gAuNP-7,** c) **Gal-gAuNP-12**, and d) **Gal-gAuNP-20** with (600 nM LTB).

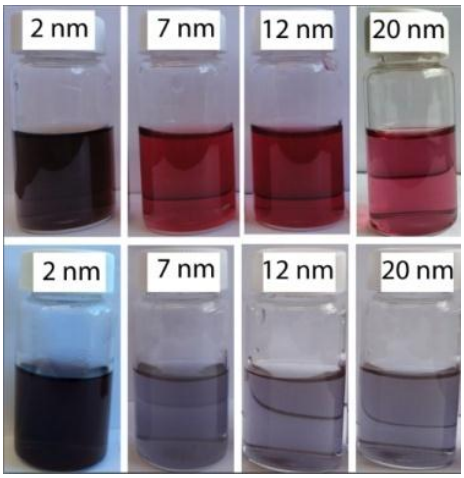

Figure 3.5. Gal-gAuNPs of various sizes before (top row) and after (bottom row) the addition of LTB (600 nM).

As shown in Figure 3.6a, the original SPR peak of **Gal-gAuNP-7**, centred at 518 nm, did not undergo a significant shift when LTB was added to give final LTB concentrations of either 150 or 300 nM. However, when the final LTB concentration was increased to 450 nM, the SPR peak shifted to 536 nm and the solution turned purple, indicating that

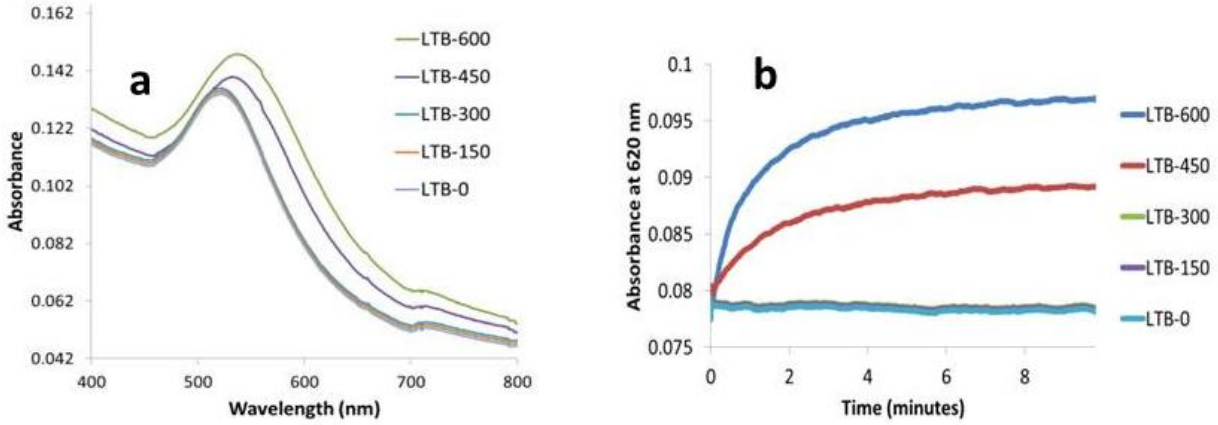

Figure 3.6. UV-Vis absorption spectra of **Gal-gAuNP-7**: (a) with varying nM concentrations of LTB (each spectrum was recorded 10 min after mixing with LTB) and (b) time dependence of absorbance at 620 nm.

significant aggregation of the Gal-gAuNPs had occurred. When the LTB concentration was increased further to 600 nM, an even more pronounced red-shift was observed, and the SPR maximum moved to 542 nm. Kinetic studies of these reactions were also carried out by monitoring the time dependence of changes in the absorption at 620 nm (Figure 3.6b).[19,20] At final LTB concentrations of 450 and 600 nM, 95% of the total increase in absorbance (I_{95}) occurred within two minutes, whilst 99% of the total increase (I_{99}) occurred within 5 minutes, indicating that aggregation of the Gal-gAuNPs was relatively fast, and that rapid detection of LTB is possible by this method.

With **Gal-gAuNP-12** (Figure 3.7a), aggregation was even observed after the addition of only 150 nM LTB. Therefore even lower LTB concentrations were used in order to determine the minimum detection limit of LTB by **Gal-gAuNP-12**. Although no SPR peak shift was observed using 50 nM LTB, at 100 nM a shift in the SPR peak was observed from 523 to 528 nm. These results indicated that **Gal-gAuNP-12** was more

effective than the **Gal-gAuNP-7** for the colorimetric detection of LTB. With **Gal-gAuNP-12**, when the LTB concentration was increased from 150 to 600 nm, the SPR maxima shifted gradually from 533 to 557 nm, indicating increased aggregation. Kinetic studies of **Gal-gAuNP-12** aggregation (Figure 3.7b), again involving monitoring the absorbance at 620 nm, revealed that I_{95} occurred within 2 minutes and that I_{99} occurred within 4.5 minutes at all LTB concentrations investigated (100-600 nM).

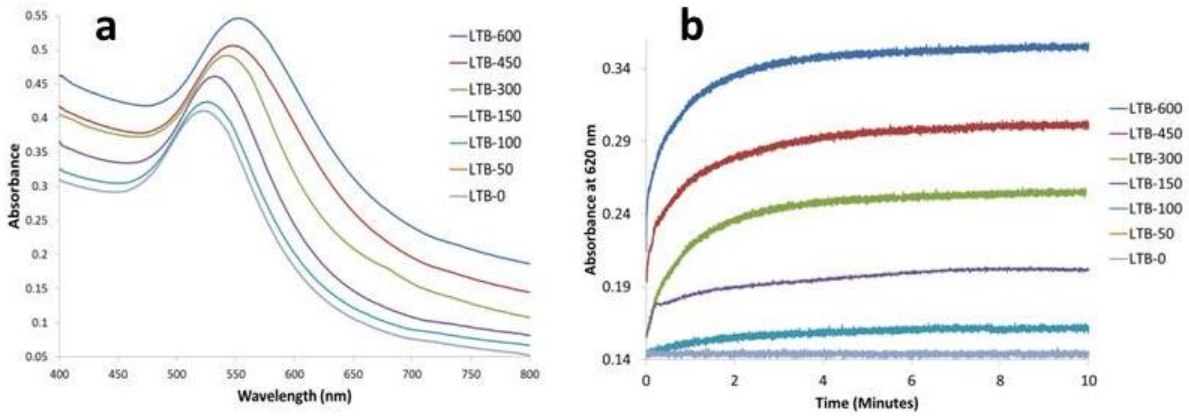

Figure 3.7. UV-Vis absorption spectra of **Gal-gAuNP-12**: (a) with varying nM concentrations of LTB (each spectrum was recorded 10 min after mixing with LTB) and (b) time dependence of absorbance at 620 nm.

When the size of the Gal-gAuNPs was further increased to 20 nm, the minimum concentration of LTB required to produce a red-shift of the SPR maximum was found to be 300 nM, i.e. a higher LTB concentration than was required for **Gal-gAuNP-12,** but lower than for **Gal-gAuNP-7** (Figure 3.8a). Kinetic data obtained for **Gal-gAuNP-20** are shown in Figure 3.8b; similarly to the cases of both **Gal-gAuNP-7** and **Gal-gAuNP-12**, I_{95} occurred within two minutes, and I_{99} occurred within 5 minutes.

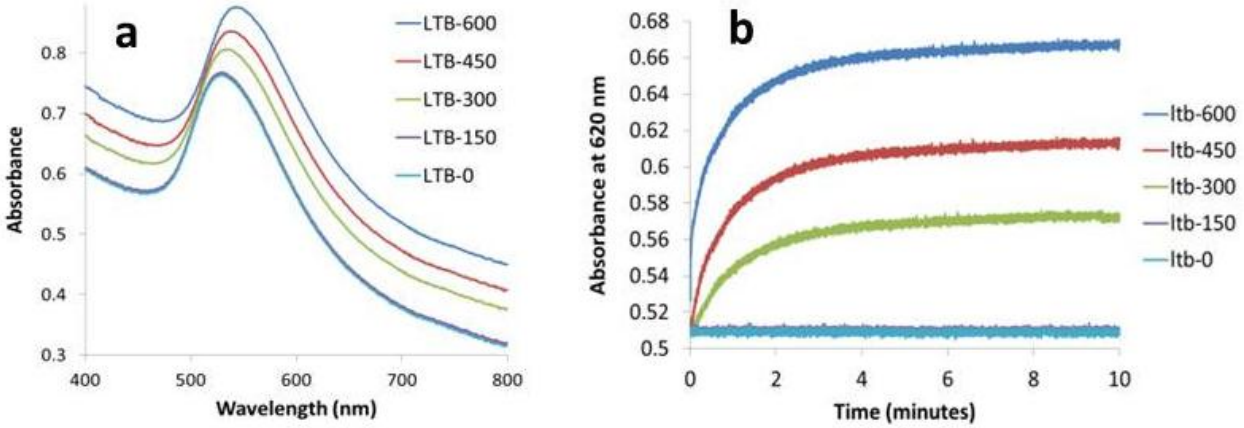

Figure 3.8. UV-Vis absorption spectra of **Gal-gAuNP-20:** (a) with varying nM concentrations of LTB (each spectrum was recorded 10 min after mixing with LTB) and (b) time dependence of absorbance at 620 nm.

To further understand the size-dependence of LTB detection by the Gal-gAuNPs, the ratio of the absorbance intensity measured at 620 nm with and without LTB ($[I^{LTB}/I^{0}]_{620}$) was plotted against the LTB concentration for all of the Gal-gAuNPs (Figure 3.9). These data show that **Gal-gAuNP-12** was not only capable of detecting LTB at much lower concentrations, but also that the increase in absorbance intensity that was observed as the LTB concentration was increased was much higher for **Gal-gAuNP-12** as compared to the other Gal-gAuNPs.

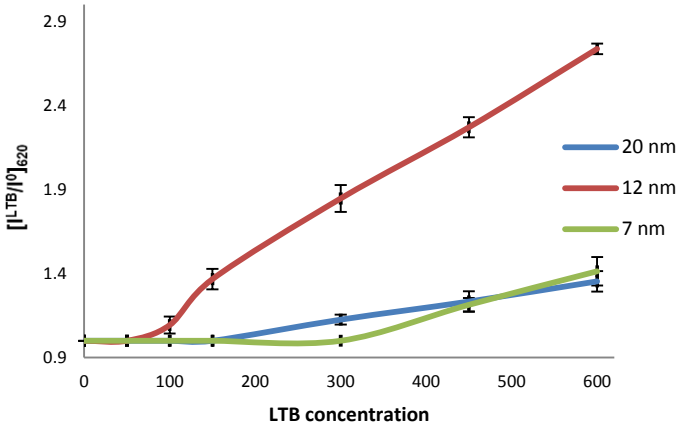

Figure 3.9. Plot of the ratio of the absorbance intensity at 620 nm both with and without LTB *vs* LTB concentration for Gal-gAuNPs of different sizes. Each point is the average of three measurements with the error bars representing the standard error.

In the cases of the 7, 12, and 20 nm Gal-gAuNPs the NP concentration used for the colorimetric study was 10 nM. In the case of **Gal-gAuNP-2** a much higher NP concentration (1 µM) was required because at a AuNP concentration of 10 nM absorption by the colloid was too low to be detected by the UV-Vis spectrometer; this was due to a combination of the significantly lower total amount of Au present, and a low extinction coefficient, which decreases as particle size decreases.[68-69] At the much higher concentration of 1 µM, it was anticipated that a higher concentration of LTB would be required to aggregate **Gal-gAuNP-2**. However even with a correspondingly higher concentration of LTB (10 µM, *i.e.* the same overall molar ratio which caused the onset of the SPR shift for **Gal-gAuNP-12**), no shift in the SPR peak was observed, and TEM (Figure 3.4a) confirmed that the **Gal-gAuNP-2** had not aggregated in the presence of LTB. Moreover the 2 nm sized **Gal-gAuNP-2** are not ideally suited to colorimetric sensing since they fall at the borderline of non-metallic/metallic NPs; as a result they have a shoulder peak instead of a prominent SPR peak in their UV-Vis spectrum (Figure

3.3).[70-71] The precise reason why **Gal-gAuNP-12** was more effective at detecting LTB than either **Gal-gAuNP-7** or **Gal-gAuNP-20** is not yet clear, and further investigations are required in order to adequately explain this finding. Furthermore, whether this size-related phenomenon is specific to this particular toxin, or is dependent on the spatial arrangement of the different carbohydrate-binding sub-units of the toxin, also remains to be demonstrated.

3.3.4. Gal-gAuNP aggregation in the presence of LTB

A pictorial representation of the LTB-induced aggregation of Gal-gAuNPs, based on previous reports on related analyte-induced aggregation-effected sensors,[4, 20] is shown in Figure 3.10. The performance of a AuNP-based colorimetric sensing system depends on how efficiently the AuNP dispersion is converted to AuNP aggregates, or vice versa, in the presence the analyte of interest.

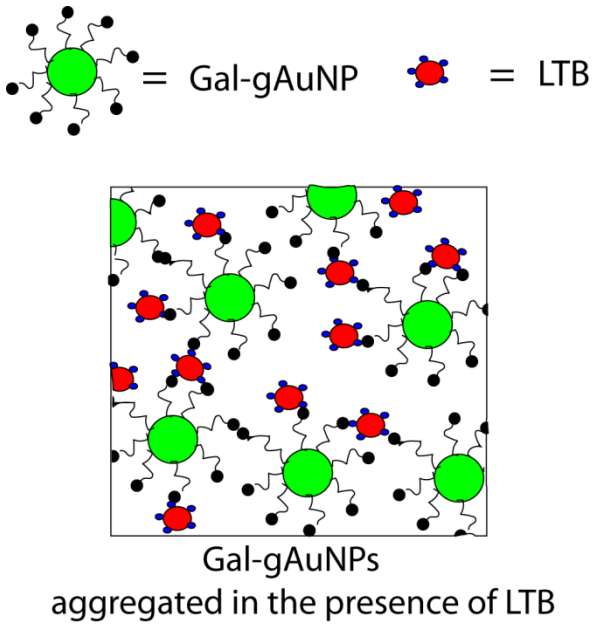

Figure 3.10. Schematic representation of the mechanism of aggregation Gal-gAuNPs in the presence of LTB.

In general, gAuNPs are stabilized against attractive van der Waals forces by steric repulsion of the surface capping ligands; in this study the thiol-terminated galactose ligands.[3] Aggregation of gAuNPs can be achieved in two ways - either *via* non-crosslinking or *via* interparticle crosslinking.[3] In non-crosslinking approach, particle aggregation is achieved by the controlled loss of electrostatic (Figure 3.11A), electrosteric (Figure 3.11B), or steric stabilizations (Figure 3.11C) without any interparticle bond formation.

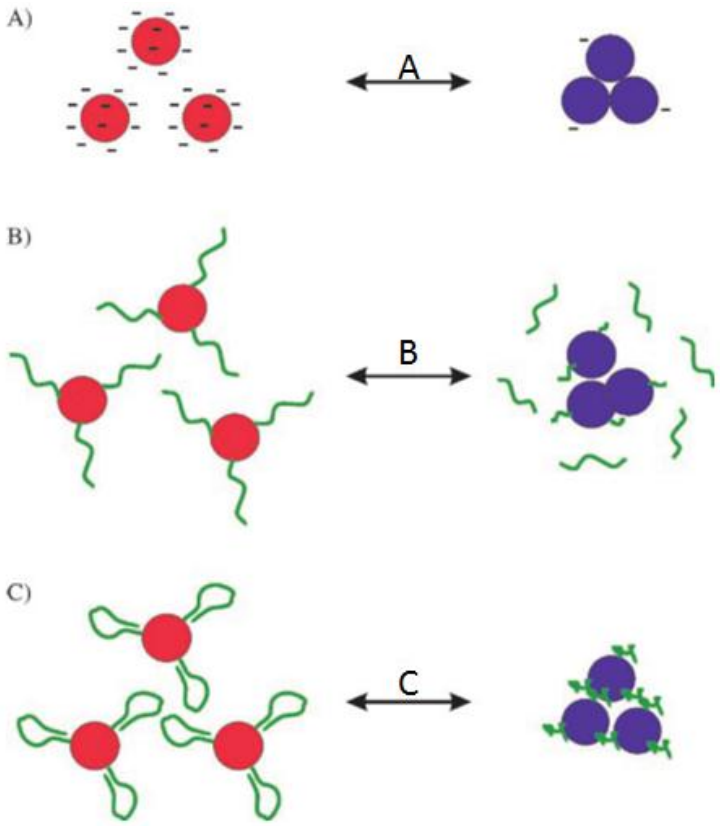

Figure 3.11. AuNP aggregation through non-crosslinking approach. A) In pathway A, AuNPs are aggregated when they lose their electrostatic stabilization provided by small charged molecules on their surface. Representative examples include the use of AuNPs to monitor a biological reaction in which the reactant and product have different effects on the surface charge properties of AuNPs; B) In pathway B, the loss of (electro)steric stabilization for (charged) polymer-stabilized AuNPs, such as the removal of DNA molecules from AuNPs by endonuclease cleavage causes the particle aggregation; C) In Pathway C, (charged) polymer conformational transitions, such as DNA aptamer folding upon binding to its target causes the AuNP aggregation. Image reprinted from Ref. 3.

The alternative interparticle crosslinking aggregation mechanism can works in either of two ways (Figure 3.12). In the first case, particles are made to aggregate by using target analytes (crosslinkers) that possess multiple binding sites for the ligands attached on the surface of AuNPs. In the second case, two sets of AuNPs are used to achieve the aggregation; one set is capped with receptor molecules and the other set with complementary molecules (anti-receptor). The direct interaction between these two set of AuNPs results in particle aggregation.[3]

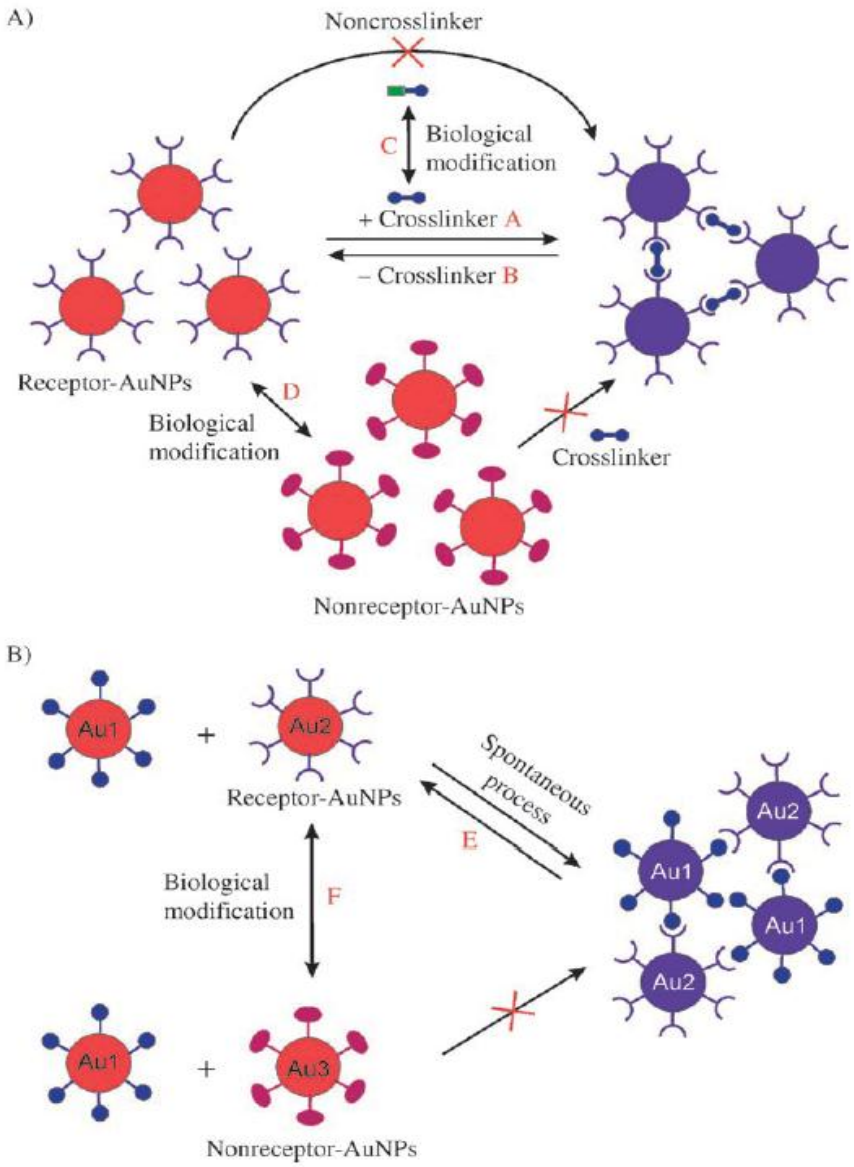

Figure 3.12. AuNP aggregation through interparticle crosslinking approach. A) In pathway A, AuNPs are aggregated by crosslinkers that posess multiple binding sites for the ligands on AuNP surface. In pathway B, the processes that remove crosslinkers deaggregates the AuNPs. Processes that modifies the crosslinkers (pathway C) or the ligands on AuNP surface (pathway D) controls the particle aggregation and dispersion. B) AuNP aggregation is achieved by direct interaction (without any crosslinker molecules) of receptor- and anti-receptor-capped AuNPs. Processes that remove these direct interactions result in deaggregation (pathway E). The aggregation can also be controlled by processes that alter the surface-bound receptors (pathway F). Image reprinted from Ref. 3. Copyright (2016) WILEY-VCH Verlag GmbH & Co. KGaA.

Interparticle crosslinking aggregation can be postulated as the basis of the sensing response reported here; controlled aggregation of the Gal-gAuNPs occurs because of binding of the multiple galactose recognition domains present in LTB to the galactose moieties present on the Gal-gAuNPs.[33]

3.3.5. Stability and selectivity of the Gal-gAuNPs

In order to demonstrate the selectivity of toxin detection aliquots of a **Gal-gAuNP-12** solution were mixed with Bovine Serum Albumin (BSA, aqueous solutions of 300-1200 nM), the lectins ConA and Hemagglutinin (aqueous solutions of 600 nM), and a variety of metal ions and anions (K^+, Na^+, Ca^{2+}, Mg^{2+}, Cl^-, NO_3^-, HCO_3^-, SO_4^{2-}, PO_4^{3-}, all at a concentration of 100 μM). It was found that none of these species had any effect on either the UV-Vis absorption spectrum or the colour of the **Gal-gAuNP-12** solution, confirming that the Gal-gAuNPs did not undergo non-specific aggregation, and that amongst the species investigated the detection was selective for LTB. Furthermore the Gal-gAuNPs were found to be stable in an electrolyte solution (a solution containing Cl^- at 100 mM, Na^+ at 135 mM, K^+ at 15 mM, and HCO_3^- at 45 mM) that was selected to mimic the typical 'watery stool' of diarrhoea patients.[72,73-74] **Gal-gAuNP-12** was then used to detect LTB in this electrolyte solution. A plot of the absorbance intensity at 620 nm *vs* LTB concentration (Figure 3.13) shows that in the electrolyte solution the minimum concentration required for the change in the absorbance at 620 nm was also found to be 100 nM; a similar result to that shown in Figure 3.9. Thus the AuNP sensor was also effective in an ionic environment that was deemed 'typical' of a clinical sample. Gal-

gAuNPs were found to be stable at least for three months at 4 ^{o}C; re-testing them after this time period gave similar results for the detection of LTB.

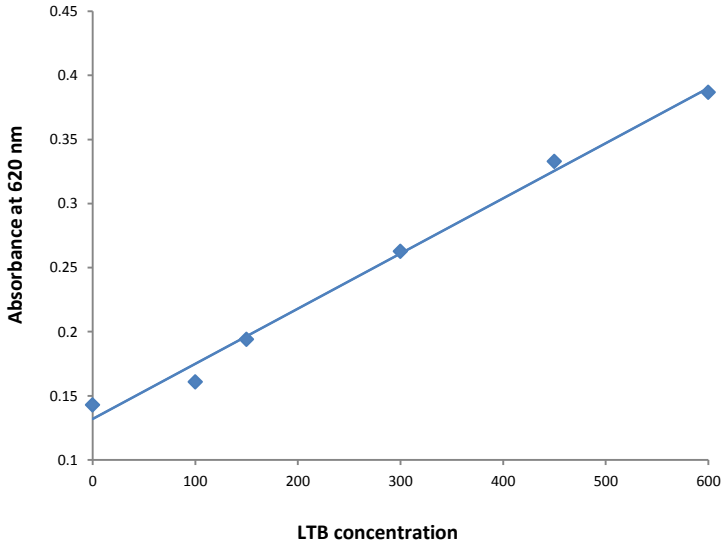

Figure 3.13. Plot of the absorbance intensity at 620 nm *vs* LTB concentration for **Gal-gAuNP-12** in an electrolyte solution selected to mimic the watery stool of diarrhoea patients.

3.4. Conclusions

This chapter has described the synthesis and use of Gal-gAuNPs for the simple and rapid colorimetric detection of LTB at nanomolar concentrations. A series of Gal-gAuNPs of different sizes (2, 7, 12, and 20 nm) were synthesized and assayed for their ability to detect LTB. The presence of multiple binding sites on LTB, together with the specific binding of these receptors to galactose units attached to the Gal-gAuNPs, caused NP aggregation as the basis for LTB detection. The 2 nm Gal-gAuNPs did not aggregate in the presence of LTB, and did not show any shift in the surface plasmon band. However, as the size of the NPs was increased from 7 to 12 and then to 20 nm, the colorimetric

detection level of LTB at first improved from 450 nM down to 100 nM and then declined to 300 nM, indicating that the optimal size for Gal-gAuNPs for the colorimetric detection of LTB was 12 nm. These results indicate that the size of gAuNPs is also an important parameter that should be considered, alongside those of linker-length and the percentage of ligand coverage, in order to construct efficient and optimised colorimetric sensors for toxic lectin detection. Kinetic studies revealed that the response developed within 2 minutes after the addition of LTB. Furthermore the Gal-gAuNPs did not undergo any non-specific aggregation in the presence of BSA, the lectins ConA and hemagglutinin, or various ions.

3.5. References

1. Zhao, P.; Li, N.; Astruc, D. *Coord. Chem. Rev.* **2013,** *257* (3), 638-665.
2. Zhou, Y.; Wang, S.; Zhang, K.; Jiang, X. *Angew. Chem. Int. Ed.* **2008,** *120* (39), 7564-7566.
3. Zhao, W.; Brook, M. A.; Li, Y. *ChemBioChem* **2008,** *9* (15), 2363-2371.
4. Marin, M. J.; Schofield, C. L.; Field, R. A.; Russell, D. A. *Analyst* **2015,** *140* (1), 59-70.
5. Lin, S.-Y.; Liu, S.-W.; Lin, C.-M.; Chen, C.-h. *Anal. Chem.* **2002,** *74* (2), 330-335.
6. Lin, S.-Y.; Chen, C.-h.; Lin, M.-C.; Hsu, H.-F. *Anal. Chem.* **2005,** *77* (15), 4821-4828.
7. Kim, Y.; Johnson, R. C.; Hupp, J. T. *Nano Lett.* **2001,** *1* (4), 165-167.
8. Lisowski, C. E.; Hutchison, J. E. *Anal. Chem.* **2009,** *81* (24), 10246-10253.
9. Beer, P. D.; Gale, P. A. *Angew. Chem. Int. Ed.* **2001,** *40* (3), 486-516.
10. Aslan, K.; Lakowicz, J. R.; Geddes, C. D. *Anal. Chem.* **2005,** *77* (7), 2007-2014.

11. Storhoff, J. J.; Elghanian, R.; Mucic, R. C.; Mirkin, C. A.; Letsinger, R. L. *J. Am. Chem. Soc.* **1998,** *120* (9), 1959-1964.

12. Saha, K.; Agasti, S. S.; Kim, C.; Li, X.; Rotello, V. M. *Chem. Rev.* **2012,** *112* (5), 2739-2779.

13. Berg, J. M.; Tymoczko, J. L.; Stryer, L. *Biochemistry*. 5 ed.; W H Freeman: New york, 2002.

14. Cohen, P.; Van Heyningen, S. *Molecular action of toxins and viruses*. Elsevier: 2012.

15. Walsh, M. J.; Dodd, J. E.; Hautbergue, G. M. *Virulence* **2013,** *4* (8), 774-784.

16. Otsuka, H.; Akiyama, Y.; Nagasaki, Y.; Kataoka, K. *J. Am. Chem. Soc.* **2001,** *123* (34), 8226-8230.

17. Hone, D. C.; Haines, A. H.; Russell, D. A. *Langmuir* **2003,** *19* (17), 7141-7144.

18. Liener, I. *The lectins: properties, functions, and applications in biology and medicine*. Elsevier: 2012.

19. Schofield, C. L.; Mukhopadhyay, B.; Hardy, S. M.; McDonnell, M. B.; Field, R. A.; Russell, D. A. *Analyst* **2008,** *133* (5), 626-634.

20. Schofield, C. L.; Field, R. A.; Russell, D. A. *Anal. Chem.* **2007,** *79* (4), 1356-1361.

21. Minke, W. E.; Roach, C.; Hol, W. G.; Verlinde, C. L. *Biochemistry* **1999,** *38* (18), 5684-5692.

22. Wei, J.; Zheng, L.; Lv, X.; Bi, Y.; Chen, W.; Zhang, W.; Shi, Y.; Zhao, L.; Sun, X.; Wang, F. *ACS nano* **2014,** *8* (5), 4600-4607.

23. Storhoff, J. J.; Lazarides, A. A.; Mucic, R. C.; Mirkin, C. A.; Letsinger, R. L.; Schatz, G. C. *J. Am. Chem. Soc.* **2000,** *122* (19), 4640-4650.

24. Reynolds, A. J.; Haines, A. H.; Russell, D. A. *Langmuir* **2006,** *22* (3), 1156-1163.

25. Wang, X.; Ramström, O.; Yan, M. *Anal. Chem.* **2010,** *82* (21), 9082-9089.

26. Takae, S.; Akiyama, Y.; Otsuka, H.; Nakamura, T.; Nagasaki, Y.; Kataoka, K. *Biomacromolecules* **2005,** *6* (2), 818-824.

27. Bergen, J. M.; von Recum, H. A.; Goodman, T. T.; Massey, A. P.; Pun, S. H. *Macromol. Biosci.* **2006,** *6* (7), 506-516.

28. Marin, M. J.; Rashid, A.; Rejzek, M.; Fairhurst, S. A.; Wharton, S. A.; Martin, S. R.; McCauley, J. W.; Wileman, T.; Field, R. A.; Russell, D. A. *Org. Biomol. Chem.* **2013,** *11* (41), 7101-7107.

29. Zeng, S.; Cai, M.; Liang, H.; Hao, J. *Anal. Methods* **2012,** *4* (8), 2499-2505.

30. Krpetić, Ž.; Guerrini, L.; Larmour, I. A.; Reglinski, J.; Faulds, K.; Graham, D. *Small* **2012,** *8* (5), 707-714.

31. Niikura, K.; Nagakawa, K.; Ohtake, N.; Suzuki, T.; Matsuo, Y.; Sawa, H.; Ijiro, K. *Bioconjugate Chem.* **2009,** *20* (10), 1848-1852.

32. Richards, S.-J.; Fullam, E.; Besra, G. S.; Gibson, M. I. *J. Mater. Chem. B.* **2014,** *2* (11), 1490-1498.

33. Mudrak, B.; Kuehn, M. J. *Toxins* **2010,** *2* (6), 1445-1470.

34. Merritt, E. A.; Sarfaty, S.; Feil, I. K.; Hol, W. G. *Structure* **1997,** *5* (11), 1485-1499.

35. Merritt, E. A.; Hol, W. *Curr. Opin. Struct. Biol.* **1995,** *5* (2), 165-171.

36. Sixma, T. K.; Pronk, S. E.; Kalk, K. H.; Wartna, E. S.; van Zanten, B. A.; Witholt, B.; Hoi, W. G. *Nature* **1991,** *351*, 317-377.

37. Van Den Akker, F.; Feil, I. K.; Roach, C.; Platas, A. A.; Merritt, E. A.; Hol, W. G. J. *Protein Sci.* **1997,** *6* (12), 2644-2649.

38. Sixma, T.; Pronk, S.; Kalk, K.; van Zanten, B. *Nature* **1992**, 365,561-564.

39. Kulkarni, A. A.; Fuller, C.; Korman, H.; Weiss, A. A.; Iyer, S. S. *Bioconjugate Chem.* **2010,** *21* (8), 1486-1493.

40. Chien, Y. Y.; Jan, M. D.; Adak, A. K.; Tzeng, H. C.; Lin, Y. P.; Chen, Y. J.; Wang, K. T.; Chen, C. T.; Chen, C. C.; Lin, C. C. *ChemBioChem* **2008,** *9* (7), 1100-1109.

41. Binsztein, N.; Jouve, M.; Viboud, G.; Moral, L. L.; Rivas, M.; Orskov, I.; Ahren, C.; Svennerholm, A. *J. Clin. Microbiol.* **1991,** *29* (9), 1893-1898.

42. Lopez-Vidal, Y.; Klemm, P.; Svennerholm, A. *J. Clin. Microbiol.* **1988,** *26* (10), 1967-1972.

43. Lopez-Vidal, Y.; Svennerholm, A. *J. Clin. Microbiol.* **1990,** *28* (9), 1906-1912.

44. Qadri, F.; Das, S. K.; Faruque, A.; Fuchs, G. J.; Albert, M. J.; Sack, R. B.; Svennerholm, A.-M. *J. Clin. Microbiol.* **2000,** *38* (1), 27-31.

45. Svennerholm, A.; Wiklund, G. *J. Clin. Microbiol.* **1983,** *17* (4), 596-600.

46. Svennerholm, A.; Wikström, M.; Lindblad, M.; Holmgren, J. *J. Clin. Microbiol.* **1986,** *24* (4), 585-590.

47. Viboud, G. I.; Binsztein, N.; Svennerholm, A. *J. Clin. Microbiol.* **1993,** *31* (3), 558-564.

48. Steinsland, H.; Valentiner-Branth, P.; Grewal, H.; Gaastra, W.; Mølbak, K. å.; Sommerfelt, H. *Diagn. Micr. Infec. Dis.* **2003,** *45* (2), 97-105.

49. Reischl, U.; Youssef, M. T.; Wolf, H.; Hyytia-Trees, E.; Strockbine, N. A. *J. Clin. Microbiol.* **2004,** *42* (9), 4092-4100.

50. Vidal, R.; Vidal, M.; Lagos, R.; Levine, M.; Prado, V. *J. Clin. Microbiol.* **2004,** *42* (4), 1787-1789.

51. Sjöling, Å.; Wiklund, G.; Savarino, S.; Cohen, D.; Svennerholm, A.-M. *J. Clin. Microbiol.* **2007,** *45* (10), 3295-3301.

52. Ito, T.; Kuwahara, S.; Yokota, T. *J. Clin. Microbiol.* **1983,** *17* (1), 7-12.

53. Ristaino, P. A.; Levine, M. M.; Young, C. R. *J. Clin. Microbiol.* **1983,** *18* (4), 808-815.

54. Menezes, C. A.; Imamura, S. Y.; Trabulsi, L. R.; Fernandes-Filho, A.; Martinez, M. B.; Guth, B. E.; Girão, D. M.; Piazza, R. M. *Mem Inst Oswaldo Cruz* **2006,** *101* (8), 875-880.

55. Spangler, B. D.; Wilkinson, E. A.; Murphy, J. T.; Tyler, B. J. *Anal. Chim. Acta* **2001,** *444* (1), 149-161.

56. Jyoti, A.; Singh, S. P.; Yashpal, M.; Dwivedi, P. D.; Shanker, R. *J. Biomed. Nanotechnol.* **2011,** *7* (1), 170-171.

57. Wolfrom, M. L.; Thompson, A.; Inatome, M. *J. Am. Chem. Soc.* **1957,** *79* (14), 3868-3871.

58. Liu, Z.; Byun, H.-S.; Bittman, R. *Org. Lett.* **2010,** *12* (13), 2974-2977.

59. Barrientos, Á. G.; de la Fuente, J. M.; Rojas, T. C.; Fernández, A.; Penadés, S. *Chem. Eur. J.* **2003,** *9* (9), 1909-1921.

60. Brust, M.; Fink, J.; Bethell, D.; Schiffrin, D.; Kiely, C. *J. Chem. Soc., Chem. Commun.* **1995,** (16), 1655-1656.

61. de la Fuente, J. M.; Barrientos, A. G.; Rojas, T. C.; Rojo, J.; Cañada, J.; Fernández, A.; Penadés, S. *Angew. Chem. Int. Ed.* **2001,** *40* (12), 2257-2261.

62. Lin, S.-Y.; Liu, S.-W.; Lin, C.-M.; Chen, C.-h. *Anal. Chem.* **2001,** *74* (2), 330-335.

63. Frens, G. *Nat. Phys. Sci.* **1973,** *241*, 20.

64. Sivaraman, S. K.; Kumar, S.; Santhanam, V. *J. Colloid Interface Sci.* **2011,** *361* (2), 543-547.

65. Haiss, W.; Thanh, N. T. K.; Aveyard, J.; Fernig, D. G. *Anal. Chem.* **2007,** *79* (11), 4215-4221.

66. de La Fuente, J.; Barrientos, A.; Rojas, T.; Rojo, J.; Canada, J.; Fernandez, A.; Penades, S. *Angew. Chem. Int. Ed.* **2001,** *40* (12), 2257.

67. Huang, K.; Ma, H.; Liu, J.; Huo, S.; Kumar, A.; Wei, T.; Zhang, X.; Jin, S.; Gan, Y.; Wang, P. C. *ACS nano* **2012,** *6* (5), 4483-4493.

68. Liu, X.; Atwater, M.; Wang, J.; Huo, Q. *Colloid. Surface. B.* **2007,** *58* (1), 3-7.

69. Jain, P. K.; Lee, K. S.; El-Sayed, I. H.; El-Sayed, M. A. *J. Phys. Chem. B.* **2006,** *110* (14), 7238-7248.

70. Bond, G. C.; Thompson, D. T. *Catal. Rev.* **1999,** *41* (3-4), 319-388.

71. Turner, M.; Golovko, V. B.; Vaughan, O. P. H.; Abdulkin, P.; Berenguer-Murcia, A.; Tikhov, M. S.; Johnson, B. F. G.; Lambert, R. M. *Nature* **2008,** *454* (7207), 981-983.

72. Spangler, B. D. *Microbiol. rev.* **1992,** *56* (4), 622-647.

73. Kaper, J. B.; Morris, J. G.; Levine, M. M. *Clin. Microbiol. Rev.* **1995,** *8* (1), 48-86.

74. Fais, M.; Karamanska, R.; Allman, S.; Fairhurst, S. A.; Innocenti, P.; Fairbanks, A. J.; Donohoe, T. J.; Davis, B. G.; Russell, D. A.; Field, R. A. *Chem. Sci.* **2011,** *2* (10), 1952-1959.

Chapter 4: Influenza virus detection by gold nanoparticles decorated with sialic acid terminated bi-antennary complex N-glycans

4.1. Objective

The aim of this chapter was to develop a simple and rapid colorimetric and DLS-based sensing system for the influenza virus by detection of viral hemagglutinin using thiol-modified sialylglycan capped glycogold nanoparticles (SG-gAuNPs). The SG-gAuNP-based sensor reported in this chapter is a step towards the development of an easy to use, cheap, selective, and highly sensitive sensing platform for the detection of the influenza virus.

4.2. Introduction

4.2.1. AuNP-based colorimetric assay

Constructs comprised of metal NPs attached to a variety of chemical entities with specific binding properties have attracted significant interest in the fields of therapeutics,[1] diagnostics,[2] and sensing.[3-4] AuNPs are particularly suited to such applications for a number of reasons; there are well-established methods for the synthesis of AuNPs with defined sizes and shapes, it is easy to modify their surfaces, and they have excellent stability and biocompatibility.[5-9] In particular, interest in the application of modified AuNPs as colorimetric sensors has increased exponentially over the past decade. A

detailed discussion on the major advantages of AuNP-based colorimetric assays is provided in Chapter 3, Section 3.1.1.

4.2.2. Influenza virus

The influenza virus is a respiratory pathogen which causes an acute febrile respiratory infection in humans and other mammals. Influenza causes regular seasonal epidemics and occasional pandemics in the human population.[10] Recent reports show that seasonal influenza epidemics result in ~300,000 human deaths annually.[11] The influenza virus particle contains two types of surface glycoprotein, neuraminidase (NA) and hemagglutinin (HA), and influenza A viruses are subtyped according to the variations of these two glycoproteins, for example as H1N1.[12] Viral HA is an integral membrane glycoprotein and has a trimeric binding pocket on the globular head of each monomer (Figure 4.1a).[13]

HA from the influenza virus is made up of ~556 amino acids, and accounts for more than 80% of the envelope proteins of the virus.[10,14] One of the essential steps in influenza viral infection is binding of the viral particles to host cells, a process which is mediated by specific interaction between the HA of the virus and sialic acid residues present on the host cell.[15] It has been found that human-adapted influenza viruses preferentially bind to sialylglycans with terminal α(2→6) linkages, whereas avian influenza viruses preferentially bind to α(2→3) linked sialylglycans (Figure 4.1).[16] Whilst the binding constant of HA for a single sialic acid residue is relatively weak (10^3 M^{-1}), the binding constant between the multiple HAs of a viral particle with the multiple sialic acids

present on a host cell has been estimated to be 10^{13} M^{-1}.[17-19] Thus a multivalent effect significantly increases binding, and prevents dissociation of the virus from the host cell.[19]

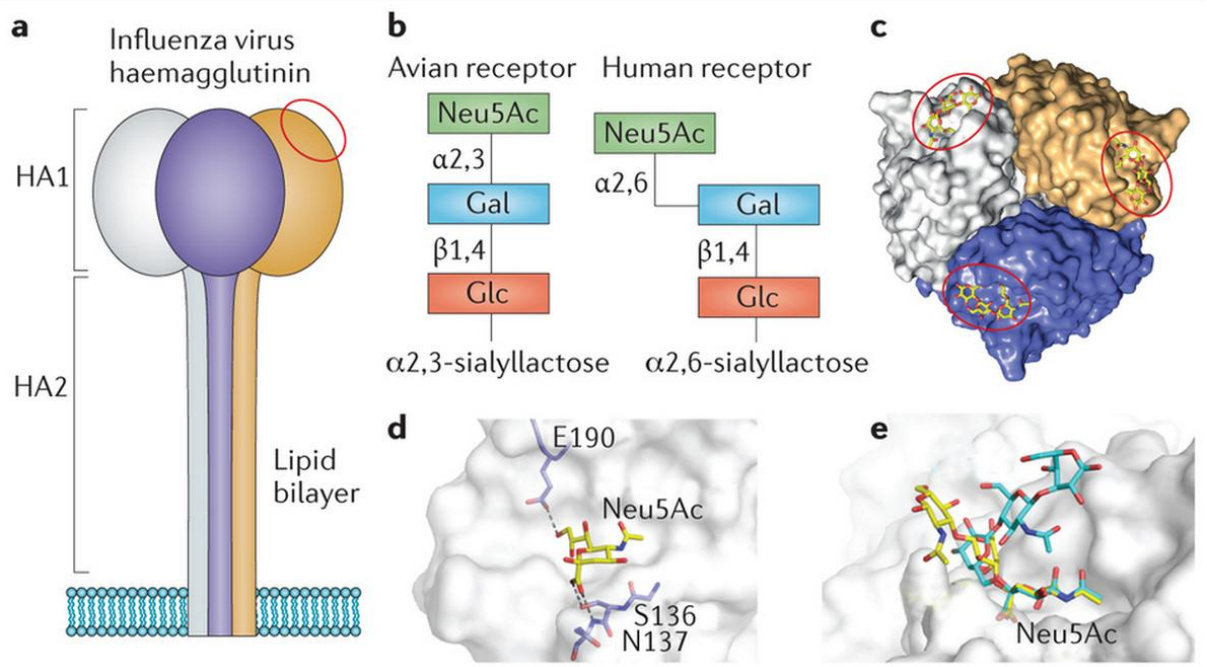

Figure 4.1. a) A schematic representation of the trimeric influenza viral hemagglutinin, with the monomers shown in purple, orange, and grey. Hemagglutinin (HA) is a transmembrane protein that is made of the stalk-like HA2 part and globular HA1 part. Each HA1 domain binds to sialic acid, and the binding site in one monomer is shown with a red circle; **b)** schematics of an example of an avian influenza virus receptor α(2→3)-sialyllactose and a human influenza virus receptor α(2→6)-sialyllactose; **c**) trimeric hemagglutinin surface representation (monomers are shown in grey, orange and purple) in complex with N-acetylneuraminic acid (Neu5Ac) (as a stick representation in yellow) (Protein Data Bank (PDB) accession 1HGG). Red circles show the glycan-binding site; **d**) close-up image of the sugar-binding site of hemagglutinin. Selected important contacts between the Neu5Ac (yellow) and hemagglutinin residues Ser136, Asn137, and Glu190 (purple) are highlighted (grey dashes). The sugar moieties are depicted in stick representation, with nitrogen atoms in blue and oxygen atoms in red; **e**) superposition of an avian influenza virus hemagglutinin in complex with α2,3-sialyllactosamine (yellow) (PDB accession 2WR2) and the human receptor α2,6-sialyllactosamine (cyan) (PDB accession 2WR7). Image reprinted with permission from Ref. 20.

4.2.3. Sialylglycopeptide

Sialylglycopeptide (SGP) **4.1**, a sialic acid terminated bi-antennary complex-type N-glycan attached to a short peptide (H-Thr-Lys-Asn-Ala-Val-Lys-OH, and the peptide is attached to the sugar through the Asn, Figure 4.2), is one of the components present in hens' egg yolk. SGP has drawn significant interest in recent years due to its antiviral and antimicrobial properties.[21] It has also been shown that SGP and its derivatives have the potential to be

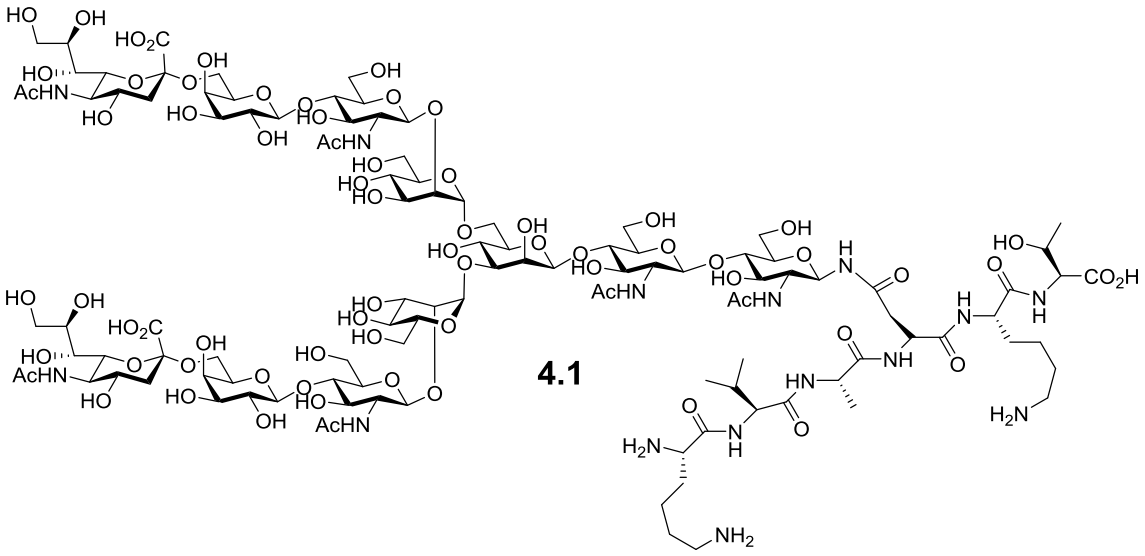

Figure 4.2. The structure of SGP.

developed into prophylactic drugs (*i.e.* drugs that are designed and used to prevent a disease from occurring) against bacterial and viral infections.[21-22] In 1997, Seko *et al.* demonstrated for the first time that SGP is naturally found in hens' unfertilized egg yolks.[23] The yield of SGP from egg yolks was compared with the other major yolk proteins such as phosvitin, α- and β-lipovitellins, and low density lipoprotein (LDL); the yield of SGP per gram of yolk was found to be lower than that of other yolk proteins.

However, due to the low molecular weight of SGP as compared to other proteins the molar yield of SGP was actually comparable with the other yolk proteins.[23]

Three egg yolk glycoproteins; riboflavin-binding protein (RBP), immunoglobulin Y (IgY), and phosvitin have N-linked silalylglycans.[24-26] The glycan of SGP is similar to those of phosvitin and RBP, as none possess either bisecting-N-acetylglucosamine residues or high mannose-type structures.[26] The difference in the structure of the glycans of the various yolk glycopeptides and glycoproteins is probably due to the different tissues in which they are formed.[23] The origin of SGP in egg yolks still remains unclear.

Due to the homogeneity seen in the amino acid sequence in SGP, it might be possible that enzymatic proteolysis of certain glycoproteins results in its formation.[23] Seko *et al.* have suggested that vitellogenin, one of the major storage protein precursors in yolk, could be the source of SGP; Vtg II, a major chicken vitellogenin, has the same amino acid sequence in the peptide of SGP.[23] However this hypothesis has yet to be verified.

4.2.4. gAuNPs and influenza virus and viral HA detection

gAuNPs have been used as sensors for various biomolecules and toxins,[27-32] including the detection of pathogenic agents such as bacteria and viruses.[33-35] Indeed the detection of both the influenza virus itself and viral HA using gAuNPs have been reported very recently,[36-38] and gAuNPs have also been tested for their efficiency in inhibiting influenza virus infection.[19] In 2010, Papp *et al*. used a synthetic sialic acid-terminated glycerol-based dendron (Scheme 4.1) to functionalize 2 and 14 nm sized AuNPs.[19] These gAuNPs

were tested for their inhibition of influenza virus infection. TEM results showed that the 14 nm sized gAuNPs were effective in influenza virus inhibition, whilst 2 nm sized gAuNPs did not have any significant effect. The procedure used for the synthesis of the sialic acid-terminated glycerol dendrimer is shown in the Scheme 4.1. The Brust-Schiffrin method (BSM) was used to synthesize 2 nm gAuNPs, and the Turkevich reaction followed by

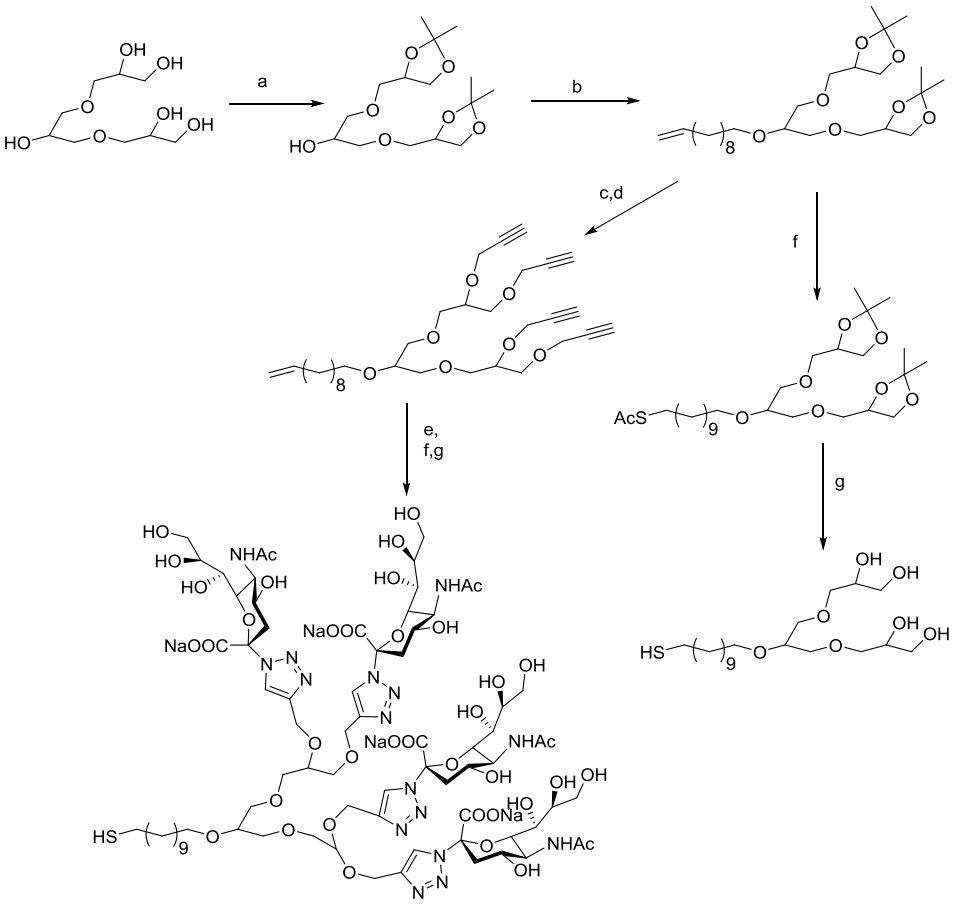

Scheme 4.1. Synthetic procedures for the sialic acid-terminated glycerol dendron and the spacer ligand. Reagents and conditions: a) 2,2'-Dimethoxypropane (DMP), *p*-toluenesulfonic acid (PTSA); b) NaOH, tetrabutylammonium iodide (TBAI), $C_{11}H_{21}Br$; c) Dowex-H^+, MeOH, reflux; d) propargyl bromide, NaH; e) azido-sialic acid, click reaction, sodium ascorbate, $CuSO_4 \cdot 5H_2O$; f) AcSH, azobisisobutyronitrile (AIBN), MeOH, *hv*; g) NaOMe, MeOH, NaOH; Adapted from Papp *et al*.[19]

ligand exchange was used to prepare the 14 nm gAuNPs. In a related work, Lee *et al.* synthesized sialic acid-functionalized gAuNPs (20 nm size) in one-pot without chemically modifying the sialic acid.[36] In this case sialic acid acted as both the reducing agent and the stabilizing ligand for Au during the gAuNP synthesis. These gAuNPs were then used for the colorimetric detection of the influenza virus (Scheme 4.2).

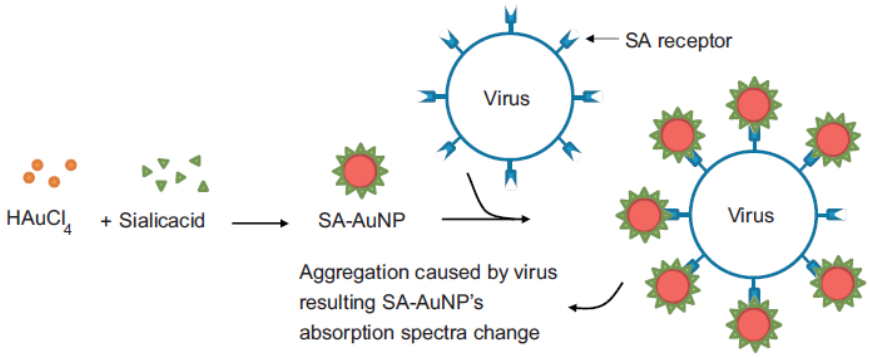

Scheme 4.2. Synthesis of sialic acid reduced and stabilized gAuNPs (SA-AuNP), and their application as colorimetric sensor for the influenza virus. Image reproduced from Ref. 36 with permission from Elsevier.

In a similar fashion Marín *et al*. synthesized gAuNPs (16 nm size) that were functionalized with both a thiolated trivalent α(2→6)-thio-linked sialic acid derivatives (Scheme 4.3) and a thiolated polyethylene glycol (PEG) derivative.[37] Use of the Turkevich reaction followed by ligand exchange allowed them to prepare 16 nm sized gAuNPs that were functionalized with different ratios of the sialic acid and the PEG ligands. A optimum colorimetric detection of the human influenza virus X31 (H3N2) was achieved when the ratio of thiolated trivalent α(2→6)-thio-linked sialic acid derivatives and a thiolated polyethylene glycol (PEG) derivative was 25:75. Moreover, the gAuNPs selectively detected human-adapted influenza viral particles which have binding

specificity for α(2→6)-linked sialylglycans over an avian-adapted virus with α(2→3) specificity.

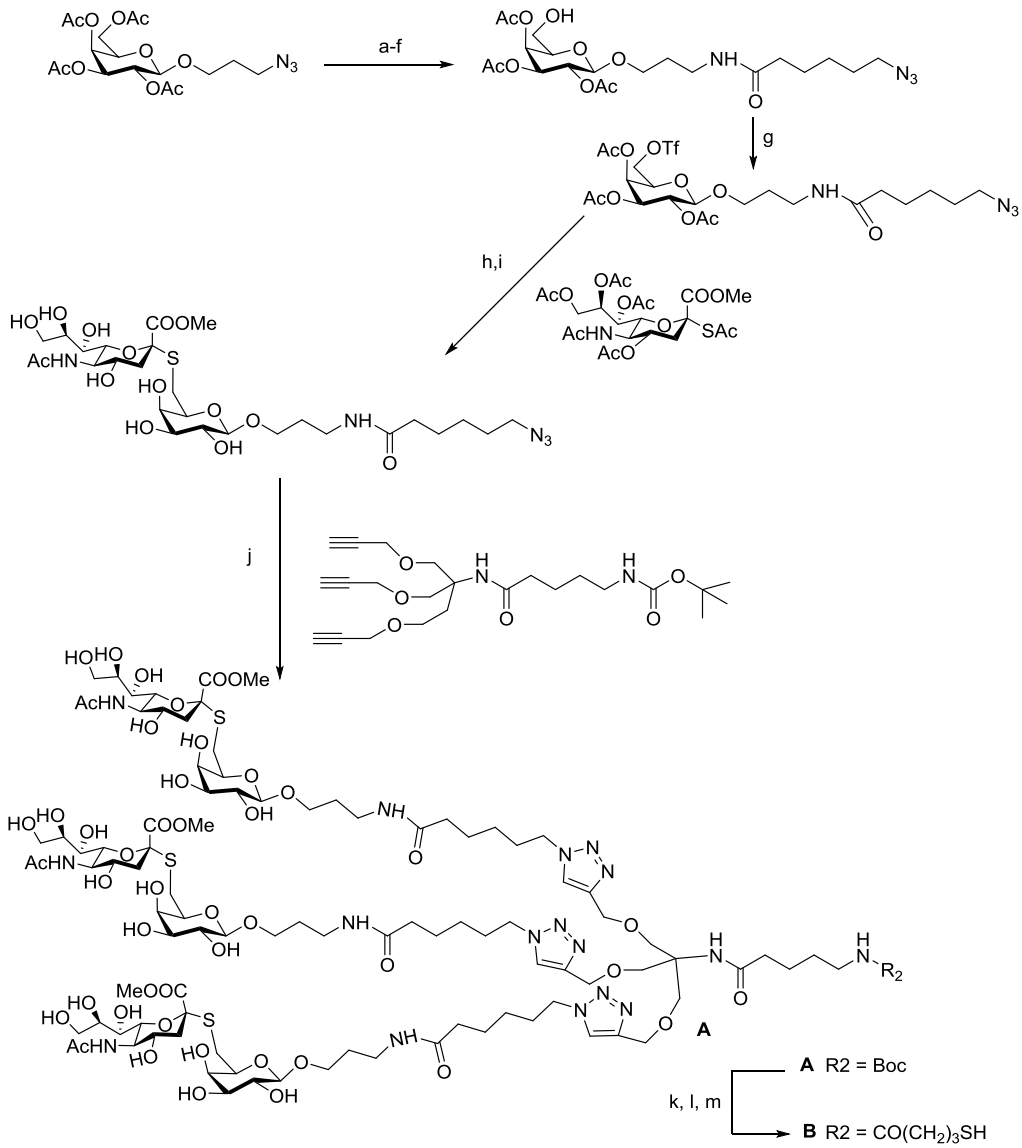

Scheme 4.3. Synthesis of thiolated trivalent α(2→6)-thio-linked sialic acid derivative (B). Reagents and conditions: (a) 10% Pd-C, EtOAc; (b) azidohexanoic acid NHS ester, Et_3N, CH_2Cl_2; (c) NaOMe-MeOH; (d) *t*butyldimethylsilyl chloride/DMF; (e) Ac_2O/Pyridine; (f) 10% TFA in 80% aq. AcOH; (g) triflic anhydride/Pyridine; (h) Et_2NH/DMF; (i) NaOMe/MeOH; (j) $CuSO_4$-sodium ascorbate, $^tBuOH/H2O$ 1 : 1; (k) 1 M aq. NaOH; (l) 80% aq. TFA; and (m) γ-thiobutyrolactone/DTT/0.5 M aq. $NaHCO_3$/EtOH 1.5 : 1.[37]

Most recently in 2014, Wei *et al*. synthesised a series of gAuNPs (13 nm size) functionalized with sialic acid derivatives, with either α(2→6) or α(2→3) linkages, as shown in Scheme 4.4.[38] The Turkevich reaction followed by ligand exchange was used to prepare the 13 nm sized gAuNPs functionalized with the sialic acid derivatives. The sialic acids were modified by sulfation, fucosylation, and *N*-acetylation. Thus these compounds represented the termini of naturally occurring glycans seen in cell surface glycolipids and glycoproteins. It was demonstrated that these gAuNPs could be effectively used for the selective colorimetric detection of both human-adapted and avian-adapted influenza virus particles.

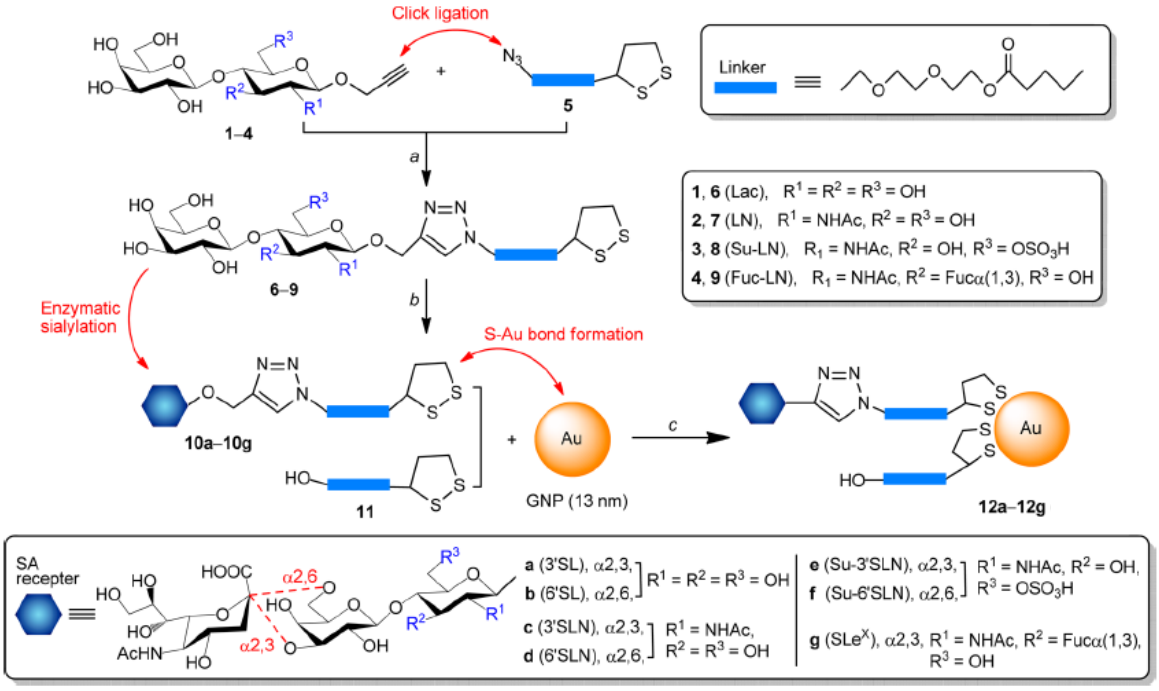

Scheme 4.4. Chemoenzymatic synthesis of gAuNPs functionalized with sialic acid derivatives, with either α(2→6) or α(2→3) linkages (**12a-12g**). Reagents and conditions: (a) CuI, DMF/MeOH, rt, 50-80%; (b) α(2→3)-SiaT or α(2→6)-SiaT, CMP-Neu5Ac, Tris-HCl buffer (pH 8.0), 37 °C, 2 h, 17-87%; (c) deionized water, rt, 24 h. Abbreviations: SiaT, sialyltransferase; CMP, cytidine 50-monophosphate; GNP, Cit-AuNPs. Reprinted with permission from Ref. 38. Copyright (2016) American Chemical Society.

Thus, the majority of previous studies have involved gAuNPs decorated with synthetic oligosaccharides of various lengths that were terminated in sialic acid. Although none of these materials corresponded to the full-length N-glycans that are typically found on the mammalian cell surface, their syntheses were nonetheless time-consuming, expensive, and logistically demanding.[19, 37-38] Additionally in the case where sialic acid itself was used as the ligand for gAuNPs,[36] the selective detection of human-adapted influenza viruses that prefer α(2→6)-linked sialylglycans was not possible.

The remaining sections of this chapter will detail the extraction of SGP from egg yolks, the synthesis of SG-gAuNPs, and investigations into their performance for the detection of the influenza virus and viral hemagglutinin.

4.3. Results and Discussion

4.3.1. Extraction of SGP and conversion to a thiol

The original procedure developed by Seko *et al.* for the extraction of SGP from egg yolks was quite tedious; it involved a phenol extraction, centrifugation, an EtOAc wash, and then repeated size exclusion and ion exchange chromatographies.[23] Also, the 9% phenol aqueous solution used to precipitate the unrelated proteins and to extract the SGP from yolks caused significant emulsification due to the blending of soluble proteins, lipids, phenol, and water. Emulsification meant that separation of supernatant and precipitates was always incomplete, even under high-speed centrifugation. Zou *et al.* simplified the final stage of the purification by employing porous graphite carbon extraction instead of the multiple gel-filtration procedure.[39] In 2012, Sugawara *et al.* reported the use of water

to extract defatted egg yolks, and that the supernatant could be consequently treated with organic solvents to precipitate SGP.[40] However, all these procedures had the drawbacks of emulsification, the need of high-speed centrifugation for long duration, and protracted purification procedures which limited the large-scale extraction of SGP. Therefore we followed the most recent extraction procedure recently developed by Sun *et al.* in which they managed to reduce the amount of emulsification and avoid the use of centrifugation.[41]

Egg yolks were separated from 300 chicken eggs purchased from super market, and the yolks were lyophilized. The yolk powder obtained was successively washed with diethyl ether and 70% aqueous acetone solution to remove the lipids present. The removal of lipids in this step significantly reduced the amount of emulsification during the later steps. The SGP in the yolk powder was then extracted into 40% aqueous acetone solution, and the residual yolk powder was removed by simple filtration of the extract through Celite®. Sun *et al.*[41] reported that 40% aqueous acetone solution was the a better solvent system to use for this extraction as compared to all other possible combination of water and acetone, and also the 9% aqueous phenol solution used by Seko *et al.*[23] SGP was purified from the extract using an active carbon/Celite® (1:1) chromatography purification. The active carbon/Celite® column was sequentially washed with 5% and 10% aqueous MeCN followed by elution with 30% aqueous MeCN afforded 1.2 g of SGP **4.1** (Scheme 4.5). In active carbon/Celite® column the activated carbon acts as a 'reverse phase' column by inducing hydrophobic interaction with eluent. As activated carbon is a very compact material, the Celite® was used to increase the porosity of the

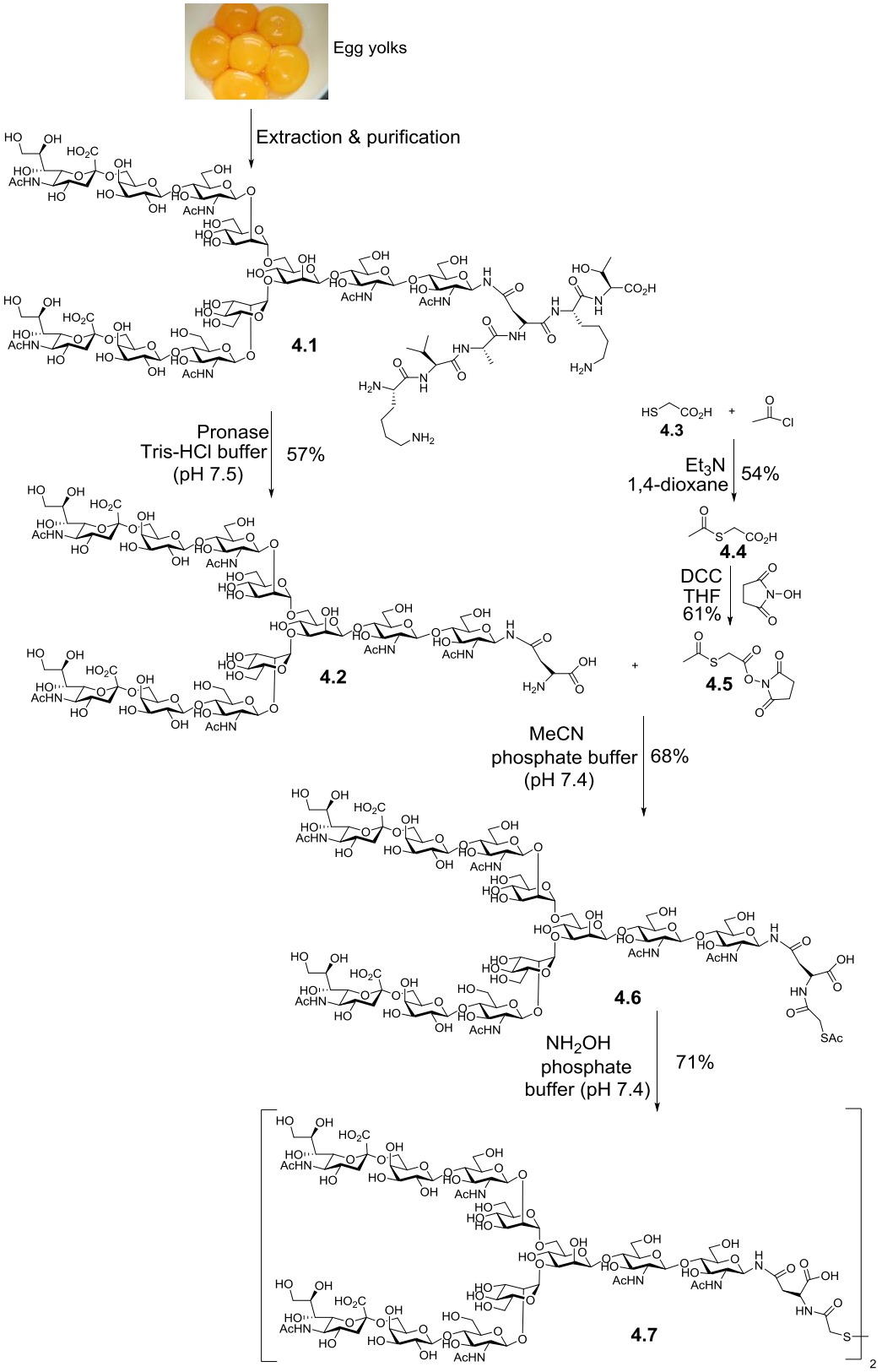

Scheme 4.5. Isolation and synthesis of the sialyloligosaccharide disulfide ligand **4.7.**

column to allow faster elution; it is thought that the Celite® did not interact significantly with the eluted species.

Incubation of the SGP **4.1** with pronase (from *Streptomyces griseus*) in Tris-HCl buffer (pH 7.5) at 37 ^{o}C then afforded the asparagine-linked complex bi-antennary N-glycan **4.2**.[42] The term pronase actually refers to a group of proteolytic enzymes that are generated in the culture supernatant of *Streptomyces griseus* (a species of bacteria in the genus *Streptomyces* generally found in soil).[43] Pronase contains at least ten proteolytic components, and thus has a very broad specificity and is used when extensive degradation of proteins is required.[43] Reaction of thioglycolic acid **4.3** with acetyl chloride and triethylamine in 1,4-dioxane afforded S-acetylmercaptoacetic acid **4.4**.[44] Reaction of **4.4** with *N*-hydroxysuccinimide and dicyclohexylcarbodiimide (DCC) in THF gave the activated ester **4.5**,[45] which was then reacted with the Asn-linked glycan **4.2** in sodium phosphate buffer (pH 7.4) containing 20% acetonitrile to give the thioacetate **4.6**. Deacetylation of **4.6** by treatment with hydroxylamine hydrochloride, followed by air oxidation afforded the disulfide **4.7.** The procedure followed here meant that the disulfide **4.7** could typically be made on a multi-hundred milligram scale.

4.3.2. Synthesis and characterization of SG-gAuNPs

The 12 nm sized SG-gAuNPs were synthesised using a ligand exchange reaction on Cit-AuNPs (12 nm) with the disulfide **4.7** (Scheme 4.6). Reaction of trisodium citrate with $HAuCl_4$ in water under reflux afforded 12 nm sized Cit-AuNPs. Reaction of disulfide **4.7**

with Cit-AuNPs in water for 48 h yielded SG-gAuNPs. Excess unbound disulfide **4.7** and other impurities were removed by centrifugal filtration with water as the solvent. Membrane filters with a molecular weight cut off of 10 kDa was used for the centrifugal filtration as the SG-gAuNPs has an average molecular weight of more than 10 kDa and all the impurities from the exchange reaction has a molecular weight of less than 10 kDa. The FT-IR spectrum of the sialylglycan-capped SG-gAuNPs was similar to that of the free disulfide **4.7** (Figure 4.3), indicating both the removal of citrate and the successful incorporation of sialylglycans on the surface of the NPs.[46]

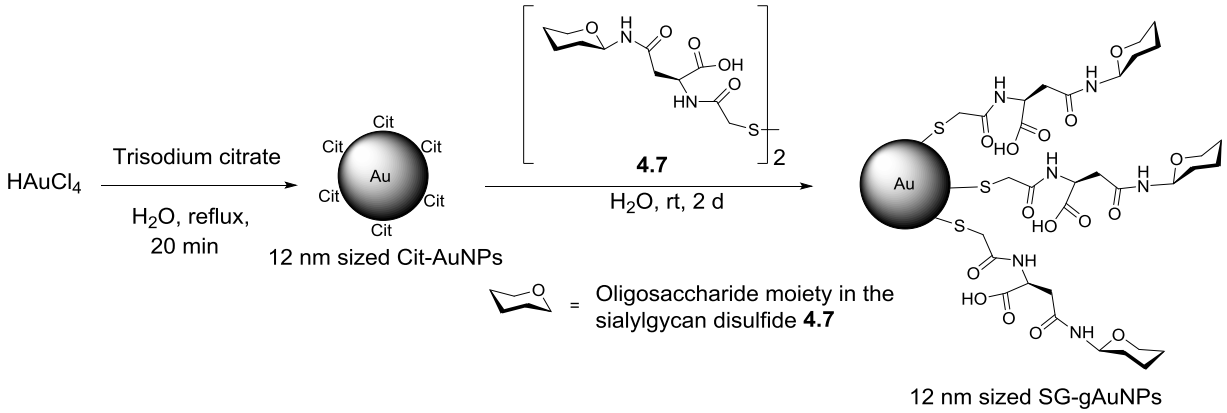

Scheme 4.6. Synthesis of 12 nm sized SG-gAuNPs by ligand exchange method.

ESI-MS results also confirmed that the sialylglycan had been successfully incorporated into the SG-gAuNPs. The particle sizes and size distributions (as demonstrated by TEM) and the UV-Vis absorption spectra (Figure 4.4) of the AuNPs were essentially the same both before and after ligand exchange, indicating that the AuNP cores had not been affected.[38]

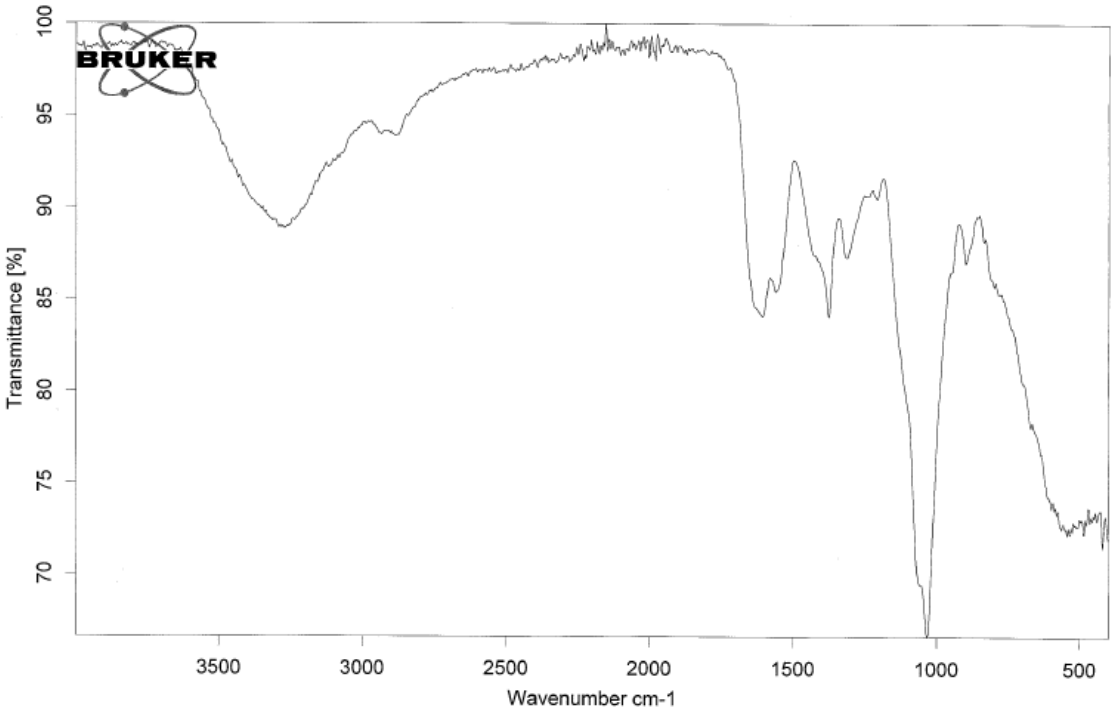

Figure 4.3. FT-IR spectra of SG-gAuNPs**.**

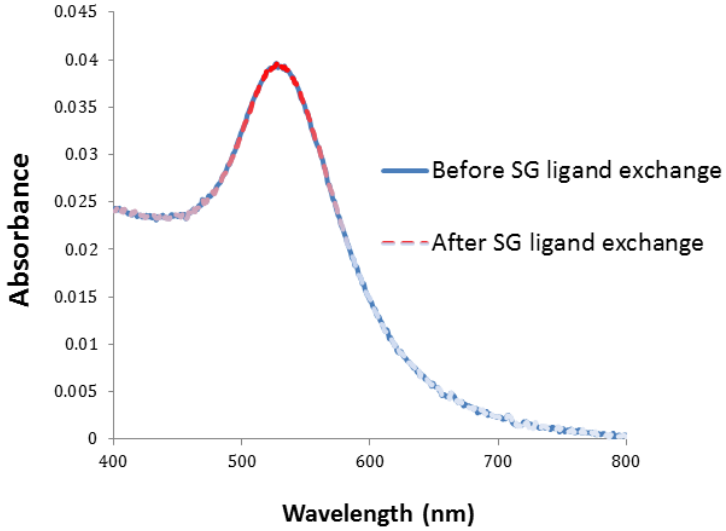

Figure 4.4. UV-Vis absorption spectra of AuNPs before and after SG ligand exchange.

Analysis of the TEM images (Figure 4.5a) of the SG-gAuNPs (at least 200 particles were measured using ImageJ software), revealed the particle sizes to be 12.1 ± 1.6 nm (Figure

4.6). The average molecular formula of the SG-gAuNPs was determined by TGA (Figure 4.7) to be $Au_{54464}(C_{90}H_{14}N_8O_{65}S)_{12404}$, which was confirmed by elemental analysis.[47-48] The average molecular formula calculations were carried out in the similar manner as described in Chapter 3, Section 3.2.2. Interestingly, this is the first report of the synthesis of gAuNPs decorated with naturally occurring full-length sialic acid terminated N-glycans.

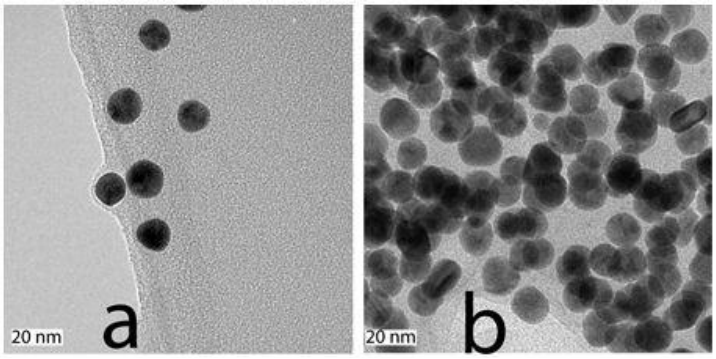

Figure 4.5. Representative TEM images of the SG-gAuNPs: a) before and b) after the addition of HA.

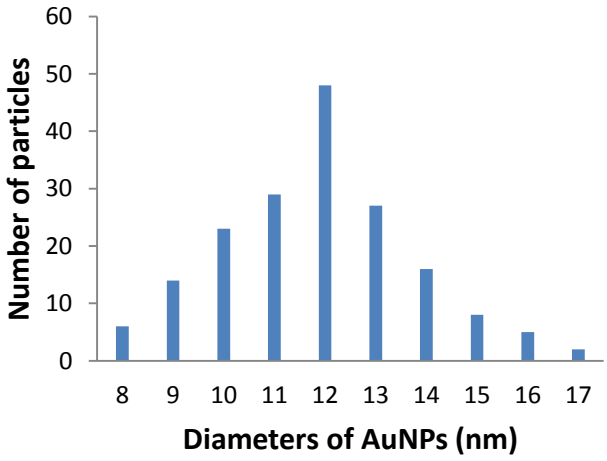

Figure 4.6. Size distribution histogram of SG-gAuNPs (12.1 ± 1.6 nm).

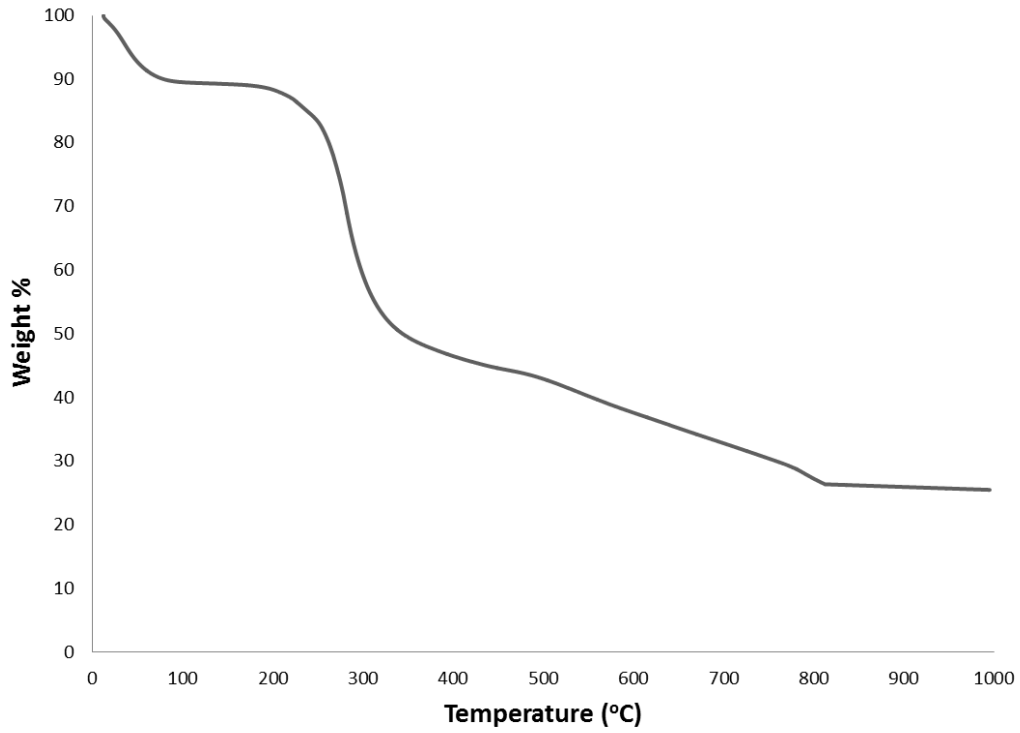

Figure 4.7. TGA plot of SG-gAuNPs

4.3.3. Colorimetric detection of influenza HA using SG-gAuNPs

In order to perform the colorimetric detection of influenza HA, a solution of SG-gAuNPs (3 nM) in phosphate buffer saline (PBS) of pH 7.4 was prepared. The NP concentration (3 nM) in the solution was confirmed by atomic absorption spectroscopy (AAS). A solution of HA (0.25 mg/mL) in PBS (pH 7.4) was prepared. Then, aliquots of the HA solution of various sizes (5, 10, 20, 30 and 40 µl) were added (with mixing) to an aliquot of the SG-gAuNP solution (200 µl), and in each case solution was made up to a total volume of 300 µl by adding PBS. The progress of the reaction in each case was monitored by UV-Vis spectroscopy at different time intervals.

When HA was added to the SG-gAuNPs (3 nM) to give a final HA concentration of 71 nM, the SPR band peak maximum of SG-gAuNPs centred at 523 nm did not undergo any significant shift, either immediately or upon standing (Figure A4.1 in the Appendix). However, when the final concentration of HA was increased to 141 nM, the SPR peak began to shift gradually in a time dependent fashion, indicating that aggregation of the SG-gAuNPs was occurring (Figure 4.8a). After 60 minutes no further change in the absorbance spectrum was observed, and the SPR peak maximum had shifted to 531 nm.

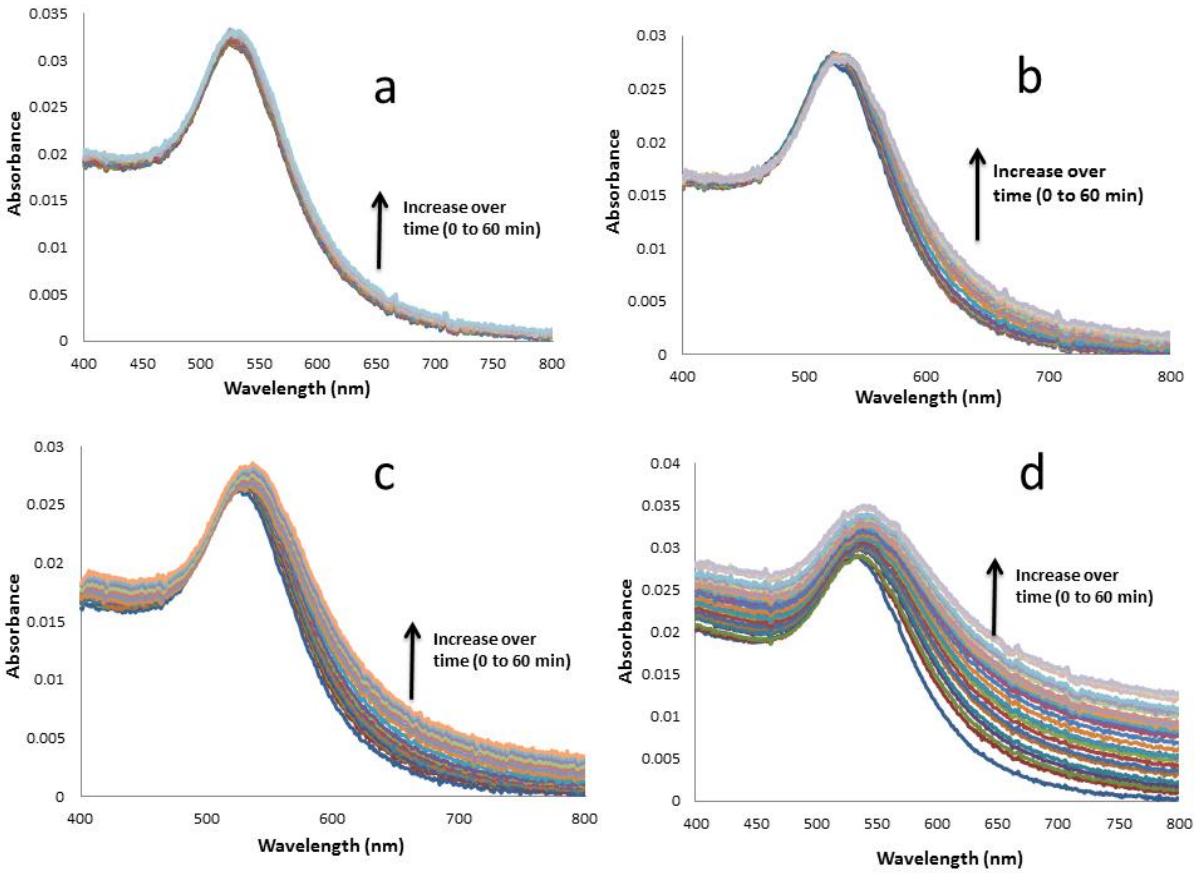

Figure 4.8. UV-Vis absorption spectra SG-gAuNP with a) 141, b) 283, c) 424, and d) 564 nM of HA.

When the HA concentration was further increased to 283, 424, and 564 nM, the SPR peak maximum underwent even more pronounced shifts to 534, 539, and 544 nm respectively over the same time period (60 minutes), indicating the formation of progressively larger SG-gAuNP aggregates as the HA concentration was increased (Figure 4.8b-d). TEM analysis also clearly showed that, following the addition of HA, the SG-gAuNPs were no longer present as individual well-separated particles (Figure 4.5a), but had assembled into networks of aggregated NPs (Figure 4.5b). HA detection was also possible with the naked eye, as the colour of the colloidal solution changed from red to purple upon SG-gAuNP aggregation (Figure 4.9).

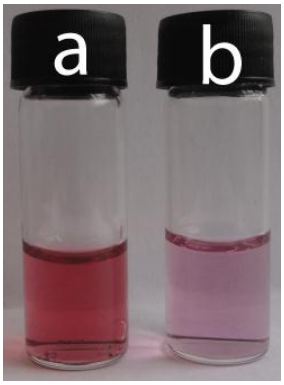

Figure 4.9. SG-gAuNP solutions: a) before and b) after the addition of HA.

A further demonstration of the effect of the HA concentration on the SPR band of the SG-gAuNPs is shown in Figure 4.10, which is a plot of the ratio of the absorbance intensity measured at 650 nm both with and without HA ($[I^{HA}/I^{0}]_{650}$) against the HA concentration between 71 and 564 nM. These data show a linear relationship between the concentration of HA added and the degree of SG-gAuNP aggregation. This change in absorbance can therefore be used to estimate the concentration of HA in an unknown

sample. Wei *et al.* reported[38] that at HA concentrations higher than 4.2 µg/mL (equivalent to 71 nM) AuNPs stabilized with synthetic mimics of sialylglycans were red-shifted. Figure 4.10 demonstrates that the SG-gAuNPs reported here are similar in terms of detection efficiency, and that the sensitivity is comparable to the results obtained from traditional methods such as ELISAs and glycan microarrays.[49-51] However considering the logistically demanding and time

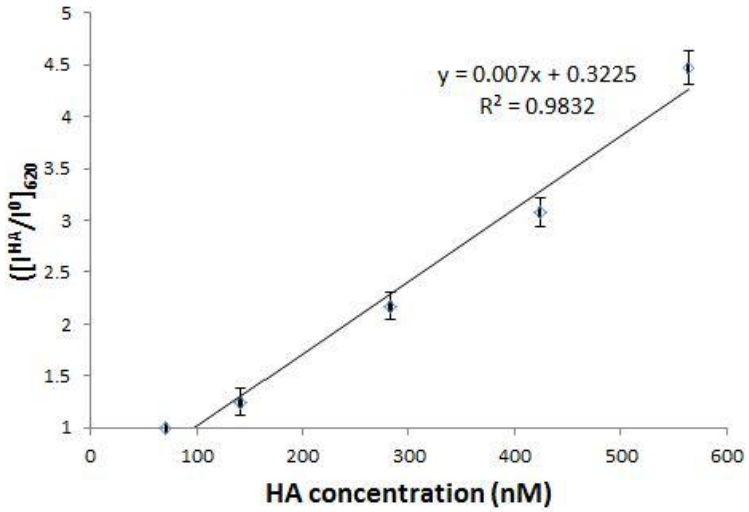

Figure 4.10. Plot of the ratio of absorbance intensity at 650 nm both with and without HA *vs* HA concentration for Sg-gAuNP. Each point is the average of three measurements with error bars representing the standard error.

consuming chemo-enzymatic synthetic procedure required to make the sialylglycan mimics in the report of Wei *et al.*,[38] the use of naturally occurring full length N-glycans that we have developed offers a simpler and more attractive method for the development of an AuNP-based sensor for HA detection.

4.3.4. Colorimetric detection of the influenza virus

It is known that in general avian-adapted influenza A viruses prefer sialylglycans with α(2→3) linkages that are present in the intestinal epithelial cells of birds, whilst human-adapted influenza A viruses prefer α(2→6) linkages which are commonly expressed in the upper respiratory tract of humans.[16] In order to investigate any selectivity of the SG-gAuNPs produced here UV-Vis studies were performed with two influenza virus strains, A/Puerto Rico/8/34 (H1N1) and A/New Caledonia/20/1999 (H1N1). This part of the work was done in collaboration with Dr. Matloob Husain`s virology group in Otago University.[52] The A/Puerto Rico/8/34 strain (hereafter referred as the Puerto Rico strain) specifically binds α(2→3)-linked sialylglycans,[53] whilst the influenza A/New Caledonia/20/1999 strain (hereafter referred as the New Caledonia strain) has specificity for α(2→6)-linked glycans.[54]

The New Caledonia (6 x 10^5 PFU/mL) and Puerto Rico strains (2 x 10^7 PFU/mL) were prepared in PBS (pH 7.4). In virology, PFU or Plaque Forming Unit is a measure of the viral particles capable of forming plaques (a plaque is a visible structure formed within a cell culture and counting the number of plaques is used as a method of virus quantification) per unit volume. PFU is a functional measurement and not a measurement of the exact number of viral particles. For example, viral particles that fail to infect the target cell will not generate a plaque and therefore they will not be counted.

In order to perform the colorimetric detection of influenza virus particles, aliquots of the New Caledonia solution (1.6, 8, 16.7, 33.4, and 50.1 µl) were added (with mixing) to an

aliquot of the SG-gAuNP solution (30 µl of 20 nM solution) and formalin (15 µL of 10% stock solution). Formalin was used to inactivate the live virus. In each case solution was made up to a total volume of 300 µl by adding PBS. The progress of the reaction was monitored by UV-Vis spectroscopy at different time intervals. In the case of the A/Puerto Rico/8/34 (H1N1) virus 1.5 µl of the stock solution was added to the SG-gAuNP solution.

Upon the addition of 10,000 PFU of the New Caledonia strain to the SG-gAuNPs (3 nM), there was a significant increase in the absorbance intensity at 650 nm (Figure 4.11). However the addition of the same number of PFU of the Puerto Rico strain (and additionally with 30,000 PFU, data not shown) did not cause any increase in the absorbance intensity at 650 nm, confirming that the SG-gAuNPs selectively detected viral particles which have an α(2→6) specificity (Figure 4.11).

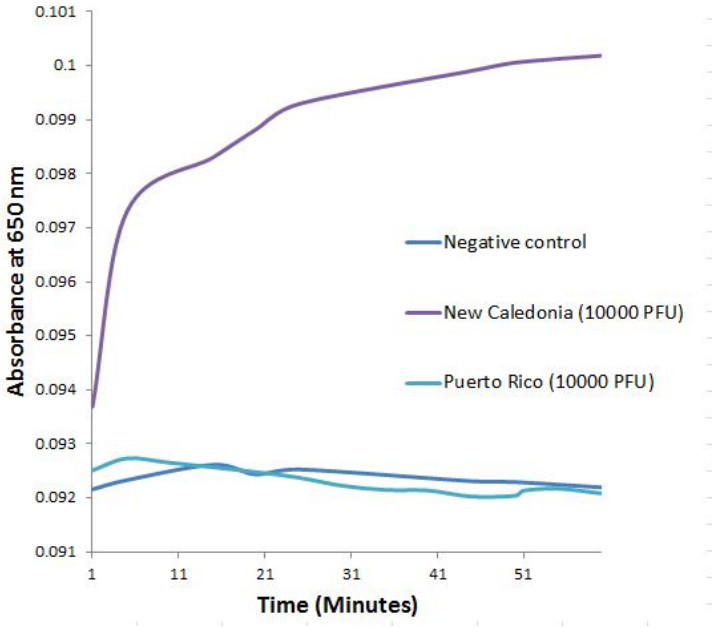

Figure 4.11. Plot of the absorbance intensity at 650 nm *vs* time for SG-gAuNPs with two different influenza viral strains, and a negative control.

A further demonstration of the effect of the influenza virus concentration on the SPR peak of the SG-gAuNPs, is shown in Figure 4.12, which plots the ratio of the absorbance intensity measured at 650 nm both with and without the New Caledonia strain ($[I^{HA}/I^{0}]_{650}$) against the New Caledonia strain concentration between 1,000 and 30,000 PFU. These data show a linear relationship between the concentration of virus added and the degree of SG-gAuNP aggregation, which is similar to the case of HA shown in Figure 4.10. Additionally, the binding of the SG-gAuNPs to the virus was found to be faster than to HA. The virus-SG-gAuNP interaction was complete within 30 minutes, in line with the report of Wei *et al.*[38] It is clear from Figure 4.12 that the SG-gAuNPs used here can readily detect the New Caledonia strain in amounts as low as 10,000 PFU.

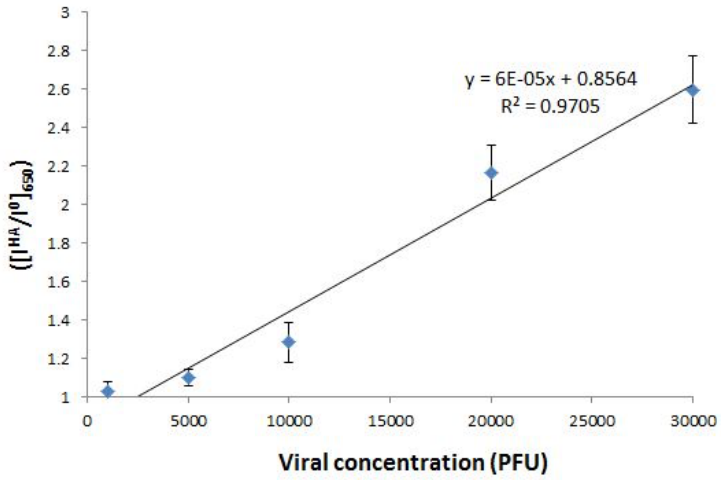

Figure 4.12. Plot of the ratio of the absorbance intensity at 650 nm with and without the New Caledonia strain *vs* the New Caledonia viral concentration. Each point is the average of three measurements with error bars representing the standard error.

4.3.5. SG-gAuNP aggregation in the presence of HA

A pictorial representation of the HA-induced aggregation of SG-gAuNPs, based on previous reports on similar analyte-induced aggregation-effected sensors, is depicted in Figure 4.13.[38, 55] The performance of an AuNP-based colorimetric sensing system depends on how effectively the AuNP dispersion is converted to AuNP aggregates by the analyte of interest. Typically, gAuNPs are stabilized against attractive van der Waals forces by the steric effects of the surface capping ligands; in this study the sialic acid terminated complex bi-antennary N-glycans.[56] Aggregation of gAuNPs can be achieved in two ways - either *via* interparticle crosslinking or *via* non-crosslinking.[56] Interparticle crosslinking aggregation is presumed to be the basis of the sensing response reported here; controlled aggregation of the SG-gAuNPs occurs because of binding of the multiple sialic acid binding sites of HA to the sialic acid-

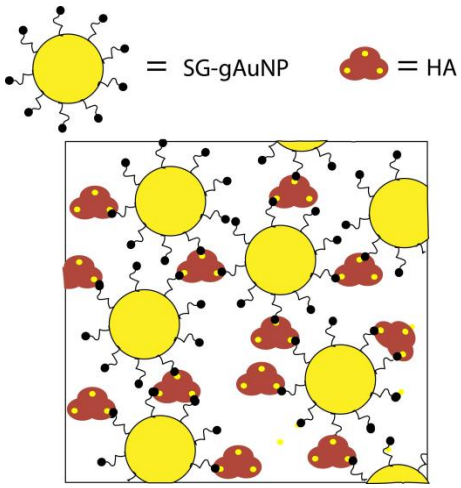

Figure 4.13. Schematic representation of the mechanism of aggregation of SG-gAuNPs in the presence of HA.

terminated ligands present on the SG-gAuNPs.[16] A detailed discussion of the theory of aggregation of gAuNPs is provided in Chapter 3, Section 3.2.4. Indeed it was found that the addition of excess sialic acid (10 mM) to a solution of SG-gAuNP aggregates formed in the presence of HA (564 nM) resulted in aggregate re-dispersion, as demonstrated by a colour change (from blue to red) and by a blue-shift in the SPR peak maximum to 523 nm. The dissociation of these aggregates to individual particles in the presence of sialic acid showed that binding of the SG-gAuNPs to HA was reversible, and also provides strong supporting evidence for the mechanism of aggregation depicted in Figure 4.13.

4.3.6. Dynamic light scattering detection of HA using SG-gAuNPs

The aggregation of SG-gAuNPs by the addition of varying concentrations of viral HA was also investigated using Dynamic Light Scattering (DLS), a technique which can provide a quantitative estimate of the average diameter of the AuNP aggregates produced.[57] As the ability of AuNPs to scatter light is significantly higher than that of

biomolecules, DLS is selective for the AuNPs present in these solutions.[58] In the DLS assays carried out here, the HA-induced SG-gAuNP aggregates were not physically separated from any remaining non-aggregated NPs that may have been present. However, the inherent bias of DLS towards larger particles/aggregates means that estimated diameters are representative of only the particle aggregates.[59]

In order to perform the DLS assay of influenza HA, a solution of the SG-gAuNPs (3 nM) was prepared in phosphate buffer saline (PBS) of pH 7.4. A solution of HA (0.25 mg/mL) was also prepared in PBS (pH 7.4). Then, aliquots of the HA solution (5, 10, 20, 30 and 40 µl) were added (with mixing) to an aliquot of the SG-gAuNP solution (200 µl), and in each case solution was made up to a total volume of 300 µl by adding PBS. The sample was equilibrated at 25 ^{o}C for 120 seconds before DLS analysis. Each DLS measurement consisted of 12 scans, each of 30 seconds duration.

DLS results can be reported in terms of intensity, volume, or number-based distributions. The fundamental size distribution produced by DLS is intensity-based distribution and therefore this measurement is less prone to error. Intensity distribution can be converted to a volume distribution using Mie theory. The volume-based distribution can further be transformed to a number-based distribution. Since the volume and number-based distributions are derived using various equations using several assumptions the probability of obtaining biased results in these measurements are large.

Number-based distribution is preferred for studying particles with smaller sizes as this generally reports the smallest size measured. However, for noisy data the number-based size distribution could be misleading; for example, when transforming from intensity to number, small noise in the intensity distribution could be over-amplified and lead to wrong conclusions. The best choice to detect and report even small amounts of aggregation of particles is the intensity-based size distribution as aggregated particles will be highlighted and the smaller individual particles will be suppressed in this measurement. Thus, in this study we have used intensity-based size distribution data to analyse the aggregation of SG-gAuNPs in the presence of HA.

From the DLS measurements the size of the "as made" SG-gAuNPs was found to be 21 ± 1 nm (Figure 4.14a). The diameter of the AuNPs in solution measured by DLS is always larger than the AuNP core diameters as measured by TEM[60] because organic ligands on the Au surface are transparent to electrons and so do not contribute to the size of the AuNPs when measured by TEM,[61] whereas DLS measures the hydrodynamic radius of the particles, which in this case includes the sialylglycan ligands and any trapped water molecules.[62]

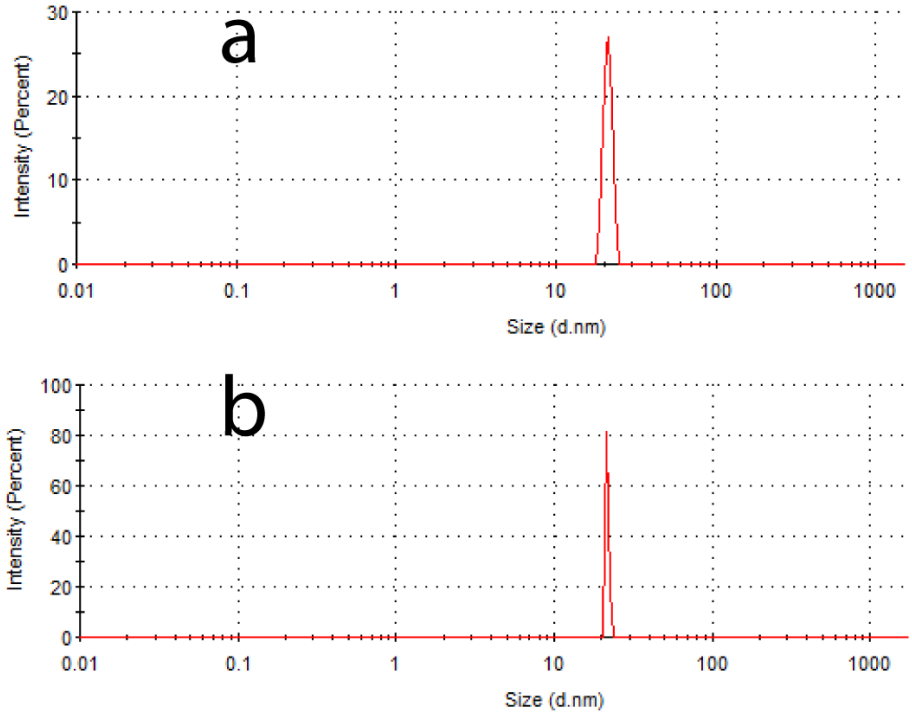

Figure 4.14. DLS measurements of the average diameters of a) SG-gAuNP and b) SG-gAuNP in the presence of 71 nM of HA

When HA was added to SG-gAuNPs (3 nM) to obtain a final HA concentration of 71 nM, DLS assay gave a particle size of 21 ± 1 nm, indicating that no aggregation had occurred at that HA concentration (Figure 4.14b). All DLS measurements were carried out 60 minutes after the addition of HA to the SG-gAuNP solution, as after that point the SPR band of the solutions remained constant. When the final HA concentration was increased to 141 nM, DLS indicated that the mean diameter of the SG-gAuNPs had increased to 97 ± 4 nm, clearly indicating aggregate formation in the presence of the HA at this concentration (Figure 4.15a). When the final HA concentration was further increased to 283, 424, and 564 nM, the mean diameter of the SG-gAuNP aggregates formed correspondingly increased to 183 ± 5, 389 ± 11, and 596 ± 21 nm respectively (Figure 4.15b-d). The larger standard deviation observed for the larger aggregates

indicates that that the polydispersity of the aggregates also increased as the concentration of HA increased.

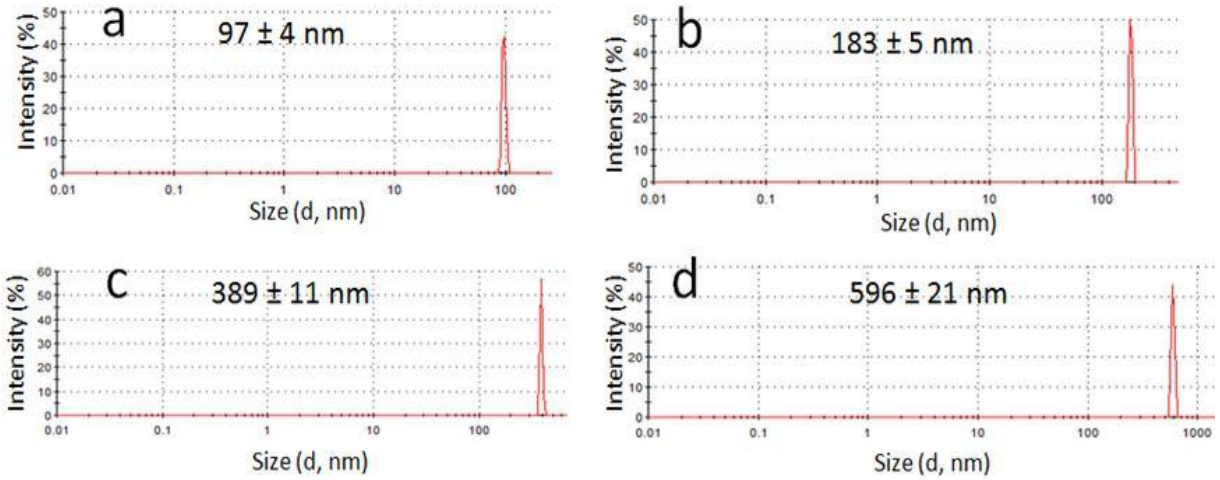

Figure 4.15. DLS measurements of the average diameters of the SG-gAuNP aggregates formed in the presence of a) 141, b) 283, c) 424, and d) 564 nM HA.

A plot of the size of SG-gAuNP aggregates measured by DLS *vs* the HA concentration (Figure 4.16) was found to be linear, with an R^2 value of 0.9748. This linear relationship can therefore be used to estimate an unknown concentration of HA, in a similar fashion to the change in absorbance intensity at 650 nm using UV-Vis spectroscopy (as shown in Figure 4.10). The proportionality constants of the two corresponding linear equations, 0.007 and 1.143 for the colorimetric and DLS assays respectively, indicate that the DLS assay is the more sensitive towards NP aggregation in accordance with previous reports.[63-64]

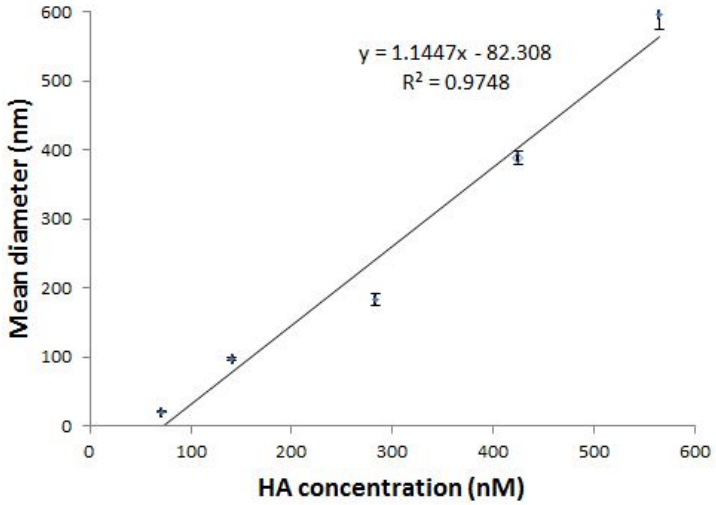

Figure 4.16. A plot of the SG-gAuNP aggregate size *vs* concentration of the HA added. Each point is the average of three measurements with error bars representing the standard error.

4.3.7. Selectivity of the SG-gAuNPs for HA

In order to demonstrate the selectivity of HA/influenza virus detection by the SG-gAuNPs aliquots of a SG-gAuNP solution were mixed with BSA, and the lectins Con A and LTB (each at 600 nM). It was found that none of these species had any effect on either the UV-Vis absorption band or the DLS measurements, confirming that the SG-gAuNPs did not undergo non-specific aggregation and that amongst the species investigated detection was selective for HA and virus.

4.4. Conclusions

This chapter has described the use of AuNPs capped with naturally occurring sialic acid terminated complex bi-antennary N-glycans for the simple and highly selective detection of viral HA and the influenza virus, by the use of both DLS and UV-Vis spectroscopy. A homogeneous SGP, isolated from egg yolks by a simple procedure, was converted to a

thiol and then used in a ligand exchange reaction with Cit-AuNPs to obtain SG-gAuNPs. The presence of sialic acid binding sites on viral HA, and their specific and multivalent binding to sialic acid residues at the termini of the ligands on the SG-gAuNPs, caused AuNP aggregation as the basis for HA/virus detection. Both UV-Vis and DLS measurements revealed a linear relationship between SG-gAuNP aggregation and the concentration of HA that was added. Additionally the SG-gAuNPs selectively detected viral particles which had binding specificity for α(2→6)-linked sialylglycans. The SG-gAuNPs did not undergo any non-specific aggregation in the presence of BSA, or two lectins.

4.5. References

1. Boisselier, E.; Astruc, D. *Chem. Soc. Rev.* **2009,** *38* (6), 1759-1782.
2. Wilson, R. *Chem. Soc. Rev.* **2008,** *37* (9), 2028-2045.
3. De, M.; Ghosh, P. S.; Rotello, V. M. *Adv. Mater.* **2008,** *20* (22), 4225-4241.
4. Willner, I.; Baron, R.; Willner, B. *Biosens. Bioelectron.* **2007,** *22* (9–10), 1841-1852.
5. Wang, Z.; Ma, L. *Coord. Chem. Rev.* **2009,** *253* (11–12), 1607-1618.
6. Sardar, R.; Funston, A. M.; Mulvaney, P.; Murray, R. W. *Langmuir* **2009,** *25* (24), 13840-13851.
7. Sperling, R. A.; Rivera Gil, P.; Zhang, F.; Zanella, M.; Parak, W. J. *Chem. Soc. Rev.* **2008,** *37* (9), 1896-1908.
8. Anker, J. N.; Hall, W. P.; Lyandres, O.; Shah, N. C.; Zhao, J.; Van Duyne, R. P. *Nat Mater* **2008,** *7* (6), 442-453.
9. Jain, P. K.; Huang, X.; El-Sayed, I. H.; El-Sayed, M. A. *Acc. Chem. Res.* **2008,** *41* (12), 1578-1586.

10. Awazu, K.; Fujimaki, M.; Gopinath, S. C. In *Palmtop waveguide-mode sensor: Comparison of sensitivity and subtyping of influenza viruses with SPR, ELISA and Immunochromatography*, Sensors, 2013 IEEE, IEEE: 2013; pp 1-3.

11. Li, X.; Wu, P.; Gao, G. F.; Cheng, S. *Biomacromolecules* **2011,** *12* (11), 3962-3969.

12. Neumann, G.; Noda, T.; Kawaoka, Y. *Nature* **2009,** *459* (7249), 931-939.

13. Subbarao, K.; Katz, J. *Cell. Mol. Life. Sci.* **2000,** *57* (12), 1770-1784.

14. Gopinath, S. C.; Awazu, K.; Fujimaki, M. *Anal. Methods.* **2010,** *2* (12), 1880-1884.

15. Sauter, N. K.; Hanson, J. E.; Glick, G. D.; Brown, J. H.; Crowther, R. L.; Park, S. J.; Skehel, J. J.; Wiley, D. C. *Biochemistry* **1992,** *31* (40), 9609-9621.

16. Imai, M.; Kawaoka, Y. *Curr. Opin. Virol.* **2012,** *2* (2), 160-167.

17. Mammen, M.; Choi, S.-K.; Whitesides, G. M. *Angew. Chem. Int. Ed.* **1998,** *37* (20), 2754-2794.

18. Mammen, M.; Choi, S.-K.; Whitesides, G. M. *Angew. Chem. Int. Ed.* **1998,** *110* (20), 2908-2953.

19. Papp, I.; Sieben, C.; Ludwig, K.; Roskamp, M.; Böttcher, C.; Schlecht, S.; Herrmann, A.; Haag, R. *Small* **2010,** *6* (24), 2900-2906.

20. Stencel-Baerenwald, J. E.; Reiss, K.; Reiter, D. M.; Stehle, T.; Dermody, T. S. *Nat. Rev. Microbiol.* **2014,** *12* (11), 739-749.

21. Tian-Bai, Z.; Zhen-Yu, P.; Hua-Jie, Z.; Zhong-Rui, M.; Min, C. *Letters in Biotechnology* **2014,** (5), 734-737.

22. Koketsu, M.; Nitoda, T.; Juneja, L. R.; Kim, M.; Kashimura, N.; Yamamoto, T. *J. Agric. Food. Chem.* **1995,** *43* (4), 858-861.

23. Seko, A. *Biochim. Biophys. Acta Gen. Subj.* **1997,** *1335* (1-2), 23-32.

24. Brockbank, R. L.; Vogel, H. J. *Biochemistry* **1990,** *29* (23), 5574-5583.

25. Tarutani, M.; Norioka, N.; Mega, T.; Hase, S.; Ikenaka, T. *J. Biochem.* **1993,** *113* (6), 677-682.

26. Ohta, M.; Hamako, J.; Yamamoto, S.; Hatta, H.; Kim, M.; Yamamoto, T.; Oka, S.; Mizuochi, T.; Matsuura, F. *Glycoconj. J.* **1991,** *8* (5), 400-413.

27. de La Fuente, J.; Barrientos, A.; Rojas, T.; Rojo, J.; Canada, J.; Fernandez, A.; Penades, S. *Angew. Chem. Int. Ed.* **2001,** *40* (12), 2257.

28. Marradi, M.; Martín-Lomas, M.; Penadés, S. *Adv. Carbohydr. Chem. Biochem.* **2010,** *64*, 211-290.

29. Hone, D. C.; Haines, A. H.; Russell, D. A. *Langmuir* **2003,** *19* (17), 7141-7144.

30. Schofield, C. L.; Mukhopadhyay, B.; Hardy, S. M.; McDonnell, M. B.; Field, R. A.; Russell, D. A. *Analyst* **2008,** *133* (5), 626-634.

31. Otsuka, H.; Akiyama, Y.; Nagasaki, Y.; Kataoka, K. *J. Am. Chem. Soc.* **2001,** *123* (34), 8226-8230.

32. Schofield, C. L.; Field, R. A.; Russell, D. A. *Anal. Chem.* **2007,** *79* (4), 1356-1361.

33. Richards, S.-J.; Fullam, E.; Besra, G. S.; Gibson, M. I. *J. Mater. Chem. B.* **2014,** *2* (11), 1490-1498.

34. Lin, C.-C.; Yeh, Y.-C.; Yang, C.-Y.; Chen, C.-L.; Chen, G.-F.; Chen, C.-C.; Wu, Y.-C. *J. Am. Chem. Soc.* **2002,** *124* (14), 3508-3509.

35. Niikura, K.; Nagakawa, K.; Ohtake, N.; Suzuki, T.; Matsuo, Y.; Sawa, H.; Ijiro, K. *Bioconjugate Chem.* **2009,** *20* (10), 1848-1852.

36. Lee, C.; Gaston, M. A.; Weiss, A. A.; Zhang, P. *Biosens. Bioelectron.* **2013,** *42*, 236-241.

37. Marín, M. J.; Rashid, A.; Rejzek, M.; Fairhurst, S. A.; Wharton, S. A.; Martin, S. R.; McCauley, J. W.; Wileman, T.; Field, R. A.; Russell, D. A. *Org. Biomol. Chem.* **2013,** *11* (41), 7101-7107.

38. Wei, J.; Zheng, L.; Lv, X.; Bi, Y.; Chen, W.; Zhang, W.; Shi, Y.; Zhao, L.; Sun, X.; Wang, F. *ACS nano* **2014,** *8* (5), 4600-4607.

39. Zou, Y.; Wu, Z.; Chen, L.; Liu, X.; Gu, G.; Xue, M.; Wang, P. G.; Chen, M. *J. Carbohydr. Chem.* **2012,** *31* (4-6), 436-446.

40. Sugawara, S.; Osumi, K. *PCT Int. Appl.* **2012,** *WO2011/027868*.

41. Sun, B.; Bao, W.; Tian, X.; Li, M.; Liu, H.; Dong, J.; Huang, W. *Carbohydr. Res.* **2014,** *396* (0), 62-69.

42. Yamamoto, N.; Ohmori, Y.; Sakakibara, T.; Sasaki, K.; Juneja, L. R.; Kajihara, Y. *Angew. Chem. Int. Ed.* **2003,** *42* (22), 2537-2540.

43. Sweeney, P. J.; Walker, J. M. Pronase (EC 3.4. 24.4). In *Enzymes of Molecular Biology*, Springer: 1993; pp 271-276.

44. Deaton, D. N.; Gao, E. N.; Graham, K. P.; Gross, J. W.; Miller, A. B.; Strelow, J. M. *Bioorg. Med. Chem. Lett.* **2008,** *18* (2), 732-737.

45. Hideo, S.; Yasuhiro, M.; Yasushi, A.; Norio, Y. *PCT Int. Appl.* **2000,** *EP 1 046 401 A2*.

46. Lin, S.-Y.; Liu, S.-W.; Lin, C.-M.; Chen, C.-h. *Anal. Chem.* **2001,** *74* (2), 330-335.

47. Huang, K.; Ma, H.; Liu, J.; Huo, S.; Kumar, A.; Wei, T.; Zhang, X.; Jin, S.; Gan, Y.; Wang, P. C. *ACS nano* **2012,** *6* (5), 4483-4493.

48. Barrientos, Á. G.; de la Fuente, J. M.; Rojas, T. C.; Fernández, A.; Penadés, S. *Chem. Eur. J.* **2003,** *9* (9), 1909-1921.

49. Xu, R.; McBride, R.; Nycholat, C. M.; Paulson, J. C.; Wilson, I. A. *J. Virol.* **2012,** *86* (2), 982-990.

50. Stevens, J.; Blixt, O.; Glaser, L.; Taubenberger, J. K.; Palese, P.; Paulson, J. C.; Wilson, I. A. *J. Mol. Biol.* **2006,** *355* (5), 1143-1155.

51. Chandrasekaran, A.; Srinivasan, A.; Raman, R.; Viswanathan, K.; Raguram, S.; Tumpey, T. M.; Sasisekharan, V.; Sasisekharan, R. *Nat. Biotechnol.* **2008,** *26* (1), 107-113.

52. Dr. Matloob Husain. http://micro.otago.ac.nz/our-people/matloob-husain/ (accessed Jan 30).

53. Guo, C.-T.; Takahashi, N.; Yagi, H.; Kato, K.; Takahashi, T.; Yi, S.-Q.; Chen, Y.; Ito, T.; Otsuki, K.; Kida, H. *Glycobiology* **2007,** *17* (7), 713-724.

54. Chen, L.-M.; Rivailler, P.; Hossain, J.; Carney, P.; Balish, A.; Perry, I.; Davis, C. T.; Garten, R.; Shu, B.; Xu, X. *Virology* **2011,** *412* (2), 401-410.

55. Marin, M. J.; Schofield, C. L.; Field, R. A.; Russell, D. A. *Analyst* **2015,** *140* (1), 59-70.

56. Zhao, W.; Brook, M. A.; Li, Y. *ChemBioChem* **2008,** *9* (15), 2363-2371.

57. Wang, X.; Ramström, O.; Yan, M. *Analyst* **2011,** *136* (20), 4174-4178.

58. Jans, H.; Huo, Q. *Chem. Soc. Rev.* **2012,** *41* (7), 2849-2866.

59. Driskell, J. D.; Jones, C. A.; Tompkins, S. M.; Tripp, R. A. *Analyst* **2011,** *136* (15), 3083-3090.

60. Ahonen, P.; Laaksonen, T.; Nykänen, A.; Ruokolainen, J.; Kontturi, K. *J. Phys. Chem. B.* **2006,** *110* (26), 12954-12958.

61. Witten, K. G.; Bretschneider, J. C.; Eckert, T.; Richtering, W.; Simon, U. *PCCP* **2008,** *10* (14), 1870-1875.

62. Diegoli, S.; Manciulea, A. L.; Begum, S.; Jones, I. P.; Lead, J. R.; Preece, J. A. *Sci. Total Environ.* **2008,** *402* (1), 51-61.

63. Kalluri, J. R.; Arbneshi, T.; Afrin Khan, S.; Neely, A.; Candice, P.; Varisli, B.; Washington, M.; McAfee, S.; Robinson, B.; Banerjee, S. *Angew. Chem. Int. Ed.* **2009,** *121* (51), 9848-9851.

64. Dasary, S. S.; Senapati, D.; Singh, A. K.; Anjaneyulu, Y.; Yu, H.; Ray, P. C. *ACS Appl. Mater. Interfaces.* **2010,** *2* (12), 3455-3460.

Chapter 5: An attempt towards the development of a one-pot synthesis of glycogold nanoparticles by use of Click Chemistry.

5.1. Objective

The aim of this chapter was to develop a facile one-pot synthesis of gAuNPs decorated with unprotected sugars using the Cu(I)-catalysed azide-alkyne Huisgen cycloaddition (CuAAC). The scarcity of reports on the use of the CuAAC reaction for gAuNP synthesis, and the discovery of a facile protecting-group free one-pot synthesis of glycoconjugates using CuAAC[1] in our group motivated us to investigate the use of Click Chemistry to synthesize gAuNPs. From the work detailed in the preceding chapters it is evident that the development of a facile one-pot synthesis of glycogold nanoparticles would enable us to synthesize a wide variety of sugar-decorated gold nanoparticle-based sensors by following one simple synthetic procedure.

5.2. Introduction

The three most common methods used to synthesize gAuNPs stabilized with thiolated-sugar derivatives are: (1) direct reduction of $HAuCl_4$ in the presence of carbohydrate derivatives with linkers bearing a thiol end-group, (2) ligand exchange on previously synthesized AuNPs with carbohydrate derivatives attached to linkers bearing a thiol end group, and (3) modification of functional groups present on the surface of AuNPs with suitably functionalized carbohydrates.[2] A detailed discussion of these three methods is provided in Chapter 1, Section 1.4.5. One of the potential approaches that can be used to

modify the ligands on the surface of AuNPs with sugars to produce gAuNPs is by using Click chemistry, which is the focus of this Chapter.

5.2.1. 1,3-Dipolar cycloaddition

The 1,3-dipolar cycloaddition is a chemical reaction between a 1,3-dipole and a dipolarophile to give a five-membered ring product.[3] A 1,3-dipole is a molecule containing four electrons in three parallel atomic p-orbitals, in which the centre atom has a formal positive charge that compensates the negative charge spread over the two terminal atoms.[4] The most widely used dipolarophiles are alkynes and alkenes. The first reports on 1,3-dipolar cycloaddition reactions appeared in the literature during the late 19th century, after the discovery of 1,3-dipoles.[4] At present, the 1,3-dipolar cycloaddition reaction is widely used to perform the regio- and stereoselective synthesis of five-membered heterocycles.[5]

The generally accepted mechanism of 1,3-dipolar cycloaddition, as proposed by Rolf Huisgen, consists a concerted pericyclic cycloaddition as shown in Scheme 5.1.[3] A 1,3-dipole reacts with a dipolarophile in a concerted and symmetry-allowed [$4\pi_s + 2\pi_s$] manner through a thermal six-electron Huckel aromatic transition state (Scheme 5.1).[6]

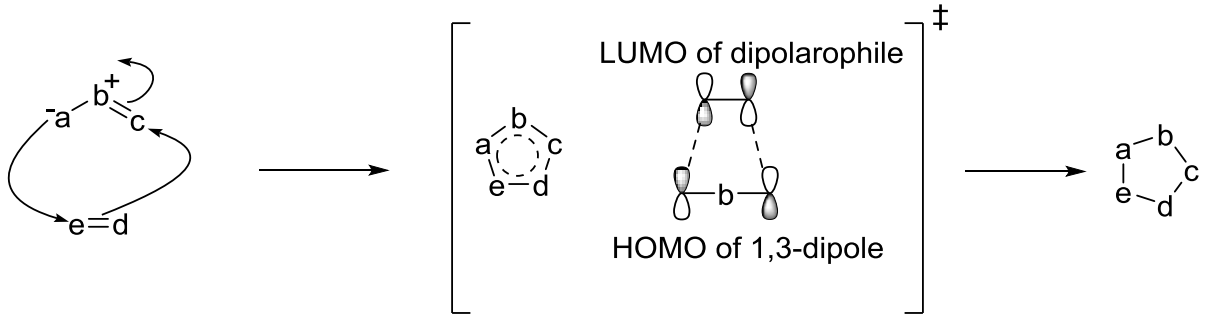

Scheme 5.1. Mechanism of 1,3-dipolar cycloaddition.

5.2.2. The Cu-catalysed Azide-alkyne Huisgen Cycloaddition (CuAAC)

The azide-alkyne Huisgen cycloaddition (AAC) is a 1,3-dipolar cycloaddition between an organic azide and an alkyne to give triazole ring products, as shown in Scheme 5.2 (a mixture of the 1,4-triazole and the 1,5-triazole is typically formed).[7] In the 1960s, Rolf Huisgen established the mechanism and explored the synthetic application of this reaction. The AAC reaction has been referred to as "the cream of the crop"[8] of click reactions, and has been extensively used in drug discovery applications.[9]

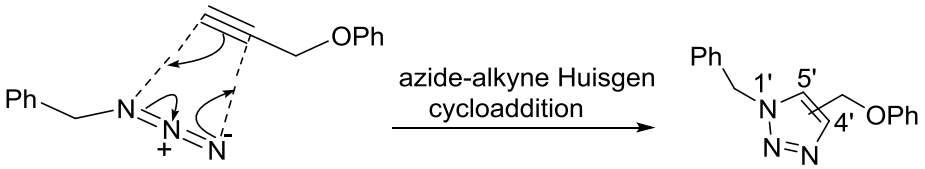

Scheme 5.2. AAC reaction between an organic azide (1,3-dipole) and an alkyne (dipolarophile) resulting in the formation of triazole products.

In 2001, Barry Sharpless defined click chemistry to be a group of reactions that "…must be modular, wide in scope, give very high yields, generate only inoffensive by-products that can be removed by non-chromatographic methods, and be stereospecific (but not necessarily enantioselective). The required process characteristics include simpler

reaction conditions (ideally, the process should be insensitive to oxygen and water), readily available starting materials and reagents, the use of no solvent or a solvent that is benign (such as water) or easily removed, and simple product isolation. Purification, if required, must be by non-chromatographic methods, such as crystallization or distillation, and the product must be stable under physiological conditions."[8]

The AAC has gained significant interest over the past decade, especially since the introduction of Cu(I) catalysis, which led to major improvements in both the regioselectivity and rates of the reaction.[10-12] Without the Cu(I) catalyst, the Huisgen cycloaddition is very slow and gives a mixture of 1,4- and 1,5-traizoles.[7] The versatility of the Cu(I)-catalysed azide-alkyne Huisgen cycloaddition (CuAAC) has been demonstrated by its robustness, insensitivity to water and oxygen, and capability to use a wide range of substrates, and has been exemplified with several applications in the biological and chemical sciences.[13] CuAAC works under water- and oxygen-tolerant conditions, and gives products in good yields with minimal side product formation. Indeed, triazole chemistry has been effectively used to enhance antibacterial, antitumor, antiviral, and antifungal properties of various compounds.[14-16] Thus, a number of catalytic conversions of azides and acetylenes in a wide range of syntheses has been performed in the last decade.[17-20] Also, CuAAC has been used in the synthesis of peptidomimetics and in bioconjugations[21-23] and has been praised as a "green" aqueous reaction.[24]

The triazole ring moiety has been shown to be chemically inert under a wide range of reaction conditions, such as hydrolysis, oxidation, and reduction. Moreover, its synthesis

can be carried out either in aqueous or in organic media.[23, 25] The CuAAC mechanism has been extensively studied and debated.[26-27] The major difference between the CuAAC and its non-catalysed counterpart (AAC) is the alteration in the activation energy barrier. Quantum mechanical calculations have shown that the transition state of the non-catalysed reaction is largely non-polarized.[28] Some 18.1 of the total 29.9 kcal/mol $\Delta G^{\ddagger}$ required is associated with the energy needed for the distortion of the azide prior to the reaction with acetylene. A stepwise catalytic process decreases the transition state energy by 11 kcal/mol and thus achieves significant rate enhancement.[29] In the CuAAC reaction, first, the Cu(I) coordinates with the π-electrons of acetylene lowering the pK_a of the acetylenic proton by up to 9.8 pK_a units, allowing de-protonation to occur in an aqueous solvent without the addition of any base (Scheme 5.3). This coordination step is then followed by an exothermic formation of a Cu(I)-acetylide complex **5.2**. The complex **5.2** then coordinates to the azide **5.3**, which rearranges into a metallocycle **5.4**, and then further into the Cu-metallated triazole **5.5.** The Cu-triazole complex then releases the free triazole **5.6** and 2Cu(I)L.

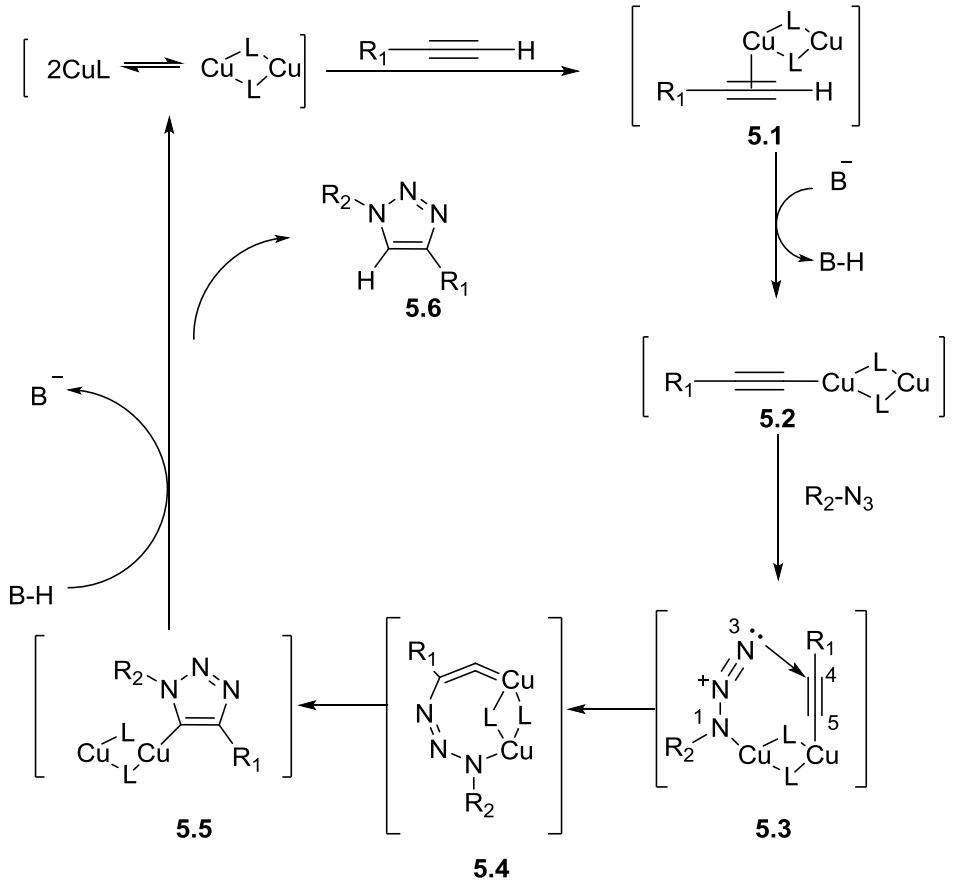

Scheme 5.3. Proposed catalytic cycle for the CuAAC reaction.

Although there have been some minor revisions to this mechanism,[26-27] the contribution of the Cu(I) catalyst in the reduction of the transition state energy remains unchallenged. The CuAAC reaction can be performed with almost any source of solvated Cu(I).[26] However, the Cu(I) can be easily oxidized to Cu(II), resulting in the inactivation of the catalyst. There are a number of methods used to produce the active catalyst for this reaction. One of the most common methods is to reduce Cu(II) salts, such as $CuSO_4 \cdot 5H_2O$, *in situ* to form Cu(I) salts. Sodium ascorbate is typically used as the reducing agent,[26] but other reducing agents, such as tris(2-carboxyethyl)phosphine (TCEP)[30] and hydrazine[31] have also been used successfully.

Alternatively, it is possible to directly add Cu(I) salts, such as CuBr, CuI, $[Cu(NCCH_3)_4][PF_6]$, or $CuOTf{\cdot}C_6H_6$,.[32] These Cu(I) sources do not need a reducing agent, but the reaction has to be performed in a deoxygenated environment and in an organic (or mixed) solvent system meaning that protecting groups may be required. Another disadvantage with these methods is that they also tend to lead to side products.[32-33] Thus, it can be concluded that the usage of Cu(I) salts is not as reliable as the *in situ* reduction of Cu(II) salts.

5.2.3. Biological Applications of 1,2,3-triazoles

Cu(I)-catalysed triazole formation has been widely used for the modification of pharmaceuticals and natural products. CuAAC allows the attachment of various chemical entities to a drug in order to enhance important properties, such as solubility and/or bioavailability.[34-35] A number of reviews are available which describe the benefits of using click chemistry for pharmaceutical applications.[36] The biological interest in triazoles arises from the fact that they are easy to make and are very stable under biological conditions.[9, 37] The ability of triazoles to tolerate oxygen, water, biological molecules, a wide range of solvents, and the *in vivo* conditions of living systems (hydrolysis, reductive environment *etc*.) makes them suitable candidates as isosteres of the amide bond in biological compounds.[9, 26, 30]

The CuAAC reaction has also been used to click carbohydrates to a wide variety of entities. In fact, a prominent method for attaching saccharides to other organic molecules has been to introduce an azide in the 1-, 2-, or 6-positions of the saccharide and then to

react it with a variety of organic alkynes using CuAAC.[1, 38-40] The CuAAC reaction has also been used to attach carbohydrate functionality to different carbohydrates and also to amino acids.[41-42]

5.2.4. AuNP surface modification using AAC

In 2006, Fleming *et al.* used the AAC reaction to attach a series of different molecules to AuNPs.[43] For the AAC reaction, small AuNPs (1.8 nm) were used because of their easy synthesis, high solubility, and good ligand exchange properties. A two-phase Brust-Schiffrin method (BSM) was firstly used to synthesize decanethiol-stabilized AuNPs. These particles were then reacted with $BrC_{11}H_{22}SH$ to replace some of the decanethiol ligands with Br-terminated undecanethiol ligands (Scheme 5.4). Nucleophilic substitution of the Br termini with NaN_3 then resulted in AuNPs decorated with azide functionalities on their outermost periphery (Scheme 5.4). Alkyne derivatives of nitrobenzene (NB), ferrocene (Fc), anthracene (An), pyrene (Pyr), aniline (Ani), and poly(ethylene glycol) (PEG) were synthesized for the click reaction with the AuNP surface (Figure 5.1). All these compounds contained a carbonyl group next to the terminal alkyne to provide a more electron withdrawing environment that would increase the rate of the AAC reaction. It was observed that a small amount of AuNPs underwent irreversible aggregation during the reaction. However, a majority of the AuNPs (> 90%) remained soluble and could be separated from the aggregates after the reaction. Although Fleming *et al.* successfully performed the AAC reaction on AuNPs, the yields (*i.e.* the extent of the azide conversion to triazole) were low (22%, or 54% in one specific case) even after 60 h.[43-44]

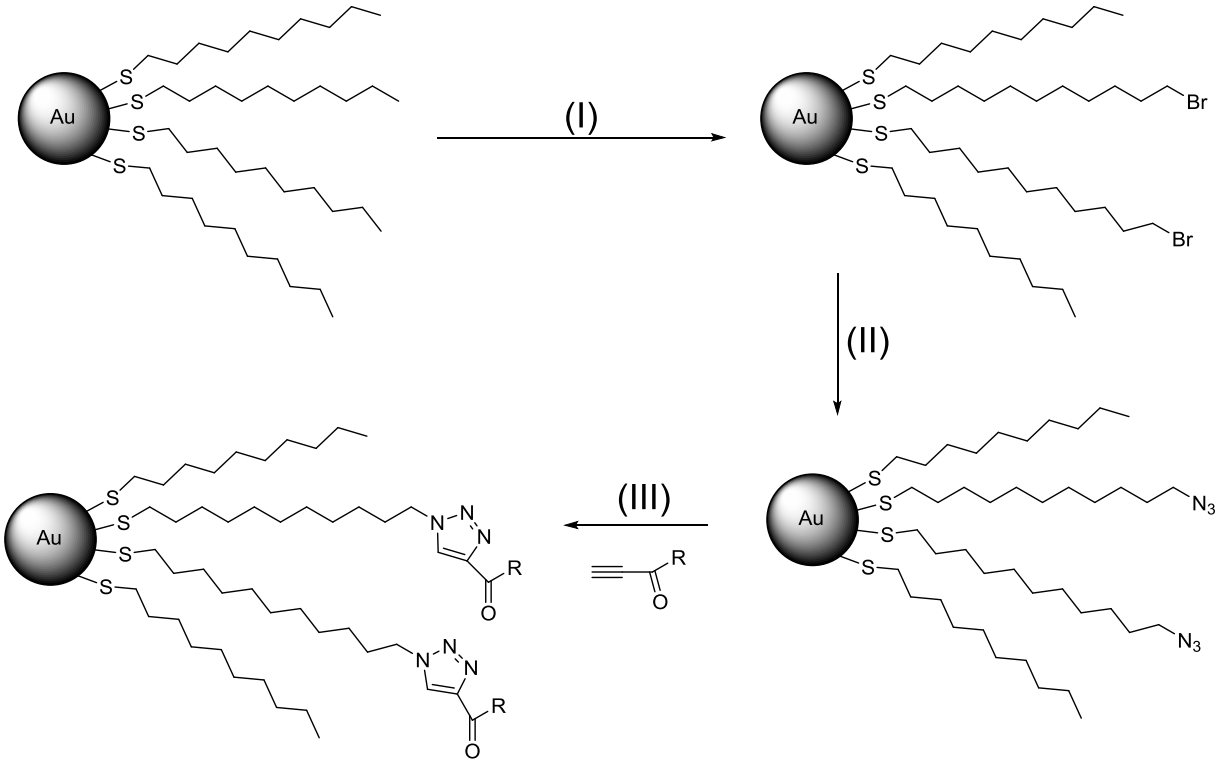

Scheme 5.4. The functionalization and the AAC reaction on AuNP surface. Reagents and conditions: (i) $Br(CH_2)_{11}SH$ in DCM, 60 h, rt; (ii) NaN_3 in DCM/DMSO solution, 48 h; (iii) R = propyn-1-one derivatized compounds (shown in Figure 5.1), 24-96 h in dioxane or 1:1 hexane/dioxane.[43]

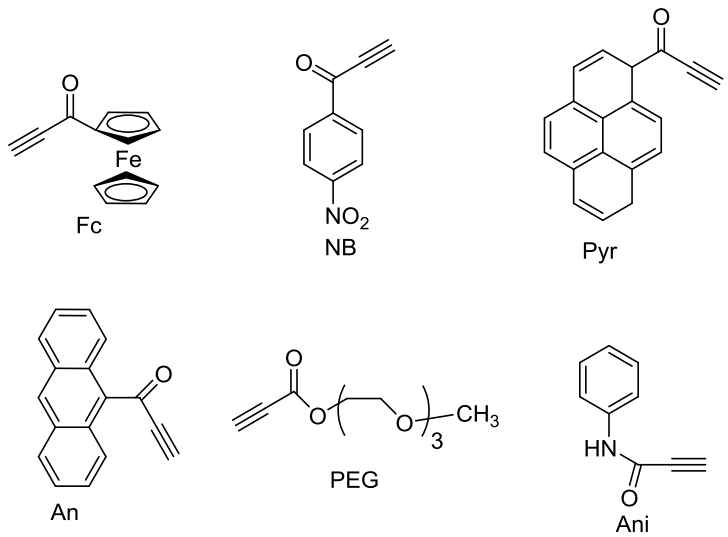

Figure 5.1. The propyn-1-one derivatized compounds used for the AAC reaction.[43]

Following the work of Fleming *et al.* various groups have used different conditions to try and increase the efficiency of the AAC reaction on AuNP surfaces. Limapichat *et al.* used electron deficient alkyne derivatives to perform the AAC reaction and observed that 75% of the azide on AuNP surface underwent cycloaddition in 16 h (Scheme 5.5).[45] Ismaili *et al.* carried out the AAC reaction with a number of terminal-acyl alkynes under hyperbaric conditions (11000 atm) and observed 80% or higher conversions within 15 to 24 h (Scheme 5.6).[46]

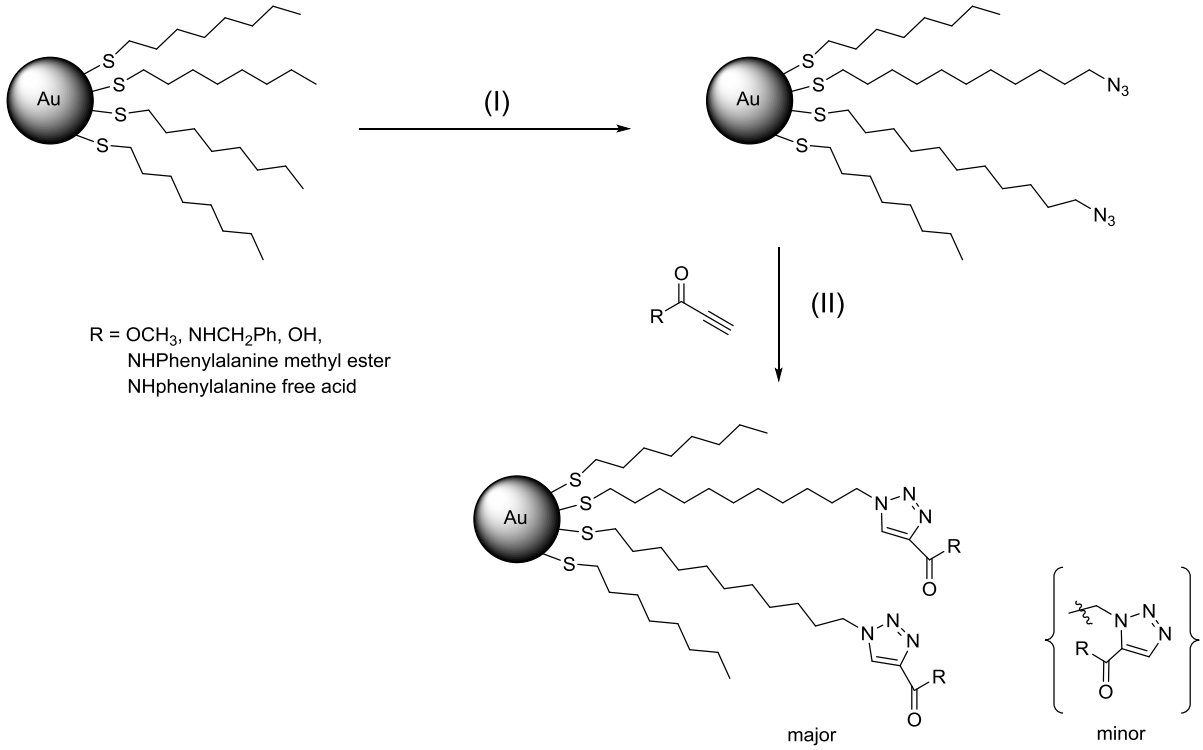

Scheme 5.5. Azide functionalization and AAC reaction on AuNP surface using electron deficient alkynes. Reagents and conditions: (I) $HS(CH_2)_{11}N_3$, C_6H_6, rt, 7 h; (II) THF, rt, 16 h.[45]

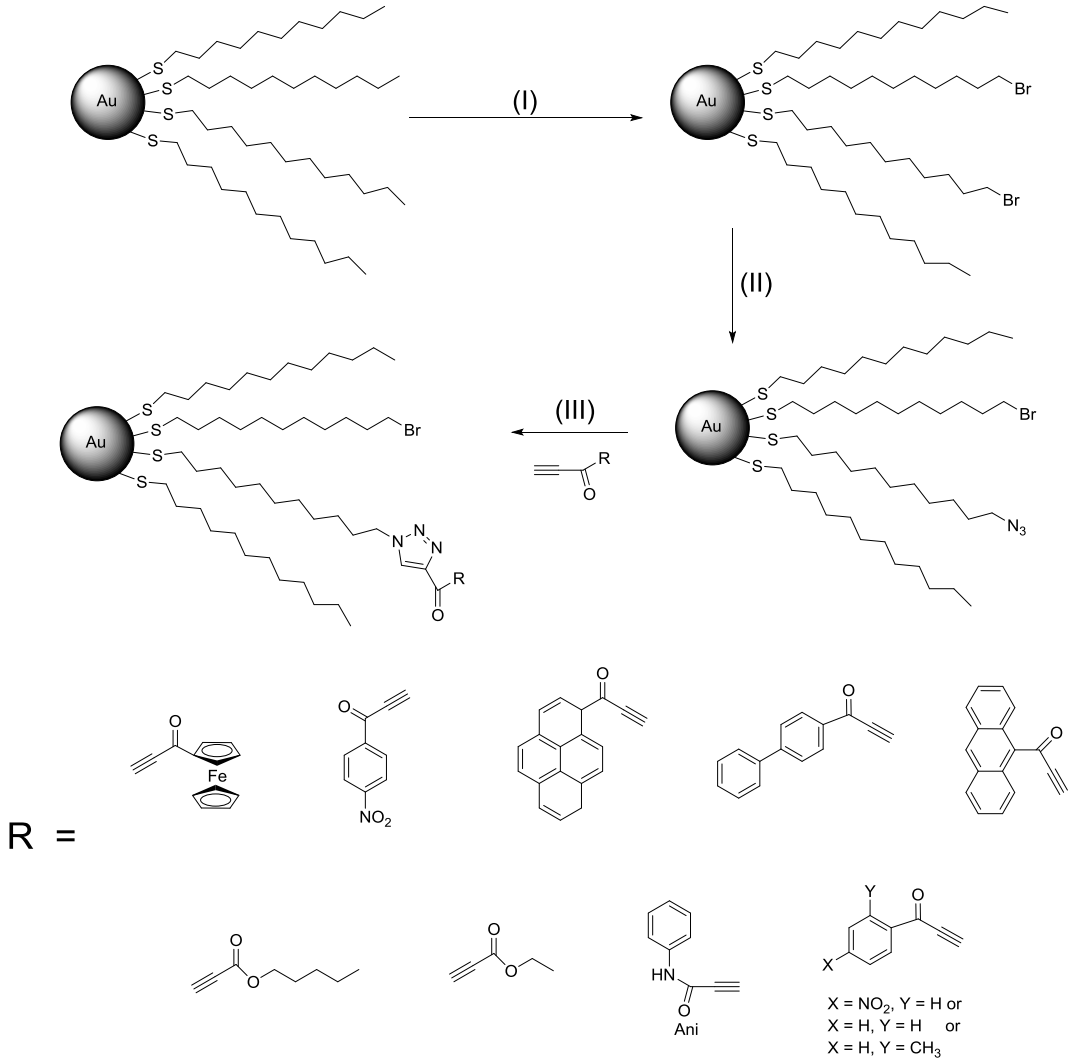

Scheme 5.6. AAC reaction performed under hyperbaric conditions. Reagents and conditions: (i) $Br(CH_2)_{11}SH$ in C_6H_6, 48 h, rt; (ii) NaN_3 in C_6H_6/DMSO solution, 48 h; (iii) R = propyn-1-one derivatized compounds, DCM, 11000 atm, 25 ^oC, 15-24 h.[46]

In 2014, Gobbo *et al.* used *interfacial* strain promoted azide-alkyne cycloaddition (I-SPAAC) to modify AuNP surfaces.[47] 2.8 nm Sized AuNPs functionalized with strained dibenzocyclooctyne derivative (DBCO-AuNP) were synthesized as shown in Scheme 5.7. These AuNPs were treated with azide-decorated polymersomes (a class of artificial vesicles) which were successfully functionalized with AuNPs in 1 h (Scheme 5.8).

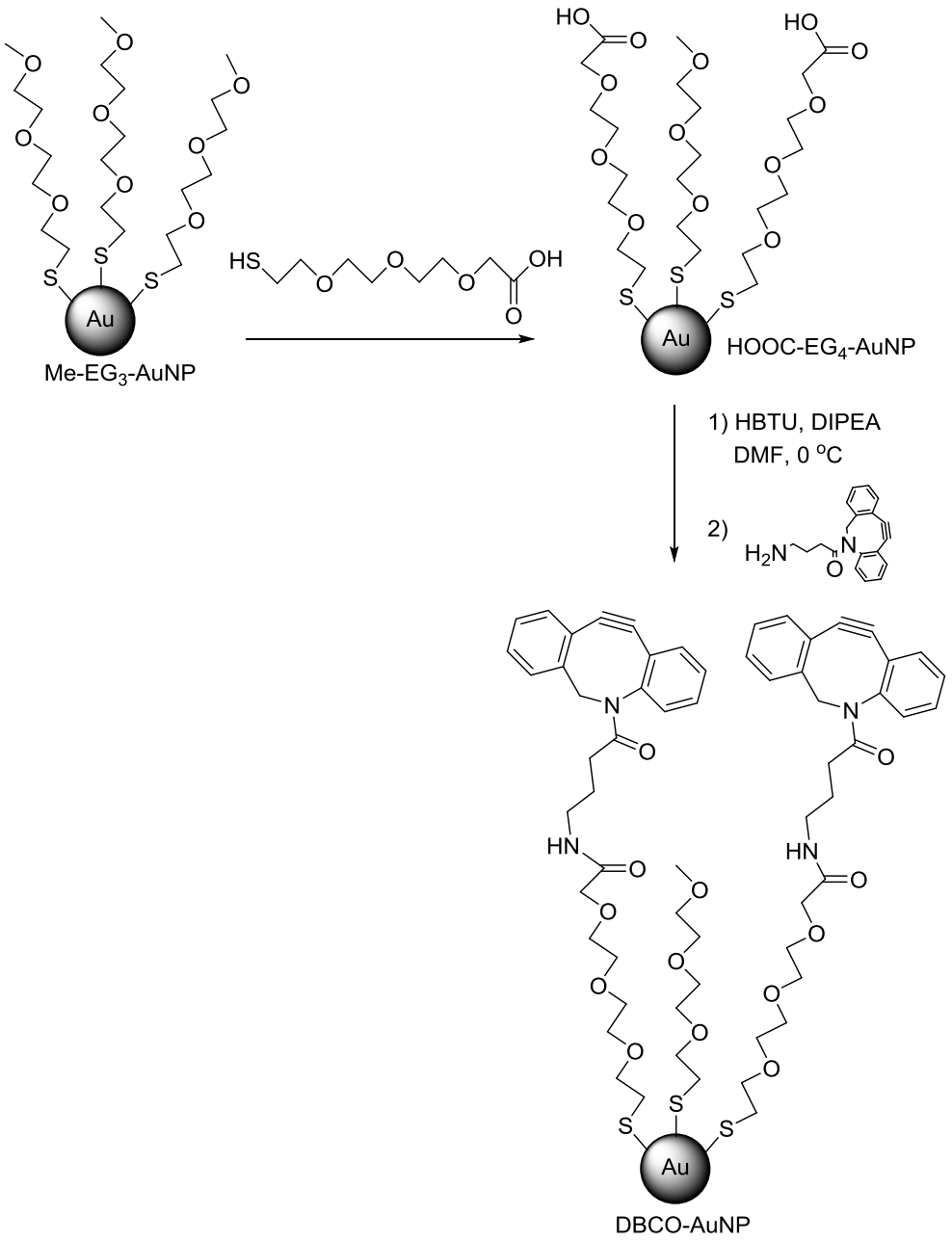

Scheme 5.7. Synthetic scheme of AuNPs functionalized with strained alkyne derivatives. HBTU = O-Benzotriazole, N,N,N',N'-tetramethyl-uroniumhexafluoro-phosphate (coupling agent), DIPEA = *N*,*N*-diisopropylethylamine.[47]

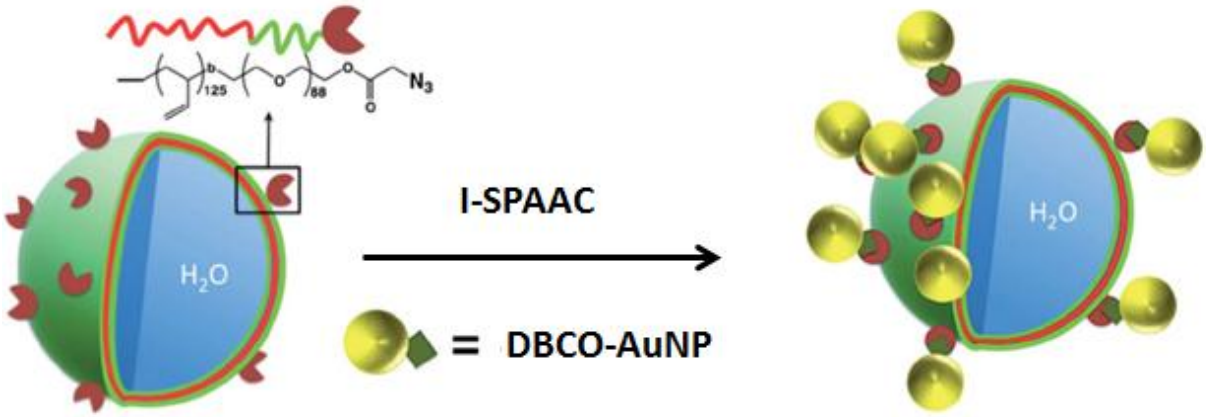

Scheme 5.8. A schematic representation of the I-SPAAC reaction between azide-functionalized polymersomes and strained alkyne functionalized AuNPs (DBCO-AuNPs) in water. Image reproduced from Ref. 47 with permission from the Royal Society of Chemistry.

5.2.5. AuNP surface modification by CuAAC

In 2006, Brennan *et al.* demonstrated that enzyme-AuNP conjugates could be synthesized by click chemistry.[48] Azide-functionalized AuNPs were synthesized by treating standard Cit-AuNPs (14 nm size) with an aqueous solution of thiolated azide ligand, as shown in Scheme 5.9. An acetylene-functionalized *Thermomyces lanuginosus* lipase was attached to these azide-functionalized water-soluble AuNPs by CuAAC (Scheme 5.9). The enzymes retained their activity after the click reaction. However, the excess of Cu (million-fold excess in comparison to the azide) and lipase used, the long reaction duration (3 days), the extensive purification procedure required, and the poor conversion of azide to triazole (less than 1%) limited further use of this procedure.

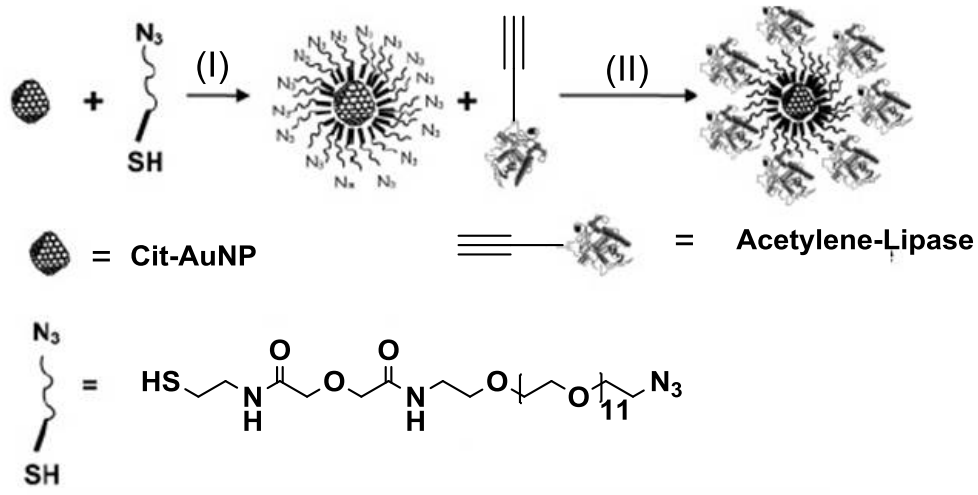

Scheme 5.9. Functionalization of AuNPs with thiolated-azide ligand, and attaching of lipase to these AuNPs using Click Chemistry. Reagents and conditions: (I) H_2O, rt, 18 h; (II) H_2O, $CuSO_4$, ascorbic acid, rt, 3 d. Reprinted with permission from Ref. 48. Copyright (2016) American Chemical Society.

Later, in 2007, Sommer *et al.* developed a simpler method to perform CuAAC on AuNP surface.[49] Microwave-assisted CuAAC was used to attach a variety of alkyne derivatives to azide functionalized AuNPs (Scheme 5.10). The use of the microwave heating for the CuAAC reaction reduced the reaction time to 5-10 min and also gave nearly quantitative conversion of the azides to triazoles. However, significant particle decomposition or aggregation was observed when AuNPs were treated for more than 15 min in the microwave reactor.

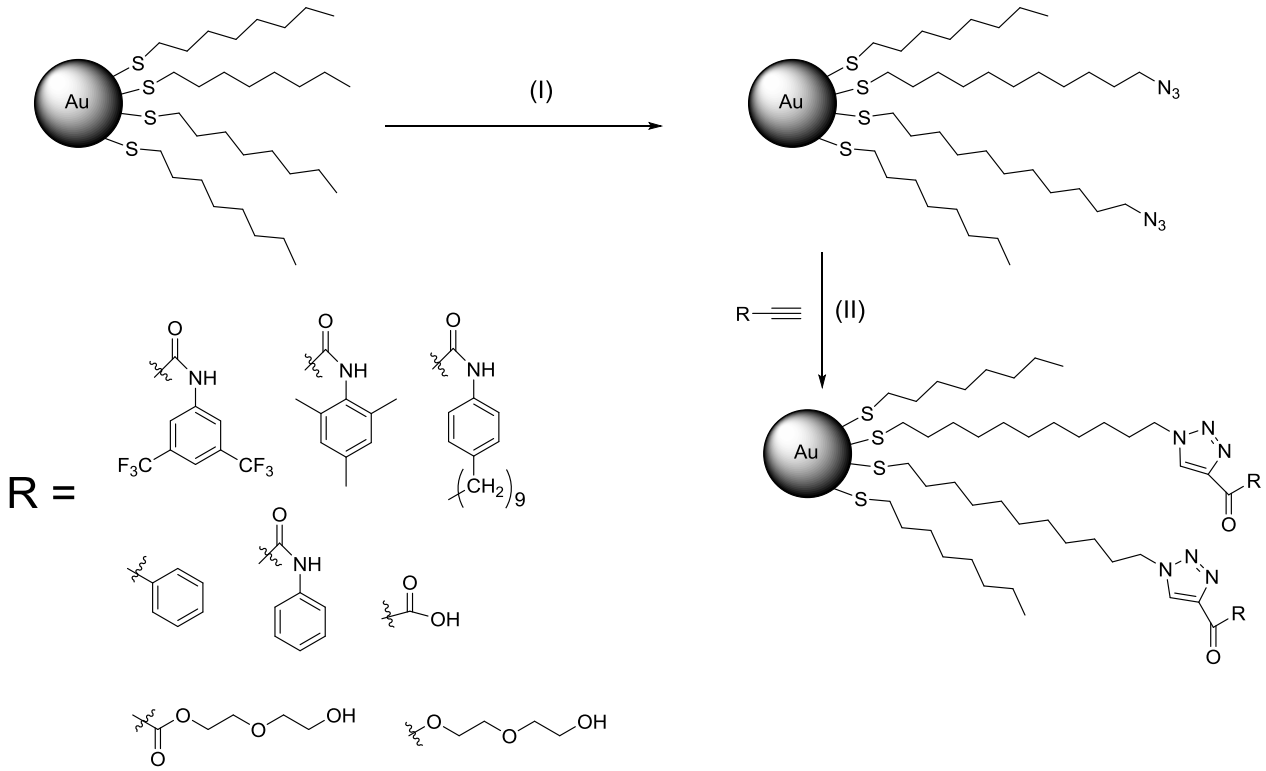

Scheme 5.10. The CuAAC reactions performed under microwave heating. Reagents and conditions: (I) $HS(CH_2)_{11}N_3$, C_6H_6, rt, 7 h; (II) dioxane/^{t}BuOH/H_2O or THF, $CuSO_4$, sodium ascorbate, microwave heating (1000 W), 5-10 min.[49]

Boisselier *et al.* reported several modifications to try and overcome the common problems faced in the CuAAC reaction of the AuNPs.[50] They reasoned that one important constraint that needed to be addressed to perform an efficient click reaction was the solubility of the reagents; alkanethiol-functionalized AuNPs are soluble in organic solvents, whereas water is required to dissolve the catalyst $CuSO_4$. In order to circumvent the solubility problem, a homogenous water-THF solvent system was used where AuNPs in THF were added to either an aqueous solution containing water-soluble alkyne derivatives or a THF-water solution of organic soluble alkyne derivatives. The amount of ascorbic acid and Cu(I) catalyst was also increased to stoichiometric amounts with respect to alkyne and azide. Also, the click reaction was performed under an inert

atmosphere. It was observed that if any of the above mentioned conditions were not met, the reaction gave a very poor yield, but when all the conditions were fulfilled, the azide to triazole conversion was virtually quantitative at rt. The reaction was performed with a variety of alkynes and good results were obtained despite the different sizes of the alkynes and their hydrophilicity. The overall reaction scheme is shown in Scheme 5.11 and the variety of alkynes used is shown in Figure 5.2.

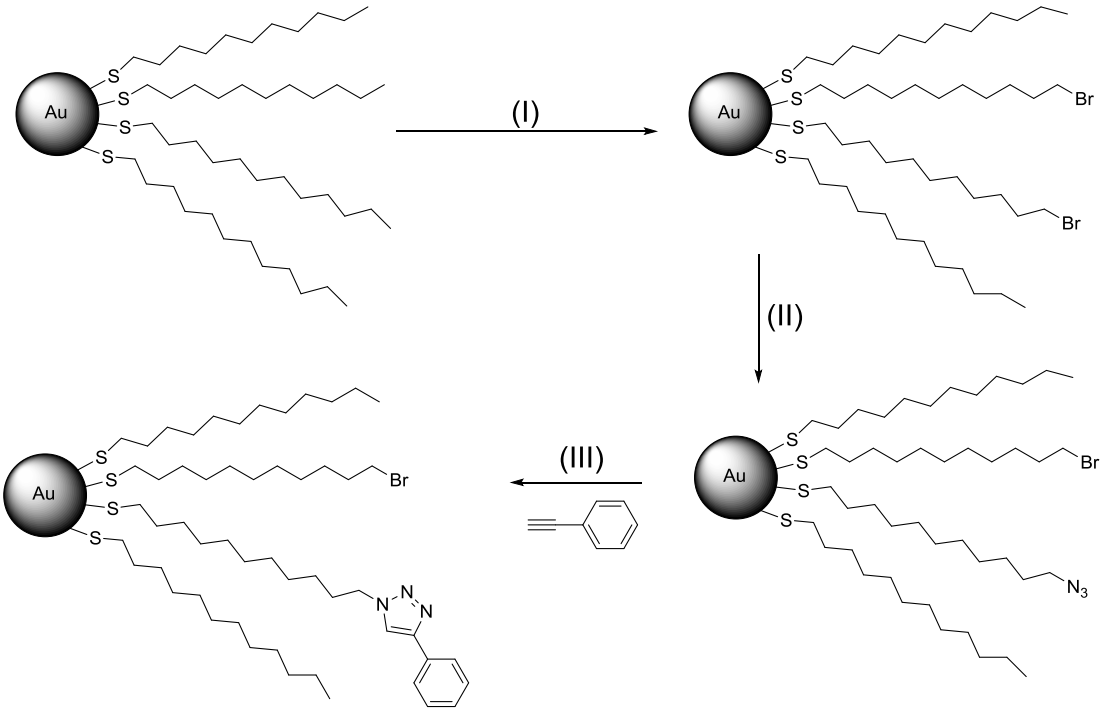

Scheme 5.11. The overall synthetic scheme of AuNP functionalization and the click reaction by Boisselier *et al*.[50] Reagents and conditions: (I) $HS(CH_2)_{11}Br$, DCM, rt, 5 d; (II) NaN_3, DCM/DMSO, rt, 2 d; and (III) $CuSO_4$, sodium ascorbate, THF/H_2O, 2 d, inert atmosphere.

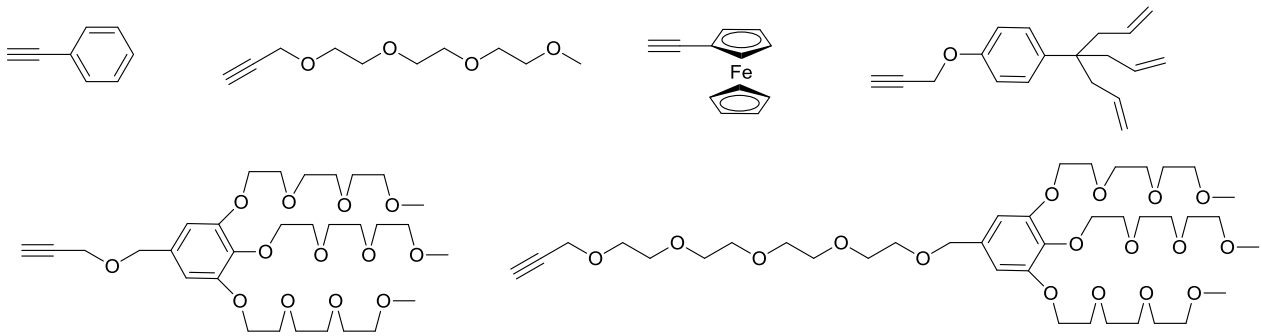

Figure 5.2. Various alkyne ligands used for the click reaction in the work of Boisselier *et al.*[50]

Following these reports, several other groups have used the CuAAC reaction on AuNPs for the detection of copper (II) salts,[51-53] ascorbic acid,[54] and protein quantification (for proteins capable of reducing Cu (II) to Cu (I)).[55] In general, two systems of AuNP, one functionalized with azide ligands and other with alkyne ligands, were synthesized and the CuAAC reactions were performed. The aggregation of AuNPs due to the click reaction was considered as the basis for the detection of various analytes.

Although, several groups have used the CuAAC reaction to attach thiolated ligands to various sugars and then subsequently attach these thiolated-sugar derivatives to AuNPs,[56-58] there has only been one study that has reported the use of the CuAAC reaction to click sugars directly onto the AuNP surface . In 2008, Chikae *et al.* first functionalized AuNPs electrodeposited on a carbon electrode with an alkyne-terminated symmetric disulfide (4,7,10,13,38,41,44,47-octaoxa-25,26-dithiapentaconta1,49-diyne).[59] Then azide-terminated sialic acid derivatives were attached to the AuNPs by the CuAAC as shown in Scheme 5.12.

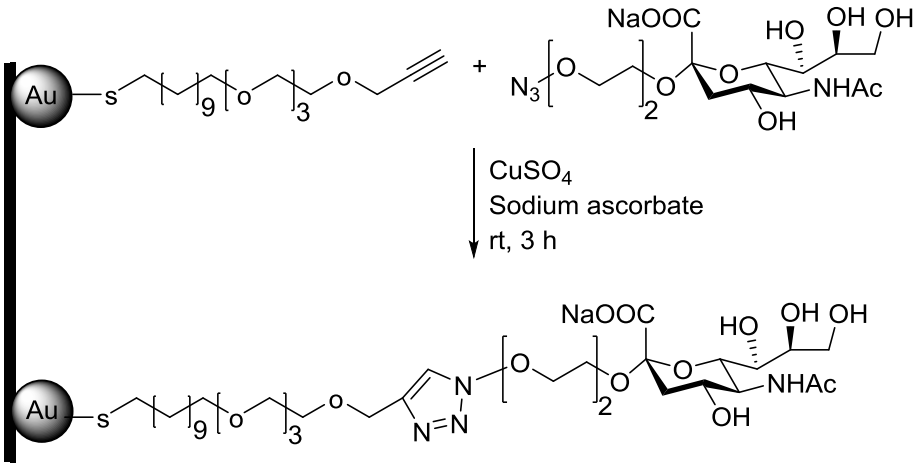

Scheme 5.12. Conversion of AuNPs electrodeposited on carbon electrode into gAuNPs by CuAAC.[59]

However, in contrast to these reports of the successful use of CuAAC for the modification of AuNPs, at least three groups have reported that attempts to modify azide-functionalized AuNPs with alkyne derivatives by CuAAC either resulted in the reversible aggregation of the particles, or in negligible conversions.[43, 45, 47] Fleming *et al.* attempted to increase the yield of the AAC reaction using several catalyst systems.[43] As the particles (AuNPs functionalized with a mixture of decanethiol, Br-terminated undecanethiol, and azide-terminated undecanethiol) were insoluble in aqueous solutions, the most frequently used $CuSO_4$-ascorbic acid system could not be used. Thus, catalysts soluble in organic solvents such as CuI, CuBr/2,6-lutidine, and bromotris(triphenylphosphinato) copper (I) were used, and, in all cases rapid and extensive particle aggregation or decomposition was observed. Limapichat *et al.* also reported similar results when Cu catalysts were used to try and enhance the cycloaddition reaction.[45] Gobbo *et al.* reacted water soluble AuNPs (particles functionalized with a mixture of Me-EG_3-SH and N_3-EG_4-SH) with 2-propyn-1-amine hydrochloride or 1-ethynylpyrene, in the presence of $CuSO_4$ and sodium ascorbate, and faced the same

problem of irreversible particle aggregation.[47] It was suggested that the particles underwent aggregation/decomposition during the CuAAC reaction due to the reaction of Cu(I) salts with the Au surface.[47]

The remaining sections of this chapter will detail the synthesis of a thiolated ligand which possesses a terminal alkyne group, the attachment of these ligands to AuNPs, and attempts to perform the one-pot synthesis of gAuNPs from these alkyne functionalized AuNPs using the CuAAC reaction.

5.3. Results and Discussion

5.3.1. Synthesis of alkyne-terminated thiol ligand (ATT).

Reaction of triethylene glycol **5.7** (1 equivalent) by stirring with NaH (0.65 equivalent) in THF followed by the addition of propargyl bromide (0.5 equivalent) gave a mixture of the alkyne **5.8** (major product, Scheme 5.13) and a triethylene glycol derivative with propargyl group at both ends (minor product). Compound **5.8** was then reacted with mesylchloride (MsCl) and triethylamine in DCM, to form an intermediate mesylate, which was then reacted with potassium thioacetate in DMF at 65 ^{o}C to afford the thioacetate **5.9.** Deacetylation of **5.9** with sodium methoxide in methanol, followed by neutralization with 1 M aqueous HCl, afforded a mixture of the disulfide **5.10** and the thiol **5.11**. Initial attempts to reduce disulfide **5.10** to thiol **5.11** using Zn powder as the reducing agent and CH_3COOH as an H^+ donor in DCM gave a mixture of **5.11** and a compound bearing an alkene unit instead of the desired alkyne. Grimmer *et al*. have reported that alkynes can be reduced to alkenes by Zn/CH_3COOH.[60] An alternative

approach was attempted using $NaBH_4$ as the reducing agent in MeOH, but this did not yield the desired thiol **5.11**. Oae *et al.* have reported that although $NaBH_4$ is capable of reducing diaryl disulfides to the corresponding thiols, it does not reduce dialkyl disulfides.[61] Finally it was found that the use of dithiothreitol in the presence of *N*,*N*-diisopropylethylamine effected reduction of the disulfide **5.10** to afford the alkyne-terminated thiol (ATT) **5.11** (Scheme 5.13).

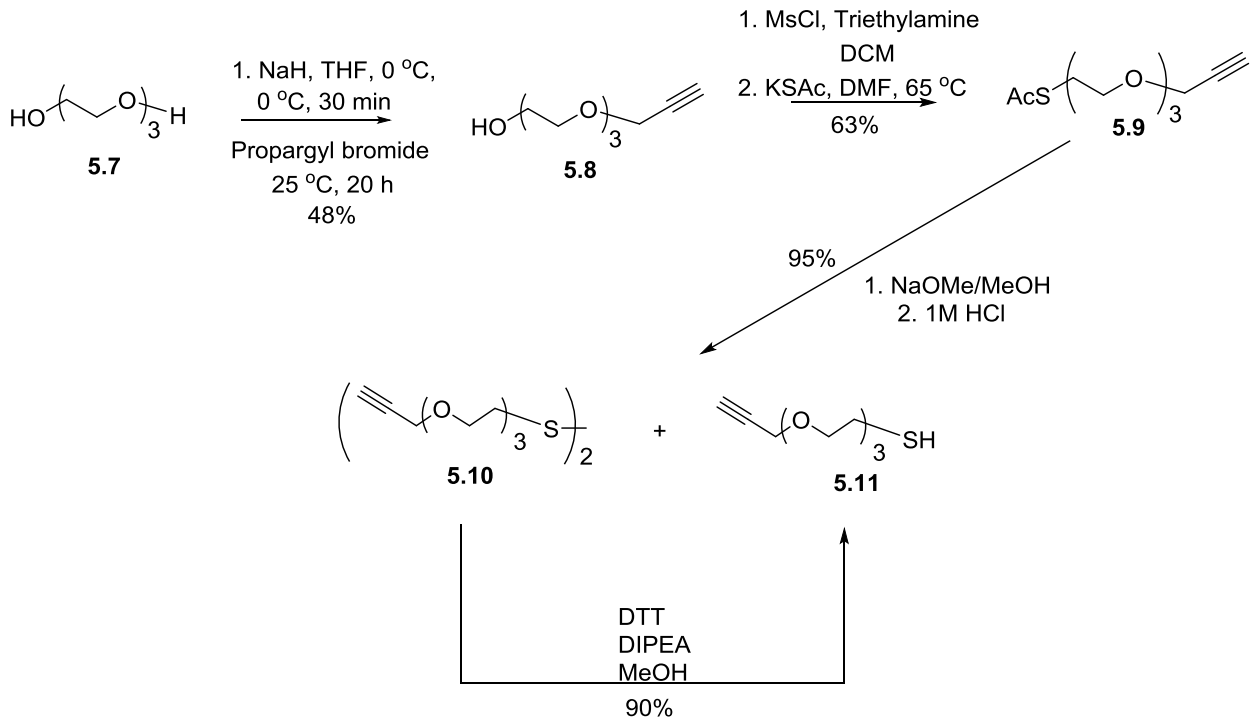

Scheme 5.13. Synthesis of the alkyne-terminated thiol (ATT) ligand.

5.3.2. Synthesis of AuNPs functionalized with alkyne-terminated thiol ligand (ATT-AuNPs)

Initially, an attempt was made to synthesize smaller sized (~2 nm) ATT-AuNPs both by a two-phase (water-toluene), and one-phase (MeOH) Brust-Schiffrin method (BSM). In two-phase BSM, $HAuCl_4$ was transferred from water to toluene using

tetraoctylammonium bromide (TOAB) and then ATT **5.11** was added to the toluene phase followed by the addition of an aqueous solution of $NaBH_4$. In one-phase BSM, ATT **5.11** dissolved in MeOH was added to a solution of $HAuCl_4$ in MeOH followed by the addition of an aqueous solution of $NaBH_4$. However, the AuNPs obtained from both the one-phase and two-phase BSM were found to be unstable and aggregated/decomposed a few hours into the reaction. Hashmi *et al.* have reported that alkynes are the most successful and most commonly used substrate in a variety of Au^{3+}/Au^{+} catalysed addition reactions.[62] The triple bond of alkynes coordinates to Au^{3+}/Au^{+} complexes resulting in the efficient activation of the bond for the attack of a nucleophile as shown in Scheme 5.14.[63] For example, Thomas *et al.* have reported that $HAuCl_4$ can be used as a catalyst for the conversion of a terminal alkyne in aqueous MeOH to a ketone (major product) by a Markovnikov addition as shown in Scheme 5.15.[64] Thus, we assume that a similar catalytic reaction of $HAuCl_4$ with the terminal alkyne in ATT interfered with the Brust-Schiffrin reaction and resulted in the formation of unstable AuNPs.

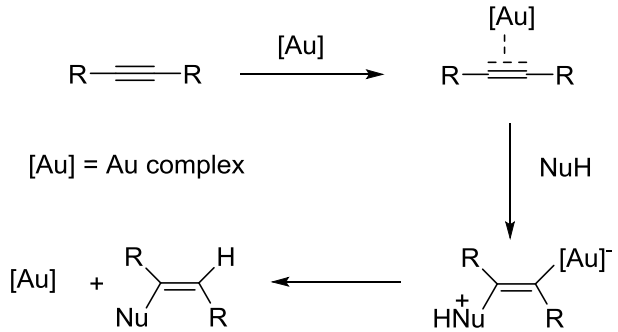

Scheme 5.14. Activation of a triple bond by Au complex followed by the attack of a nucleophile.

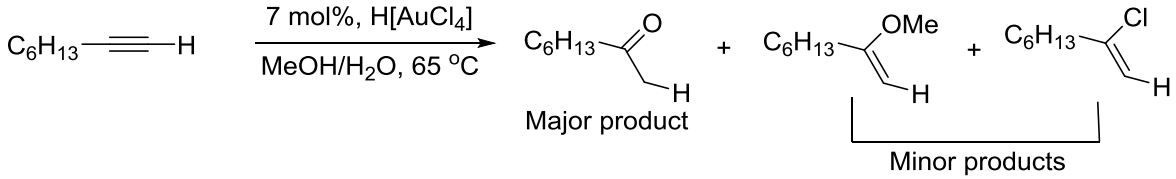

Scheme 5.15. $HAuCl_4$ catalysed conversion of a terminal alkyne to a ketone.

Next 12 nm sized ATT-AuNPs were synthesized by a ligand exchange reaction of Cit-AuNPs (12 nm) with ATT **5.11** (Scheme 5.16). Compound **5.11** was dissolved in MeOH, and was then added to the Cit-AuNPs in water and stirred. After 24 h, the reaction yielded the ATT-AuNPs, which were not soluble in water or polar organic solvents, such as MeOH or MeCN, but which were soluble in non-polar organic solvents, such as DCM, $CHCl_3$, and THF. The ATT-AuNPs were then purified by washing with water (to remove citrate), followed by repeated centrifugation (4 x 6000 rpm) in MeOH until no ATT ligands were found in the supernatant by ^{1}H NMR analysis. The broad peaks corresponding to the ligand ATT protons in the ^{1}H NMR spectra (Figure A5.1 in Appendix) confirmed the binding of the ATT ligands to the surface of AuNPs. The average molecular formula of the SG-gAuNPs was determined by TGA (Figure A5.2 in the Appendix) to be $Au_{53568}(C_9H_{15}O_3S)_{43174}$. The average molecular formula calculations were carried out in the similar manner as described in Chapter 3, Section 3.2.2. The size distribution histograms of both the Cit-AuNPs and the ATT-AuNPs are shown in Figure A5.3 in Appendix.

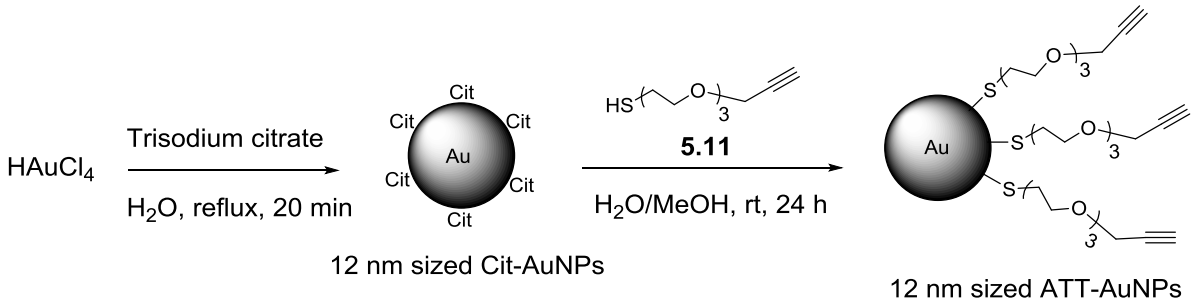

Scheme 5.16. Synthesis of 12 nm sized ATT-AuNPs by a ligand exchange method.

Previously, when water soluble ligands were used to perform the exchange reactions on Cit-AuNPs (Chapter 3 and 4), the wine-red colour of the AuNP solution, the dispersed state of the AuNPs (as determined by TEM images), and the SPR peak (obtained in UV-Vis spectrophotometer measurements) was same both before and after the ligand exchange reaction. However, in this case, when this water-insoluble ligand was used, the solution turned purple (Figure 5.3), the SPR peak shifted to a higher wavelength (523 nm to 541 nm) and became broader (Figure 5.4), and the TEM images revealed partial aggregation of the particles (Figure 5.5). Despite the partial aggregation seen in TEM images, the ATT-AuNP solution remained stable without any precipitation at least for three months at 4 ^{o}C.

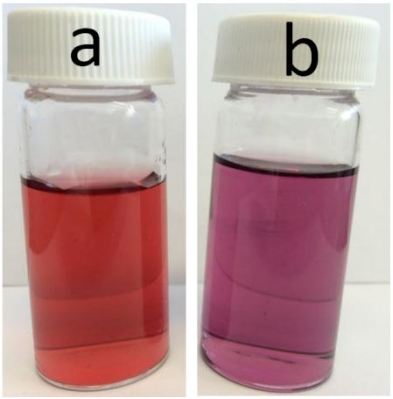

Figure 5.3. Photographs of AuNP solutions (a) Cit-AuNPs in water and (b) ATT-AuNPs in DCM

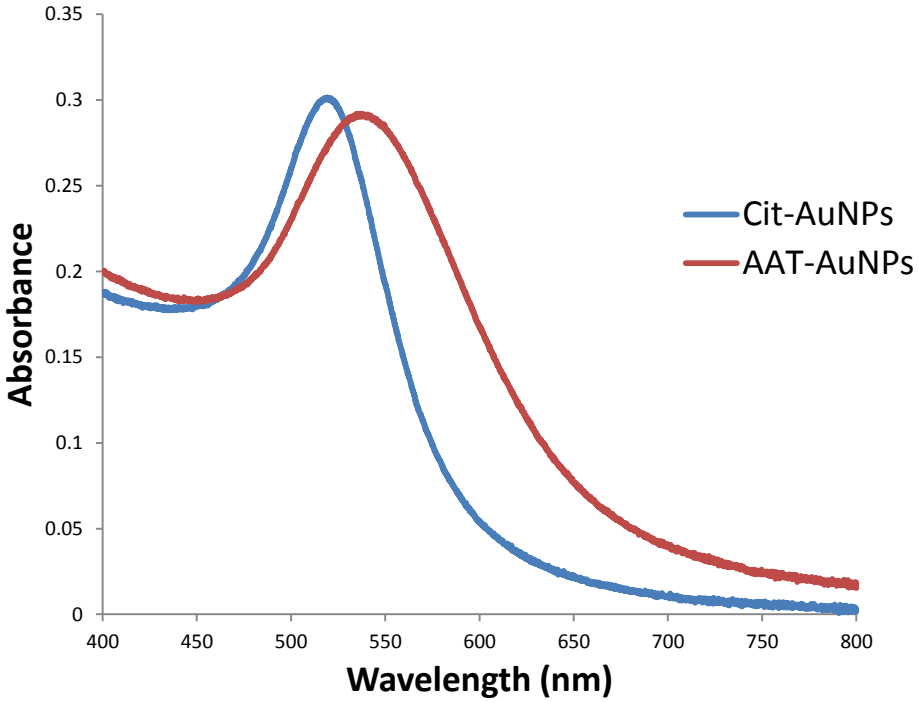

Figure 5.4. UV-Vis absorbance spectra of the Cit-AuNPs in water and AAT-AuNPs in DCM.

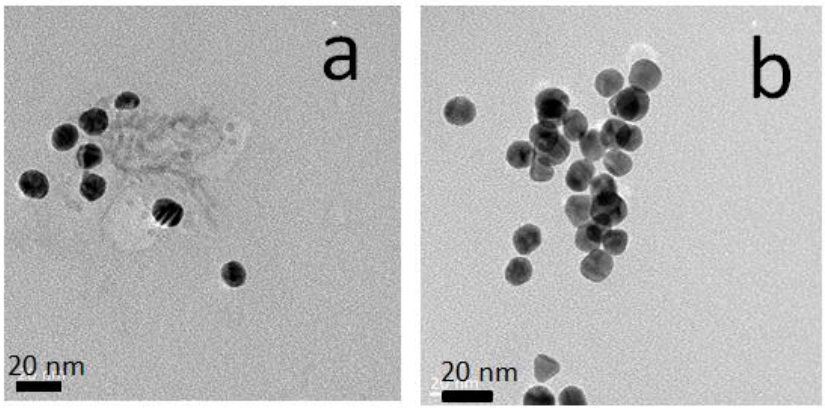

Figure 5.5. Representative TEM images of (a) Cit-AuNPs and (b) AAT-AuNPs

Baranov *et al*. observed similar results when a ligand exchange reaction was performed with 11-azidoundecane-1-thiol on 15 nm sized Cit-AuNPs.[65] In their work, 11-azidoundecane-1-thiol dissolved in DMF was added to the Cit-AuNPs in water. The AuNP solution turned from red to violet and, occasionally, small dark flakes (aggregated thiol-functionalized AuNPs) were observed on top of the solution. The thiol-stabilized AuNPs were found to be soluble in all organic solvents. The SPR peak shifted from 518 to 530 nm after the ligand exchange, and the particles were found to be self-assembled in the TEM images.

The problems associated with the phase transfer of AuNPs from water to an organic solvent following a ligand exchange process still remain to be solved.[65] The mode of binding of the ligands to the particles is entirely different in the two systems. In Cit-AuNPs, the electrostatic forces between the negatively charged citrate anions and the electron-deficient AuNP surface bind them together, and this interaction is supported by water due to its high dielectric constant; whereas in thiolated AuNPs, the covalent interaction between the Au atoms on AuNP surface and the sulfur in the thiol ligands is

responsible for the binding of the ligands with the particles. Organic solvents have a much lower dielectric constant than water. During the transfer of Cit-AuNPs from water to an organic solvent, and before they are completely stabilized with organic thiols, the citrate ligands dissociate in the organic solvent resulting in the aggregation of the particles.[65] The scattered and ambiguous experimental data present in the literature on the phase transfer of AuNPs from water to an organic solvent indicates that more detailed research has to be carried out to understand the phase transfer reaction in more depth.[66]

5.3.3. Synthesis of glycosyl azides

The traditional method used to synthesize unprotected glycosyl azides involves at least three or four protecting group manipulations to obtain the desired product. A synthetic route generally involves converting the desired sugar, for example *N*-acetyl-D-glucosamine (GlcNAc), into a protected glycosyl halide **5.13**, followed by a nucleophilic displacement by azide to give the glycosyl azide **5.14** (Scheme 5.17). Finally, the acetyl protecting groups are removed by Zemplén deacetylation to give the desired deprotected glycosyl azide **5.15**.[67]

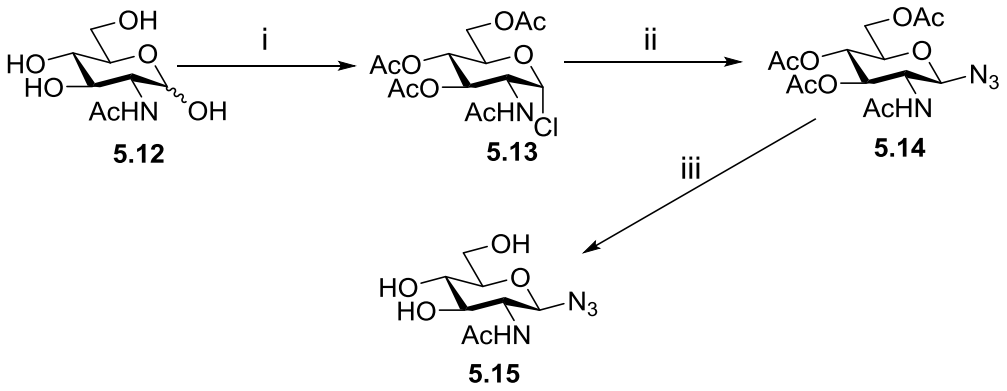

Scheme 5.17. Synthesis of de-protected glycosyl azides. Conditions: i) AcCl; ii) NaN_3, sat. aq. $NaHCO_3$, $^tBuNH_4.HSO_4$, DCM; iii) Na, MeOH.

5.3.4. Synthesis of glycosyl azides using 2-azido-1,3-dimethylimidazolinium hexafluorophosphate

In 2014, the Fairbanks' group demonstrated that 2-azido-1,3-dimethylimidazolinium hexafluorophosphate (ADMP) could be used to synthesize glycosyl azides efficiently.[1] Prior to that, 2-chloro-1,3-dimethylimidazolinium chloride (DMC) has been used as the activating agent and NaN_3 as the nucleophile source.[68] The Fairbanks group also showed that ADMP was capable of the dual roles of activating the reducing sugars, and providing an azide source without the use of sodium azide. ADMP **5.19** has also been used on several occasions in the literature as an efficient diazo-transfer reagent.[69-70] Friction and impact sensitivity tests have demonstrated that ADMP is not explosive,[70] making it in fact safer to handle than sodium azide. ADMP was synthesized following the procedure reported by Kitamura *et al.* (Scheme 5.18).[69] Reaction of 1,3-dimethylimidazolidinone **5.16** with oxalyl chloride in toluene afforded 2-chloro-1,3-dimethylimidazolinium chloride (DMC) **5.17**. This was then converted to its hexafluorophosphate salt **5.18** by reaction with $NaPF_6$ in MeCN, and then treated with sodium azide in MeCN to afford ADMP **5.19**.

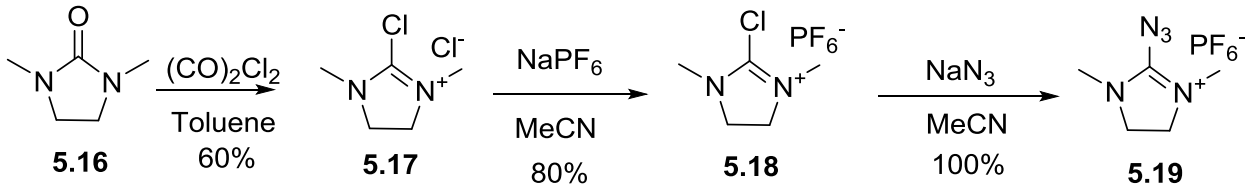

5.16 **5.17** **5.18** **5.19**

Scheme 5.18. Synthesis of ADMP **5.19**.

For the synthesis of the glycosyl azide, GlcNAc **5.12** was reacted with ADMP (3 equivalents) in the presence of triethylamine (5 equivalents) in a D_2O/MeCN mixture (Scheme 5.19).[1] The reaction yielded a mixture of the desired β-azide **5.20** and the oxazoline **5.21** (from ^{1}H NMR analysis in Figure 5.6). Five equivalents of triethylamine were used based on the need to deprotonate the anomeric hydroxyl group as well as accounting for any hydrolysis of ADMP. A solvent mixture of D_2O/MeCN (4:1) was used to improve the solubility of ADMP. The crude reaction mixture (β-azide **5.20** and oxazoline **5.21**) was then treated dropwise with 1 M aqueous HCl until the solution turned acidic, and then immediately neutralized using an aqueous solution of saturated $NaHCO_3$. After the acid and base treatment, the anomeric oxazoline proton (5.9 ppm) completely disappeared from the ^{1}H NMR spectrum, and the desired azide **5.20** was obtained as the sole product (Figure 5.6). When D-glucose **5.22** was treated with ADMP under the same conditions, the β-D-glucosyl azide **5.23** was obtained without the need for the acid and base treatment, along with 20% of 1,6-anhydro-β-D-glucose **5.24** as a side product (Scheme 5.20).

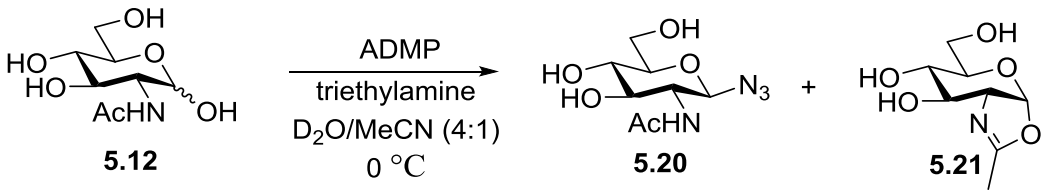

Scheme 5.19. Reaction of GlcNAc **5.12** with ADMP **5.19**.

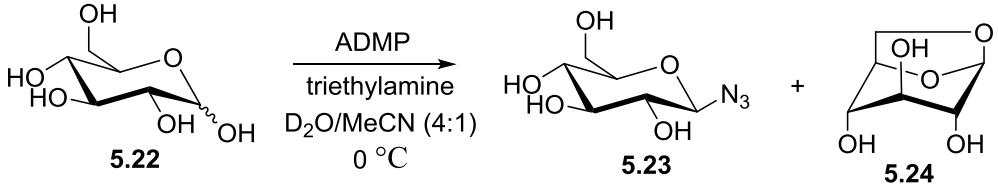

Scheme 5.20. Reaction of D-glucose **5.22** with ADMP **5.19**.

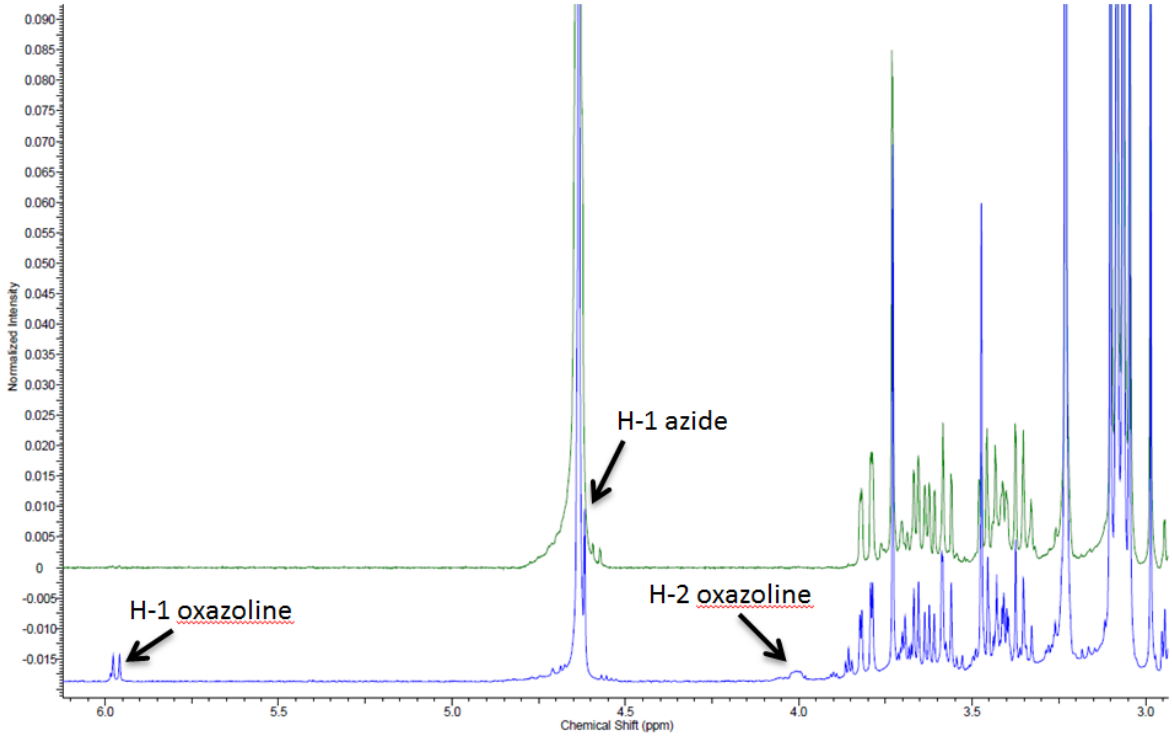

Figure 5.6. ^{1}H NMR spectra of before (bottom) and after (top) acid workup of reaction of GlcNAc with ADMP.

5.3.5. Synthesis of glycosyl triazoles with alkyne-terminated thioacetate (5.9) in a one-pot reaction

The Fairbanks' group have developed a protecting-group-free one-pot synthesis of glycoconjugates directly from reducing sugars with the combined use of ADMP and the CuAAC reaction.[1] It was shown that the reaction was entirely stereoselective and could be applied to attach a wide variety of alkyne derivatives to reducing sugars, including oligosaccharides. The coupling of GlcNAc **5.12** with propargyl alcohol performed by Fairbanks' group is shown in Scheme 5.21. After the formation of the glycosyl azide (the GlcNAc reaction with ADMP as explained in Section **5.2.4**) was complete, propargyl alcohol, $CuSO_4 \cdot 5H_2O$, and L-ascorbic acid were added, and the mixture was heated to 50 °C, which led to the formation of the glycosyl triazole in excellent yield (85%) and with complete stereoselectivities.

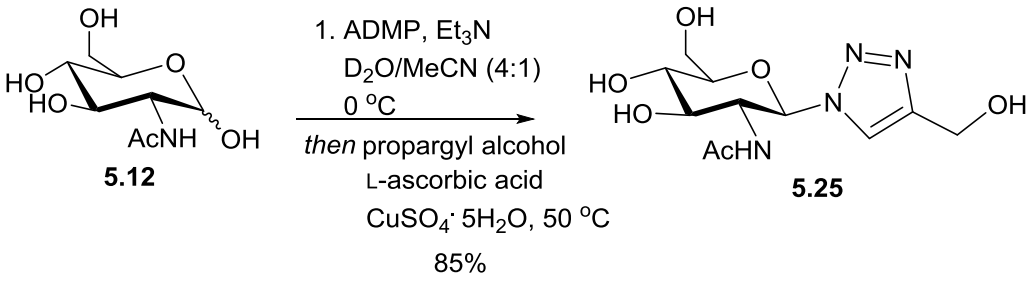

Scheme 5.21. One-pot synthesis of GlcNAc triazole from propargyl alcohol by Lim *et al.*[1]

In this work, the same procedure was used to develop a one-pot reaction to functionalize the AAT-AuNPs with various reducing sugars. In order to establish the conditions, the reaction was performed with the alkyne-terminated thioacetate **5.9**, before performing the reaction with the AAT-AuNPs. The thioacetate was used instead of the thiol **5.11** in order to avoid the possible interference of the thiol group in CuAAC reaction. GlcNAc **5.12**

was used as the reducing sugar. After the formation of the glycosyl azide (the GlcNAc reaction with ADMP as explained in Section **5.2.4**) was complete, thioacetate **5.9** dissolved in THF (as **5.9** was insoluble in water), $CuSO_4 \cdot 5H_2O$, and L-ascorbic acid were added, and the mixture was heated to 50 °C. Even after 24 h, t.l.c did not show any progress of the reaction. Therefore, the reaction mixture was heated to 90 ^oC (Scheme 5.22). After 14 h, t.lc. ($CHCl_3$/MeOH, 4:1) indicated the complete consumption of starting material (R_f 0.3) and the formation of a major product (R_f 0.5). The product obtained was found to be a mixture of triazole thioacetate **5.26** and triazole thiol **5.27**. Deacetylation was performed by treating with Na in MeOH, followed by neutralization with 1 M aqueous HCl, converted all the thioacetate to thiol. Although the click reaction was successful, the purification of the triazole thiol **5.27** was found to be very difficult. Compound **5.27** always co-eluted with ascorbic acid-related impurities (Figure A5.4 in Appendix) in flash chromatography purification. Since the click reaction went to completion and pure **5.27** was not the primary goal of the project, further purification attempts were not made.

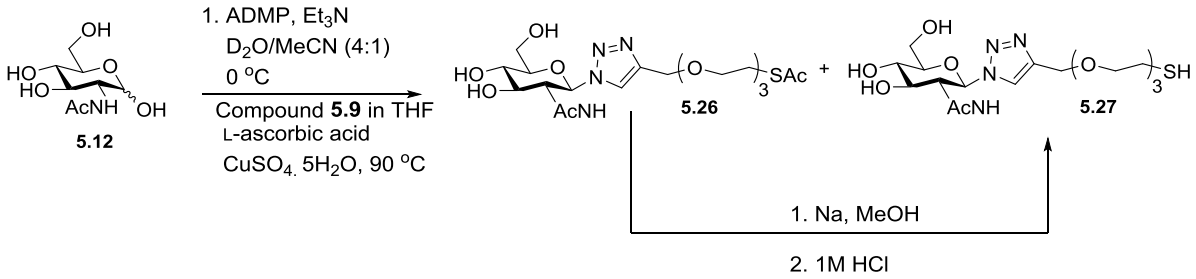

Scheme 5.22. One-pot synthesis of GlcNAc triazole from the alkyne-terminated thioacetate **5.9.**

5.3.6. One-pot gAuNP synthesis by CuAAC

It was then investigated if the one-pot reaction procedure developed by the Fairbanks group could be used to convert the AAT-AuNPs into gAuNPs. After the formation of GlcNAc azide **5.20** was complete (the GlcNAc reaction with ADMP as explained in Section **5.2.4**), AAT-AuNPs dissolved in THF, L-ascorbic acid, and $CuSO_4 \cdot 5H_2O$ (dissolved in water) were added and the mixture was stirred overnight at rt. Initially, 1.5 mol% $CuSO_4 \cdot 5H_2O$ with respect to the ligands on the AAT-AuNPs was used for the reaction. After 24 h, the solvent was removed *in vacuo,* and the residue obtained was dissolved in and then dialyzed against water for 3 d. Dialysis tubing with 10 kDa molecular weight cut off (MWCO) was used for the dialysis process. The AuNP solution was freeze dried after the dialysis, and the ^{1}H NMR analysis of the AuNPs revealed that the particles had not reacted with the glycosyl azide.

Following the observation of Boisselier *et al.*,[50] a stoichiometric amount of $CuSO_4 \cdot 5H_2O$ with respect to the alkyne ligand on the AAT-AuNPs was used and the reaction was run under an inert atmosphere. Reagents were added to the glycosyl azide in the following order; firstly the AAT-AuNPs in THF, followed by ascorbic acid, and then finally the $CuSO_4 \cdot 5H_2O$ dissolved in water. When the AuNP solution was added to the azide solution, the colour turned to that of the AuNP solution (purple), i.e. there was no change in the colour of the AuNP solution. The addition of the ascorbic acid did not cause any change in the physical properties of the solution. However, when the $CuSO_4 \cdot 5H_2O$ was added, the particles immediately precipitated. Yet surprisingly after 15 to 20 minutes, a portion of the precipitate was found to have re-dispersed in the solution, and the solution

regained the original purple colour. After 24 h, the solvent was removed *in vacuo,* and the residue obtained was dissolved in and dialyzed against water for 3 d. Unfortunately, the particles precipitated completely during the dialysis treatment. However, in one particular experiment, some of the particles remained dispersed in water and a ^{1}H NMR analysis was performed. The ^{1}H-NMR of the freeze-dried sample (Figure 5.7) clearly showed the peaks corresponding to the triazole proton (8.15 ppm) and the H-1 proton of the glycosyl traizole (5.70 ppm) along with other sugar and ATT-AuNP protons. Additionally, these particles were found to be soluble in water and were insoluble in organic solvents. The change in particle solubility, from organic to aqueous soluble, and the ^{1}H NMR spectrum, both suggest that polar sugar molecules had been clicked onto the particle surface. However, even this particular sample precipitated entirely within 24 h.

In further experiments the CuAAC reaction was performed with the purified GlcNAc azide **5.20**. However precipitation of the particles could not be prevented, although this did confirm that neither the triethylammonium salts or the ADMP urea (the by-products formed during the azide synthesis) were responsible for the particle aggregation. Similar results were obtained when the glucosyl azide was used as the sugar unit.

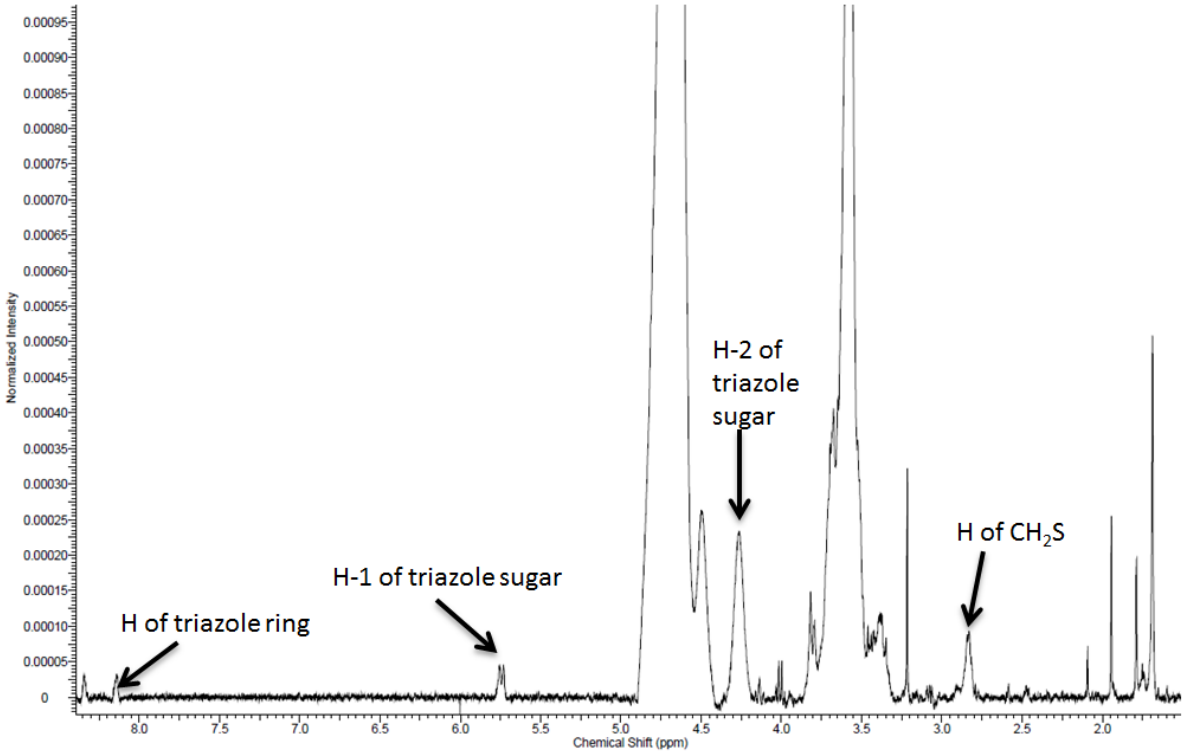

Figure 5.7. ^{1}H NMR spectra of the AuNPs obtained from the one-pot reaction of AAT-AuNPs with GlcNAc.

5.4. Conclusions and future work

The results from this project suggest that the water-insoluble AAT-AuNPs used here were incompatible with the CuAAC reaction conditions and thus prevented the one-pot synthesis of gAuNPs. A number of different groups have obtained the similar results, *i.e*, have observed AuNP precipitation under CuAAC reaction conditions.[43, 45, 47] The immediate precipitation of ATT-AuNPs upon the addition of $CuSO_4 \cdot 5H_2O$ here indicates that the Cu catalyst reacted with the particles and caused precipitation. The precise reason as to how the Cu catalyst caused the aggregation of AuNPs is not yet clear, and further investigations are required in order to adequately explain this observation. Furthermore,

the very specific conditions that have enabled some groups to perform the CuAAC reaction without causing any AuNP precipitation also need to be explained.

With respect to future work, the *interfacial* strain promoted azide-alkyne cycloaddition (I-SPAAC) is one of the potential methods that could be used to convert these AuNPs to gAuNPs without causing any particle precipitation. The procedure developed by Gobbo *et al.*[47] can be used to synthesise DBCO-AuNPs (Scheme 5.7), and these particles could be reacted with glycosyl azides to obtain gAuNPs as shown in Scheme 5.23.

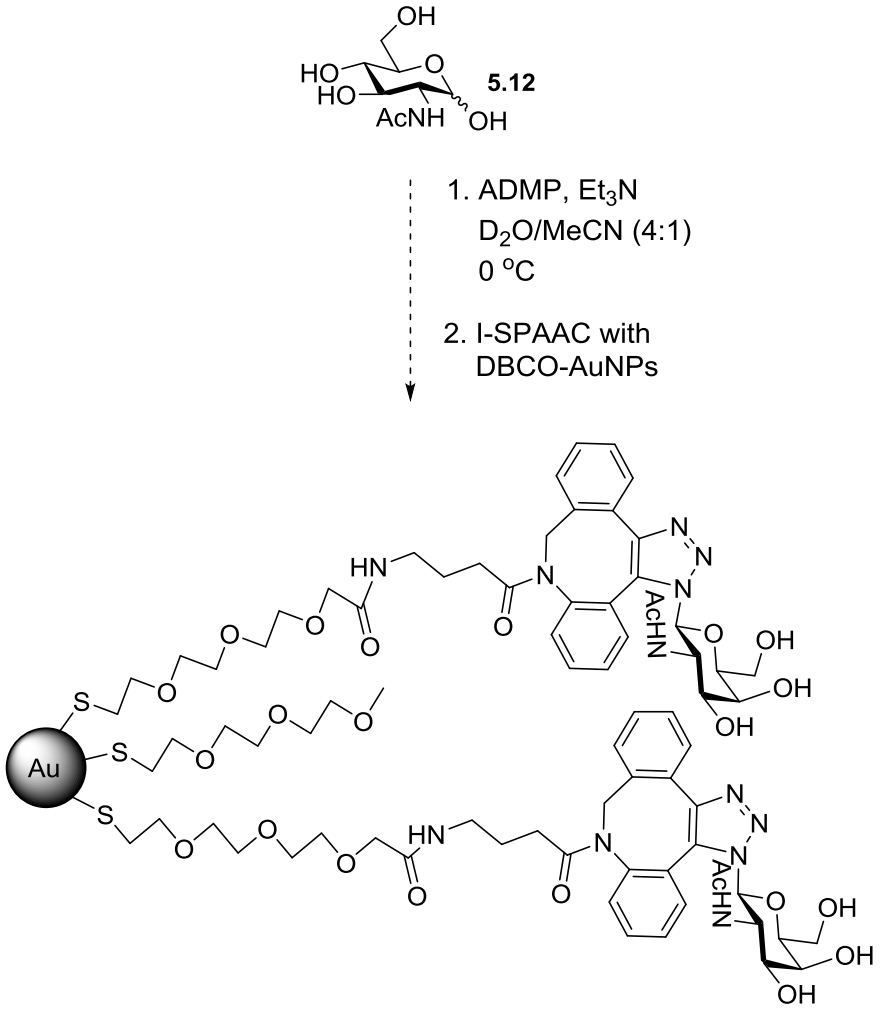

Scheme 5.23. The conversion of AuNPs to gAuNPs by I-SPAAC reaction.

5.5. References

1. Lim, D.; Brimble, M. A.; Kowalczyk, R.; Watson, A. J. A.; Fairbanks, A. J. *Angew. Chem. Int. Ed.* **2014,** *126* (44), 12101-12105.

2. Marradi, M.; Martín-Lomas, M.; Penadés, S. *Adv. Carbohydr. Chem. Biochem.* **2010,** *64*, 211-290.

3. Huisgen, R. *Angew. Chem. Int. Ed.* **1963,** *2* (11), 633-645.

4. Böhm, T.; Weber, A.; Sauer, J. *Tetrahedron* **1999,** *55* (31), 9535-9558.

5. Gothelf, K. V.; Jørgensen, K. A. *Chem. Rev.* **1998,** *98* (2), 863-910.

6. Huisgen, R. *J. Org. Chem.* **1976,** *41* (3), 403-419.

7. Huisgen, R. *Angew. Chem. Int. Ed.* **1963,** *2* (10), 565-598.

8. Kolb, H. C.; Finn, M.; Sharpless, K. B. *Angew. Chem. Int. Ed.* **2001,** *40* (11), 2004-2021.

9. Kolb, H. C.; Sharpless, K. B. *Drug Discov. Today* **2003,** *8* (24), 1128-1137.

10. Huisgen, R. *Pure Appl. Chem.* **1989,** *61* (4), 613-628.

11. Tornøe, C. W.; Christensen, C.; Meldal, M. *J. Org. Chem.* **2002,** *67* (9), 3057-3064.

12. Huisgen, R.; Szeimies, G.; Möbius, L. *Chem. Ber.* **1967,** *100* (8), 2494-2507.

13. Meldal, M.; Tornøe, C. W. *Chem. Rev.* **2008,** *108* (8), 2952-3015.

14. Duval, R. A.; Poupon, E.; Romero, V.; Peris, E.; Lewin, G.; Cortes, D.; Brandt, U.; Hocquemiller, R. *Tetrahedron* **2006,** *62* (26), 6248-6257.

15. Fu, X.; Albermann, C.; Zhang, C.; Thorson, J. S. *Org. Lett.* **2005,** *7* (8), 1513-1515.

16. Li, J.; Zheng, M.; Tang, W.; He, P.-L.; Zhu, W.; Li, T.; Zuo, J.-P.; Liu, H.; Jiang, H. *Bioorg. Med. Chem. Lett.* **2006,** *16* (19), 5009-5013.

17. Evans, R. A. *Aust. J. Chem.* **2007,** *60* (6), 384-395.

18. Goodall, G. W.; Hayes, W. *Chem. Soc. Rev.* **2006,** *35* (3), 280-312.

19. Hawker, C. J.; Wooley, K. L. *Science* **2005,** *309* (5738), 1200-1205.

20. Yeo, D. S.; Srinivasan, R.; Chen, G. Y.; Yao, S. Q. *Chem. Eur. J.* **2004,** *10* (19), 4664-4672.

21. Angell, Y. L.; Burgess, K. *Chem. Soc. Rev.* **2007,** *36* (10), 1674-1689.

22. Miller, N.; Williams, G. M.; Brimble, M. A. *Org. Lett.* **2009,** *11* (11), 2409-2412.

23. Wilkinson, B. L.; Long, H.; Sim, E.; Fairbanks, A. J. *Bioorg. Med. Chem. Lett.* **2008,** *18* (23), 6265-6267.

24. Chen, L.; Li, C. J. *Adv. Synth. Catal.* **2006,** *348* (12-13), 1459-1484.

25. Jiang, Y.; Kong, D.; Zhao, J.; Zhang, W.; Xu, W.; Li, W.; Xu, G. *Tetrahedron Lett.* **2014,** *55* (15), 2410-2414.

26. Bock, V. D.; Hiemstra, H.; Van Maarseveen, J. H. *Eur. J. Org. Chem.* **2006,** *2006* (1), 51-68.

27. Rodionov, V. O.; Fokin, V. V.; Finn, M. *Angew. Chem. Int. Ed.* **2005,** *44* (15), 2210-2215.

28. Jones, G. O.; Ess, D. H.; Houk, K. N. *Helv. Chim. Acta* **2005,** *88* (7), 1702-1710.

29. Himo, F.; Lovell, T.; Hilgraf, R.; Rostovtsev, V. V.; Noodleman, L.; Sharpless, K. B.; Fokin, V. V. *J. Am. Chem. Soc.* **2005,** *127* (1), 210-216.

30. Zhan, W.-h.; Barnhill, H. N.; Sivakumar, K.; Tian, H.; Wang, Q. *Tetrahedron Lett.* **2005,** *46* (10), 1691-1695.

31. Golas, P. L.; Tsarevsky, N. V.; Sumerlin, B. S.; Matyjaszewski, K. *Macromolecules* **2006,** *39* (19), 6451-6457.

32. Rostovtsev, V. V.; Green, L. G.; Fokin, V. V.; Sharpless, K. B. *Angew. Chem. Int. Ed.* **2002,** *114* (14), 2708-2711.

33. Horne, W. S.; Stout, C. D.; Ghadiri, M. R. *J. Am. Chem. Soc.* **2003,** *125* (31), 9372-9376.

34. Aher, N. G.; Pore, V. S. *Synlett* **2005,** *14*, 2155-2158.

35. Zinzalla, G.; Milroy, L.-G.; Ley, S. V. *Org. Biomol. Chem.* **2006,** *4* (10), 1977-2002.

36. Hein, C. D.; Liu, X.-M.; Wang, D. *Pharm. Res.* **2008,** *25* (10), 2216-2230.

37. Bräse, S.; Gil, C.; Knepper, K.; Zimmermann, V. *Angew. Chem. Int. Ed.* **2005,** *44* (33), 5188-5240.

38. Wilkinson, B. L.; Bornaghi, L. F.; Houston, T. A.; Innocenti, A.; Supuran, C. T.; Poulsen, S.-A. *J. Med. Chem.* **2006,** *49* (22), 6539-6548.

39. Wilkinson, B. L.; Bornaghi, L. F.; Poulsen, S.-A.; Houston, T. A. *Tetrahedron* **2006,** *62* (34), 8115-8125.

40. Wróblewski, A. E.; Głowacka, I. E. *Tetrahedron: Asymmetry* **2005,** *16* (24), 4056-4064.

41. Gouin, S. G.; Bultel, L.; Falentin, C.; Kovensky, J. *Eur. J. Org. Chem.* **2007,** *2007* (7), 1160-1167.

42. Hotha, S.; Kashyap, S. *J. Org. Chem.* **2006,** *71* (1), 364-367.

43. Fleming, D. A.; Thode, C. J.; Williams, M. E. *Chem. Mater.* **2006,** *18* (9), 2327-2334.

44. Thode, C. J.; Williams, M. E. *J. Colloid Interface Sci.* **2008,** *320* (1), 346-352.

45. Limapichat, W.; Basu, A. *J. Colloid Interface Sci.* **2008,** *318* (1), 140-144.

46. Ismaili, H.; Alizadeh, A.; Snell, K. E.; Workentin, M. S. *Can. J. Chem.* **2009,** *87* (12), 1708-1715.

47. Gobbo, P.; Mossman, Z.; Nazemi, A.; Niaux, A.; Biesinger, M. C.; Gillies, E. R.; Workentin, M. S. *J. Mater. Chem. B.* **2014,** *2* (13), 1764-1769.

48. Brennan, J. L.; Hatzakis, N. S.; Tshikhudo, T. R.; Dirvianskyte, N.; Razumas, V.; Patkar, S.; Vind, J.; Svendsen, A.; Nolte, R. J.; Rowan, A. E. *Bioconjugate Chem.* **2006,** *17* (6), 1373-1375.

49. Sommer, W. J.; Weck, M. *Langmuir* **2007,** *23* (24), 11991-11995.

50. Boisselier, E.; Salmon, L.; Ruiz, J.; Astruc, D. *Chem. Commun.* **2008,** (44), 5788-5790.

51. Zhou, Y.; Wang, S.; Zhang, K.; Jiang, X. *Angew. Chem. Int. Ed.* **2008,** *120* (39), 7564-7566.

52. Hua, C.; Zhang, W. H.; De Almeida, S. R.; Ciampi, S.; Gloria, D.; Liu, G.; Harper, J. B.; Gooding, J. J. *Analyst* **2012,** *137* (1), 82-86.

53. Zhang, Z.; Li, W.; Zhao, Q.; Cheng, M.; Xu, L.; Fang, X. *Biosens. Bioelectron.* **2014,** *59*, 40-44.

54. Zhang, Y.; Li, B.; Xu, C. *Analyst* **2010,** *135* (7), 1579-1584.

55. Zhu, K.; Zhang, Y.; He, S.; Chen, W.; Shen, J.; Wang, Z.; Jiang, X. *Anal. Chem.* **2012,** *84* (10), 4267-4270.

56. Papp, I.; Sieben, C.; Ludwig, K.; Roskamp, M.; Böttcher, C.; Schlecht, S.; Herrmann, A.; Haag, R. *Small* **2010,** *6* (24), 2900-2906.

57. Marín, M. J.; Rashid, A.; Rejzek, M.; Fairhurst, S. A.; Wharton, S. A.; Martin, S. R.; McCauley, J. W.; Wileman, T.; Field, R. A.; Russell, D. A. *Org. Biomol. Chem.* **2013,** *11* (41), 7101-7107.

58. Wei, J.; Zheng, L.; Lv, X.; Bi, Y.; Chen, W.; Zhang, W.; Shi, Y.; Zhao, L.; Sun, X.; Wang, F. *ACS nano* **2014,** *8* (5), 4600-4607.

59. Chikae, M.; Fukuda, T.; Kerman, K.; Idegami, K.; Miura, Y.; Tamiya, E. *Bioelectrochemistry* **2008,** *74* (1), 118-123.

60. Grimmer, J.; Muller, T. Method for Reducing Alkyne Compuonds. 2007.

61. Oae, S.; Doi, J. *Organic Sulfur Chemistry*. CRC Press: Florida, 1991.

62. Hashmi, A. S. K. *Gold Bull. 36* (1), 3-9.

63. Hashmi, A. S. K. *Chem. Rev.* **2007,** *107* (7), 3180-3211.

64. Norman, R. O. C.; Parr, W. J. E.; Thomas, C. B. *J. Chem. Soc., Perkin Trans. 1* **1976,** (18), 1983-1987.

65. Baranov, D.; Kadnikova, E. N. *J. Mater. Chem.* **2011,** *21* (17), 6152-6157.

66. Huang, S.; Minami, K.; Sakaue, H.; Shingubara, S.; Takahagi, T. *J. Appl. Phys.* **2002,** *92* (12), 7486-7490.

67. Lim, D. Synthesis of O-Linked Glycopeptides Using Enzymatic Catalysis. Ph.D. Thesis, University of Canterbury, 2016.

68. Tanaka, T.; Nagai, H.; Noguchi, M.; Kobayashi, A.; Shoda, S.-I. *Chem. Commun.* **2009,** (23), 3378-3379.

69. Kitamura, M.; Tashiro, N.; Miyagawa, S.; Okauchi, T. *Synthesis* **2011,** (7), 1037-1044.

70. Kitamura, M.; Kato, S.; Yano, M.; Tashiro, N.; Shiratake, Y.; Sando, M.; Okauchi, T. *Org. Biomol. Chem.* **2014,** *12* (25), 4397-4406.

Chapter 6: Experimental Section

6.1. General experimental procedures and instruments

All chemical reagents were of analytical grade and used as supplied without further purification unless otherwise stated. Solvents were removed under reduced pressure using a Buchi^{TM} rotary evaporator. Water used for the synthesis of AuNPs was purified by a MilliQ system (Millipore). Thin Layer Chromatography (t.l.c.) was carried out on Merck Silica Gel 60F_{254} aluminium backed plates. Plate visualization was achieved using a UV lamp (λ_{max} = 254 or 365 nm), and/or ammonium molybdate (5% in 2M H_2SO_4). Flash column chromatography was carried out using Sorbsil C60 40/60 silica.

Proton and carbon nuclear magnetic resonance (^1H, ^{13}C) spectra were recorded on Bruker AV400 (400 MHz), or Bruker AV500 (500 MHz) spectrometers. All chemical shifts are quoted on the δ-scale in ppm using residual solvent as an internal standard. ^1H and ^{13}C spectra were assigned using COSY, DEPT, HSQC, HMBC, and TOCSY. High resolution mass spectra were recorded on a Bruker FT-ICR mass spectrometer using electrospray ionisation (ESI) or chemical ionisation (CI) techniques as stated. *M/z* values are reported in Daltons. Optical rotations were measured on a Perkin-Elmer 241 polarimeter with a water-jacketed 1 cm^3 cell with a path length of 1 dm, and are quoted in units of $^o.cm^2.g^{-1}$. Infrared spectra were recorded on a Perkin-Elmer Spectrum One FTIR instrument operating in diffuse reflectance mode with samples prepared as KBr pellets or on a Bruker FTIR spectrometer with Alpha's Platinum ATR single reflection diamond where the neat samples were recorded.

TGA was performed with an Alphatech SDT Q600 TGA/DSC apparatus, on 6 - 8 mg of purified, dry materials (alumina crucible was used as the sample holder), under N_2 (with a flow rate of 100 mL/min), recording data from 25 to 1000 °C at a heating rate of 10 °C/min. Elemental analyses were performed by the Campbell Microanalytical Laboratory at the University of Otago. TEM images of AuNPs were obtained using a Philips CM200 TEM operating at 200 kV. Samples for TEM imaging were prepared by dropping 2 µL of a freshly prepared solution of nanostructured Au onto a holey carbon-coated copper grid (300 mesh, SPI Supplies, USA) and drying at room temperature. Analysis of the TEM images of the AuNPs (in each case at least 200 particles were measured) were performed using ImageJ software. UV-Vis absorption spectra were recorded with a Varian Cary 100 UV-Vis spectrophotometer or a multimode reader (Varioskan Flash, Thermo Scientific). DLS measurements were performed using a Malvern Zetasizer Nano ZS DLS system (Malvern Instruments Ltd., UK). The DLS system is equipped with a λ=633 nm He-Ne laser and an avalanche photodiode detector configured to collect backscattered light at 173^{o}.

6.2. Experimental for Chapter 2

Synthesis of tetrachloroauric (III) acid trihydrate ($HAuCl_4 \cdot 3H_2O$)[1]

Pure Au metal (99.99%, 15 g) was added to freshly prepared *aqua regia* (150 mL) at 60 ^{o}C. After 3 d Au was completely dissolved in *aqua regia*. The solution was concentrated *in vacuo* to afford **tetrachloroauric (III) acid trihydrate ($HAuCl_4 \cdot 3H_2O$)** as a yellow solid (28 g).

Synthesis of Au nanomaterials

All experiments were performed under an air atmosphere. In a typical reaction, 150 mL of 0.25 mM aqueous solution of $HAuCl_4 \cdot 3H_2O$ was refluxed (**2.1a**) or heated to the desired temperature (70 ^oC for **2.1b**, **2**.**2a**, **2**.**3a**, and **2**.**4b**, and 95 ^oC for **2.4a**) in a temperature-controlled oil bath with continuous magnetic stirring (500 rpm). The required amount of trisodium citrate as an aqueous solution (38.8 mM) was added rapidly to the solution and the reaction was continued for 15 min, after which the reaction mixture was cooled to rt. In the case of **2.4a**, the reaction was carried out for 60 min as well.

6.3. Experimental for Chapter 3

Reagents

All chemicals and reagents other than those listed below were supplied by Sigma-Aldrich Chemical Co. The heat-labile enterotoxin B-subunit was purchased from Reagent Proteins (San Diego, USA). Recombinant influenza A virus H1N1 hemagglutinin (A/California/04/2009) was purchased from Sino Biological Inc. (Beijing, China).

Colorimetric bioassay for LTB using Gal-gAuNPs

Purified Gal-gAuNPs were freeze-dried, and then re-suspended in phosphate buffer (10 mM, pH 7.2) to give a nanoparticle concentration of 10 nM. A series of solutions with a range of LTB concentrations (300, 600, 900 and 1200 nM) were prepared separately in Milli-Q water. Then, an aliquot of each of the LTB solutions (150 μl) was added (with

mixing) to an aliquot of the Gal-gAuNP solution (150 µl), and the progress of the reaction was monitored by UV-Vis spectroscopy, recording the absorption at 620 nm prior to recording of the whole UV-Vis absorbance spectrum. Aliquots of the Gal-gAuNP solution were also mixed with bovine serum albumin (BSA, aqueous solutions of 300-1200 nM) and a variety of metal ions and anions (K^+, Na^+, Ca^{2+}, Mg^{2+}, Cl^-, NO_3^-, HCO_3^-, SO_4^{2-}, PO_4^{3-}, all at a concentration of 100 µM) to confirm that the Gal-gAuNPs did not undergo non-specific aggregation and also with Con A and Hemagglutinin (each 600 nM) to confirm that the particles were selective only towards LTB. Additionally, an electrolyte that mimicked the typical watery stool of diarrhoea patients, namely a solution containing Cl^- at 100 mM, Na^+ at 135 mM, K^+ at 15 mM, and HCO_3^- at 45 mM,[2-4] was prepared to test the stability and the efficiency of toxin detection of the Gal-gAuNPs.

Synthesis

1,2,3,4,6-Penta-*O*-acetyl-β-D-galactopyranose 3.1[5-6]

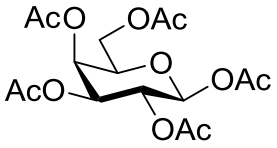

Sodium acetate (41 g, 500 mmol) was added to acetic anhydride (315 mL), and the mixture was refluxed at 120 °C for 30 min. D-Galactose (30.0 g, 165 mmol) was then added slowly over 30 min. After a further 120 min, t.l.c (petrol:EtOAc, 1:1) showed complete consumption of starting material (R_f 0) and the formation of single product (R_f 0.7). The reaction mixture was then cooled to rt and a mixture of water and ice (400 mL) was added. The ensuing precipitate was filtered, and then recrystallized (EtOH) to give

pentaacetate **3.1** (20.0 g, 31%) as white crystalline solid; m.p. 135-138 °C [lit. m.p. 137-139 °C][5]; $[\alpha]_D^{20}$ +29.3 (*c*, 1.0 in $CHCl_3$)[6] [lit. $[\alpha]_D^{23.5}$ +27.1 (*c*, 1.03 in $CHCl_3$)]; δ_H (500 MHz, $CDCl_3$)[7] 1.99, 2.04, 2.11, 2.16 (15H, 4 x s, 5 x CH_3CO_2), 4.07 (1H, m, H-5), 4.13-4.16 (2H, m, H-6, H-6'), 5.06 (1H, dd, $J_{3,4}$ 3.5 Hz, H-3), 5.32 (1H, dd, $J_{2,3}$ 10.5 Hz, H-2), 5.42 (1H, m, H-4), 5.69 (1H, d, $J_{1,2}$ 8.3 Hz, H-1).

8-Hydroxy-3,6-dioxa-octyl 2,3,4,6-tetra-*O*-acetyl-β-D-galactopyranoside 3.2[8]

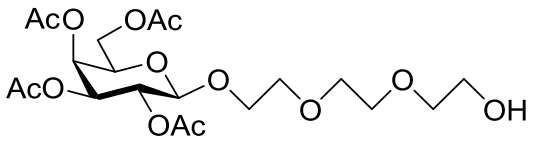

$BF_3{\cdot}Et_2O$ (1.9 mL, 15.4 mmol) was added to a solution of compound **3.1** (3.0 g, 7.7 mmol) and triethylene glycol (2.2 mL, 17 mmol) in dry DCM (30 mL) and the resulting solution was stirred at rt for 5 h. The solution was then diluted with DCM (30 mL) and washed successively with an aqueous solution of saturated $NaHCO_3$ (2 × 30 mL), H_2O (2 × 30 mL), and brine (30 mL). The organic extracts were dried (Na_2SO_4), filtered, and concentrated *in vacuo*. The residue was then purified by flash chromatography (petrol:EtOAc, 1:1) to afford alcohol **3.2** (1.5 g, 40 %) as a yellow syrup; $[\alpha]_D^{20}$ + 0.3 (*c*, 1.0 in MeOH); δ_H (400 MHz, $CDCl_3$)[8] 2.15, 2.06, 2.04, 1.98 (12H, 4 x s, 4 x CH_3), 3.77-3.59 (10H, m, 5 x OCH_2), 3.95 (2H, m, 1 x CH_2O), 4.15 (3H, m, H-5, H-6, H-6`), 4.58 (1H, d, $J_{1,2}$ 7.8 Hz, H-1), 5.02 (1H, dd, $J_{3,4}$ 2.1 Hz, H-3), 5.19 (1H, dd, $J_{1,2}$ 7.8 Hz, $J_{2,3}$ 8.7 Hz, H-2), 5.38 (1H, m, H-4); HRMS (ESI) Calcd. For $C_{20}H_{33}O_{13}$ (MH^+) 481.1916. Found 481.1914.

8-Thioacetyl-3,6-dioxa-octyl 2,3,4,6-tetra-*O*-acetyl-β-D-galactopyranoside 3.3[8]

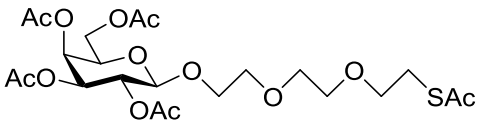

Triethylene glycol galactoside **2.7** (2.5 g, 5.3 mmol) was dissolved in dry DCM (100 mL) under nitrogen at 0 ^{o}C and stirred. Mesyl chloride (0.7 mL, 10 mmol) was added dropwise, and then triethylamine (1.4 mL, 10 mmol) was added. The reaction mixture was then allowed to warm to rt. After 2h, t.l.c (EtOAc) indicated the formation of a single product (R_f 0.3) and the complete consumption of the starting material (R_f 0). The reaction was quenched by the addition of MeOH (10 mL) and concentrated *in vacuo.* The residue was dissolved in DMF (25 mL), and potassium thioacetate (2 g, 20 mmol) was added and the reaction was then stirred at 65 ^{o}C. After 16 h, t.l.c. (EtOAc) indicated the formation of a major product (R_f 0.4) and the complete consumption of the starting material (R_f 0.3). The reaction mixture was cooled, diluted with EtOAc (30 mL) and washed successively with an aqueous solution of saturated $NaHCO_3$ (2 x 30 mL), H_2O (2 x 30 mL), and brine (30 mL). The organic layer was separated, dried (Na_2SO_4), filtered, and concentrated *in vacuo*. The residue was purified by flash chromatography (petrol:EtOAc, 1:3) to afford 8-thioacetyl-3,6-dioxaoctyl 2,3,4,6-tetra-*O*-acetyl-β-D-galactopyranoside **3.3** (1.9 g, 64.5%) as a yellow syrup. $[\alpha]_D^{20}$ -3.0 (*c*, 1.0 in $CHCl_3$)]; δ_H (400 MHz, $CDCl_3$)[8] 2.14, 2.06, 2.04, 1.98 (12H, 4 x s, 4 x CH_3CO_2), 2.34 (3H, s, 1 x CH_3COS), 3.09 (2H, t, 2 x $C\underline{H_2}S$), 3.58-3.75 (8H, m, 4 x CH_2O), 3.92 (2H, m, 1 x CH_2O), 4.14 (3H, m, H-5, H-6, H-6`), 4.57 (1H, d, $J_{1,2}$ 7.8 Hz, H-1), 5.02 (1H, dd, $J_{3,4}$ 2.1 Hz, H-3), 5.21 (1H, dd, $J_{2,1}$ 7.8 Hz, $J_{2,3}$8.7 Hz, H-2), 5.39 (1H, m, H-4); HRMS (ESI) Calcd. For $C_{22}H_{34}O_{13}SNa(MNa^+)$ 561.1612. Found 561.1617.

8,8`-Dithiobis(3,6-dioxaoctyl-β-D-galactopyranoside) 3.4[8]

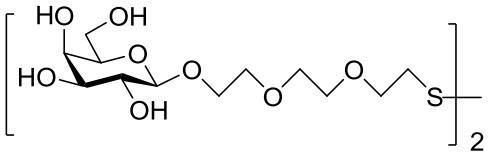

NaOMe (0.17 M in MeOH, 1 mL) was added to a solution of compound **3.3** (500 mg, 0.93 mmol) in MeOH (10 mL), and the solution was stirred at rt for 2 h. The solution was then neutralized by the addition of Amberlite IR-120 (H^+ resin), filtered, and then air oxidized by bubbling air continuously through the solution for a total of 64 h. The solvent was then removed *in vacuo* to afford disulfide **3.4** (295 mg, 97 %) as a yellow syrup. $[\alpha]_D^{20}$ –1.6 (*c*, 1.0 in D_2O); δ_H (500 MHz, d_6-DMSO)[8] 2.81 (2H, t, CH_2S), 3.40 (1H, m, H-2), 3.48-3.65 (10H, m, 4 x CH_2O, H-6, H-6`), 3.69 (3H, m,1 x CH_2O, H-4), 3.77 (1H, m, H-3), 3.93 (1H, m, H-5), 4.28 (1H, d, $J_{1,2}$ 8.5 Hz, H-1); HRMS (ESI) Calcd. For $C_{24}H_{46}O_{16}S_2$ (MNa^+) 677.2119. Found 677.2110

Gal-gAuNP-2

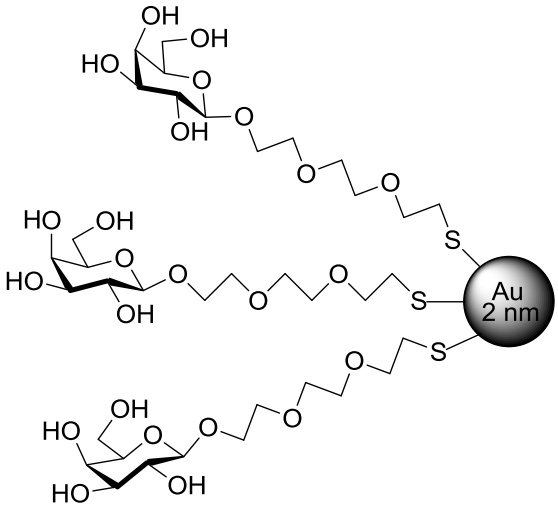

A solution of disulfide **3.4**[8] (50 mg, 0.076 mmol) in MeOH (12 mL) was added to a solution of $HAuCl_4 \cdot 3H_2O$ (15 mg, 0.038 mmol) in water (3 mL) and stirred (500 rpm). A solution of $NaBH_4$ (14.37 mg, 0.38 mmol) in water (1.7 mL) was added in small portions, and the reaction was then stirred for 2 h. The mixture was concentrated *in vacuo,* the residue was dissolved in Milli-Q water (10 mL), and then purified by centrifugal filtering (Amicon Ultra 10K, Millipore, MWCO=10,000, 1h, 5000 x g). The addition of 10 mL of Milli-Q water and centrifugal filtration was repeated until the NPs were free of salts and starting material (as seen by the absence of signals arising from disulfide **3.4** in the ^1H NMR spectrum). The residue was then dissolved in water (2 mL) and lyophilized to obtain **Gal-gAuNP-2.** TEM: 2.3 ± 0.5 nm; IR (KBr): 3300 (br, OH), 2933, 2873, 1062 cm^{-1}; UV: 508 nm; TGA: ligand 41.6%, Au 58.4 %; Elemental analysis Found: C, 18.23; H, 3.31; S, 4.32. Calc. for $Au_{377}(C_{12}H_{24}O_8S)_{162}$: C, 18.3; H, 3.08; S, 4.08%; HRMS (ESI) Calcd. For $C_{24}H_{46}O_{16}S_2$ (MNa^+) 677.2119. Found 677.2133.

Gal-gAuNP-7

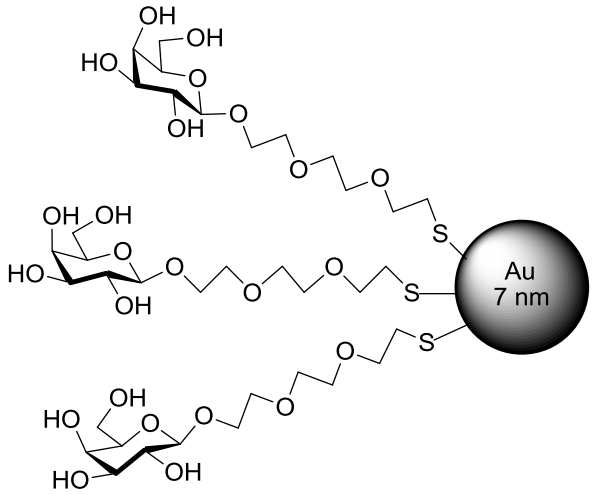

An aqueous solution of $HAuCl_4 \cdot 3H_2O$ (0.25 mL, 0.254 mM, pH 1.6) was added to a boiling aqueous solution of trisodium citrate (34.25mL, 5.3 mM) with constant stirring (500 rpm). After 15 min, the reaction mixture was cooled to rt, and a solution of disulfide **3.4**[8] (500 mg, 0.76 mmol) was added. The reaction was then stirred for 48 h at rt. The reaction mixture was concentrated *in vacuo*, the residue was dissolved in Milli-Q water (10 mL), and then purified by centrifugal filtering (Amicon Ultra 10K, Millipore, MWCO=10,000, 1h, 5000 x g). The residue was then dissolved in water (2 mL) and lyophilized to obtain **Gal-gAuNP-7**. TEM: 7.3 ± 0.9 nm; IR (KBr): 3300 (broad band), 2933, 2873, 1062 cm^{-1}; UV: 517 nm; TGA: ligand 23.1%, Au 76.9%; Elemental analysis Found: C, 10.21; H, 1.49; S, 2.37. Calc. for $Au_{12060}(C_{12}H_{24}O_8S)_{2181}$: C, 10.16; H, 1.62; S, 2.26%; HRMS (ESI) Calcd. For $C_{24}H_{46}O_{16}S_2$ (MNa^+) 677.2119. Found 677.2121.

Gal-gAuNP-12

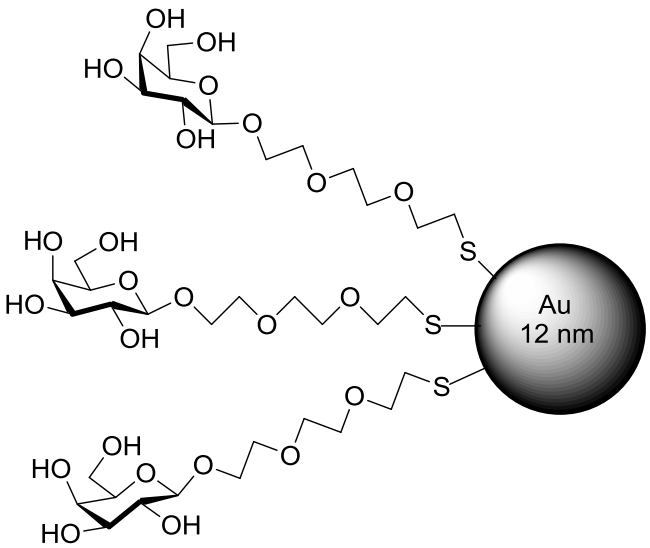

An aqueous solution of trisodium citrate (5.6 mL, 38.8 mM) was added to a boiling aqueous solution of $HAuCl_4 \cdot 3H_2O$ (25mL, 1 mM) with constant stirring (500 rpm). After 15 min, the reaction mixture was cooled to room temperature, and a solution of disulfide **3.4**[8] (650 mg, 1 mmol) was added. The reaction was then stirred for 48 h at rt. The reaction mixture was concentrated *in vacuo*, the residue was dissolved in Milli-Q water (10 mL), and then purified by centrifugal filtering (Amicon Ultra 10K, Millipore, MWCO=10,000, 1h, 5000 x g). The residue was then dissolved in water (2 mL) and lyophilized to obtain **Gal-gAuNP-12**. TEM: 12.0 ± 1.7 nm; IR (KBr): 3300 (broad band), 2933, 2873, 1062 cm^{-1}; UV: 523 nm; TGA: ligand 8.70%, Au 91.3%; Elemental analysis Found: C, 4.06; H, 0.64; S 0.97%. Calc. for $Au_{53568}(C_{12}H_{24}O_8S)_{3074}$: C, 4.15; H, 0.64; S, 0.92%; HRMS (ESI) Calcd. For $C_{24}H_{46}O_{16}S_2$ (MNa^+) 677.2119. Found 677.2121.

Gal-gAuNP-20

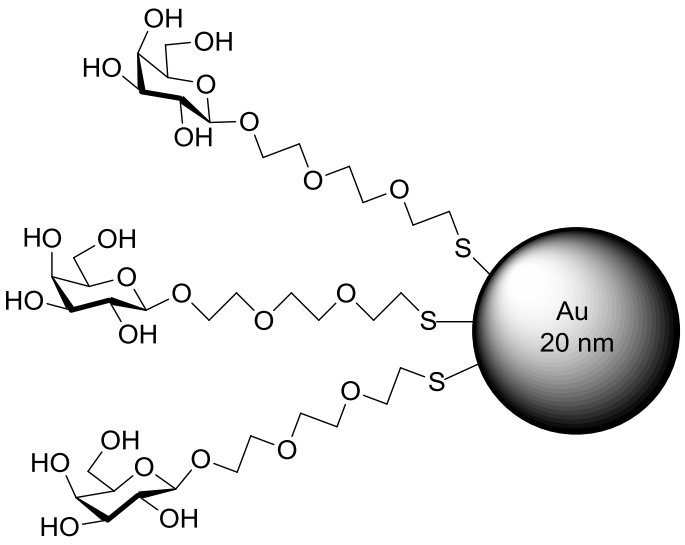

An aqueous solution of trisodium citrate (1.24 mL, 16.9 mM) was added to a boiling aqueous solution of $HAuCl_4 \cdot 3H_2O$ (25.4 mL, 0.3 mM) with constant stirring (500 rpm).

After 15 min, the reaction mixture was cooled to rt, and a solution of disulfide **3.4**[8] (81 mg, 0.12 mmol) was added. The reaction was then stirred for 48 h at rt. The reaction mixture was concentrated *in vacuo*, the residue was dissolved in Milli-Q water (10 mL), and then purified by centrifugal filtering (Amicon Ultra 10K, Millipore, MWCO=10,000, 1h, 5000 x g). The residue was then dissolved in water (2 mL) and lyophilized to obtain **Gal-gAuNP-20**. TEM: 20.3 ± 1.8 nm; IR (KBr): 3300 (broad band), 2933, 2873, 1062 cm^{-1}; UV: 527 nm; TGA: ligand 5.90 wt%, Au 94.10 wt%; Elemental analysis Found: C, 2.58; H, 0.41; S, 0.58. Calc. for $Au_{53568}(C_{12}H_{24}O_8S)_{3074}$: C, 2.58; H, 0.42; S, 0.57%; HRMS (ESI) Calcd. For $C_{24}H_{46}O_{16}S_2$ (MNa^+) 677.2119. Found 677.2118.

6.4. Experimental for chapter 4

Reagents

Recombinant influenza A virus H1N1 hemagglutinin (A/California/04/2009) was purchased from Sino Biological Inc. (Beijing, China). The influenza virus A/Puerto Rico/8/34 (H1N1) and A/New Caledonia/20/1999 (H1N1) strains were propagated in 10-day old embryonated chicken eggs, and titrated on Madin-Darby Canine Kidney (MDCK) cells (this part was done by our collaborators, Dr. Matloob Husain`s virology group, in Otago University).

Colorimetric detection of HA using SG-gAuNPs

Purified SG-gAuNPs were freeze-dried, and then re-suspended in PBS (pH 7.4) to give a NP concentration of 3 nM. A solution of HA in (0.25 mg/mL) PBS (pH 7.4) was prepared. Then, aliquots of the HA solution (5, 10, 20, 30 and 40 µl) were added (with

mixing) to an aliquot of the SG-gAuNP solution (200 µl), and in each case solution was made up to a total volume of 300 µl by adding PBS, and the progress of the reaction was monitored by UV-Vis spectroscopy at different time intervals. Additionally, an aliquot of the SG-gAuNP solution (200 µl) were also mixed with bovine serum albumin (BSA) (600 nM) to confirm that the SG-gAuNPs did not undergo non-specific aggregation and also with Con A and B subunit of heat-labile enterotoxin (each at 600 nM) to confirm that the particles were selective only towards HA.

Colorimetric detection of viral particles using SG-gAuNPs

Egg allantoic fluid containing influenza A/New Caledonia/20/1999 (H1N1) (6×10^5 PFU/mL) or influenza A/Puerto Rico/8/34 (H1N1) (2×10^7 PFU/mL) strain was prepared in PBS. Aliquots of the A/New Caledonia/20/1999 (H1N1) solution (1.6, 8, 16.7, 33.4, and 50.1 µl) were added (with mixing) to an aliquot of the SG-gAuNP solution (30 µl of 20 nM solution) and formalin (15 µL of 10% stock solution). In each case solution was made up to a total volume of 300 µl by adding PBS. The progress of the reaction was monitored by UV-Vis spectroscopy at different time intervals. In the case of the A/Puerto Rico/8/34 (H1N1) virus 1.5 µl of the stock solution was added to the SG-AuNP solution.

DLS assay

The sample was equilibrated at 25 ^{o}C for 120 seconds before analysis. Each measurement was for 12 scans, each of 30 seconds duration. The mean particle hydrodynamic diameters reported were calculated from intensity based particle size distributions.

Extraction and synthesis

Extraction of sialylglycopeptide (SGP) from egg yolks 4.1 [9]

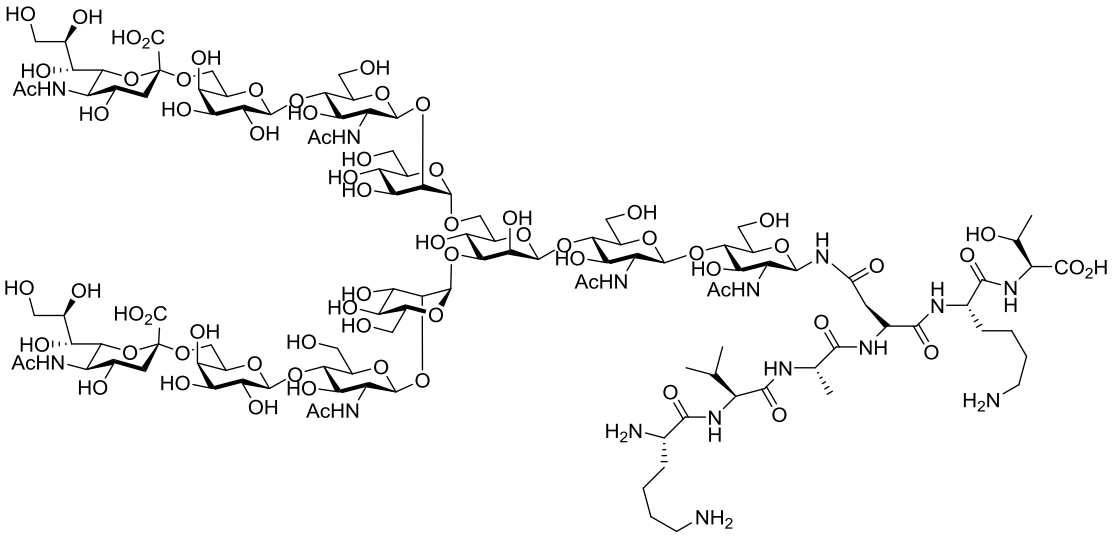

Three hundred egg yolks (3.3 L) were stirred in water (1.5 L) and then freeze-dried to obtain 2.1 kg of yolk powder. This powder was washed successively with diethyl ether (6 L x 2) and 70 % aqueous acetone (6 L) after thorough mixing. Aqueous acetone (40%, 3 L x 2) was added, with vigorous mixing, and the solution was then filtered through Celite®. The filtrate was concentrated and freeze-dried to give 30 g of yolk extract powder. This powder (30 g) was dissolved in H_2O, and purified by solid-phase extraction with an active carbon/Celite®(300 g:300 g) column (the column was sequentially washed with 5% and 10% aqueous MeCN, before elution of SGP with 30% aqueous MeCN) to afford 1.2 g of sialylglycopeptide (SGP) **4.1**[9] as a white powder; δ_H (400 MHz, D_2O)[1] 0.84 (6H, d, γ CH_3 of Val), 1.04 (3H, d, γ CH_3 of Thr), 1.25 (3H, d, β CH_3 of Ala), 1.31 (2H, m, γ CH_2 of Lys), 1.52-1.64 (3H, m, δ CH_2 of Lys, H-3_{ax}NeuAc7, H-3_{ax}NeuAc7`), 1.75 (2H, m, β $CH_2$ of Lys), 2.54 (1H, m, H-$3_{eq}$NeuAc7, H-$3_{eq}$NeuAc7`), 2.70 (2H, m, β CH_2 of Asn), 2.87 (2H, t, ε CH_2 of Lys), 4.33 (2H, d, H-1Gal-6, H-1Gal6`), 4.47 (3H, m,

H-1GlcNAc2, H-1GlcNAc5, H-1GlcNAc5`), 4.63 (1H, m, H-1Man3), 4.82 (1H, m, H-1Man4`), 4.91 (1H, d, H-1GlcNAc1), 5.00 (1H, m, H-1Man-4); HRMS (ESI): calcd. For $C_{112}H_{189}N_{15}O_{70}(MH^+)$ 2865.1763. Found 2865.1734 (MH^+).

Asparagine-linked complex bi-antennary N-glycan 4.2 [10]

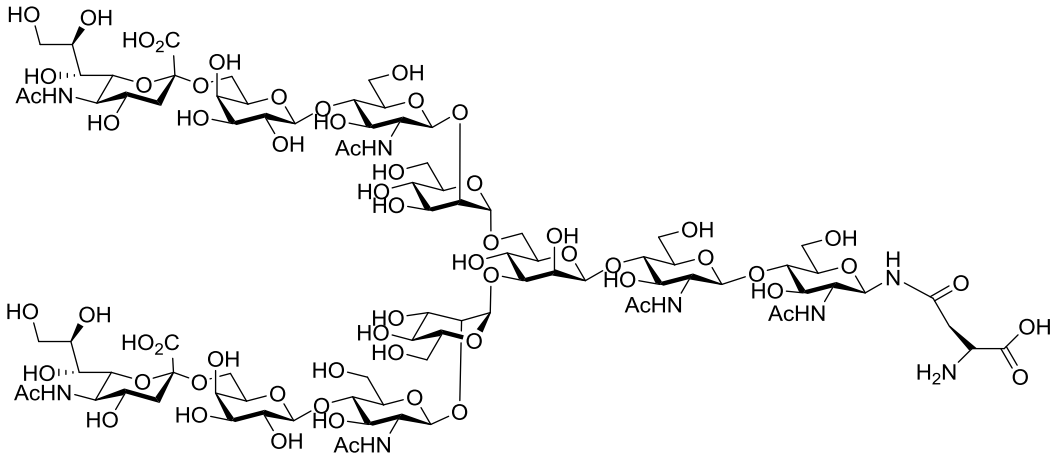

Pronase (3 mg, from *Streptomyces griseus*) was added to a solution of SGP **4.1**[9] (20 mg) and NaN_3 in Tris-HCl buffer (50 mM, pH 7.5, 1 ml), and the mixture was incubated at 37 ^oC. The pH of the solution was checked regularly and adjusted to 7.5. After 7 d, the mixture was purified by gel filtration using a Sephadex G-25 column (8.7 x 1.7 cm) which was pre-equilibrated and eluted with 0.01% aqueous NH_3. Fractions of 8 ml were collected at a flow rate of 0.5 mL/min, and examined for their sugar content using the phenol/sulfuric acid test. The fractions which showed positive results were pooled and lyophilized to obtain asparagine-linked N-glycan **4.2**[10] (10 mg, 57%) as a white powder; δ_H (400 MHz, D_2O)[2] 1.80 (2H, dd, *J* 12.4 Hz, H-3_{ax}NeuAc7, H-3_{ax}NeuAc7`), 2.10-2.2

(18H, s, 6 x CH_3CO_2), 2.76 (2H, m, H-3_{eq} NeuAc7, H-3_{eq}NeuAc7`), 2.95 (1H, dd, *J* 8 Hz, J 16 Hz, β-$CH_2$ of Asn), 3.03 (1H, dd, *J* 4 Hz, J 16 Hz, β-$CH_2$ of Asn), 4.17 (1H, bd, H-2Man4`), 4.24 (1H, bd, H-2Man4), 4.30 (1H, bs, H-2Man3), 4.49 (2H, d, *J* 7.6 Hz, H-1Gal6, H-1Gal6`), 4.66 (3H, m, H-1GlcNAc2, H-1GlcNAc5, H-1GlcNAc5`), 4.86 (1H, s, H-1Man3), 5.15 (1H, d, *J* 9.5 Hz, H-1GlcNAc), 5.18 (1H, s, H-1Man4); HRMS (ESI) Calcd. For $C_{88}H_{144}N_8O_{64}$ (MH^+) 2337.8332. Found 2337.8340.

_S_-Acetylmercaptoacetic acid 4.4[11]

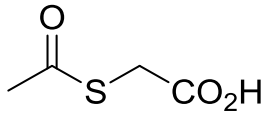

Acetyl chloride (3.8 mL, 0.054 mmol) was added drop-wise to a stirred mixture of triethylamine (15 mL, 0.108 mol) and thioglycolic acid **4.3** (5.22 g, 0.054 mol) in 1,4-dioxane (100 mL) at 0 ^oC under nitrogen, and the reaction was then warmed to rt. After 12 h, t.l.c (EtOAc) showed the formation of a major product (R_f 0) and the complete consumption of starting material (R_f 0.5). The reaction mixture was filtered through Celite® and concentrated *in vacuo.* 1 M Aqueous HCl (30 mL) was added, and the reaction was stirred for 1 h. The reaction mixture was extracted with DCM (3 x 30 mL), dried ($MgSO_4$), filtered, and concentrated *in vacuo* to give *S*-acetylmercaptoacetic acid **4.4**[11] (4.2 g, 54%) as a yellow oil; δ_H (400, d_6-DMSO)[11] 2.35 (3H, s, CH_3COS), 3.66 (2H, s, CH_2CO_2), 12.75 (1H, br s, COOH).

_N_-Hydroxysuccinimide ester 4.5[12]

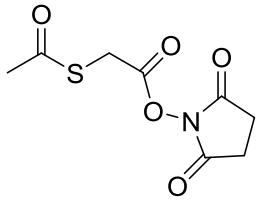

_S_-Acetylmercaptoacetic acid **4.4**[11] (2.6 g, 0.019 mol) and _N_-hydroxysuccinimide (2.2 g, 0.019 mol) were dissolved in THF (50 mL), and the reaction mixture was stirred at rt for 10 min before cooling to 0 ^{o}C. Dicylohexylcarbodiimide (DCC) (3.97 g, 0.019 mol) was dissolved in THF (5 mL), and then added to the reaction mixture. The reaction mixture was warmed to rt and stirred under nitrogen. After 12 h, t.l.c (EtOAc:MeOH, 4:1) showed the formation of a major product (R_f 0.6) and the complete consumption of the starting material (R_f 0.4). The residue was purified by flash column chromatography (petrol:EtOAc, 2:1) to afford _N_-hydroxysuccinimide ester **4.5**[12] (1.9 g, 61%) as a yellow oil. δ_H (400MHz, CD_3Cl_3)[12] 2.43 (3H, s, $COCH_3$), 2.85 (4H, s, $COCH_2CH_2CO$), 3.99 (2H, s, SCH_2CO_2).

Sialylglycan thioacetate 4.6

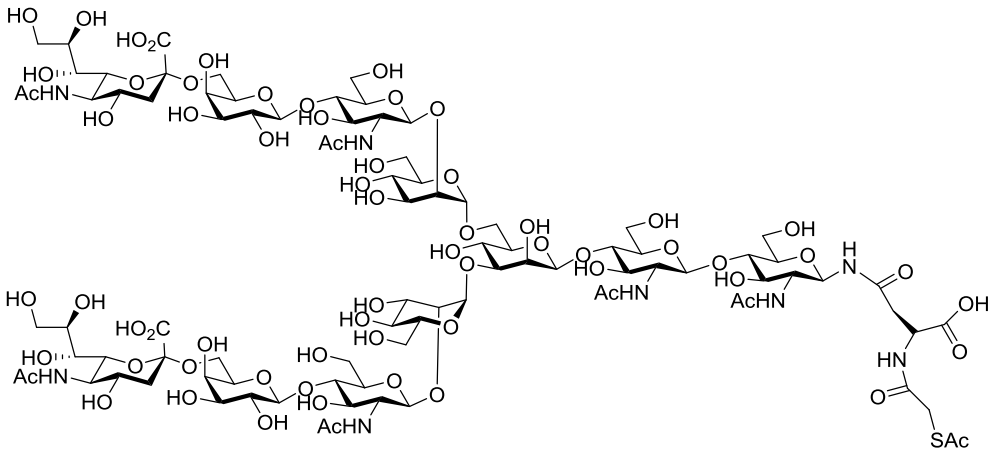

A solution of *N*-hydroxysuccinimide ester **4.5**[12] (12 mg, 0.049 mmol) in MeCN (0.3 mL) was added to a solution of asparagine-linked N-glycan **4.2**[10] (7.6 mg, 0.003 mmol) in sodium phosphate buffer (50 mM, 1 ml, pH 7.4) containing 20% MeCN. The mixture was stirred at rt for 12 h and then lyophilized. The residue was purified by gel filtration on a Sephadex G-25 column (8.7 x 1.7 cm), which was pre-equilibrated and eluted with 0.01% aqueous ammonia, to obtain thioacetate **4.6** (5 mg, 68%) as a white powder; δ_H (400 MHz, D_2O) 1.80 (dd, 2H, *J* 12.4 Hz, H-3_{ax}NeuAc7, H-3_{ax}NeuAc7`), 2.10-2.2 (18H, s, 6 x $CH_3CO_2$), 2.30 (3H, s, $CH_3COS$), 2.53-2.67 (4H, m, β-$CH_2$ of Asn, H-$3_{eq}$ NeuAc7, H-$3_{eq}$NeuAc7`), 4.17 (1H, bd, H-2Man4`), 4.24 (1H, bd, H-2Man4), 4.30 (1H, bs, H-2Man3), 4.49 (2H, d, *J* 7.6 Hz, H-1Gal6, H-1Gal6`), 4.66 (3H, m, H-1GlcNAc2, H-1GlcNAc5, H-1GlcNAc5`), 4.86 (1H, s, H-1Man3), 5.15 (1H, d, *J* 9.5 Hz, H-1GlcNAc), 5.18 (1H, s, H-1Man4); HRMS (ESI) Calcd. For $C_{92}H_{148}N_8O_{66}S$ (MH^+) 2453.8264. Found 2453.8191.

Sialylglycan disulfide 4.7

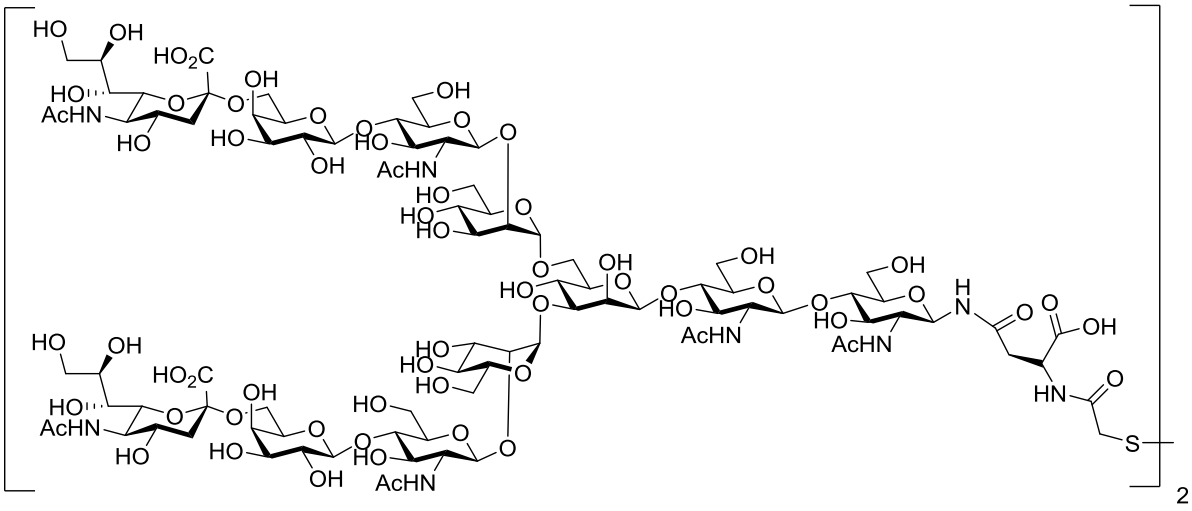

Hydroxylamine hydrochloride (51 mg, 0.73 mmol) was added to a solution of thioacetate **4.6** (300 mg, 0.122 mmol) in sodium phosphate buffer (100 mM, 80 ml, pH 7.4). The mixture was stirred at rt for 2 h and then lyophilized. The residue was purified by gel filtration on a Sephadex G-25 column (8.7 x 1.7 cm), which was pre-equilibrated and eluted with 0.01% aqueous NH_3, followed by air oxidation by bubbling air continuously through the solution for a total of 64 h to obtain sialylglycan disulfide **4.7** (210 mg, 71%) as a white powder; δ_H (400 MHz, D_2O) 1.80 (dd, 2H, *J* 12.4 Hz, H-3_{ax}NeuAc7, H-3_{ax}NeuAc7`), 2.10-2.2 (18H, s, 6 x $CH_3CO_2$), 2.53-2.67 (4H, m, β-$CH_2$ of Asn, H-$3_{eq}$ NeuAc7, H-$3_{eq}$NeuAc7`), 4.17 (1H, bd, H-2Man4`), 4.24 (1H, bd, H-2Man4), 4.30 (1H, bs, H-2Man3), 4.49 (2H, d, *J* 7.6 Hz, H-1Gal6, H-1Gal6`), 4.66 (3H, m, H-1GlcNAc2, H-1GlcNAc5, H-1GlcNAc5`), 4.86 (1H, s, H-1Man3), 5.15 (1H, d, *J* 9.5 Hz, H-1GlcNAc), 5.18 (1H, s, H-1Man4); HRMS (ESI) Calcd. For $C_{90}H_{146}N_8O_{65}S$ $(M+2H)^{2+}$ 1206.4116. Found 1206.4155.

Sialylglycan-capped gold nanoparticles (SG-gAuNPs)

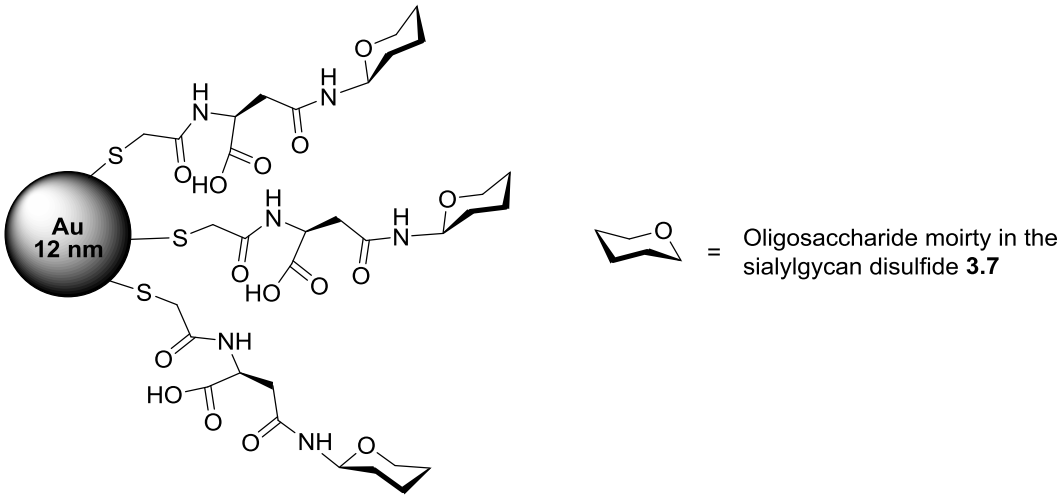

An aqueous solution of trisodium citrate (1.7 mL, 39.0 mM) was added to a boiling aqueous solution of $HAuCl_4 \cdot 3H_2O$ (7.6 mL, 1 mM) with constant stirring (500 rpm). After 15 min, the reaction mixture was cooled to rt, and a solution of disulfide **4.7** (144 mg, 1 mmol) was added. The reaction was stirred for 48 h at rt. The reaction mixture was concentrated *in vacuo*, the residue was dissolved in Milli-Q water (10 mL), and then purified by centrifugal filtering (Amicon Ultra 10K, Millipore, MWCO=10,000, 1h, 5000 x g). The residue was then dissolved in water (2 mL) and lyophilized to obtain **SG-gAuNP**. TEM: 12.1 ± 1.6 nm; IR (KBr): 3300 (broad band), 2933, 2873, 1062 cm^{-1}; UV: 523 nm; TGA: ligand 73.6%, Au 26.4%; Elemental analysis Found: C, 32.65; H, 4.50; N, 3.44; S, 1.04. Calcd. for $Au_{54464}(C_{12}H_{24}O_8S)_{12404}$: C, 32.96; H, 4.47; N, 3.42; S, 1.01%; HRMS (ESI) Calcd. For $C_{90}H_{146}N_8O_{66}S$ $(M+2H)^{2+}$ 1206.4116. Found 1206.4155

6.5. Experimental for chapter 5

3,6,9-Trioxadodec-11-yne-1-ol 5.8 [13]

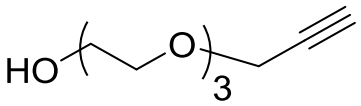

Triethylene glycol **5.7** (15.02 g, 100 mmol) was dissolved in 40 mL of dry THF. NaH (2.60 g, 65 mmol, 60% dispersion in mineral oil) was slowly added under nitrogen at 0 ^{o}C, and stirred for 30 min. Propargyl bromide (7.9 mL, 50 mmol) was added dropwise, and the mixture was stirred at 0 ^{o}C for 2 h, and then at 25 ^{o}C for 20 h. After this time, t.l.c (petrol:EtOAc, 1:3) showed the complete consumption of the starting material (R_f 0) and the formation of a major product (R_f 0.3). The reaction was quenched by the addition of MeOH (20 mL), and the mixture was then filtered through Celite® and concentrated *in vacuo*. The residue was purified by flash column chromatography (petrol:EtOAc, 2:1) to give 3,6,9-trioxadodec-11-yne-1-ol **5.8** (9 g, 48%) as a yellow oil. δ_H (400 MHz, $CDCl_3$)[13] 2.26 (1H, br s, OH), 2.42 (1H, t, *J* 2.3 Hz, $H_2CCC\underline{H}$), 3.55 - 3.79 (12H, m, 6 x CH_2O), 4.20 (2H, d, *J* 2.3 Hz, $\underline{H_2}CCCH$); HRMS (ESI) Calcd. For $C_9H_{17}O_4$ (MH^+) 189.1049. Found 189.1054.

1-Thioacetyl-3,6,9-trioxadodec-11-yne 5.9

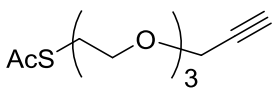

Alkyne **5.8** (9 g, 47.8 mmol) was dissolved in dry DCM (150 mL) under nitrogen at 0 ^{o}C and stirred. Mesyl chloride (7.4 mL, 96 mmol) was added dropwise, followed by triethylamine (13.3 mL, 96 mmol). The reaction mixture was then warmed to rt. After 2h, t.l.c (petrol:EtOAc, 2:1) indicated the formation of a single product (R_f 0.4), and the complete consumption of the starting material (R_f 0.2). The reaction was quenched by the addition of MeOH (30 mL) and concentrated *in vacuo.* The residue was dissolved in DMF (150 mL), potassium thioacetate (22 g, 191 mmol) was added, and the reaction was then stirred at 65 ^{o}C. After 16 h, t.l.c. (petrol:EtOAc, 2:1) indicated the formation of a major product (R_f 0.6), and the complete consumption of the starting material (R_f 0.4). The reaction mixture was cooled to rt, diluted with EtOAc (100 mL) and washed successively with aqueous solution of saturated $NaHCO_3$ (2 × 60 mL), H_2O (2 × 60 mL), and brine (30 mL). The organic layer was separated, dried (Na_2SO_4), filtered, and concentrated *in vacuo*. The residue was purified by flash chromatography (petrol:EtOAc, 10:1) to afford 1-thioacetyl-3,6,9-trioxadodec-11-yne **5.9** (7.4 g, 63%) as a yellow syrup. ν_{max} (KBr disc) 3271 (s, $H_2CC\underline{C}\text{-}\underline{H}$) 2865 (s, $H_2C\underline{C}\text{-}\underline{H}$) , 1685 (s, C=O) cm^{-1}. δ_H (400 MHz, $CDCl_3$) 2.31 (1H, s, CH_3CO), 2.42 (1H, t, *J* 2.3 Hz, $H_2CCC\underline{H}$), 3.08 (2H, t, *J* 6.5 Hz, CH_2S), 3.53 - 3.73 (10H, m, 5 x CH_2O), 4.20 (2H, d, *J* 2.3 Hz, $\underline{H_2}CCCH$); δ_C (100 MHz, $CDCl_3$) 28.8 (t, CH_2S), 30.5 (q, $\underline{C}H_3CO$), 58.4 (t, $H_2\underline{C}CCH$), 69.1 (t, CH_2O) 69.7 (t, CH_2O), 70.3 (t, CH_2O), 70.5 (t, CH_2O), 70.7 (t, CH_2O), 74.5 (d, $H_2CC\underline{C}H$), 79.6 (s, H2C$\underline{C}$CH), 195.5 (s, CO);; HRMS (ESI) Calcd. For $C_{11}H_{19}O_4S$ (MH^+) 247.0999. Found 247.0990.

1,1`-Dithiobis (3,6,9-trioxadodec-11-yne) 5.10

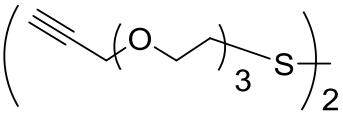

NaOMe (8.1 M solution in MeOH) was added to a solution of compound **5.9** (2 g, 8.1 mmol) in MeOH (50 mL), and the solution was stirred at rt. After 2 h, the solution was neutralized (confirmed by pH paper) by the addition of 1M HCl, and then air-oxidized by bubbling air continuously through the solution for a total of 72 h. The solvent was then removed *in vacuo* to afford disulfide **5.10** (1.6 g, 95%) as a yellow syrup; ν_{max} (KBr disc) 3253 (w, $H_2CC\underline{C\text{-}H}$), 2865 (s, $H_2C\underline{C\text{-}H}$ stretch), 1349 (w, $H_2C\underline{C\text{-}H}$ bend), 1092 (s, C-O) cm^{-1}; δ_H (400 MHz, $CDCl_3$) 2.42 (1H, t, *J* 2.2 Hz, $H_2CCC\underline{H}$), 2.86 (2H, t, *J* 8 Hz, CH_2S), 3.55 - 3.77 (10H, m, 5 x CH_2O), 4.18 (2H, d, *J* 2.4 Hz, $\underline{H_2}CCCH$); δ_C (100 MHz, $CDCl_3$) 38.4 (t, CH_2S), 58.4 (t, $H2\underline{C}CCH$), 69.1 (t, CH_2O), 69.6 (t, CH_2O), 70.3 (t, CH_2O), 70.4 (t, CH_2O), 70.5 (t, CH_2O), 74.5 (d, $H2CC\underline{C}H$), 79.6 (s, $H2C\underline{C}CH$); HRMS (ESI) Calcd. For $C_{18}H_{30}O_6S_2Na$ (MNa^+) 429.1376. Found 429.1375

1-Mercapta-3,6,9-trioxadodec-11-yne 5.11

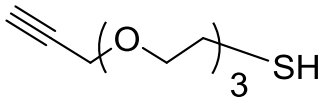

Dithiothreitol (DTT) (569 mg, 3.69 mmol) was added to a solution of the disulfide **5.10** (300 mg, 0.739 mmol) and *N*, *N*-diisopropylethyl amine (DIPEA) (0.65 mL, 3.69 mmol)

in MeOH and stirred under nitrogen at room rt. After 3 h, t.l.c (petrol:EtOAc, 1:1) indicated the formation of a single product (R_f 0.4), and the complete consumption of the starting material (R_f 0.3). The reaction mixture was concentrated *in vacuo*, diluted with EtOAc (30 mL) and washed successively with 1 M aqueous HCl solution (2 x 30 mL), an aqueous solution of saturated $NaHCO_3$ (2 × 30 mL), H_2O (2 × 30 mL), and brine (30 mL). The organic layer was separated, dried (Na_2SO_4), filtered, and concentrated *in vacuo*. The residue was purified by flash chromatography (petrol:EtOAc, 10:1) to afford 1-mercapta-3,6,9-trioxadodec-11-yne **5.11** (270 mg, 90.0%) as a yellow syrup. ν_{max} (KBr disc) 3250 (w, $H_2CC\underline{C\text{-}H}$), 2865 (s, $H_2C\underline{C\text{-}H}$), 1348 (w, $H_2C\underline{C\text{-}H}$ bend), 1090 (s, C-O) cm^{-1}; δ_H (400 MHz, $CDCl_3$) 1.56 (1H, t, *J* 8 Hz, SH), 2.42 (1H, t, *J* 2.2 Hz, $H_2CCC\underline{H}$), 2.66 (2H, m, CH_2S), 3.55 - 3.71 (10H, m, 5 x CH_2O), 4.18 (2H, d, *J* 2.4 Hz, $\underline{H_2}CCCH$); δ_C (100 MHz, $CDCl_3$) 23.5 (t, CH_2S), 58.4 (t, $H_2\underline{C}CCH$), 69.1 (t, CH_2O), 70.2 (t, CH_2O), 70.4 (t, CH_2O), 70.5 (t, CH_2O), 72.8 (t, CH_2O), 74.5 (d, $H_2CC\underline{C}H$), 79.6 (s, $H_2C\underline{C}CH$); HRMS (ESI) Calcd. For $C_9H_{16}O_3SNa$ (MNa^+) 227.0712. Found 227.0721.

2-Chloro-1,3-dimethylimidazolinium chloride 5.17 [14]

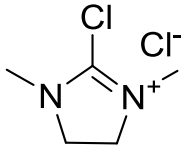

1,3-Dimethylimidazolidinone **5.16** (56.7 mL, 524 mmol) was dissolved in toluene (500 mL) and stirred under a nitrogen atmosphere. Oxalyl chloride (59.4 mL, 693 mmol) was added dropwise, and the reaction was stirred at 50 °C. After 3 h, the flask was cooled to rt and then stirred overnight. After 18 h, the precipitate was filtered, washed with cold

toluene and then recrystallized (MeCN/Et_2O). The white solid was filtered and dried under vacuum to yield 2-chloro-1,3-dimethylimidazolidinium chloride **5.17** (53 g, 60%) as a white powdery solid, m.p. 91-96 °C [lit. m.p. 95-100 °C];[14] δ_H (400 MHz, CD_3CN)[14] 3.17 (6H, s, 2 x CH_3), 4.02 (4H, s, 2 x CH_2); HRMS (ESI) Calcd. For $C_5H_{10}ClN_2$ (M+) 133.0527. Found 133.0529.

2-Chloro-1,3-dimethylimidazolinium hexafluorophosphate 5.18 [14]

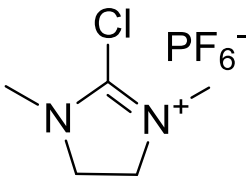

2-Chloro-1,3-dimethylimidazolidinium chloride **5.17** (37 g, 220 mmol) was dissolved in anhydrous MeCN (300 mL) and stirred under a nitrogen atmosphere. $NaPF_6$ (40.5 g, 220 mmol) was added and the reaction was stirred at rt. After 30 min, the solution was filtered through Celite® which was washed with MeCN (100 mL). The combined washings were concentrated *in vacuo,* and the resultant solid was dissolved in a minimal amount of MeCN. Et_2O was added until a precipitate formed, which was collected by suction filtration to afford 2-chloro-1,3-dimethylimidazolinium hexafluorophosphate **5.18** (49 g, 80%) as a white solid, m.p. 226-232 °C [lit. 230-231 °C];[14] δ_H (400 MHz, CD_3CN)[14] 3.14 (6H, s, 2 x CH_3), 3.95 (4H, s, 2 x CH_2); HRMS (ESI) Calcd. For $C_5H_{10}ClN_2$(M+) 133.0527. Found 133.052

2-Azido-1,3-dimethylimidazolinium hexafluorophosphate (ADMP) 5.19 [14]

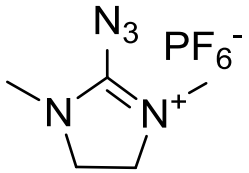

2-Chloro-1,3-dimethylimidazolidinium hexafluorophosphate **5.18** (11.6 g, 41.7 mmol) was dissolved in anhydrous MeCN (120 mL) and stirred at 0 °C under a nitrogen atmosphere. Sodium azide (3.8 g, 58.5 mmol) was added to the reaction mixture. After 3 h, the mixture was filtered through Celite® which was washed with MeCN. The filtrate was concentrated *in vacuo*, and the resulting solid dissolved in a minimal amount of MeCN. Et_2O was added until a precipitate formed, which was collected by suction filtration to afford 2-azido-1,3-dimethylimidazolinium hexafluorophosphate **5.19** (11.8 g, quant.) as a white solid, m.p. 201-205 ^oC [lit. 205-207 °C];[14] δ_H (400 MHz, CD_3CN)[14] 3.08 (s, 6H, 2 x CH_3), 3.81 (s, 4H, 2 x CH_2); HRMS (ESI) Calcd. For $C_5H_{10}N_5$ (M+) 140.0931. Found 140.0925.

2-Acetamido-2-deoxy-β-D-glucopyranosyl azide 5.20[14]

N-Acetyl-D-glucosamine **5.12** (250 mg, 1.13 mmol) and triethylamine (0.8 mL, 5.7 mmol) were stirred in D_2O/MeCN (4:1, 5 mL) and cooled to 0 °C. ADMP **5.19** (0.95 g, 3.4 mmol) was added. After 1 h, t.l.c. ($CHCl_3$/MeOH, 2:1) indicated complete consumption of starting material (R_f 0.2) and the formation of two major products (R_f

0.5, 0.6). The reaction mixture was acidified to pH 2 by dropwise addition of aqueous 1.2 M HCl and then neutralized by addition of $NaHCO_3$ (5 mL of a saturated aqueous solution). The solution pH was followed by using pH paper. The reaction mixture was concentrated, and the residue was dissolved in ethanol (10 mL), filtered through Celite®, and concentrated *in vacuo*. The residue was then redissolved in water (10 mL), washed with DCM (2 x 20 mL), filtered through a column of Amberlite® IR120 (H^+, previously treated with aqueous 1 M NaOH solution), and concentrated *in vacuo*. Purification by flash column chromatography ($CHCl_3$:MeOH, 5:1) gave 2-acetamido-2-deoxy-β-D-glucopyranosyl azide **5.20** (240 mg, 84%) as a white solid; m.p. 127 - 131 °C [lit. m.p. 125-130 °C];[15] $[\alpha]_D^{20}$ -34 (*c*, 1.0 in MeOH) [lit. $[\alpha]_D^{20}$ -34 (*c*, 1.0 in MeOH)];[15] δ_H (400 MHz, D_2O)[29] 1.88 (3H, s, CH_3), 3.32 (1H, m, H-4), 3.35-3.42 (2H, m, H-3, H-5), 3.53 (1H, at, *J* 9.5 Hz, H-2), 3.60 (1H, dd, $J_{5,6}$ 5.4 Hz, $J_{6,6'}$ 12.2 Hz, H-6), 3.75 (1H, m, H-6'), 4.58 (1H, d, $J_{1,2}$ 9.3 Hz, H-1); HRMS (ESI) Calcd. For $C_8H_{14}N_4O_5$ (MNa^+) 269.0862. Found 269.0852.

1-(2'-Acetamido-2'-deoxy-β-D-glucopyranosyl)-4-(1-Mercapta-3,6,9-trioxadodecyl)-1,2,3-triazole 5.27

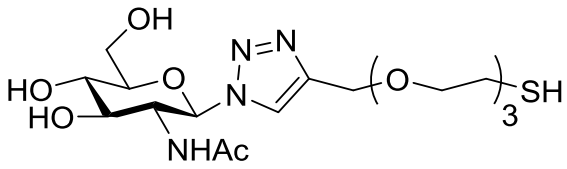

N-Acetyl-D-glucosamine **5.12** (100 mg, 0.45 mmol) and triethylamine (313 µL, 2.26 mmol) were dissolved in D_2O/MeCN (4:1, 2 mL) and the mixture was cooled to 0 °C.

ADMP **5.19** (387 mg, 1.3 mmol) was then added, and the reaction was stirred at 0 °C. After 1 h, t.l.c. ($CHCl_3$/MeOH, 2:1) indicated the complete consumption of the starting material (R_f 0.2), and the formation of two major products (R_f 0.5, 0.6). The reaction mixture was acidified to pH 2 by the dropwise addition of aqueous 1.2 M HCl and then neutralized by addition of saturated aqueous $NaHCO_3$ solution. Alkyne **5.9** (223 mg, 0.9 mmol) dissolved in 10 mL of MeCN, $CuSO_4 \cdot 5H_2O$ (1.7 mg, 7 µmol), and L-ascorbic acid (15.9 mg, 0.09 mmol) were added, and the reaction mixture was stirred at 90 °C. After 14 h, t.l.c. ($CHCl_3$/MeOH, 4:1) indicated the complete consumption of starting material (R_f 0.3) and the formation of a major product (R_f 0.5). The reaction mixture was concentrated, and the residue was dissolved in MeCN (20 mL), filtered through Celite®, and concentrated *in vacuo*. The residue was dissolved in MeOH (30 mL), and then NaOMe (3.2 M solution in MeOH) was added. The reaction was stirred at rt for 12 h. The solution was neutralized (confirmed by pH paper) by the addition of aqueous 1M HCl, and concentrated *in vacuo*. An unsuccessful attempt was made to purify the residue by flash chromatography ($CHCl_3$:MeOH, 10:1). The product co-eluted along with ascorbic acid-related impurities. δ_H (400 MHz, CD_3OD) 1.67 (3H, s, NHCO$\underline{CH_3}$), 2.90 (2H, m, CH_2S), 3.52-3.83 (14H, m, H-3, H-4, H-5, H-6, 5 x CH_2O), 3.90 (1H, m, H-6`), 4.20 (1H, m, H-2), 4.60 (2H, s, CH_2O), 5.80 (1H, d, $J_{1,2}$ 10 Hz, H-1), 8.17 (1H, s, C=CH); HRMS (ESI) Calcd. For $C_{17}H_{31}N_4O_8S$ (MH+) 451.1857. Found 451.1850.

1-Mercapta-3,6,9-trioxadodec-11-yne-functionalized AuNPs (ATT-AuNPs)

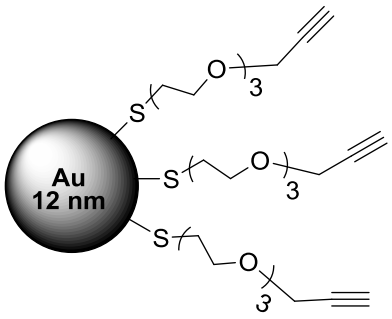

An aqueous solution of trisodium citrate (10 mL, 42.9 mM) was added to a boiling aqueous solution of $HAuCl_4 \cdot 3H_2O$ (100 mL, 1 mM) with constant stirring (500 rpm). After 15 min, the reaction mixture was cooled to rt, and a solution of ATT **5.11** (150 mg, 0.74 mmol) in MeOH (50 mL) was added. The reaction was stirred for 24 h at rt. The reaction mixture was concentrated *in vacuo,* and the residue was washed with water (3 x 10 mL). It was then dissolved in MeOH and purified by centrifugation (4 x 6000 rpm) to afford ATT-AuNPs (20 mg). TEM: 12.0 ± 1.4 nm; IR (KBr): 2921 (s, $H_2C\underline{C\text{-}H}$ stretch), 1458 (w, $H_2C\underline{C\text{-}H}$ bend), 1084 (s, C-O) cm^{-1}; UV: 541 nm; TGA: ligand 45.4%, Au 54.6%; δ_H (400 MHz, $CDCl_3$) 2.44 (br. s, $H_2CCC\underline{H}$), 2.70-3.03 (br. m, CH_2S), 3.50 - 3.80 (br. m, CH_2O), 4.20 (br. s, $\underline{H_2}CCCH$); HRMS (ESI) Calcd. For $C_9H_{16}O_3SNa$ (MNa^+) 227.0712. Found 227.0721.

AuNPs functionalized with the GlcNAc triazole 5.27

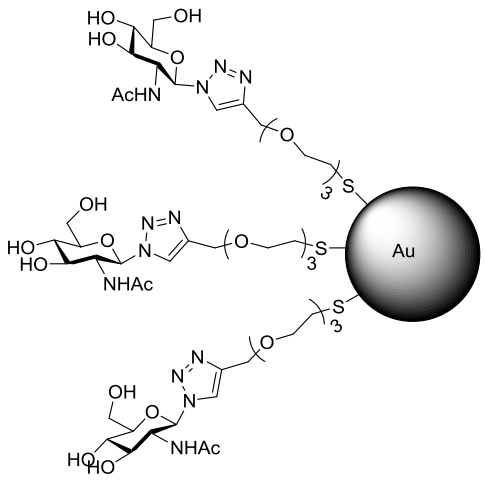

N-Acetyl-D-glucosamine **5.12** (10 mg, 0.045 mmol) and triethylamine (32 µL, 0.26 mmol) were dissolved in D_2O/MeCN (4:1, 0.2 mL) and the mixture was cooled to 0 °C. ADMP **5.19** (38 mg, 0.13 mmol) was then added, and the reaction was stirred at 0 °C. After 1 h, t.l.c. ($CHCl_3$/MeOH, 2:1) indicated the complete consumption of the starting material (R_f 0.2), and the formation of two major products (R_f 0.5, 0.6). The reaction mixture was acidified to pH 2 by the dropwise addition of aqueous 1.2 M HCl and then neutralized by addition of saturated aqueous $NaHCO_3$ solution. The solution pH was followed by using pH paper. ATT-AuNP (3 mg) dissolved in 2 mL of THF, L-ascorbic acid (25 mg, 0.14 mmol), $CuSO_4 \cdot 5H_2O$ (2.5 mg, 0.01 mmol) dissolved in H_2O were added to the reaction and stirred under nitrogen at rt. After 24 h, reaction mixture was dialyzed in H_2O for 3 d and then lyophilized to obtain AuNPs functionalized with the GlcNAc triazole **5.27** (aggregated) (1 mg). δ_H (400 MHz, D_2O) 1.67 (br. s, NHCOC$\underline{H_3}$),

2.80-2.90(m, CH_2S), 3.30-3.80 (m, H-3, H-4, H-5, H-6, 5 x CH_2O), 4.00 (br. s, H-6`), 4.2 (br. s, H-2), 4.52 (s, CH_2O), 5.76 (d, $J_{1,2}$ 10 Hz, H-1), 8.15 (br. s, C=CH).

6.6. Reference

1. Brawer, J. *Handbook of preperative inorganic chemistry* 2ed.; Academic Press: New York, 1963.

2. Spangler, B. D. *Microbiol. rev.* **1992,** *56* (4), 622-647.

3. Kaper, J. B.; Morris, J. G.; Levine, M. M. *Clin. Microbiol. Rev.* **1995,** *8* (1), 48-86.

4. Fais, M.; Karamanska, R.; Allman, S.; Fairhurst, S. A.; Innocenti, P.; Fairbanks, A. J.; Donohoe, T. J.; Davis, B. G.; Russell, D. A.; Field, R. A. *Chem. Sci.* **2011,** *2* (10), 1952-1959.

5. Wolfrom, M. L.; Thompson, A.; Inatome, M. *J. Am. Chem. Soc.* **1957,** *79* (14), 3868-3871.

6. Liu, Z.; Byun, H.-S.; Bittman, R. *Org. Lett.* **2010,** *12* (13), 2974-2977.

7. Mukthavaram, R.; Marepally, S.; Venkata, M. Y.; Vegi, G. N.; Sistla, R.; Chaudhuri, A. *Biomaterials* **2009,** *30* (12), 2369-2384.

8. Schofield, C. L.; Mukhopadhyay, B.; Hardy, S. M.; McDonnell, M. B.; Field, R. A.; Russell, D. A. *Analyst* **2008,** *133* (5), 626-634.

9. Sun, B.; Bao, W.; Tian, X.; Li, M.; Liu, H.; Dong, J.; Huang, W. *Carbohydr. Res.* **2014,** *396* (0), 62-69.

10. Yamamoto, N.; Ohmori, Y.; Sakakibara, T.; Sasaki, K.; Juneja, L. R.; Kajihara, Y. *Angew. Chem. Int. Ed.* **2003,** *42* (22), 2537-2540.

11. Deaton, D. N.; Gao, E. N.; Graham, K. P.; Gross, J. W.; Miller, A. B.; Strelow, J. M. *Bioorg. Med. Chem. Lett.* **2008,** *18* (2), 732-737.

12. Hideo, S.; Yasuhiro, M.; Yasushi, A.; Norio, Y. *PCT Int. Appl.* **2000,** *EP 1 046 401 A2*.

13. Lu, G.; Lam, S.; Burgess, K. *Chem. Commun.* **2006,** (15), 1652-1654.

14. Lim, D.; Brimble, M. A.; Kowalczyk, R.; Watson, A. J. A.; Fairbanks, A. J. *Angew. Chem. Int. Ed.* **2014,** *126* (44), 12101-12105.

15. Lim, D. Synthesis of O-Linked Glycopeptides Using Enzymatic Catalysis. Ph.D. Thesis, University of Canterbury, 2016.

Appendix

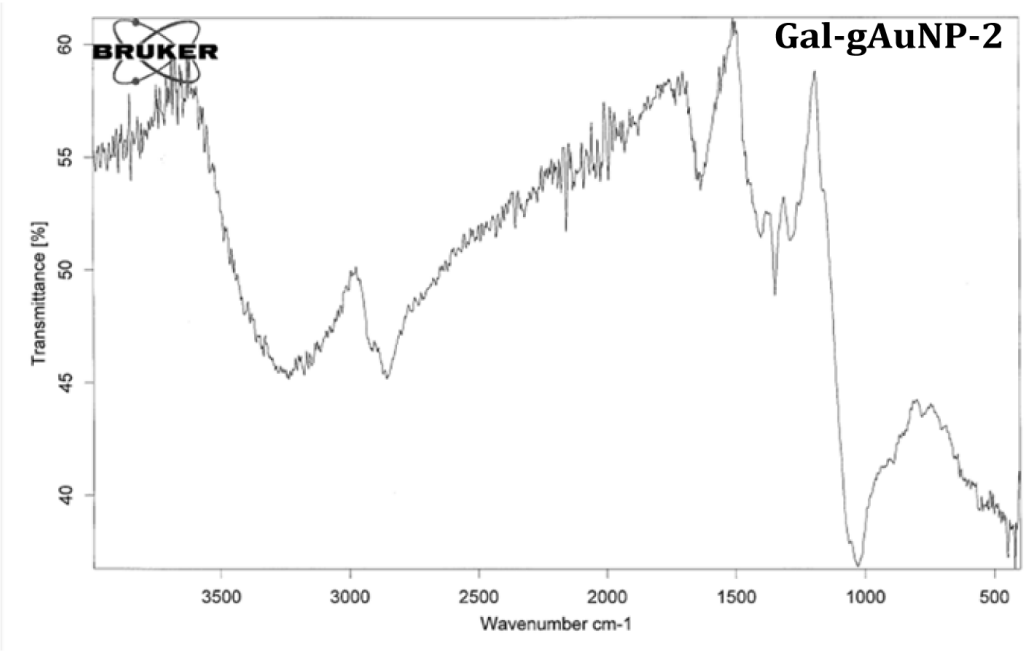

Figure A3.1. FT-IR spectra of **Gal-gAuNP-2.**

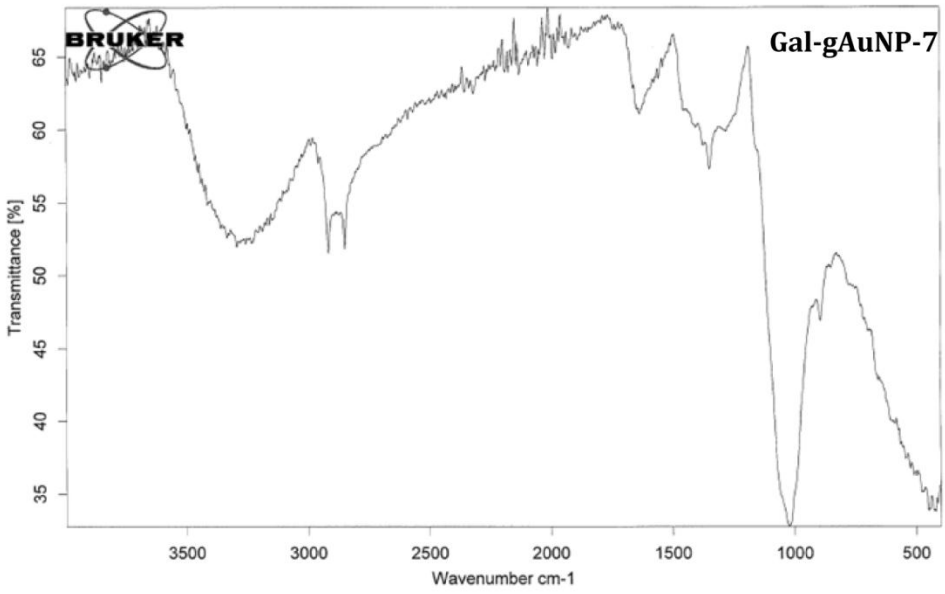

Figure A3.2. FT-IR spectra of **Gal-gAuNP-7.**

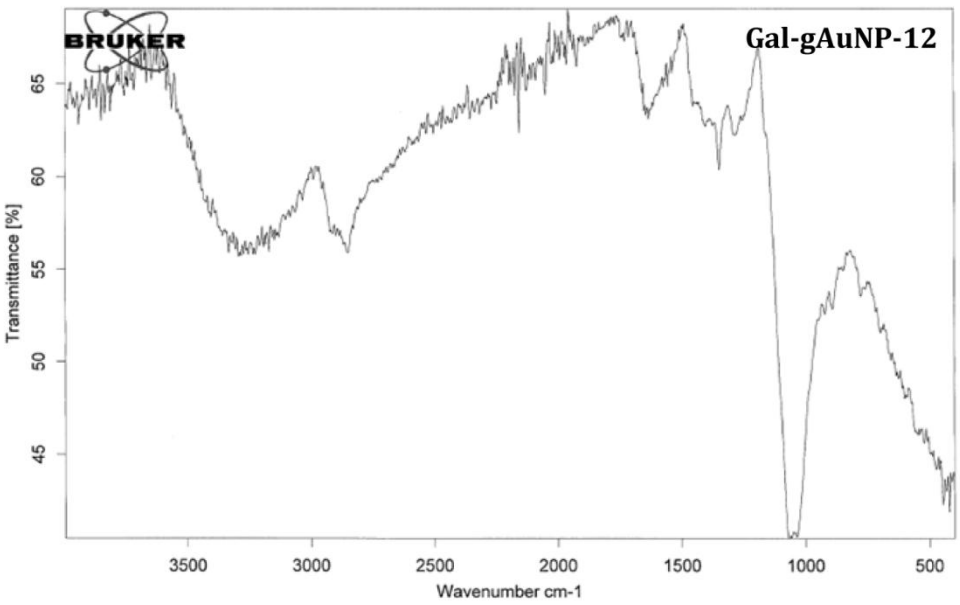

Figure A3.3. FT-IR spectra of **Gal-gAuNP-12.**

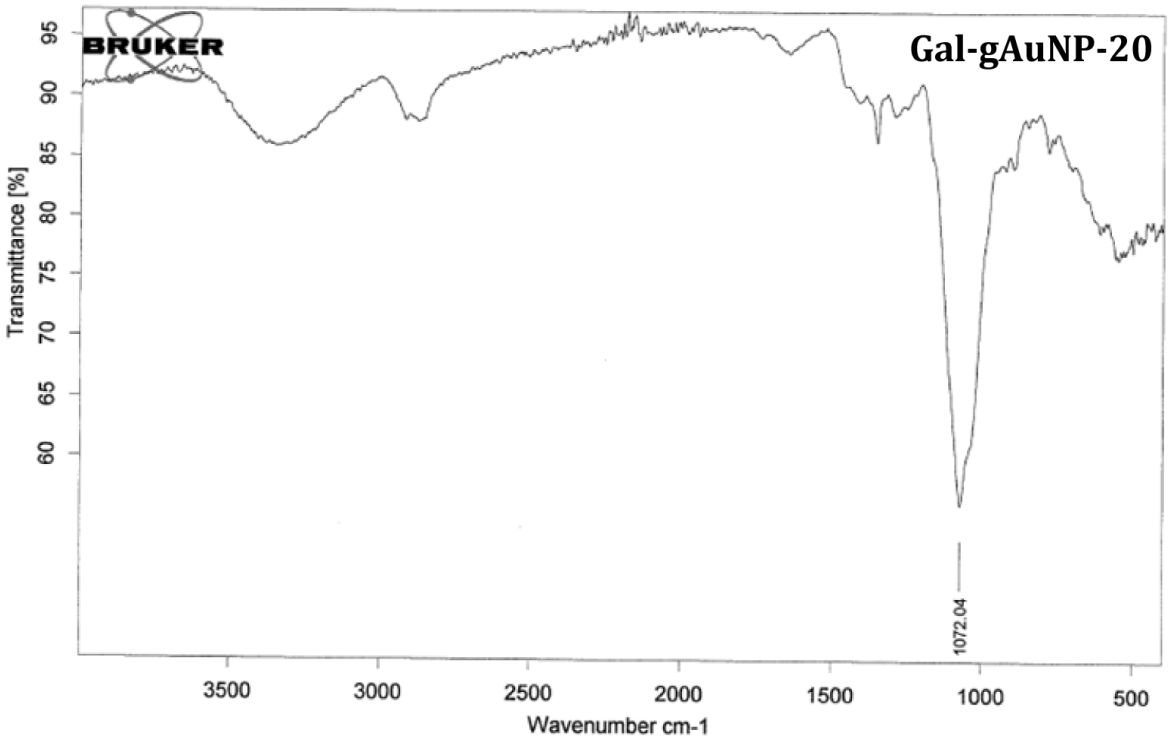

Figure A3.4. FT-IR spectra of **Gal-gAuNP-20.**

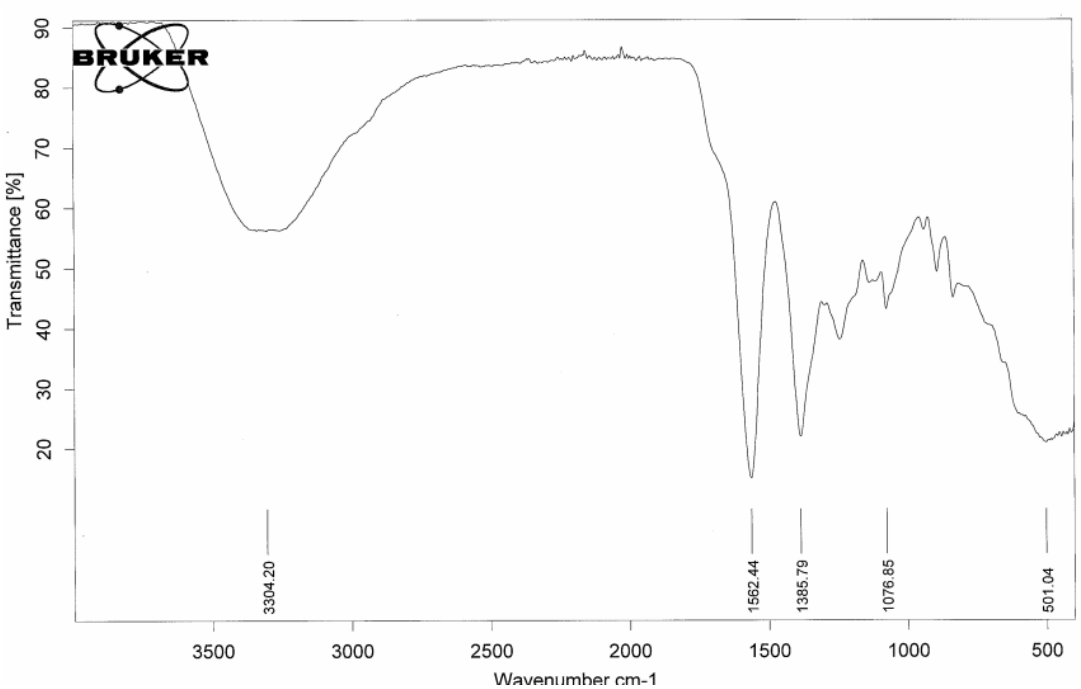

Figure A3.5. FT-IR spectra of Cit-AuNPs.

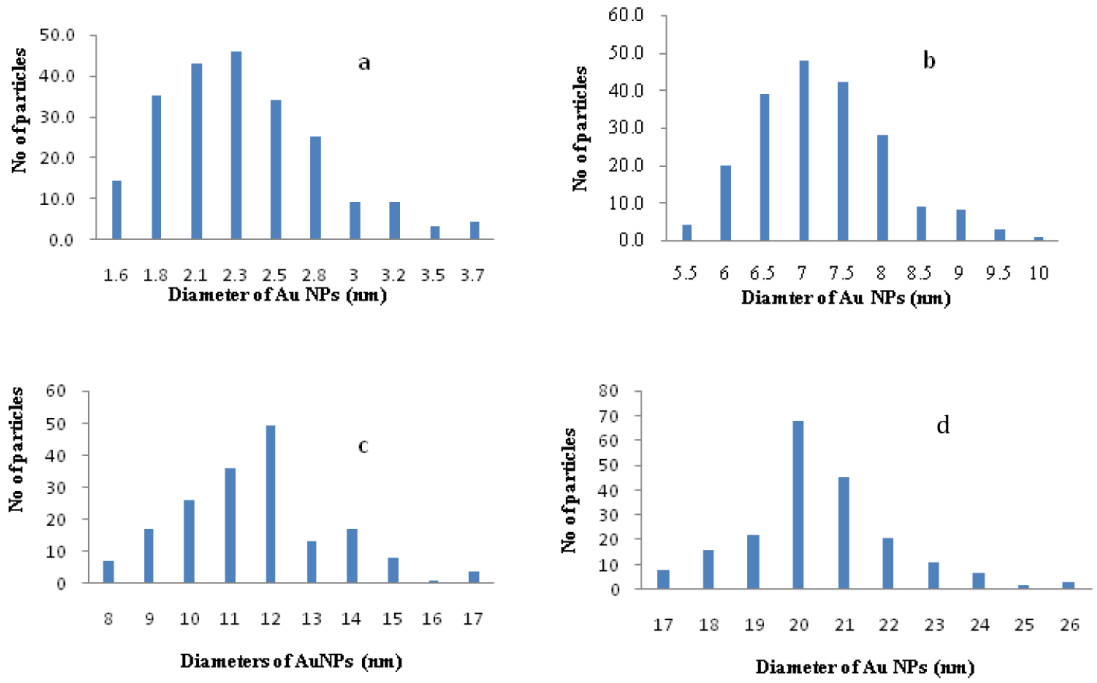

Figure A3.6. Size distribution histograms of a) **Gal-gAuNP-2** (2.3 ± 0.5 nm), b) **Gal-gAuNP-7** (7.3 ± 0.9 nm), c) **Gal-gAuNP-12** (12.0 ± 1.7 nm), and (d) **Gal-gAuNP-20** (20.3 ± 1.8 nm). At least 200 AuNPs were measured for the statistics of particle size distributions in all cases.

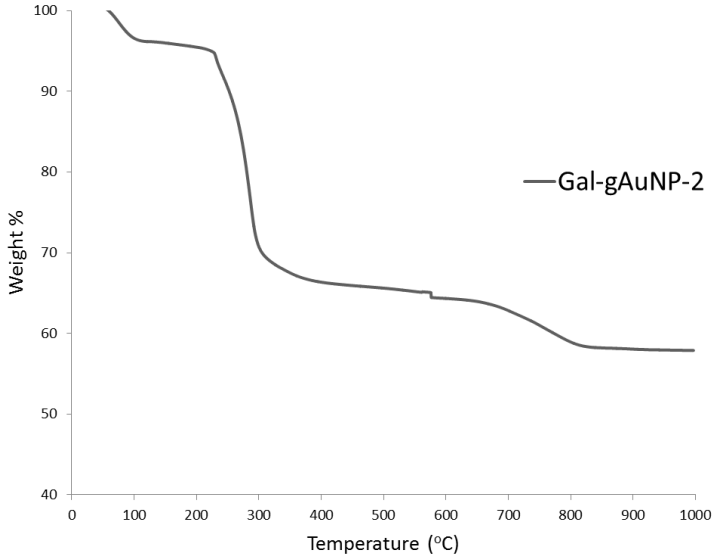

Figure A3.7. TGA plot of **Gal-gAuNP-2.**

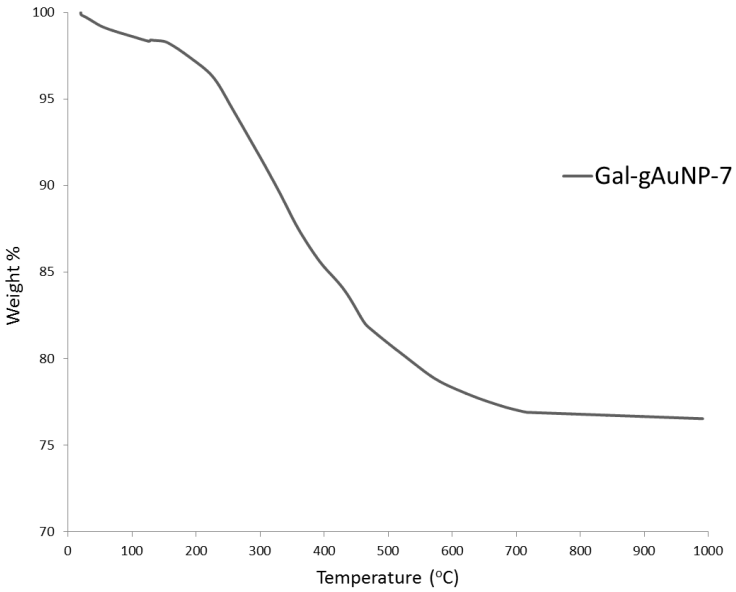

Figure A3.8. TGA plot of **Gal-gAuNP-7.**

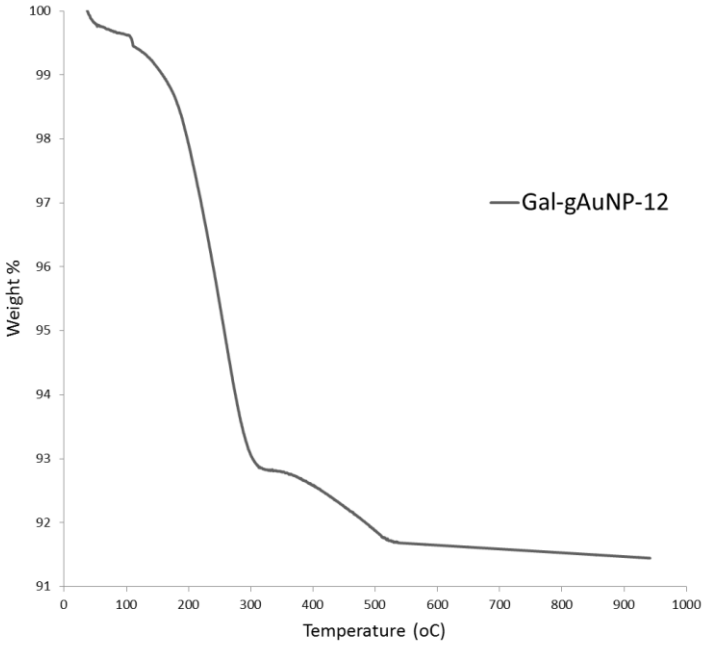

Figure A3.9. TGA plot of **Gal-gAuNP-12.**

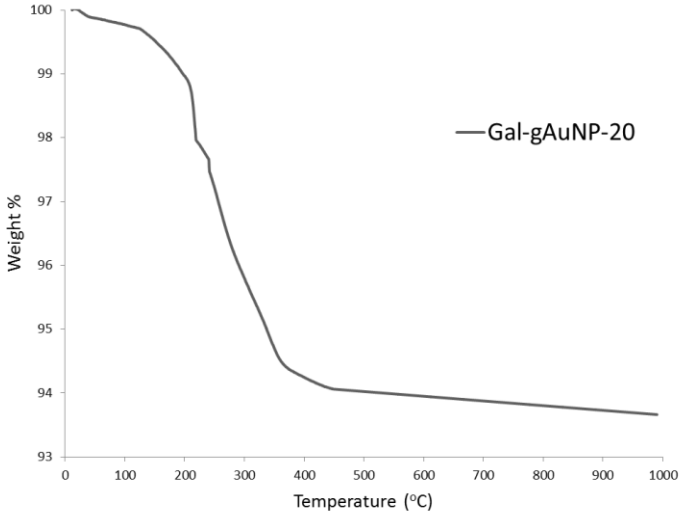

Figure A3.10. TGA plot of **Gal-gAuNP-20.**

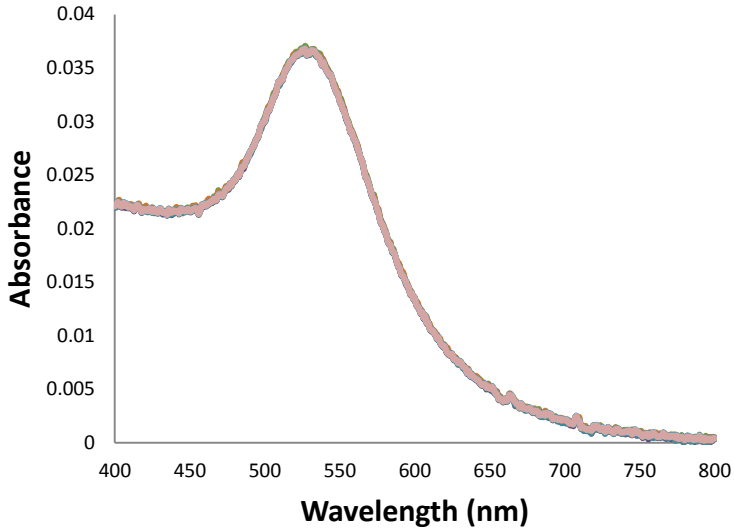

Figure A4.1. UV-Vis spectrum of SG-gAuNP in the presence of 71 nM HA

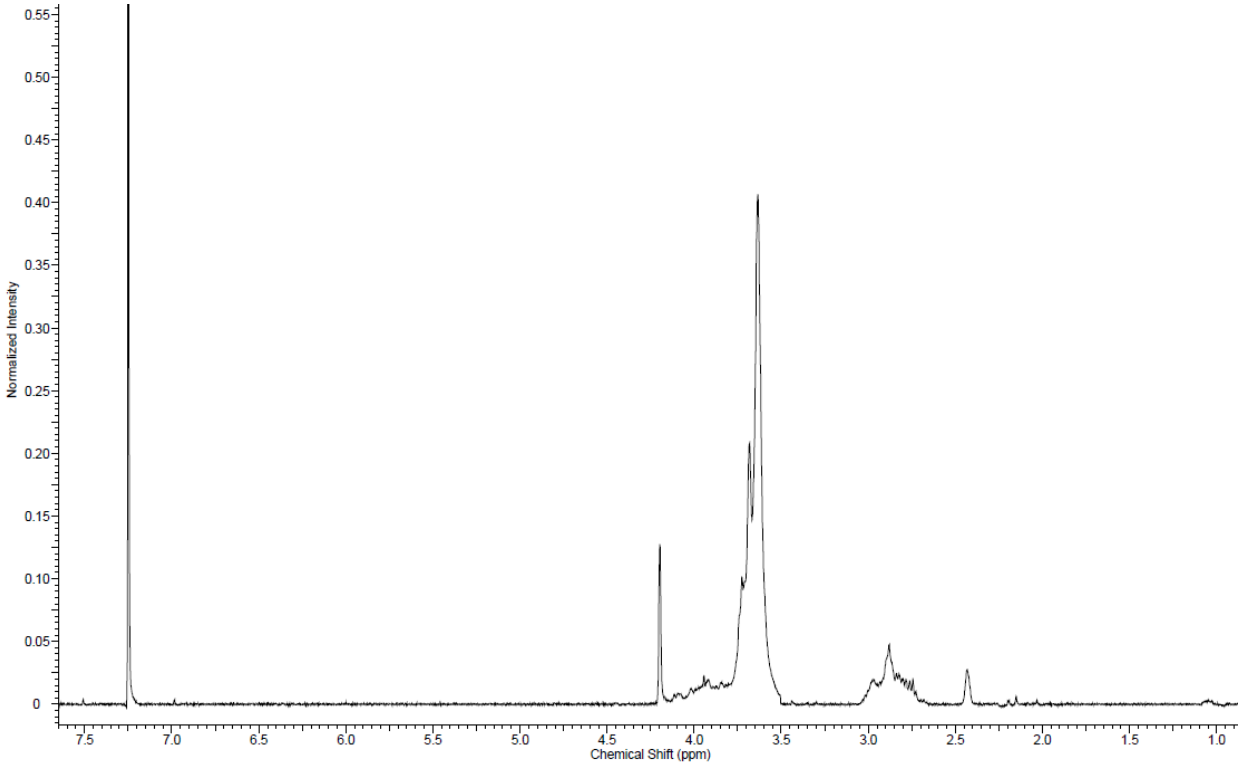

Figure A5.1. ^{1}H-NMR spectrum of ATT-AuNPs.

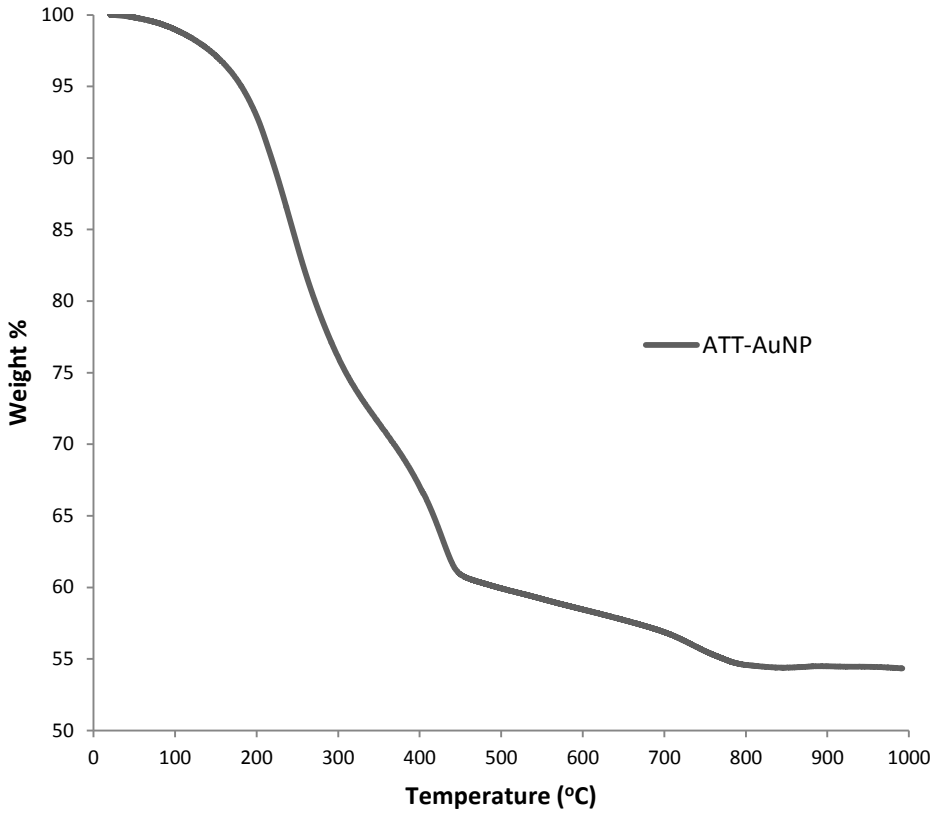

Figure A5.2. TGA plot of ATT-AuNPs.

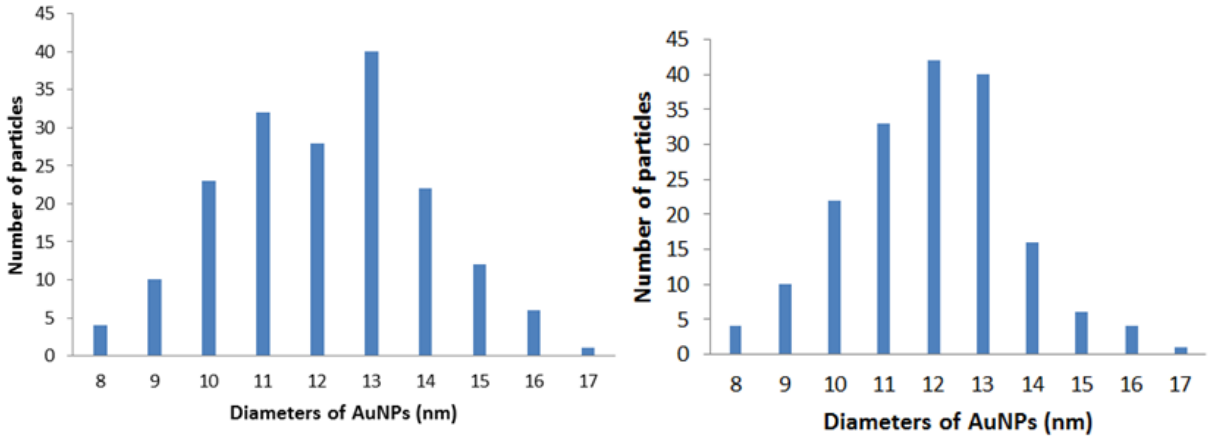

Figure A5.3. Size distribution histograms of Cit-AuNPs (12.1 ± 1.5 nm) and ATT-AuNPs (12.0 ± 1.4 nm).

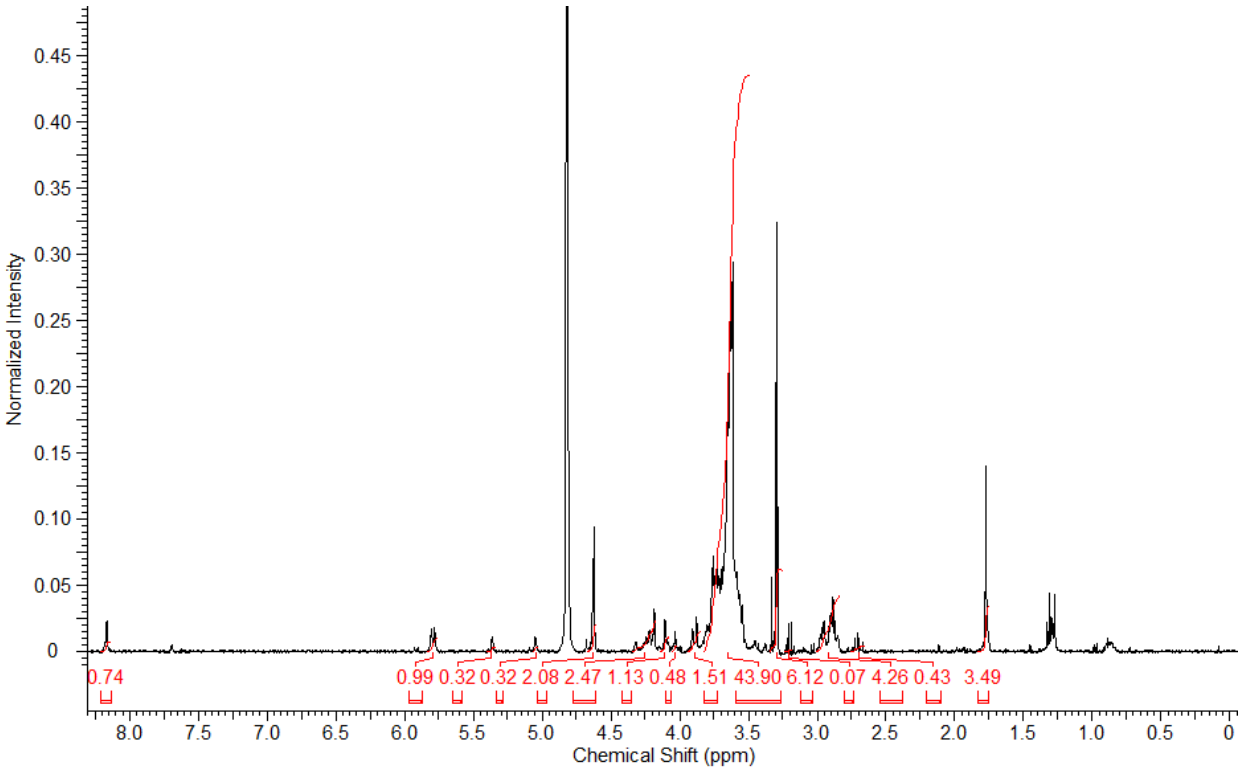

Figure A5.4. ^{1}H-NMR spectrum of the compound **5.27** co-eluted with ascorbic acid-related impurities.